STRATIGRAPHY, STRUCTURAL GEOLOGY, AND TECTONIC IMPLICATIONS OF THE SHOO FLY COMPLEX AND THE CALAVERAS-SHOO FLY THRUST, CENTRAL SIERRA NEVADA, CALIFORNIA

Charles Merguerian

Submitted in partial fulfillment of the
requirements for the degree
of Doctor of Philosophy
in the Graduate School of Arts and Sciences

COLUMBIA UNIVERSITY
1985

ABSTRACT

Stratigraphy, Structural Geology, and Tectonic Implications of the Shoo Fly Complex and the Calaveras-Shoo Fly Thrust, Central Sierra Nevada, California

Charles Merguerian

Mylonitic rocks of the Shoo Fly Complex form a region of epidote-amphibolite grade quartzose and granitoid gneiss, subordinate schist and calcareous rocks, and rare amphibolite in the foothills of the Sierra Nevada range in central California. The Shoo Fly has endured a complicated Phanerozoic structural development involving seven superposed deformations at variable crustal depths. The first four of these (D_1-D_4) involved tight to isoclinal folding and shearing under medium grade metamorphic conditions. The last three (D_5-D_7) are marked by open folding and retrograde metamorphism of older fabric elements.

The Shoo Fly is in ductile fault contact with east-dipping argillite, chert, and marble of the Calaveras Complex. The Calaveras-Shoo Fly thrust formed during D_3 and is a 1-2 km wide syn-metamorphic ductile shear zone. Recognition of D_3 overprinting of older D_1+D_2 fabrics along the thrust zone indicates that upper plate Shoo Fly rocks record an earlier and more complex structural history than the lower plate Calaveras rocks.

Paleozoic gneissic granitoids, an important lithologic component of the Shoo Fly, were intruded as a series of plutons ranging from calc-alkaline gabbro to granitoid (predominate) to syenite. They truncated the early S_1 foliation in the Shoo Fly and were folded during regional D_2 and D_3 events when they were penetratively deformed into augen gneiss, blastomylonite, and ultramylonite.

The Sonora dike swarm occurs as an areally extensive (> 1500 km^2) subvertical consanguineous suite of andesite, lamprophyre, and basalt dikes that trend east-west across the Calaveras and Shoo Fly Complexes. The metamorphic complexes form the basement to a middle Jurassic calc-alkaline plutonic arc (Jawbone granitoid sequence). A middle Jurassic K-Ar age on the dikes (157-159 m.y.) together with the data of this report indicate that they are petrogenetically related to the Jawbone granitoid sequence and that the dikes probably formed during subduction beneath a continental arc.

The dikes provide an important structural marker in the Shoo Fly and Calaveras Complexes. Intrusion of the dike swarm was sensitive to a structural anisotropy in the basement complexes. Since they intruded east-west along a spaced regional schistosity developed during folding of the Calaveras-Shoo Fly thrust, thrusting and subsequent folding were clearly pre-middle Jurassic events.

Available geochronologic data sets middle Ordovician to late Devonian intrusive ages for the gneissic granitoids, establishing a pre-late Devonian depositional age for the Shoo Fly. D_1 and intrusion of the orthogneiss protoliths may have been precursors of the Late Devonian to Early Mississippian Antler orogeny or, alternatively, may have occurred significantly earlier than the Antler orogeny. Based on cross-cutting relations, D_2 formed during the Antler orogeny, D_3 and possibly D_4 during the Sonoma orogeny, and D_5 and D_6 during the Nevadan orogeny.

TABLE OF CONTENTS

	Page #
Preface	1
Chapter 1 - Stratigraphy and structural geology of the Shoo Fly Complex and the Calaveras-Shoo Fly thrust, Sierra Nevada foothills belt, Tuolumne and Mariposa Counties, California	3
Chapter 2 - Paleozoic gneissic granitoids in the Shoo Fly Complex, central Sierra Nevada, California	90
Chapter 3 - Geology and geochemistry of the Sonora dike swarm, central Sierra Nevada foothills belt, California	140
References	197
Plates (in pocket)	

[**Note:** Electronic copies of plates are available on-line in .pdf format at www.Dukelabs.com]

ACKNOWLEDGEMENTS

A study of such duration and breadth is driven by the help and inspiration of many individuals. First and foremost I thank Dr. Richard A. Schweickert for his initial introduction to the problem and his unerring support throughout. The chapters were critically reviewed by Drs. Hannes K. Brueckner, Ian W. D. Dalziel, and Terry Engelder. In addition to these gentlemen, discussions with Nicholas L. Bogen, Patrick and Pamela Brock, Rhodes W. Fairbridge, David S. Harwood, Peter H. Mattson, Dennis Radcliffe, and Warren Sharp have proved fruitful in the generation of many of the ideas presented herein.

I was assisted in the field and laboratory by Jay and Joyce Brown, Peter Carucci, Maria and Merlin Dyball, Altan Gulumoglu, Tim Harnett, P. LaJuke, Will Kaufman, K. K. Kurkjian, Susan Logan, Myriam Ogburn, Des and Betty Parrish, Elizabeth Lee Riggs, and Deb Stoner. This work was funded by the National Science Foundation (grants # EAR-76-10979 and EAR-79-14779), the California Division of Mines and Geology, Duke Geological Laboratory, and the Geological Society of America.

The Sierra Nevada

PREFACE

The western flank of the Sierra Nevada range in California is underlain by a diverse assemblage of Paleozoic and Mesozoic metamorphic rocks. The lower Paleozoic Shoo Fly Complex, the oldest of these units, forms an elongate outcrop belt along the eastern margin of the metamorphic belt. The Shoo Fly was first described in the northern Sierra in the early 1900s but until now little was known about the distribution and structure of the Shoo Fly Complex in the central Sierra except for reconnaissance mapping by R.A. Schweickert in the 1970^{s}.

The following three chapters report the results of an in-depth study of various aspects of the geology of the Shoo Fly Complex and associated rocks in Tuolumne County, California. All of the chapters have been submitted to professional journals for publication. The geologic map (Plate 1) is being published by the California Division of Mines and Geology as an open-file report (scale 1:24,000).

Chapter l describes the lithology, structure, and metamorphism of the Shoo Fly and structure and deformation related to the Calaveras-Shoo Fly thrust. The Shoo Fly endured a long and complicated structural history involving seven superposed deformational events (D_l-D_7), each with distinctive structural and metamorphic characteristics.

The Calaveras-Shoo Fly thrust is a major deep-seated ductile shear zone that separates the Lower Paleozoic Shoo Fly Complex from upper Paleozoic to lower Mesozoic rocks of the Calaveras Complex to the west. The unique ductile fault textures developed in both the Shoo Fly and Calaveras are described and interpreted to indicate that the fault marks an important plate boundary that experienced a protracted history of thrust motion. Finally, the Shoo Fly Complex of this report is correlated with the Shoo Fly of the northern Sierra and similar rocks in north-central Nevada, the Klamath Mountains, and British Columbia.

Chapter 2 provides a detailed account of lithology, petrology, geochemistry, and structural geology of Paleozoic gneissic granitoid rocks which are an important lithologic component of the Shoo Fly Complex. These studies indicate that the gneisses were derived from igneous protoliths that were sequentially intruded as plutons ranging from gabbro (oldest) to granite and granodiorite (median age) to syenite (youngest). The gneisses post-date the oldest deformational event in the Shoo Fly (D_1). Preliminary geochronologic data (Sharp and others, 1982) on some of the gneiss bodies indicate apparent early Paleozoic igneous ages, and thus set a pre-late Devonian age for D_1 in the Shoo Fly and establishes a younger age limit on deposition of the Shoo Fly.

Chapter 3 reports on the field occurrence, lithology, petrography, and geochemistry of the Sonora dike swarm, an areally extensive suite of calc-alkaline andesite, lamprophyre, and basalt dikes that were intruded in the middle Jurassic sub-parallel to an east-west-trending schistosity in the Shoo Fly and Calaveras Complexes. Data presented in Chapter 3 suggests that the dikes formed within a composite marginal magmatic arc whose basement consisted of polyphase deformed rocks of the Calaveras and Shoo Fly Complexes. Emplacement of the dikes was strongly influenced by the crustal anisotropy created by the east-west schistosity in the basement and possibly by east-west-directed compressive forces transmitted into the overriding plate during middle Jurassic subduction to the west.

The present study of the Stanislaus, Tuolumne, and. Merced river drainages was undertaken to document and describe the lithology, structural geology, and geochemistry of the Shoo Fly Complex and associated rocks. This report provides the first detailed record of the geology of this region and places critical constraints on the tectonic interpretations of the foothills metamorphic belt.

CHAPTER 1

Stratigraphy and structural geology of the Shoo Fly Complex and the Calaveras-Shoo Fly thrust, Sierra Nevada foothills belt, Tuolumne and Mariposa Counties, California

ABSTRACT

Mylonitic rocks of the Shoo Fly Complex form a region of epidote-amphibolite grade quartzose and granitoid gneiss, schist, subordinate calcareous rocks, and rare amphibolite in the west-central foothills of the Sierra Nevada range in California. The region, described here for the first time, is engulfed to the east by the Sierra Nevada batholith and to the west is in thrust contact with east-dipping argillite, chert, and marble of the Calaveras Complex. The thrust juxtaposes rocks of constrasting lithology, age, structure, and metamorphism. The Shoo Fly probably originated as a thick sequence of slope and rise sediments deposited near the lower Paleozoic shelf edge of ancestral North America. The Calaveras is composed of chaotic oceanic sedimentary rocks of late Paleozoic to early Mesozoic age.

The Shoo Fly has endured a complicated Phanerozoic structural history involving seven superposed deformations occurring at variable crustal depths. The first four of these events (D_1-D_4) involved tight to isoclinal folding and local shearing under varied medium grade metamorphic conditions. The last three (D_5-D_7) are marked by open folding and retrograde metamorphism of the older fabrics. Early in this evolution, between D_1 and D_2, metasedimentary rocks of the Shoo Fly Complex were discordantly intruded by sills and plutons of gabbro, granite, and syenite which subsequently formed orthogneiss bodies, an important lithologic component of the Shoo Fly in Tuolumne County.

The Calaveras-Shoo Fly thrust formed during D_3 and is a folded synmetamorphic ductile shear zone that varies in width from 1-2 km and has been traced for over 90 km from lat. 38°05'N to 37°30'N. A remarkable along-strike D_3 textural consistency in the Calaveras-Shoo Fly thrust zone includes the formation of 1) megascopic isoclinal, intrafolial, and rootless F_3 folds with a penetrative axial-planar S_3 mica foliation, spaced ductile shears and widespread

transposition, 2) ellipsoidal slivers of foliated Shoo Fly flattened parallel to S_3 and highly elongated parallel to L_3 stretching lineations in sheathing mylonitic envelopes, 3) zones and seams of mylonite layering with highly strained and polygonized quartz ribbons with abrupt grain-size variations between layers, 4) macro- to microscopic strained quartz augen with internal sutures and core and mantle structure, rounded feldspar augen exhibiting marginal granulation, bent twins, corrosion, and cracking with local replacement by muscovite, 5) highly laminated phyllonitic textures in schistose rocks with frayed mica augen surrounded by anastomosing S_3 folia of smaller recrystallized micas and quartzose ribbons, and 6) late-stage D_3 injections of protocataclasite, pseudotachylyte, foliated granitoid sills, and minor folding.

The recognition of D_3 mylonitization of D_1+D_2 fabrics along the Calaveras-Shoo Fly thrust indicates that upper plate Shoo Fly rocks record a more complex, earlier structural history than the lower plate Calaveras rocks. During the formation of the thrust the Calaveras Complex experienced its first regional deformation which was characterized by long-limbed isoclinal folds and the development of a penetrative flattening foliation. In the thrust zone, syn-metamorphic flattening, imbrication and intense silicification of the Calaveras occurs.

The thrust and related structural features were folded by east-west-trending F_4 folds which are in turn crosscut by mid-Jurassic plutons and mafic dikes of the Sonora dike swarm. The preceding structural features and igneous bodies are cut by N32°W and N30°E steep to vertical cleavages which are traceable into open, possibly conjugate, F_5 and F_6 folds that formed during the Nevadan orogeny of Late Jurassic time. The youngest N60°W to E-W vertical cleavage (S_7) is probably of Late Cretaceous age.

This report on the Shoo Fly Complex describes and documents a complicated sequence of deep-seated folding, metamorphism, and shearing, punctuated by well-bracketed cross-cutting

igneous events. Available geochronologic data suggest that D_2 and possibly D_1, formed during the Antler orogeny, D_3 and possibly D_4 during the Sonoma orogeny, and D_5 and D_6 during the Nevadan orogeny.

INTRODUCTION

The western metamorphic belt of the Sierra Nevada range (Clark, 1964, 1976) is roughly 350 km long, 60 km wide and extends from lat. 40°15'N south-southeasterly to lat. 37°N. It is overlain by Cretaceous to Cenozoic rocks of the Great Valley sequence to the west and is intruded by the Sierra Nevada batholith to the east. South of the lat. 39°N it is composed of three ductile-fault-bounded tectonostratigraphic units (Fig. 1) which show an eastward increase in age, metamorphic grade, and structural complexity with abrupt transitions occurring at the Melones, Sonora, and Calaveras-Shoo Fly faults.

The westernmost belt (Fig. 1) consists of upper Jurassic flysch and lower to upper Jurassic volcanic arc rocks resting on pre-lower Jurassic oceanic crust, serpentinite and melange (Taliaferro, 1933, 1942, 1943; Clark, 1964, 1970, 1976). The Jurassic oceanic assemblage was tightly folded and metamorphosed to lower green schist facies during the late Jurassic Nevadan orogeny (Bateman and others, 1963; Clark, 1964).

Until recently all metamorphic rocks south of lat. 39°N and east of the Melones fault (Fig. 1) were grouped with the Calaveras Formation by Clark (1964). The terrane is composed of two parts, the central and eastern belts (Schweickert, 1977, 1981; Merguerian and Schweickert, 1980; Schweickert and others, 1984).

The central belt (the Calaveras Complex) consists of a chaotic assemblage of upper Paleozoic to lower Mesozoic(?) argillite and siltstone, massive and rhythmically-bedded-chert, marble, talc-schist, and rare basalt. The age of the Calaveras remains uncertain, but Permo

Carboniferous fossils from limestone olistoliths (Turner, 1893; Schweickert and others, 1977) indicate a maximum Carboniferous age for the complex. The Calaveras is bounded on the west by the Sonora fault (Schweickert and Bogen, 1983) and is in ductile fault contact (Calaveras-Shoo Fly thrust) with the Shoo Fly Complex to the east (Merguerian and Schweickert, 1980).

The Shoo Fly Complex of early Paleozoic(?) age of the eastern belt underlies a terrane 330 km in length and 6-20 km wide which extends southward into Mariposa County at the southern terminus (lat. 37°30 'N) of the metamorphic belt (Merguerian, 1981 ms, 1982) where batholithic rocks cut across trend (Figs. 2, 3). The Shoo Fly shows a southward increase in structural complexity and metamorphic grade. North of lat. 39°N it consists of weakly metamorphosed quartzose sandstone, graywacke, slate, chert, and limestone (Clark, 1976). South of lat. 38°05'N (Fig. 2) it is a multiply deformed (seven superposed phases of deformation) and sheared assemblage of quartzite, quartzofeldspathic gneiss, granite, syenite, and gabbroic orthogneiss, garnet schist, calc-silicate rock, marble, and rare amphibolite. As noted above, the Shoo Fly is in ductile fault contact (Fig. 2) with the Calaveras Complex along a 1-2 km zone of mylonitization, intense flattening, imbricated rock units and transposition with overprinting metamorphism of older fabric elements (Merguerian, 1981). The Calaveras Complex, which forms the lower plate of the east-dipping thrust, is highly flattened and silicified and exhibits a less complicated structural history than the Shoo Fly.

This report presents new data on the stratigraphy and the nature and timing of structure and metamorphism of the Shoo Fly Complex and the Calaveras-Shoo Fly thrust in Tuolumne and Mariposa Counties, California. Isotopically dated intrusives indicate that the deformational and metamorphic history recorded in the Shoo Fly Complex may be the result of periodic

Phanerozoic orogeny (including the Antler, Sonoma, and Nevadan orogenies) each with its distinctive structural and metamorphic signature.

Area of this report and methods

The western metamorphic belt of the Sierra Nevada, the focus of gold-seeking prospectors since the mid-1800's, is deeply incised by a system of southwestward-flowing rivers that coalesce ultimately near San Francisco Bay. Draining the seasonal snowfields that form in the higher elevations of the range, from north to south these are the Feather, Yuba, American, Cosumnes, Mokelumne, Stanislaus, Tuolumne, and Merced Rivers (Fig. 2, inset Fig. 4). The principal erosion of the southern half of the metamorphic belt began in the Oligocene (Huber, 1981) and has continued into the Quaternary at a somewhat accelerated rate. Southwestward tilting of the Sierra Nevada block, which overlaps in time with the development of the Basin and Range province to the east, created a consequent stream system that, by the Eocene, produced an extensive planation surface.

During subsequent Quaternary rejuvenation, the main branches of the Stanislaus River and to a lesser extent its tributaries were deeply incised through the Eocene-planation surface leaving narrow hilltop residuals above 930 m elevation in the study area. A profound southwest sloping summit accordance is obvious on topographic maps. The steep v-shaped canyons have differential relief of 370-615 m, and offer the best exposures of the Shoo Fly Complex because the intervening ridges are choked with brush and mantled by Tertiary volcanic rocks or by a thick, lateritic, clayey paleosoil that formed during Cenozoic tropical climates. The trellised drainage pattern of the Stanislaus River system (Fig. 4) is indicative of emphatic control of north-northeast- and eastwest-trending brittle structural fabrics, joints, and faults in bedrock as well as the regional tilt.

Eleven months were spent in the field between 1978 and 1981 between the Middle Fork of the Stanislaus River and the southern tip of the metamorphic belt (Figs. 2, 3). Detailed mapping and structural analysis was carried out in parts of the Stanislaus, Columbia SE, Crandall Peak, and Twain Harte 7-1/2 minute quadrangles (herein called the Jupiter area after a former mining town centered in the study area). The Jupiter area lies between the towns of Murphys, Columbia, Sonora and Twain Harte and is bounded by Routes 4, 49, and 108, and by the Middle Fork Stanislaus River (Plate 1, Fig. 4).

In the Jupiter area detailed mapping was limited to water courses where abundant stream-polished exposure is common. Every outcrop in the rivers and creeks was examined for stratigraphic and structural data (>900 stations) and over 300 samples were collected for petrographic and geochemical analysis. Mapping of the Shoo Fly Complex and the Calaveras-Shoo Fly thrust south-east of Tuolumne City (Fig. 2) was accomplished in 2-1/2 months in 1981 with nearly 600 stations measured. Preliminary maps and a report on this southern region (Fig. 2) are on file with the California Division of Mines and Geology (Merguerian, 1981 ms). A detailed map (Plate 1 - 1:24,000 scale) of the Jupiter area is reproduced in simplified form in figure 5. The structural symbols defined in the legend to Plate 1 are used throughout the plates and figures of this report.

STRATIGRAPHY

Paleozoic metamorphic rocks which form parts of the Shoo Fly and Calaveras Complexes, crop out in the Jupiter area (Plate 1, Fig. 2). They were intruded by Paleozoic plutons, Mesozoic dikes, sills, and plutons, and are unconformably overlain by Tertiary volcanic rocks. The following sections describe the stratigraphy and field relations of metasedimentary,

metaigneous, and post-tectonic igneous rocks of the Jupiter area with major emphasis on the Shoo Fly Complex.

Metasedimentary rocks

The Shoo Fly Complex

Nomenclature. The "Shoo Fly beds" were originally named by Diller (1892, p. 375) for exposures near Taylorsville, California (Fig. 1) in Clear Creek about 3 km southeast of Shoo Fly Bridge. They included a limestone containing poorly preserved crinoid stems and Diller suggested they were of Carboniferous age. Diller (1892) also described adjacent outcrops of the Grizzly quartzite that contained abundant Silurian fossils. Diller (1908, p. 23) described the Shoo Fly Formation as consisting of clay slates with gray or black flinty material (chert?), quartzite with local slaty interlayers, subordinate quartz-pebble conglomerate, and minor beds with volcanic fragments and limestone lentils up to 17 m thick.

Unfortunately, Diller's original "Shoo Fly beds" are complexly folded and highly faulted and parts are now recognized as younger rocks. The name Shoo Fly Formation was retained by Clark and others (1962) for thinly-bedded quartzose and pyritic slate, siltstone, and chert, quartz-ose graywacke, plagioclase- and orthoclase-rich arkose, and subordinate quartz- and quartzite-pebble conglomerate near the American River that lie unconformably beneath bedded Mesozoic rocks.

Previous work. Folio mapping in the area of this report by Turner and Ransflme (1897, 1898) defined a "siliceous terrane" probably derived from igneous materials. They recognized but did not map quartzose rocks in drainages of the Mokelumne, Stanislaus, and Tuolumne rivers and on Elizabeth Peak, Mt. Lewis, Mt. Provo, and Duckwall Mtn. (Fig. Z). Turner (1893) suggested the quartzose rocks may be of Paleozoic age. Despite this early work, quartzose rocks

of the southern part of the western metamorphic belt were grouped into the Calaveras Formation of Turner (1893) by Clark (1964) who considered all metamorphic rocks east of the Melones Fault zone to be the Calaveras.

Schweickert (1977, 1981) re-examined the quartzose rocks as part of a regional study of the Calaveras Complex and established their continuity with "known" Shoo Fly rocks in the American River drainage. He suggested the name "Shoo Fly Complex" and mapped in reconnaissance a ductile tectonic contact (the Calaveras-Shoo Fly thrust) separating the Calaveras and Shoo Fly complexes between lat. 38°45' and lat. 37°30 'N (Fig 1.).

Lithologic units. Detailed mapping in the Jupiter area indicates that the Shoo Fly Complex consists of five mappable units; the units also occur to the south, between lat. 38° and 37°30'N. The original stratigraphic relationships among the units are unknown and no stratigraphic continuity is implied, because the assemblage is polydeformed and cut by a large number of ductile shear zones (discussed later).

In order of decreasing a real abundance (Plate 1, Fig. 5), the Shoo Fly Complex in the Jupiter area can be subdivided into quartzite and quartzofeldspathic gneiss, granitoid orthogneiss, schist, calc-silicate and marble, and amphibolite. All metasedimentary units show gradational contacts and are interlayered with one another. The gneissic granitoids are calc-alkaline metaigneous rocks that post-date an early S_1 metamorphic fabric (Schweickert and Merguerian, 1980). In many cases interlayered rocks have sharp, structurally imbricated contacts. However, undisrupted sedimentary layering is locally preserved as gradational mineralogic variations between sub-units, thick quartzofeldspathic layers with subordinate schistose layers, and laterally continuous centimeter-scale quartzite layers in schist.

Brief descriptions of the mappable units are given below. Detailed descriptions of sub-units can be found in Appendix 1.

1) <u>Quartzite and quartzofeldspathic gneiss.</u> This is a heterogeneous sequence of quartz-mica gneiss, quartzofeldspathic gneiss, pure quartzite and massive to thinly-layered black to dark-gray vitreous quartzite. The color ranges from light- and dark-gray or maroon- to brown on weathered surfaces and is generally gray-colored on fresh surfaces. Layering varies from massive- to thickly-layered and slabby but locally is highly-laminated. Outcrops are massive, tabular and quite prominent, forming vitreous stream-polished exposures and steep waterfalls at the nick-points of streams.

Interlayering of lithologies occurs at all scales and these rocks occur locally within all of the other metasedimentary units of the Shoo Fly Complex. Co-mingled calc-silicate rock and quartzite are quite common and mixed lithologies occur near contacts with schist. The following lithologies occur in minor amounts throughout the unit: 1) grayweathering, buff-colored quartzite with centimeter-scale dark quartz segregations (identical to those of the schist unit), 2) medium grained, angular and rounded quartzite-, quartz-, and chert-rich f fragmental layers, 3) flattened white- to cream-colored quartz- and chertpebble conglomerate, 4) laminated gray-weathering quartzite with f flattened (up to 1 cm) bluish quartzite pebbles, 5) pyritic schist and massive pyritic quartzite, 6) highly muscovitic zones, and 7) schistose interlayers 1 cm to 1 m thick.

2) <u>Schist.</u> The schist unit is a heterogeneous sequence of quartz-mica-plagioclase schist, phyllite and schistose gneiss. Color ranges from brown- to maroon- and gray-weathering and the schist is well foliated to highly-laminated and medium- to coarse-grained. Some outcrops are deeply weathered and create rounded masses in streams. The schistose rocks are interlayered with one another and with 0.5 cm to 0.5 m thick layers and lenses of mica-quartzite and

quartzofeldspathic gneiss. Complete transitions from mica schist to quartz-mica schistose gneiss to quartz-mica gneiss often occur within individual outcrops. Pods, lentils, and stringers of dark quartz from 2mm to 2m long occur in some zones, but they are typically 2-5 cm long and quite conspicuous. These quartz bodies are gray-black to bluish-black, flinty, extremely fine-grained and show conchoidal fracture. Minor lithologies include: dark-gray biotite phyllite, graphitic schist, pyritic schist, layers of angular to wispy quartz pebbles, and local zones of flattened quartz boulder conglomerate. Two outcrops of schist were found with sandy layers 3-50 cm thick showing relict detrital textures.

3) Calc-silicate and marble. This map unit is an assemblage of calc-silicate and calcareous rocks of diverse mineralogy and texture. They are brown- to tan- to light-green-weathering, and dark-green to gray. The rocks are well-layered, fine- to medium-grained diopside±tremolite calc-silicate rock, calcite and dolomite marble, and siliceous marble. Outcrops are not common except within larger mappable rock bodies. Where outcrops of marble are extensive a mini-karstic topographic surface exists. Small occurrences of the calc-silicate and marble that cannot be shown at 1:24,000 map scale are typically interlayered with quartzitic subunits of the quartzite and quartzofeldspathic gneiss. They also are sometimes interlayered with micaceous quartzite within sequences dominantly of quartzite and are associated with schist containing dark quartz pods. These calcareous rocks repeatedly occur near the contact between the quartzite and schist units. This may indicate some vestige of stratigraphic continuity in an otherwise thoroughly sheared complex of lithologic units. Mechanical differences between the marble and quartzites creates intricate folding patterns at their contacts that were not recognized in the schist unit.

4) Amphibolite. Two exposures of green hornblende-plagioclasebiotite amphibolite up to 120 m thick were found in Eagle and Rose Creeks (Plate 1) in the Jupiter area. Elliptical domains 10 to 15 cm across are suggestive of a fragmental texture. The rocks are crudely foliated.

The Calaveras Complex

Nomenclature and previous work. Originally named by Turner (1893) during folio mapping in the Mother Lode gold belt, the Calaveras Formation included all Paleozoic sedimentary rocks of the Sierra Nevada, excepting Silurian rocks found in the north. The term Calaveras "complex" was introduced for rocks east of the Melones fault in the vicinity of Figure 2 by Schweickert and others (1977) because of the uncertain age and clearly chaotic nature of the rocks. Quartzose rocks to the east, now recognized as the Shoo Fly, which were included in their original definition (unit Cq), were removed at a later time (Schweickert, 1981) .

Lithologic units. In the Jupiter area (Fig. 2) the Calaveras is a chaotic assemblage of massive argillite and siltstone, massive and rhythmically-bedded-chert, marble, talc-schist, basalt, and rare sandstone layers. In the study area the Calaveras is easily distinguished from the Shoo Fly due to their marked difference in rock type as described above. In addition, the Shoo Fly is more highly recrystallized, contains less marble, bears gneissic granitoids, and shows evidence for a greater number of regional deformational episodes. The age of the Calaveras remains uncertain, but Permo-Carboniferous fossils from limestone olistoliths (Turner, 1894; Schweickert and other, 1977) indicate a maximum late Paleozoic age for the sequence.

The Calaveras was not mapped in detail in the Jupiter area because Schweickert (unpub. data) has mapped extensively in the region. Descriptions of the Calaveras in this region can be found in Schweickert and Wright (1975), and Wright and Schweickert (1977), and Schweickert (1981).

Interpretation of Shoo Fly metasedimentary protoliths

Although the interpretation of pre-metamorphic protoliths is hindered in sheared medium-grade rocks by extensive recrystallization and transposition, detailed field study and examination of the metamorphic mineralogy allows some deductions to be made. Table 1 lists the interpreted pre-metamorphic protoliths of the Shoo Fly Complex from the Jupiter area (see Appendix 1 for detailed mineralogic descriptions). The dominance of siliceous lithologies comprising the Shoo Fly Complex, suggests derivation from a reworked continental source. Totally nonfeldspathic quartzite±mica±opaques with radiating extinction is interpreted as meta-chert.

The Shoo Fly evidently represents a thick sequence of subfeldspathic psammite with subordinate pelite, chert, carbonate rock of variable composition, and rare volcanic rock probably deposited near the continental margin of western North America.

Age constraints. No fossils have been found in the Shoo Fly Complex of Tuolumne County, and therefore the absolute sedimentary age of the sequence is unknown. The combined effects of multiple deformations under variable metamorphic conditions further obscures any original stratigraphic relationships. Siluro-Ordovician to Pennsylvanian U-Pb and Rb-Sr ages (Sharp and others, 1982) on some gneissic granitoid bodies in the Jupiter area indicate that the Shoo Fly is of early Paleozoic or older age.

Syntectonic meta-igneous rocks

Gneissic granitoids. This is a compositionally variable assemblage of foliated granite, syenite, and subordinate granodiorite, diorite, and gabbro orthogneiss with conspicuous augen (typically porphyroclasts of feldspar) in a finer-grained matrix of recrystallized minerals. The rocks are tan-, white-, and gray-weathering, white to dark gray, and fine- to coarse-grained. The

gneiss bodies range in size from 3 km masses showing complex internal zoning to centimeter-scale "lit-parlit injections," meter-scale sills, and larger lensoidal bodies.

The orthogneisses contain foliated xenoliths and screens of all of the various lithologies of the Shoo Fly Complex. Scattered apophyses, cross-cutting veins, fine-grained chilled margin facies, and irregular discordant contacts together mandate an igneous origin for these rocks. Mixed zones of orthogneiss and metasedimentary rocks of the Shoo Fly Complex are common but cannot be shown at 1:24,000 scale (Plate 1). The gneisses, which post-date an early episode of folding and metamorphism in the Shoo Fly (Schweickert and Merguerian, 1980), are described in detail elsewhere (Chapter 2).

Syn-tectonic granitoid dikes and sills. The Shoo Fly and Calaveras Complexes both contain foliated syn-tectonic granitoid dikes and sills that are mainly concordant to the Calaveras-Shoo Fly thrust fabric. They are brown-weathering, white to light-tan, fine- to medium-grained rocks composed of potash feldspar, plagioclase, quartz, biotite, and muscovite. The foliated sills are restricted to the Calaveras-Shoo Fly thrust zone and shear zones within the Shoo Fly Complex and occur as blebs a few cm long, as stretched boudins up to 10 cm thick, and as foliated masses up to 2.5 m thick.

Post-tectonic igneous rocks

Metamorphic basement rocks of the Shoo Fly and Calaveras Complexes are intruded by numerous post-tectonic felsic and mafic sills and dikes, granitic to mafic-ultramafic plutons, and by the Sierra Nevada batholith. Tertiary volcanic and volcaniclastic rocks drape many of the prominent ridges. For the most part the igneous rocks were not mapped in detail and the smaller dikes and sills are not shown on the maps (Plate 1, Fig. 5). These rocks are briefly described in the following sections.

Middle-Jurassic post-tectonic plutons. Near lat. 38°N a temporally constrained suite of compositionally zoned granitic through ultramafic plutons intrude across the metamorphic belt of the Sierra Nevada. One of these, the Standard pluton (Fig. 2) borders the southern edge of Plate 1 and Figure S but was not mapped in this study. Field and petrographic studies by W.D. Sharp (1984) and R.A. Schweickert (unpub. data) indicate that the pluton is a steep-walled internally zoned medium- to coarse-grained pyroxene- and hornblende-rich quartz diorite and monzodiorite with subordinate two pyroxene gabbro and ultramafic phases (W.D. Sharp - pers. comm., 1983). There are igneous foliations but no through going metamorphic fabrics have been recognized. Sillimanite found in the contact aureole southeast of the Standard pluton (Kerrich, 1970) and coexisting garnet-biotite-staurolite-sillimanite contact assemblages, found to the north in the present study, are superimposed on older penetrative fabrics in the Shoo Fly. U-Pb data from the Standard pluton yield a 164-170 m.y. middle Jurassic intrusive age (Sharp and Saleeby, 1979; Stern and others, 1981). A suite of plutonic rocks of similar age and lithology (Jawbone granitoid sequence of Stern and others, 1981) affected the metamorphic belt in the vicinity of Figure 2. The Standard pluton crosscuts the Calaveras-Shoo Fly thrust (Schweickert, 1981) and the pluton is, in turn, crosscut by slightly younger dikes of the Sonora mafic dike swarm.

Mafic dikes of the Sonora dike swarm. The Shoo Fly and Calaveras Complexes are multiply-intruded by a swarm of mafic dikes near lat. 38°N. Over 1000 dikes ranging from basalt to andesite have been mapped in the Shoo Fly and Calaveras by Merguerian and R.A. Schweickert (our unpub. data). In the Shoo Fly, the dikes are sub-parallel to E-W trending axial surface traces of folds that deform the Calaveras-Shoo Fly thrust (Fig. S). The dikes occur as solitary sheets and dikelets 3-5 cm thick and as dense 25 wide zones of profuse multiple

injections with anastomosing chilled margins. Individual dikes within these zones have an average thickness of 1 m and offshoots are common. Three textural types have been recognized:

1. light-gray to dark-gray spessartite and vogesite lamprophyres with non-oriented subhedral to euhedral phenocrysts of pargasitic amphibole, light-green amphibole, augite, and plagioclase up to 4 mm long. The dikes are generally less than 0.4 m thick.

2. gray-green to gray-black, dense, dominantly aphyric basalt and andesite dikes which locally possess augite and brown amphibole microphenocrysts and have microgabbro and microdiorite cores when thicknesses exceed 2 m.

3. dark-gray mottled medium- to coarse-grained, labradorite-phyric pyroxene-free basalt and andesite dikes. The phenocrysts are euhedral to subhedral (up to 4 mm) and the dikes are typically thicker than (1) or (2).

Cross-cutting relationships and chilled margin observations indicate that the dominantly aphyric dikes (2), which comprise over 35% of the mafic dike swarm, are of median relative age and thickness. They always cross-cut the thicker plagioclase-rich dikes (3) and are in turn cut by thinner lamprophyre dikes (1). The geology, geochemistry, and tectonic significance of the Sonora mafic dike swarm are treated elsewhere (Chapter 3). A 157-159 m.y.a. K-Ar hornblende age for the dikes has been reported by Sharp (1980).

Mesozoic post-tectonic rocks including the Sierra Nevada batholith. Granitic rocks of the Sierra Nevada batholith intrude the Shoo Fly Complex and contact metamorphose its easternmost outcrops. Internal phases within the batholith were not mapped in the present study. The rocks are dominantly medium- to coarse-grained, biotite-hornblende-granite, granodiorite, and quartz monzonite (Bateman and other, 1963). Along its western border a pronounced biotite and hornblende flow foliation, flow-oriented foliated xenoliths, and reduction in grain size occur.

Recrystallization of the Shoo Fly in these areas yields a contact induced increase in grain size. Elsewhere veins of granitic rock brecciate the Shoo Fly wall rocks. Late Jurassic to late Cretaceous ages have been reported for the batholith by many workers (Bateman and Clark, 1974; Evernden and Kistler, 1970; Stern and others, 1981).

Granitic plutons and dikes of unknown age. There are a number of small plutons in the Jupiter area (Plate 1, Fig. 5) and to the south (Fig. 2) that may be satellitic to the Sierra Nevada batholith or predate it entirely. The largest of these are, from north to south, the Knight Creek, Basin Creek, and Hazel Green plutons (Fig. 2). Most of these and the batholith crosscut the Calaveras-Shoo Fly thrust.

The Knight Creek pluton is exposed in drainages of Knight and Rose Creeks in the Stanislaus and Columbia SE 7-1/2 minute quadrangles (Plate 1). It is a medium- to coarse-grained biotite granite with local zones of pegmatite. The pluton crosscuts the Calaveras-Shoo Fly thrust and included xenoliths of the Sonora mafic dike swarm along its western contact with the Calaveras Complex (R.A. Schweickert - per. comm., 1982). The Basin Creek pluton intrudes the Shoo Fly Complex 10 km east of the Standard pluton. It is composed of medium- to coarse-grained hornblende granite, diorite, and local gabbro but was not mapped in detail. The Hazel Green pluton (Bowen, 1969; Tobisch, 1960) consists of medium-to coarse-grained granite and hornblende granodiorite with coarse-grained gabbroic to ultramafic rocks composing its northwestern border. Partly obscured by Tertiary volcanic rocks, a small coarse-grained hornblendite pluton occurs east of the Clavey river (Fig. 2). Many small plutons of granite, granodiorite and gabbro occur in the study area (Merguerian, 1981 ms).

Nearly 25 granitic dikes and sills have been mapped in the Shoo Fly Complex of the Jupiter area. They are not foliated and of variable composition and texture, and occur as aplite,

quartz-phenocrystic felsite, and granite pegmatite. They are less prevalent than the mafic dikes and are of unknown age but are possibly related to the intrusion of the Sierra Nevada batholith.

Tertiary volcanic rocks. Volcanic and volcaniclastic rocks of the Oligo-Miocene Valley Springs and Mio-Pliocene Relief Peak formations (Slemmons, 1966) occur above 1000 m elevations in the eastern part of the Jupiter area (Plate 1). White, fine-grained individual rhyolitic ash flow units up to 20 m thick of the Valley Springs Formation are found near Mount Knight (Crandall Peak quadrangle) and Grant Ridge (Twain Harte quadrangle) (Plate 1). The Relief Peak Formation is a tan- to gray-brown poorly-sorted, mudflow breccia (lahar) with rounded cobbles and boulders up to 0.5 m in diameter. The clasts are matrix supported and range in composition from predominantly volcanic rocks such as andesite, rhyolite, obsidian, and pumice, to sedimentary rocks such as chert and limestone, and rare silicified tree limbs. The matrix is composed of clay and fine-grained volcanic rock fragments and is strongly cemented creating remnant erosional surfaces with protruding, immovable boulders. Channelized lahars are found on the south rim of the Middle Fork Stanislaus River canyon.

STRUCTURAL GEOLOGY

The Shoo Fly Complex shows evidence for a long and complicated structural history involving seven superposed deformational episodes (D_1 through D_7) divisible into four discrete phases of ductile folding, shearing, and recrystallization (F_1-F_4) followed by three more brittle phases of folding and cleavage development (F_5-F_7), and finally, faulting. The various phases have been distinguished in the field by careful observation of overprinting relationships and sampling of cross-cutting axial surface foliations in regions of refolded folds. Table 2 lists

and defines the structural and metamorphic effects of the various deformational events that have affected the Shoo Fly Complex. Temporal relationships with various igneous and geomorphic events are also indicated.

In this paper ductile fault rocks are classified according to the scheme developed by Sibson (1977) who examined the Outer Hebrides Thrust and other ancient fault zones. The nomenclature for cohesive fault rocks is summarized below with percentages representing the proportion of matrix vs. porphyroclasts.

Random Fabric	**Foliated**	**% matrix**
protocataclasite	protomylonite	10-50%
cataclasite	mylonite	50-90%
ultracataclasite	ultramylonite	90-100%

In addition, according to Sibson (1977) cohesive rocks with less than 10% matrix are varieties of crush breccia and foliated mylonitic rocks with pronounced mineral growth are termed blastomylonite.

Figure 5 shows some aspects of the stratigraphic and structural complexity of the Shoo Fly Complex. The Calaveras-Shoo Fly thrust, the most obvious tectonic feature in the study area, trends northwest-southeast across the Jupiter area and dips steeply toward the east. Juxtaposition of the Shoo Fly and Calaveras Complexes took place during D_3, a regional dyamothermal event characterized by the formation of rootless isoclinal folds, imbrication of lithologies, and formation of blastomylonite under epidote-amphibolite grade conditions. Mylonitization obliterates earlier fabrics within the thrust zone and also occurs in smaller ductile shear zones throughout the Shoo Fly Complex. D_3, the most widespread deformational episode

to have affected the Paleozoic basement rocks of the region, will be treated after a discussion of preD_3 events. The geology of the Calaveras-Shoo Fly thrust and related features, and finally, post-D_3 events will be discussed in turn.

Evidence for pre-deformation

Many independent lines of evidence indicate that the Shoo Fly Complex has experienced two prograde dynamothermal events D_1 and D_2, that were separated by a period of intrusion of granitic and syenitic rocks. Figures 6, 7, and 8 are overlays for figure 5 (geologic map of the Jupiter area) and should be consulted for the following discussions. Zones where D_3 ductile shearing totally obliterates the D_1 and D_2 fabrics occur within 1-2 km of the Calaveras-Shoo Fly thrust and in a 400 m wide zone 7 km to the northeast (Figs. 5, 6). Outside of these regions, F_3 folding and small ductile shear zones are widespread but preserve between them evidence of the earlier structural history of the Shoo Fly Complex.

Regionally the F_3 folds deform a composite metamorphic layering (S_1 and S_2) and locally in the axial regions of pre-F_3 isoclinal folds (F_1 and F_2) the metamorphic layering (S_1) and mica foliation (S_2) are preserved. Together they constitute pre-Calaveras deformation as the S_3 fabric in the Shoo Fly is coeval with the development of both the earliest flattening foliation in the Calaveras and the creation of the Calaveras-Shoo Fly thrust. The F_1 and F_2 fold phases are regionally significant and regulate the northeast-southwest-trend of both lithologic units and the S_1 and S_2 metamorphic fabrics of the Shoo Fly (Figs. 5, 7) all of which are truncated nearly orthogonally by the thrust.

D_1. Younger D_2 and D_3 deformation has all but destroyed the evidence for D_1 except in regions of dominant F_2 folds. In every example of clear F_2 folding a metamorphic layering or mica foliation (S_1) is deformed about the hinge area. In a few localities S_1 is strongly mylonitic

with intrafolial F_1 folds occurring within the layering. Pre-D_3 sheath-folds have been found locally. It is unknown whether they are due to passive rotation of F_1 fold hinges during D_2 or an interference pattern resulting from the superposition of F_1 and F_2 folds. Commonly S_1 is marked by recrystallized quartzose laminae, feldspar, and mica, but F_1 folds are rare. No attempt was made to trace S_1 axial surfaces in the field and their apparently discontinuous nature is indicated in Fig. 7. In most instances the S_1 layering is transposed into parallelism with S_2, the axial surface of F_2 folds, as the D_2 event was a strongly penetrative event in this region.

Perhaps the most compelling evidence for D_1 is provided by the fact that protoliths of the orthogneiss metaplutonic unit truncated the S_1 metamorphic layering (Figs. 7, 9). The contacts have subsequently been folded together with S_1 in the Shoo Fly, by F_2 folds, and a penetrative foliation developed in the gneisses parallel to S_2.

Structural relations of the orthogneiss protoliths. Prior to 275 m.y.b.p. small plutons of gabbro, granite, and syenite with chilled margins and associated sills and dikes intruded the Shoo Fly Complex which already contained F_1 folds and an S_1 foliation (Table 2). These igneous rocks are now represented by gneissic granitoids which are intimately associated with all metasedimentary units of the Shoo Fly Complex (Plate 1; Chapter 2).

A plutonic origin for the gneissic granitoids of Tuolumne County is indicated by relict igneous contacts and textures in the interior of a larger bodies. In the larger internally-zoned bodies, cognate xenoliths occur and sharp contacts between granite, gabbro, and syenite gneisses are interpreted as primary intrusive contacts. Permeated and discordant intrusive contacts, bosses, veins, and apophyses, as well as mixed zones of orthogneiss and metasedimentary host rock occur.

The orthogneisses enclose foliated sub-equant, angular, to elongate (up to 2 m long) xenoliths and screens of every Shoo Fly lithology. Typically, the xenoliths are elongate parallel to a metamorphic layering (S_1) which suggests structural control over emplacement of the ortho-gneiss protoliths. Although highly folded, the sheet-like rather than equidimensional geometric form of the gneisses (Plate 1) supports this hypothesis. Augen gneiss locally crosscuts F_1 fold hinges and truncates the S_1 metamorphic layering of the Shoo Fly wall rocks. On the middle and north forks of the Stanislaus river, undeformed protoliths locally occur and these cut an early foliation (S_1) in the Shoo Fly.

Locally, xenoliths, sills and "lit-par-lit" injections of gneiss are deformed by F_2 folds and are affected by subsequent deformational episodes. Isoclinal to tight folding of gneiss-Shoo Fly contacts by F_2 folds and refolding by younger structures generate intricate outcrop patterns (Plate 1 , Fig. 7). Low angle truncation of S_1 in the Shoo Fly by orthogneiss and the effects of D_2 are illustrated in Fig. 9.

D_2. Strongly recrystallized penetrative mineral fabrics formed under amphibolite grade metamorphic conditions in the Shoo Fly Complex during the D_2 event. Field drawings (Fig. 10) and photographs (Figs. 11, 12) document the dominantly isoclinal style of the F_2 folds. They typically deform the S_1 metamorphic layering in long-limbed isoclinal and angular tight folds with shearing and mylonite developed along their axial surfaces (S_2) (Table 2). Locally the F_2 folds are 1) reclined with a strong down-dip lineation parallel to hingelines, 2) rootless folds with complex disharmonic patterns, and 3) eye-folds.

A penetrative mica foliation occurs parallel to the axial surfaces of F_2 folds, together with recrystallization of quartz, feldspar, and quartz veins in rocks of appropriate composition. Boudinage of D_1 quartz veins locally occur along the limbs of F_2 folds. S_2 is regionally

preserved as a folded enveloping surface in the hinge areas of F_3 folds where it is marked by recrystallized mica, quartzose laminae, or foliated compositional layering. Photomicrographs presented in a later section show relict S_2 mineral growth.

D_2 in the Jupiter area (Figs. 5, 7) involved folding (F_2) of the Shoo Fly which created apparent map-scale repetition of the schist unit and the development of an S_2 foliation in the orthogneiss parallel to F_2 axial surfaces. D_2 was thus the first deformation to have affected the plutonic protoliths of the orthogneiss. Both S_1 and S_2 are progressively transposed into parallelism with S_3 in zones of high D_3 ductile strain and the composite S_1+S_2 foliation is truncated at the Calaveras-Shoo Fly thrust together with various lithologic units (Merguerian, 1981). Because of the isoclinal nature of both F_1 and F_2 folds, which formed under lower amphibolite grade metamorphic conditions, the pre-D_3 crystalline fabrics in the Shoo Fly are essentially coplanar. It is unknown whether F_1 and F_2 were progressive events. If D_1 and D_2 mark a single orogenic pulse, the intrusion of the orthogneiss protoliths may represent synkinematic intrusions or, alternatively, they may have been intruded during a hiatus in regional compressive deformation.

D_3 deformation and thrusting

During the D_3 event, F_3 folds were superimposed on polydeformed and locally mylonitic crystalline rocks under lower-amphibolite grade metamorphic conditions during formation of the Calaveras-Shoo Fly thrust (Table 2). In general, F_3 folds have shorter wavelengths and amplitudes than either F_1 or F_2 folds and recrystallization is incomplete and at a lower grade than during D_2. The effects of D_3 vary from km-scale zones of near total shearing and ductile transportation to zones of abundant F_3 folds cut by spaced, thin biotite-rich S_3 shears. In areas of

nonpenetrative D_3 deformation between thrusts and shears, study of the older D_1 and D_2 fabrics and non-sheared F_3 folds is possible.

F_3, S_1 outside the thrust zone. The style of F_3 folds varies not only as a function of lithology but also with proximity to the Calaveras-Shoo Fly thrust zone. With the exception of local D_3 shear zones, the degree of D_3 mylonitization and attendant transposition of older D_1 and D_2 metamorphic fabrics into parallelism with S_3 decreases away from the thrust zone (Plate 2). F_3 folds and the S_2 and S_1 fabric become progressively more obvious outside of the zones of intense D_3 deformation (Fig. 13).

Away from shear zones the F_3 folds are isoclinal to tight in profile and refold F_1 and F_2 isoclines and eye-folds, S_2 quartzose laminae, and S_2 foliation in augen gneiss. The axial surfaces of F_3 folds are marked by recrystallization of quartz, mica, and to a lesser extent feldspar. On F_3 fold limbs black shears 1 mm to 1 cm thick form anastomosing networks that locally surround ellipsoidal foliated rock bodies. The shears are locally and widely spaced and separate internally folded domains in outcrop (Plate. 2). Transposition of older metamorphic fabrics into parallelism with S_3 is common in the cores of megascopic F_3 folds and shearing is common along F_3 limbs (Fig. 14a).

In the Jupiter area (Fig. 5) northwest-trending tight to isoclinal F_3 folding has produced map-scale deformation of schist-quartzite unit contracts and deformation of augen gneiss (Fig. 7). The S_3 axial surfaces are regionally folded by an F_4 east-plunging antiformal structure north of the Standard pluton (Fig. 2). Planar and linear structural elements of the Shoo Fly in the Jupiter area are plotted on equal area nets in Fig. 15. S_1 and S_2 are plotted together because they are commonly co-planar. The poles to S_1+S_2 show a strong great-circle distribution due to the

combined effects of F_3 and younger folding. F_1 and F_2 hingelines are scattered but show a weak concentration toward the east.

Poles to S_3 are strongly concentrated in the southwest quadrant indicating that the S_3 foliation generally trends northwest and dips steeply toward the northeast (Fig. 15). The great-circle distribution of S_3 poles defines a statistical F_4 fold axis that agrees well with actual measured F_4 hingelines. Tight F_4 folding about N85°W-trending axial surfaces created the digitations of the Calaveras-Shoo Fly thrust (Plate 1, Fig. 5) and concentrated S_3 poles near the north and south edges of the net. F_3 hingelines are scattered about S75°E @ 42° due to near-coaxial F_4 folding and original divergent orientations of S_1 and S_2.

Mylonite and cataclasite outside the thrust zone. In the Jupiter area over 100 ductile faults geometrically related to the thrust have been mapped in the Shoo Fly Complex (Fig. 6). These faults range in thickness from 4 mm to about 16.5 m. Usually they are less than 10 cm thick but extend for great distances across stream channels. They form spaced zones (i.e. - 2 cm mylonite seams with 12 cm spacing), anastomosing networks of thick and thin seams, and exhibit identical textures with fault rocks from the Calaveras-Shoo Fly thrust zone.

Roughly 7 km east of the Calaveras-Shoo Fly thrust in Rose Creek (Fig. 5, 6) a 400 m wide ductile shear zone is marked by F_3 folding and the formation of mylonite, imbrication of lithologies, and marked elongation of imbricated slices parallel to F_3 hingelines. Locally, within the shear zone foliated augen gneiss occurs in a zone of shredded and folded calc-silicate with abundant floating F_3 hinges (Fig. 6 (R490)). Field localities can be found in Plate 3. Elsewhere, in Eagle Creek, a 14 cm thick mylonite surrounds an ellipsoidal block of foliated (S_2) augen gneiss which is deformed by F_4 (Figs. 14b, 16 (E553, R490)).

Near Tuolumne City on the Cottonwood Road (T.2N, R.16E, Sec. 28) a 2.5 m thick zone of finely granulated black protocataclasite cuts the S_2 foliation of the Shoo Fly Complex. Clasts within the zone range up to 0.3 m3 but 1-3 cm3 fragments are most common. The random fabric clasts account for > 75% of the zone and are angular with tabular to wispy outlines and a few are rounded (Fig. 1 7a) . Most of them are composed of biotite-muscovite-quartzite, mica schist, and phyllite, typical Shoo Fly lithologies. The matrix is a finely comminuted mixture of recrystallized micro crystalline quartz, mica, magnetite, and calcite. Incipient marginal granulation of the clasts, sinuous injection of matrix across and concentration of opaques along their boundaries and development of a weak flow-foliation are evident in thin section (Fig. 17b). It is suggested that the matrix is a crush microbreccia or the result of recrystallization of original pseudo tachylyte. Injections of matrix into the country rock thin from 3 cm to a feather edge. Such seams of D_3 protocataclastic matrix are folded by F_4 folds.

The Calaveras-Shoo Fly thrust. The Calaveras-Shoo Fly thrust separates rocks of contrasting lithology, structure, crystallinity, and age. Upper plate rocks of the Shoo Fly Complex record an older and more complex structural history than lower plate rocks of the Calaveras Complex to the west (Fig. 5). The regional parallelism of S_3 axial surface traces, D_3 ductile shear zones and the Calaveras-Shoo Fly thrust (Fig. 6) and truncation with ductile transposition of the pre-D_3 fabrics (S_1+S_2) (Fig. 7) forces the conclusion that D_3 in the Shoo Fly is related to development of the thrust.

In the Calaveras Complex a flattening foliation (S_1) with local mineral elongation formed axial planar to long-limbed isoclinal folds (F_1) in silicified chert-argillite parallel to the regional trace of the thrust. D_3 in the Shoo Fly, therefore, is coeval with the oldest (D_1) deformation in the Calaveras. All younger structures (D_4-D_7) crosscut the thrust and are developed in both

units. In the thrust zone differences in mechanical properties between rocks of the Shoo Fly and Calaveras Complexes resulted in the unique ductile fault textures described below. The contact between the Calaveras and Shoo Fly Complexes is a syn-metamorphic shear zone marked by stratigraphic, structural, and metamorphic truncation of the Shoo Fly Complex (Figs. 5, 8) and total mixing of Calaveras and Shoo Fly lithologies. The trace of the thrust (Plate 1, Fig. 5) is a formline that separates regions of >50% Calaveras from >50% Shoo Fly lithologies. Discrete slivers of both units have been found interlayered away from the thrust. The thrust zone is variable but averages about 1-2 km in thickness. Various lithologies of the Shoo Fly responded differently in zones of high strain and are discussed separately in a later section.

In the thrust zone and similar intra-Shoo Fly D_3 ductile shear zones (Fig. 6) intense shearing and contemporaneous domainal recrystallization parallel to the axial surfaces of F_3 folds to form a distinctive blastomylonitic fold-thrust fabric with abundant megascopic to microscopic ellipsoidal slivers and porphyroclasts. The S_3 thrust fabric has been traced for over 90 km from the Jupiter area to the southern terminus of the foothills metamorphic belt (Fig. 2) (Merguerian, 1981 ms, 1982).

In the Jupiter area (Fig. 4, Plate 1) the Calaveras-Shoo Fly thrust is exposed on the Middle Fork Stanislaus River (*), Stony Gulch (*), Knight Creek, Eagle Creek (*), Rose Creek (*), and at the confluence of Deer Creek with the South Fork Stanislaus River. The most accessible exposures (* above) are in the Stanislaus 7-1/2 minute quadrangle (T.3N, R.15E, Sec. 6, and 8) and the Columbia SE 7-1/2 minute quadrangle (T.3N, R.15E, Sec. 15, and 23). Detailed traverses across the Calaveras-Shoo Fly thrust in the Jupiter area indicate a remarkable consistency in the nature of structural features found along strike in the Jupiter area. Plate 4 shows the folded thrust surface, the orientations of S_2, S_3, S_4, and some younger structures. The

progressive transposition of S_2 toward the thrust and positions of tectonic slivers of Calaveras and Shoo Fly lithologies and foliated granitoid sills are indicated. The discussion that follows is an account of numerous transects illustrating the deformational style of the Calaveras-Shoo Fly thrust.

Middle Fork Stanislaus River. Between the Confluence "pluton", which consists of augen gneiss, and the Calaveras-Shoo Fly thrust (Plate 4), quartzites in the Shoo Fly are highly laminated and locally gneissic. Within the S_3 foliation refolded F_2 isoclines are common. The thrust zone is marked by mixed mylonitic quartzite and slivers of strongly-penciled silicified black argillite. There is a pronounced intercalation of Calaveras argillite parallel to the laminated mylonitic foliation (S_3) of the Shoo Fly quartzite (Fig. 18a). Disharmonic F_4 folds also deform the thrust fabric. S_4 is subparallel with all older fabrics in the area because of locally intense F_4 folding and forceful intrusion of the Knight Creek pluton (Plates 1, 4).

Unnamed creeks. The thrust is never encountered in the unnamed creeks near Stony Gulch (Plate 4) but D_3 blastomylonite and mylonite are developed up to 2 km from the trace. Counterclockwise rotation of S_4, S_3 and presumably S_1+S_2 is due to intrusion of the Knight Creek pluton (Fig. 5, Plates 1, 4). F_3 isoclinal folds with floating quartzitic hinges occur but pervasive shears along S_3 define the fault fabric (Plate 2). S_3 is marked by boudinage and transposition of D_2 quartz veins and the formation of a transposition foliation with syntectonic recrystallization of biotite and quartz. Centimeter-scale mylonitic layering and spaced seams of blastomylonite occur throughout the transect.

Pervasive shearing within individual outcrops creates ellipsoidal slivers of foliated quartzite and marble (up to 7 m long) flattened parallel to S_3 and elongate parallel to both hingelines of F_3 folds and L_3 stretching lineations developed in mylonitic sheaths which surround

them. A relict S_2 foliation within the slivers is folded by F_3 folds and recrystallized S_3 biotite and S_3 shears, formed within the axial regions of the F_3 folds, crosscut the sliver boundaries. The S_3 fabrics join and are continuous with the sheared margins of the slivers. Pods of augen gneiss are sheared and the S_2 foliation is truncated by D_3 blastomylonite. The gneiss contains a strong L_3 lineation.

Stony Gulch. Within 1 km of the thrust ductile transposition of layering and recrystallization of biotite and quartz are dominant. Local F_3 isoclinal and tight folds are preserved but synmetamorphic S_3 shearing along limbs and cores of F_3 folds is well-developed (Plates 2, 4). S_3 is marked by a penetrative mica foliation, spaced ductile shears, quartz veins up to 0.5 m thick, and seams of mylonite and blastomylonite. F_3 folds of diopside-tremolite calc-silicate rock (Fig. 13b), imbrication of lithologies (Fig. 19a, b), pseudotachylyte(?), and foliated granite sills are found nearer the thrust. On a road 50 m north of Stony Gulch interleaved black siliceous argillite of the Calaveras and Shoo Fly quartzite are highly flattened and strongly lineated.

Knight Creek. D_3 blastomylonite occurs up to 3.5 km away from the thrust in Knight Creek although it is domainal and not penetrative at this distance. Within 2 km of the thrust total transposition and development of the thrust fabric is found (Plates 2, 4). Long-limbed intrafolial F_3 isoclines, rootless folds, and reclined folds with sheared-out limbs create a highly imbricated, composite S_3 fabric in the rocks. Low-angle (10°-30°) truncation of S_3 by thin shears is locally found thus suggesting multiple displacements during D_3. The S_3 foliation is marked by recrystallized mica, spaced blastomylonite shears, and mylonitic layering. Foliated meter-scale slivers of quartzite in a black argillite matrix are flattened into S_3 with elongation parallel to F_3 hingelines and L_3 stretching lineation s. Silicified and highly flattened chert-argillite of the

Calaveras is interlayered with foliated dark-gray quartzite at the thrust. A 30 m thick sliver of Calaveras argillite occurs 1 km east of the thrust and is strongly folded by F_4 (Plate 4).

Eagle Creek. Within 750 m of the thrust, rootless isoclinal F_3 folds with stretching lineations parallel to F_3 hingelines occur. F_3 isoclinal folds are developed outside of the thrust zone (Plate 2). The S_3 foliation is marked by recrystallization of mica, spaced ductile shears, abundant quartz veins, and flattened and recrystallized mineral aggregates. Toward the thrust the density and thickness of D_3 shear zones increase until the country rock becomes subordinate. Alternating 1-10 m wide zones of complete and incomplete shearing and transposition grading into zones of blastomylonite typify the transect.

Within 100 m of the thrust, S_3 encloses 0.5 m ellipsoidal masses of quartzofeldspathic gneiss containing S_2. Tight F_3 folds with sheared limbs occur within the slivers and have S_3 axial surfaces parallel to the plane of maximum flattening; elongation lineations formed within the sliver margins are parallel to F_3. Within the slivers biotite is recrystallized in the axial surfaces of F_3 folds and a biotite fabric can be traced continuously into the S_3 blastomylonite that surrounds the slivers. In the Shoo Fly synmetamorphic flow of schistose blastomylonite around quartzite, tectonic slivers of Calaveras argillite 0.5 km and 1.6 km from the thrust and late syntectonic foliated granitic sills occur (Plate 4). Local 5 cm by 1 cm pods of foliated granitoids occur parallel to the S_3 fabric and are elongate parallel to F_3. Ellipsoidal Shoo Fly slivers occur 0.5 km west of the thrust.

At the thrust, mixing of Shoo Fly quartzite, quartzofeldspathic gneiss, and phyllite with Calaveras argillite, flowage of argillite around coherent blocks of foliated quartzite, "rolled" quartzite blocks (l.0 m^3) argillite, D_3 quartz veins, silicification and strong L_1 (equivalent to L_3 in the Shoo Fly) penciling in the Calaveras are observed.

Rose Creek. On Rose Creek 1.6 km east of the thrust, shearing along the limbs of F_3 folds marks the beginning of penetrative D_3 deformation. Approaching the thrust zone, F_3 folds change from asymmetric tight folds to isoclinal folds (Plate 2). Shearing along the axial surfaces and limbs of F_3 folds creates a transposed S_3 fabric that appears shredded in outcrop.

The blastomylonitic S_3 foliation becomes dominant within 800 m of the thrust and encloses ellipsoidal slivers up to 20 m in length which are flattened parallel to S_3. The slivers are elongated parallel to L_3 in the bounding mylonite and blastomylonite. Branching veins of pseudotachylyte (Fig. 20) from 1 cm to 1 mm thick crosscut and disrupt the S_3 mylonitic layering near the Star Mine. Elsewhere ultramylonite seams, mylonite (Fig. 21 a) and foliated late syn-tectonic granitic sills occur (Plate 4). The sills range from 0.7-1 m in thickness with small foliated lenses of mica-quartzite strung out into parallelism with S_3 at the sill margins. An incipient biotite foliation in the sills can be traced into S_3 of the country rock but in detail low angle truncation of the S_3 blastomylonitic thrust fabric occurs at sill margins, indicating the sills are late syntectonic with respect to D_3. At the thrust, seams of fine-grained Calaveras argillite were injected across the margins of ellipsoidal slivers of Shoo Fly quartzite and along the axial surfaces of biotite-lined F_3 folds within them (Fig. 21 b). In addition, foliated quartzite and black argillite are interlayered on centimeter scale. Calaveras argillite is extensively veined with quartz and silicified.

Confluence of Deer Creek and South Fork Stanislaus River. D_3 ductile transposition is well-developed within 1.3 km of the thrust on both Deer Creek and the South Fork Stanislaus River. S_3 shearing along F_3 axial surfaces becomes progressively more intense as the thrust is approached (Plate 2). Near the thrust S_2 is cut by S_3 surfaces varying from spaced shears (Fig. 16) to highly recrystallized thinly-layered zones of blastomylonite (Fig. 18b), highly laminated

mylonite (Fig. 22), and 3 cm seams of ultramylonite. Late syntectonic granitic sills (Plate 4) are locally injected into the axial regions of F_3 folds.

Within 450 m of the thrust large-scale synmetamorphic imbrication results in quartzose flaser gneiss. Angular 1.0 m masses of quartzite are surrounded by massive bluish chert and argillite of the Calaveras and 3 m ellipsoidal blocks of silicified black argillite and flattened chert are surrounded by foliated quartzite. The Shoo Fly quartzite is locally cut by anastomosing seams of black argillite parallel to S_3. Slices of Calaveras argillite vary from 1-100 m thick but average about 5 m. They are complexly intercalated with Shoo Fly quartzite. Biotitic S_3 shears in the quartzite are parallel to the S_1 flattening foliation in the slices of Calaveras. The high degree of imbrication of Shoo Fly and Calaveras rock bodies along the thrust in this transect is quite possibly typical of the thrust contact. Nearly 100% exposure in the vicinity of the confluence offers control not realized elsewhere.

Petrography of the D_3 thrust fabric

Microscopic examination of Shoo Fly D_3 tectonics reveals microscale analogs of the mesoscopic features described above. Microstructural features in the Shoo Fly are described separately for each lithology.

Quartzite and quartzofeldspathic gneiss. The quartzose mylonites are typically dense, glassy, highly-laminated and flattened with a sugary texture on broken surfaces and exhibit a marked reduction in grain size compared to granoblastic rocks of the unit found elsewhere. The formation of blastomylonite-sheathed ellipsoidal porphyroclasts is characteristic of the thrust zone.

The porphyroclasts are composed of quartz, feldspar, or quartzofeldspathic aggregates. The highly strained quartz porphyroclasts were annealed into polygonized lenticles ranging from

0.07 mm - 2 mm thick with internally sutured grain boundaries. The quartz augen are bounded by microcrystalline films of biotite, muscovite, calcite and opaque minerals which are continuous or end in numerous splays. The quartz augen commonly have finer-grained tails and imbricated rinds recrystallized into sub-grains. They are cut by small oriented (S_3) crystals of biotite and muscovite and contain folia (S_2) of mica (Fig. 23a). Ribboned quartz from 0.1 mm to 3 cm locally cut porphyroclasts. In laminated mylonitic rocks (Figs. 21, 22), highly-strained and polygonized quartz-rich layers are separated by coarse mica folia. Adjacent quartz layers in various stages of strain-induced recrystallization show abrupt grain-size variations (Fig. 23b) that together with the bounding micas define S_3.

Quartzofeldspathic rocks contain angular- to rounded porphyroclasts of plagioclase and orthoclase ranging from 0.1-2 mm. They show bent twins, bodily rotation, filled cracks, edge-granulation, corrosion and replacement by quartz and muscovite (Fig. 23 c). Large quartz and feldspar augen commonly preserve the S_2 foliation at a high angle to S_3 in the form of oriented micas or opaque minerals (Fig. 23d). The elliptical quartzofeldspathic aggregates show many of the same features as the quartz and feldspar porphyroclasts.

Augen gneiss. The deformational textures of the augen gneisses are treated in Chapter 2 but are described briefly below. The dominant metamorphic fabrics in the gneiss are mylonitic and include S_2 and S_3. In regions of high strain, relict igneous textures are obliterated with the formation of a blastomylonitic S_3 foliation composed of finely recrystallized quartz, feldspar, mica, hastingsite, and stilpnomelane. The S_3 foliation anastomoses about 1-3 mm (avg.) porphyroclasts of feldspar and domains of less-deformed rock. Feldspar augen usually are cracked, have bent twins and show marginal granulation, in contrast to quartz which is flattened

and recrystallized into strained polygonized flasers with highly-undulose cores. In D_3 ductile shear zones augen are rare due to extensive grain-size reduction.

Schist. In regions of high strain the schistose rocks take on a phyllitic sheen due to a reduction of grain size during mica recrystallization. Typically they are foliated and highly-laminated with quartzose ribbons from 2 mm-1 cm thick. Phyllonitic textures occur (Fig. 24a) with large S_2 micas progressively rotated and sheared. Locally, optically continuous S_2 mica augen are strongly recrystallized (Fig. 24b). Deformation of mica results in frayed edges, intracrystalline glide planes, and anastomosing folia of smaller recrystallized flakes defining S_3. Layer parallel shear and imbrication parallel to S_3 created porphyroclasts and lenticular domains of quartz, feldspar, and mica (Fig. 24c). Vestiges of S_2 and S_1 metamorphic fabrics are locally preserved within the porphyroclasts. Strongly laminated schists have a pin striped appearance due to the alternation of penetration micaceous folia with lenticular, flattened quartz grains or ribbons (Fig. 24d). Dark quartz segregations (meta-chert?) become highly flattened and recrystallized.

Calc-silicate and marble. In regions of high strain the calc-silicate rocks are highly flattened and often appear as isoclinally folded wisps or rootless folds when interlayered with more competent quartzose units. Extremely disharmonic folding is common due to ductility contrasts between adjacent rock bodies, rolled shear-bounded ellipsoidal structures develop up to 10 m in length. Calc-silicate rocks are highly recrystallized with reduction in grain size compared to similar rocks outside of ductile shear zones. Large augen of tremolite and diopside are bent with ragged edges and locally retrograded to chlorite (Fig. 25 a). The S_3 foliation, composed of smaller oriented tremolite needles, anastomoses around the augen (Fig. 25b). The augen were evidently formed during an earlier metamorphic episode coincident with D_2. The

texture suggests similar but slightly lower grade metamorphic conditions during D_3. The marble deformed by ductile flow and pervasive recrystallization. Within calcite and dolomite marble, calcite and dolomite crystals are typically flattened with deformed twin lamellae.

Summary and significance of D_3 deformation

In the southern third of the Sierra Nevada metamorphic belt D_3 was a regionally important deformational event that affected both the Shoo Fly and Calaveras Complexes. D_3 was markedly inhomogeneous thus generating a great variety of structural features in the Shoo Fly (Table 3).

F_3 folds are well-developed in the Jupiter area and persist to the south part of the metamorphic belt (Fig. 2). They vary from isoclinal to tight folds, commonly with limbs sheared parallel to the S_3 axial surface. D_3 folding, shearing, and recrystallization of foliated meta-sedimentary and metaigneous rocks was coeval with the development of mylonite. Near the Calaveras-Shoo Fly thrust and D_3 shear zones (Fig. 6) the F_3 folds are somewhat less obvious with domains of sheared F_3 folds and mylonite grading into one another. L_3 stretching lineations formed within the S_3 foliation are invariably parallel to F_3 hingelines which plunge down-dip to the east-southeast (Fig. 15).

Ellipsoidal slivers of foliated Shoo Fly rocks are internally folded (F_3) and sheared (S_3) and sheathed by strongly lineated (L_3) mylonite and blastomylonite. The slivers are elongate parallel to F_3 and L_3 and flattened parallel to S_3. The slivers may be examples of mega-augen of strain-hardened rock (foliated Shoo Fly) with their rounded shapes due to tectonic rotation and progressive encroachment of blastomylonitic shears.

Megascopic to microscopic syn-metamorphic intercalation of Shoo Fly and Calaveras rock units occurs throughout the thrust zone. The rocks develop a flinty aspect and a general

darkening of color due to extensive silicification and grain size reduction. In the thrust zone, the older pre-thrust fabrics in the Shoo Fly are difficult to recognize because they are highly flattened into parallelism with S_3, and strongly recrystallized.

Interpretation of the Calaveras-Shoo Fly thrust. The intensity of D_3 structures and spatial coincidence of mylonite at the Calaveras-Shoo Fly contact plus the regional parallelism of F_3 axial surfaces (Figs. 5, 6) indicate that high strains developed at this boundary during D_3 time. Metamorphic recrystallization during D_3 indicate that the contact formed at moderate crustal depths. In the metasedimentary rocks of the Shoo Fly, syn-kinematic growth of biotite and muscovite parallel to S_3 and recrystallization of quartz (± ribboning parallel to L_3), feldspar, and calc-silicate minerals characterize the D_3 fabric. In the orthogneisses recrystallization of biotite, quartz, feldspar, epidote, and amphibole occur. These coexisting mineral assemblages define the epidote-amphibolite facies of Turner (1968) which correspond to temperatures of 400°-600°C and depths of 15-25 km.

As discussed earlier, the microscope shows a marked ductile vs. brittle mechanical contrast between quartz and mica vs. feldspar during the D_3 event. Such textures correspond to behavior of crustal rocks at the ductile-brittle transition experimentally determined by Tullis and Yund (1977) and Carter and others (1981) at depths of 10-15 km and temperatures of 350°-500°C. These estimates compare well with the P-T conditions defined by the epidote-amphibolite facies.

The east-dipping Calaveras-Shoo Fly thrust is a broad zone of structural discordance in that the Shoo Fly contains two phases of deformation (D_1+D_2) and an intervening intrusive event that are not present in the Calaveras. The complexes record disparate structural histories that coincided during D_3 and younger events. Near the Shoo Fly contact the Calaveras was highly

silicified, imbricated and flattened during D_3 with the formation of long-limbed isoclinal folds of compositional layering (typically bedding). Boudinage of granitic sills parallel to S_1 in the Calaveras (equivalent to S_3 in the Shoo Fly) indicates that the Calaveras was lithified before thrusting (Schweickert, pers. comm., 1983). Dewatering and compaction of the Calaveras preceded or accompanied D_3 juxtaposition with the Shoo Fly because hard rock shearing of the Shoo Fly could not have taken place if the Calaveras were unlithified and lacked sufficient shear strength. The ductility contrast between polydeformed quartzitic rocks of the Shoo Fly and chert-argillite of the Calaveras evidently resulted in the ductile fault textures described above.

The contrast in age and the high-angle truncation of lithology and D_1+D_2 fabrics in the Shoo Fly (Plate 1) suggest that the boundary is a ductile shear zone that juxtaposed deformed psammitic and plutonic rocks of the upper-plate Shoo Fly with lower-plate Calaveras chert-argillite at moderate crustal depths. The fact that older rocks of the upper plate Shoo Fly occur physically above younger rocks of the Calaveras and that L_3 and F_3 lineations and hingelines plunge down the dip of S_3 support the hypothesis that the Calaveras-Shoo Fly contact is a thrust fault and not a strike-slip boundary. The ellipsoidal slivers, which are unique to the Shoo Fly Complex, are also oriented with their long dimensions parallel to F_3. The lineations are here collectively interpreted, in concert with a thrust hypothesis, to indicate a relative D_3 tectonic transport direction up-dip along the Calaveras-Shoo Fly thrust. The intense D_3 fabrics formed in the vicinity of the thrust are identical to mylonitic rocks described from ductile shear zones of deep-seated orogenic belts found in central Australia (Bell and Etheridge, 1976), eastern Pyrenees (Carreras and others, 1980), northwestern Scotland (Christie, 1960; Sibson, 1980; White and others, 1980), eastern Connecticut (Dixon, 1968), southern Appalachians (Mitra, 1978), Morocco (Pique, Jeannette, and Michard, 1980), South Island, New Zealand (Reed,

1964), and Wyoming (Weathers and others, 1979). The literature on ductile shear zones shows that such zones typically experience geometrically varied, complex movement histories.

In addition to the ductile fabrics in the Shoo Fly described earlier, some relatively brittle fabrics formed during the late stages of D_3 deformation. Locally, thin seams of cataclasite crosscut S_3 and zones of D_3 mylonite at acute angles from 10°-15°. Post-S_3 injections of pseudotachylyte and protocataclasite occur. Furthermore, a minor, non-penetrative fold phase crenulates the S_3 foliation but is deformed by D_4 and younger structures. Late-syntectonic granitoid sills and bleb-like injections are typically found in zones of high strain and may represent partial melts derived at depth from shear heating. Local openings of the forming S_3 foliation during dike injection may record a crustal transition to lower confining pressures. Textural evidence indicates that oriented S_3 biotite is rimmed by retrograde chlorite (Fig. 26 a). The chloritized S_3 biotite foliation is crenulated by F_4 folds and cut by newly recrystallized S_4 biotite and garnet porphyroblasts.

Field and petrographic data indicate that juxtaposition of the Shoo Fly and Calaveras Complexes took place under variable P-T conditions fostered by prolonged relative motion. The presence of post-S_3 but pre-D_4 cataclastic fabrics, minor folds, and retrograde chlorite metamorphism indicates protracted translation of the upper plate Shoo Fly Complex along the Calaveras-Shoo Fly thrust to progressively higher crustal levels during the waning stages of D_3. It is unknown whether displacement between the Shoo Fly and Calaveras Complexes occurred as discrete multiple episodes or as a continuum.

The absolute age and longevity of the thrusting is unknown but the thrust is deformed by east-west-trending folds (F_4 in the Shoo Fly; F_2 in the Calaveras) and these are regionally truncated by the 164-170 m.y. Standard pluton (Schweickert, 1981; Sharp and Saleeby, 1979;

Stern and others, 1981) which engulfs the thrust (Figs. 2, 5, 7). Clearly this sets a pre-middle Jurassic age for development of the thrust. The broad spectrum of D_3 deformational styles encountered in the Jupiter area evidently reflects the complex inhomogeneous response of polylithologic, deformed (D_1+D_2) basement rocks of the Shoo Fly Complex during thrusting. The juxtaposition of polydeformed quartzitic and plutonic rocks of the Shoo Fly with younger, less deformed oceanic rocks (Calaveras), along a zone of ductile shear deformation, suggests that it represents a deep-seated plate boundary between continental basement rocks and accreted oceanic sediments.

Post-D_3 deformation

D_4. The Calaveras-Shoo Fly thrust (Figs. 5, 8), and related and older fabrics are deformed by a regionally important folding episode representing F_4 in the Shoo Fly and F_2 in the Calaveras. F_4 folds are typically tight or asymmetric crenulate folds although local isoclinal folds with a biotite rich axial-planar foliation are found (Fig. 27). F_4 folds are especially well-developed in rocks with a strong S_3 lamination and because S_3 is less well-developed east of the thrust, F_4 folds have a less obvious effect on map relations to the east (Plate 1 , Figs. 5, 8).

S_4 is also marked by a spaced biotite±muscovite±quartz schistosity or by a crenulation cleavage. Large oriented porphyroblasts of biotite and local subhedral garnet poikiloblastically overgrow the S_3 foliation in the Shoo Fly and create a spaced S_4 biotite schistosity which can be traced into the axial surfaces of F_4 folds. The intensity of the spaced S_4 schistosity increases dramatically near F_4 hinges where strong overprinting is observed. In quartzitic rocks S_4 is a spaced silicified slip cleavage. Refraction of S_4 across sills of orthogneiss and ellipsoidal slivers also occurs. The F_4 folds plunge statistically 47° into S85°E with N85°W, 90° axial surfaces (Fig. 15). They regulate the distribution of poles to S_1, S_2 and S_3 and, due to their near coaxial

orientation, conically deform the F_3 hingelines and L_3 lineations. The relative lack of north-south-trending, east-dipping S_3 f oliations may reflect a sampling error, but probably also reflects the tight regional style of F_4.

D_5 and D_6. Two related generations of open, asymmetric crenulate folds with variable plunge and weakly developed axial surface cleavage (S_5, S_6) warp S_4 and older fabrics. These structures, recognized along the length of the foothills metamorphic belt are of Late Jurassic age and are probably correlative with penetrative cleavages in all rocks west of the Calaveras (Fig. 1) (Schweickert and others, 1984).

S_5 and S_6 are spaced black residue cleavages composed of fine grained chlorite, quartz, and opaque minerals but locally brittle fractures are developed. Subhedral D_4 garnet porphyroblasts are locally cracked and replaced by chlorite. Chlorite also locally replaces "D_4" and older micas. Within the study area, S_6 is more strongly developed than S_5 which is omitted in figure 8 because it barely affects the map pattern (Plate 1 , Fig. 5). S_5 and S_6 may be conjugate cleavages.

Poles to S_5 (Fig. 15) show some scatter but average about N32°W, 780NE. Poles to S_6 are clustered about N30°E, 90°. The F_5 folds and cleavage deform and crosscut the post-S_4 mafic dikes and the Knight Creek and Basin Creek plutons (Fig. 2). F_6 folds warp the trace of the Calaveras-Shoo Fly thrust and the Sonora Fault (Figs. 1, 2) and brittle fractures parallel to S_6 regionally control the trellised drainage described earlier.

D_7. A very late, sporadically developed spaced brittle cleavage (S_7) that trends N65°W to E-W, is axial planar to broad, open F_7 folds. Although of similar orientation to S_4, S_7 can usually be distinguished from S_4 in that little or no recrystallization occurred along the S_7 cleavage, with the exception of quartz recrystallization and incipient retrograde metamorphic effects such as

chlorite replacing biotite. In contrast, S_4 is commonly marked by well-developed spaced biotite schistosity.

Summary of deformational and metamorphic features. Detailed mapping in the Jupiter area has delineated a complex structural and metamorphic history for the Paleozoic basement rocks (Table 2). Figure 28 summarizes the contrast in geologic history between the Shoo Fly and Calaveras Complexes and indicates the regional relationship of structural and igneous events. The Shoo Fly Complex bears evidence for two phases of deformation (D_1, D_2) and an intervening plutonic episode that predate juxtaposition with the Calaveras. However, beginning with the formation of the D_3 Calaveras-Shoo Fly thrust, later regional structures are superimposed upon both complexes. The Calaveras-Shoo Fly thrust and related structures were folded by east-west-trending F_4 folds (Calaveras F_2) and subsequently in the middle Jurassic time by the Standard pluton and the Sonora mafic dike swarm. S_5 and S_6 cleavage (Calaveras S_3 and S_4) deforms S_4 and older fabrics and the mafic dikes. The late S_7 cleavage is not shown due to its sporadic nature.

Structural and textural evidence indicates that the Shoo Fly Complex experienced many medium to low grade P-T conditions during its evolution. The initial phases of isoclinal folding, shearing, and regional metamorphism during D_1 and D_2 indicate that the Shoo Fly was a complexly folded and recrystallized basement terrane prior to juxtaposition with the Calaveras. The lower amphibolite grade peak of regional metamorphism during D_2 was followed by a similar metamorphic pulse during the main phase of D_3 deformation. By the waning stages of D_3, however the Shoo Fly was elevated to higher crustal levels where chlorite retrograde metamorphism, cataclastic textures, and minor folds developed.

Metamorphic recrystallization of biotite and garnet during D_4 indicate that F_4 folding took place under higher temperatures and possibly at greater depths than D_3. The lack of penetrative structural fabrics and retrograde metamorphism during D_5 through D_7 defines a post-D_4 Shoo Fly history at progressively higher crustal levels. The regional correlation of these structures are discussed below.

DISCUSSION

The deformational events that affected the Shoo Fly Complex can be related to three recognized orogenic pulses that have occurred within the SW Cordillera (Table 2) but the earliest event (D_1) may have no recognized counterpart in the region. The absolute ages of the various deformational events are not well constrained but certain limits can be placed on their timing due to dating of crosscutting igneous rocks and comparative structural studies across the strike of the metamorphic belt near lat. 38°N by Schweickert and others (1984).

Age constraints and correlation of deformational episodes. The first deformational episode to have affected the south part of the Shoo Fly Complex (Fig. 2; Table 2) involved F_1 folding, shearing, and development of an S_1 mica foliation. In Tuolumne County the S_1 fabric is cut by discordant orthogneiss bodies which yield U-Pb emplacement ages clustered at 450 and 275 m.y.a. (Sharp and others, 1982, in press). If the Siluro-Ordovician age reported is valid, D_1 would represent a preSilurian deformational event not recognized elsewhere in the SW Cordillera and could argue for an enigmatic extra-Cordilleran origin for the Shoo Fly. Preliminary Rb-Sr data by H.K. Brueckner (pers. comm., 1983) suggests a 363 m.y. emplacement age for the gneisses which conservatively suggests that D_1 occurred before latest Devonian time.

Structural and textural data presented here indicates that the D_2 event involved isoclinal folding and local mylonitization under lower amphibolite grade conditions. The timing of the D_2 event is poorly constrained but because the S_2 fabric is well-developed in the orthogneisses of the Jupiter area and D_2 predates the earliest regional deformation (D_3) to affect the late Paleozoic-early Mesozoic Calaveras, it can be bracketed between Siluro-Ordovician and Permo-Carboniferous time. Given the uncertainties, D_2 and possibly D_1, may be correlative with the Antler orogeny of Late Devonian to Early Mississippian age which marks an episode of continentward thrusting of eugeosynclinal rocks now found structurally above the Lower Paleozoic Cordilleran miogeosyncline (Roberts and others, 1958).

The D_3 event involved shearing and folding of upper and lower plate rocks during formation of the Calaveras-Shoo Fly thrust. D_2 and D_3 in the Jupiter area are not interpreted as progressive events due to the near-orthogonal truncation of the Shoo Fly S_2+S_1 axial surfaces against the thrust (Fig. 7). Since D_3 is the initial deformation to have affected the Calaveras Complex and the 164-170 m.y. Standard pluton (Sharp and Saleeby, 1979; Stern and others, 1.981) intrudes across the thrust (Figs. 2, 5), D_3 must have occurred between Permo-Carboniferous and middle Jurassic time. It probably correlates with the Late Permian to Early Triassic Sonoma orogeny which is recognized as another episode of continentward thrusting of oceanic rocks, this time structurally above the Antler allochthons.

The S_4 spaced schistosity and cleavage have been reoriented by forceful intrusion of the Knight Creek and Standard plutons (Fig. 8) and are cut by mafic dikes of the Sonora dike swarm. The middle Jurassic cooling age for the Standard pluton and 157-159 m.y. K/Ar hornblende dates on the mafic dikes (Sharp, 1980) together mandate a pre-middle Jurassic age for D_4. A 215±10 m.y. (Late Triassic) metamorphic reheating event affected the orthogneisses of

Tuolumne County (Sharp and others, in press). This reheating episode may be due to D_4 because it was the last regional episode of recrystallization before local contact metamorphism noted in the vicinity of the Standard pluton. Alternatively, the Late Triassic thermal event may be an anomalous hybrid age due to the clearly complex nature of regional deformation, metamorphism, and plutonism in the Jupiter area. A Late Triassic age for D_4 would clearly strengthen the correlation of D_3 with the Sonoma orogeny as suggested above.

During D_5 and D_6 northwest (S_5) and northeast (S_6) trending folds and cleavage were superimposed on middle Jurassic plutons, mafic dikes, and older regional structural fabrics in the Shoo Fly Complex (Fig. 8). Comparative structural studies across the foothills metamorphic belt by Merguerian and others (1983) indicate that S_5 and S_6 are of Late Jurassic age and formed synchronously with structural fabrics of identical orientation and similar metamorphic grade west of the Sonora fault during the Nevadan orogeny. The Nevadan orogeny was an abrupt collisional episode that occurred 153-158 m.y.a. when Jurassic volcanic and sedimentary rocks of island-arc affinity were juxtaposed with the Calaveras and Shoo Fly Complexes along the Melones-Sonora fault zone (Schweickert and others, 1983). Intriguingly, the Nevadan structures are penetrative in the Jurassic rocks to the west of the Sonora fault yet in the Paleozoic rocks to the east Nevadan S_5 and S_6 structures are weakly formed and involve retrograde metamorphism (chloritization) of S_4 and older fabric elements. The contrast in structural style during the Nevadan orogeny is probably due to strain hardening of the Paleozoic terranes during pre-Nevadan tectonism (Schweickert and others, 1984).

The youngest and least penetrative of all structures mapped in the Shoo Fly Complex are similar in orientation and style to structures developed in Jurassic and Lower Cretaceous metavolcanic rocks in roof pendants to the east which are cut by Upper Cretaceous plutons

(Nokleberg and Kistler, 1980; Tobisch and Fiske, 1976, 1982). S_7 may be correlative with these structures and therefore be of early Late Cretaceous age.

Correlation with the northern Sierra Shoo Fly Complex. In the northern Sierra Nevada the Shoo Fly Complex consists of at least four lithologically distinct, east-dipping thrust-bound segments (Girty and Schweickert, 1985a). The eastern and structurally highest unit is a melange consisting of sheared shale and sandstone with blocks of chert, limestone, gabbro, volcanic rock, and serpentinite (Schweickert, 1974, 1981; Bond and Schweickert, 1981). Underlying the melange unit, the Culbertson Lake allochthon (Girty and Schweickert, 1985a) consists of subarkosic to quartzose sandstone, shale, and chert, with subordinate volcanic rock, limestone, and conglomerate (D'Allura and others, 1977; Girty and Schweickert, 1979, 1985a). These units are tectonically underlain by another unit composed of chert and shale which is, in turn, underlain by a quartzose sandstone, phyllite, and marble unit.

The pre-metamorphic lithologies of the Shoo Fly Complex from the southern Sierra Nevada (Table 1) probably consisted of sub-feldspathic quartzose sandstone with subordinate shale, chert, diverse calcareous rocks, and rare mafic volcanic rocks. Table 4 compares the interpretive Shoo Fly protoliths of table 1 with published stratigraphic data from the entire outcrop belt of the Shoo Fly Complex (Fig. 1). The similarities in lithologic types and their relative abundance, as well as small scale stratigraphic features argue convincingly for a direct correlation between lower Paleozoic rocks of Tuolumne and Mariposa Counties (this report) and the "type" Shoo Fly in the northern Sierra as first suggested by Schweickert (1977). In addition, the southern Sierra Shoo Fly Complex is lithically most similar to quartzose sandstone phyllite, and marble of the structurally lowest unit to the north.

The Shoo Fly Complex is of unknown thickness partly due to structural complexity. Its base is nowhere exposed but sedimentologic and geochemical data from the northern part of the belt by Bond and Devay (1980) and Girty and Schweickert (1985a, b) indicate that the structurally highest eastern units were deposited on oceanic crust. The lower sandstone unit was deposited within a prograding sub-sea fan complex probably derived for a continental block and/or from a recycled orogenic provenance. Recent U/Pb data on detrital zircon from Shoo Fly sandstone in the Culbertson Lake allochthon (G.H. Girty, pers. comm., 1983) indicates a 2.08 b.y. provenance age which is consistent with derivation from the Salmon River (Lemhi) Arch in east-central Idaho as suggested by Bond and Devay (1980) and Schweickert and Snyder (1981). D'Allura and others (1977) and Schweickert (1974) suggested that the northern Sierra Shoo Fly represents a deformed outer continental margin sequence. Stratigraphic and structural evidence presented in this report (Tables 2, 4) are consistent with the concept that the Shoo Fly was deposited adjacent to North America in late Precambrian(?) to lower Paleozoic time.

The Sr^{87}/Sr^{86} 0.706 line of Kistler and Peterman (1973, 1978) isotopically defines the inferred westward limit of buried Precambrian crust in the SW Cordillera (Fig. 29). The 0.706 line, therefore, delimits the inferred lower Paleozoic shelf edge of western North America. Sharp and others (1982, in press) report an initial Sr^{87}/Sr^{86} ratio of 0.709±.001 from the Confluence augen gneiss body (Fig. 5) and report a 1.9 b.y. inherited Pb component in augen gneiss elsewhere in the Jupiter area. The 1.9 b.y. Pb component in the augen gneiss of the Shoo Fly of Tuolumne County may be due to passage through and assimilation of Proterozoic zircon from sediments of the Shoo Fly thus strengthening correlation with "type" Shoo Fly rocks of the northern Sierra Nevada. The Sr^{87}/Sr^{86} data might record complicated isotopic mixing between

the Shoo Fly and orthogneiss protoliths or, alternatively, be due to the presence of continental or quasi-continental crust beneath the southern Sierra Shoo Fly Complex.

Regional correlation. Although structurally imbricated in the north and highly deformed and metamorphosed in the south, the structurally lowest lithologic unit of the Shoo Fly is remarkably continuous for over 330 km making it the most extensive terrane of lower Paleozoic metamorphic rock in the SW Cordillera (Fig. 29). The Shoo Fly Complex seems similar to and may be correlative with deformed lower Paleozoic rocks of the Central Metamorphic Belt of the Klamath mountains (Fig. 29) (cf - Cashman, 1980; Churkin and Langenheim, 1960; Churkin and Eberlein, 1977; Irwin, 1966, 1981; and Lanphere and Irwin, 1965) and possibly the Lardeau Group and Hamill-Badshot sequence south of the Selkirk and Purcell mountains in the Kootenay arc of the SE British Columbia (Reesor and Moore, 1971). The sedimentologic studies of Bond and Devay (1980) and Girty and Schweickert (1985c) independently provide direct comparison between parts of the northern Sierra Nevada Shoo Fly Complex with units in the Roberts Mountains allochton of east-central Nevada (Fig. 29).

As suggested by Schweickert (1981), other rocks possibly correlative with the Shoo Fly occur in the eastern Sierra Nevada in roof pendants such as Saddlebag Lake (Brook, 1977; Seitz, 1983), and Mount Morrison in the John Muir wilderness area (duBray, 1981; Morgan and Rankin, 1972; Rinehart and Ross, 1964; and Russell and Nokleberg, 1977). Other possibly correlative rocks occur in the Mokelumne Wilderness Area (McKee and Howe, 1981), on Dunderberg Peak in the Hoover Wilderness Area (Keith and Seitz, 1981), in the Mount Raymond roadless area (Huber, 1982), in the Tick-Tac-Toe pendant (Bateman and others, 1982), and in the Dinkey Creek pendant (Dodge, 1982) (Fig. 29).

Tectonic significance of the Calaveras-Shoo Fly thrust. North of lat. 39°N, the Shoo Fly is unconformably overlain to the east by a thick sequence of Late Devonian volcanic arc rocks (McMath, 1966). Similar rocks also occur in the southeast Klamath mountains and in northwestern Nevada (Fig. 29). According to Schweickert and Cowan (1975) and Schweickert and Snyder (1981), the Shoo Fly forms the basement to an arc which sutured to North America during the Permo-Triassic Sonoma orogeny. Schweickert and Merguerian (in press) suggest that the Calaveras-Shoo Fly thrust marks a deep-seated dislocation between the arc massif (Shoo Fly) and the upper Paleozoic to lower Mesozoic(?) subduction complex (Calaveras) that was thrust beneath it. Alternatively, as suggested by Saleeby (1981) the thrust may mark a former late Triassic to early Jurassic subduction boundary between North American basement rocks (Shoo Fly) and accreted oceanic rocks (Calaveras). Both of these tectonic scenarios are possible given the expanse of available age control on the timing of D_3.

CONCLUSIONS

The Shoo Fly Complex is a significant tectonostratigraphic element in the metamorphic belt of the western Sierra Nevada. This report describes and documents an elaborate structural sequence for the southern Sierra Shoo Fly Complex which is lithologically correlative with areally extensive lower Paleozoic oceanic rocks deposited near the North American continental margin. In the central and southern Sierra, the Shoo Fly Complex consists of quartzite and quartzofeldspathic gneiss, schist, subordinate calc-silicate rocks and marble, and rare amphibolite. The Shoo Fly has experienced a total of seven superposed deformational events throughout its evolution. The first four of these involved tight to isoclinal folding and local shearing under variable medium grade metamorphic conditions. The last three are characterized by open folding

and low grade metamorphic recrystallization. During the D_3 event, juxtaposition of the Shoo Fly and Calaveras Complexes took place along the Calaveras-Shoo Fly thrust. Formation of the thrust at depths of 10-15 km developed a 2 km wide zone of intense localized folding, imbricated lithologies, and mylonite. Local overprinting of the ductile D_3 fabrics by pre-D_4 cataclastic fabrics suggests protracted motion along the Calaveras-Shoo Fly thrust and possibly other shear zones in the Shoo Fly.

The metasedimentary units of the Shoo Fly were intruded after the oldest D_1 phase of folding and metamorphism by a suite of granite, syenite, and gabbro sills and plutons. They now occur as gneissic granitoid bodies throughout Tuolumne County complexly deformed along with their Shoo Fly host rocks. At various later times the Shoo Fly was also intruded by felsic and mafic dikes, granitic to ultramafic plutons, and ultimately the Sierra Nevada batholith. The igneous rocks, some of which are geochronically dated, are well-bracketed with respect to deformational episodes of the Shoo Fly Complex. The resulting integration of geochronologic, structural, and metamorphic data produces a correlation, with some uncertainties, between deformational events of the Shoo Fly and Phanerozoic tectogenesis recognized elsewhere in the SW Cordillera.

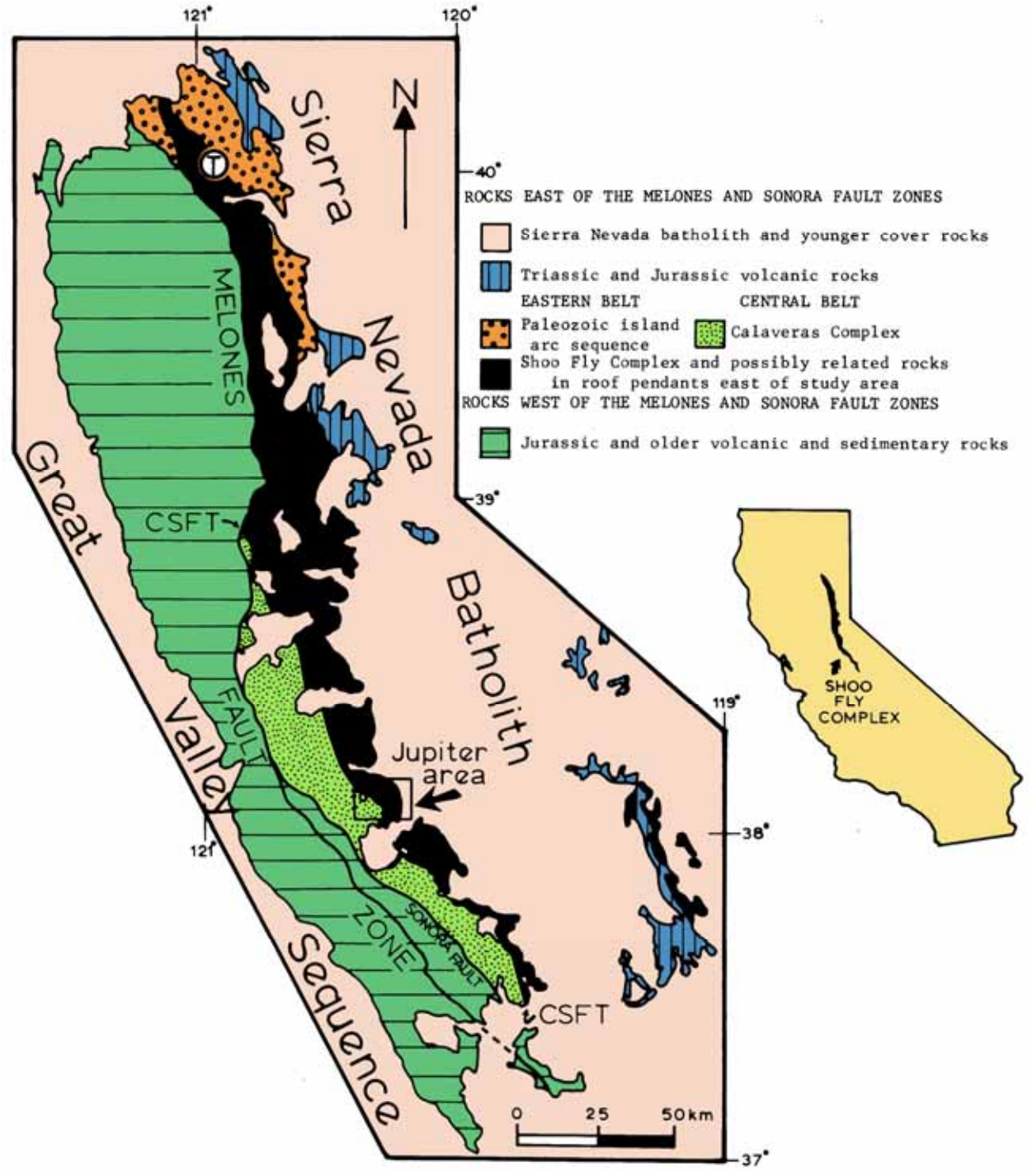

Figure 1 - Sketchmap of the Shoo Fly Complex (black) and other tectonostratigraphic units of the Sierra Nevada foothills metamorphic belt. CSFT = Calaveras-Shoo Fly thrust. After Schweickert and Merguerian (in press).

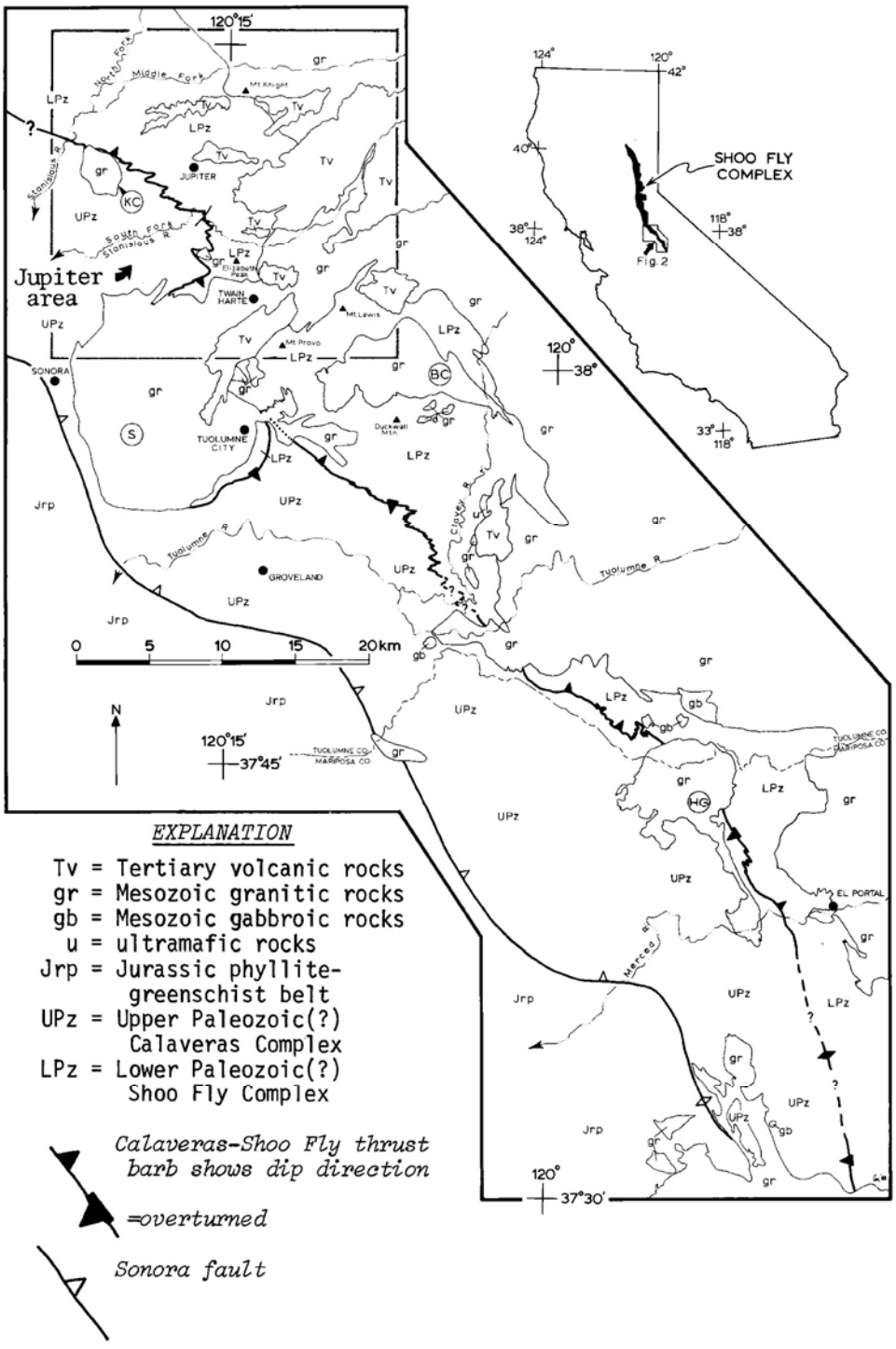

Figure 2 - Geologic sketch map of the Shoo Fly Complex and the Calaveras Shoo Fly thrust in Tuolumne and Mariposa Counties, California. The distribution of the Shoo Fly Complex and geometry of the thrust are outlined from detailed bedrock mapping at 1:24,000 scale accomplished during 1978-1981. Solid circles indicate cities and towns and solid triangles mark geographic localities mentioned in the text. Some map contacts are from Bowen (1969), Strand and Koenig (1965), Tobisch, (1960); Schweickert, (unpub. data); Schweickert and Bogen (1983), Turner and Ransome, (1897, 1898); and Wagner and others (1981).

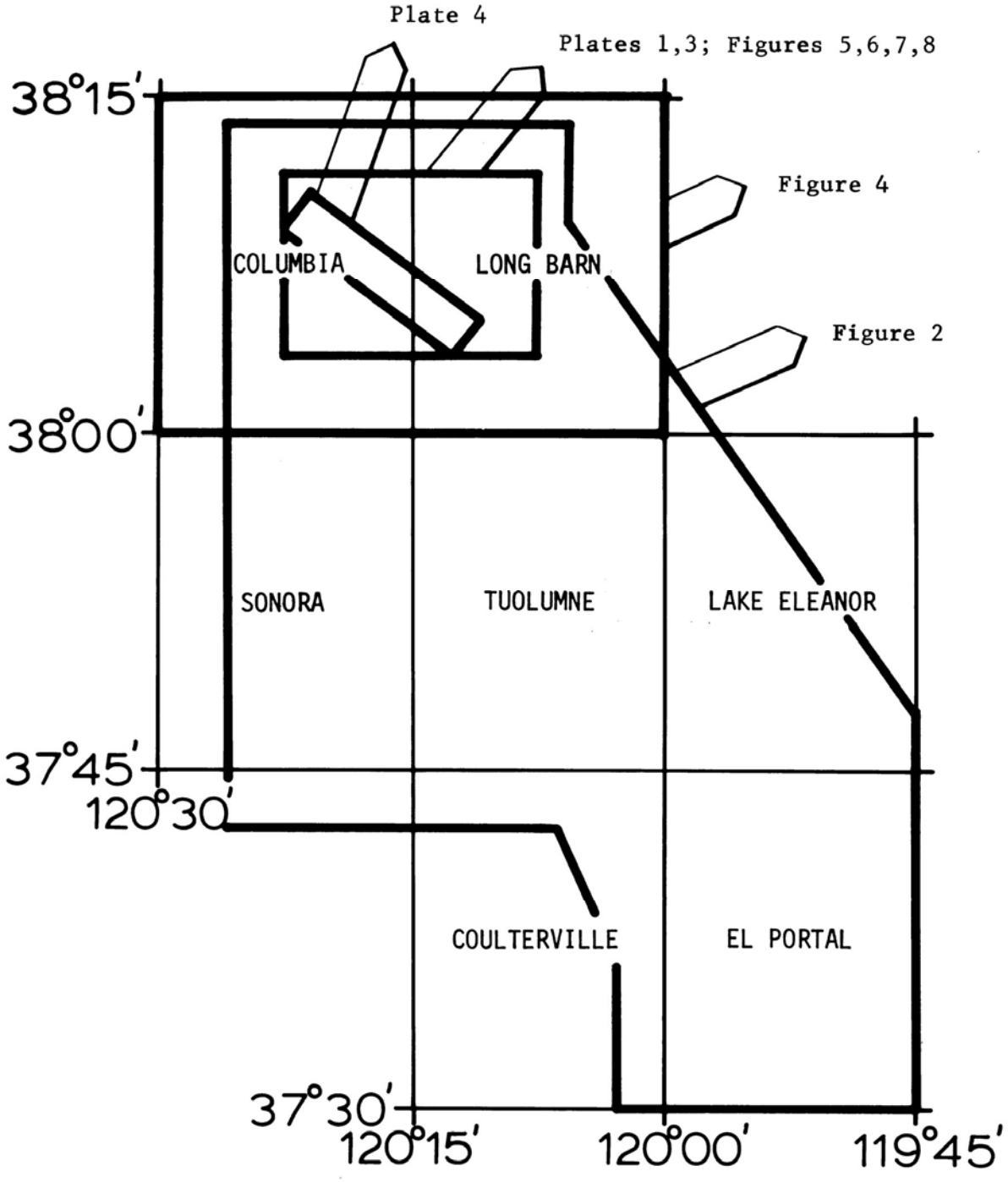

Figure 3 - Index of figures and plates of this report with respect to 15' quadrangles in the central Sierra Nevada. The 7-1/2 minute quadrangle maps of the Shoo Fly and parts of the Calaveras Complexes shown on Figure 2 are on open-file at the California Division of Mines and Geology in San Francisco. The 7-1/2 minute quadrangles comprising the Jupiter area appear in Plate 1.

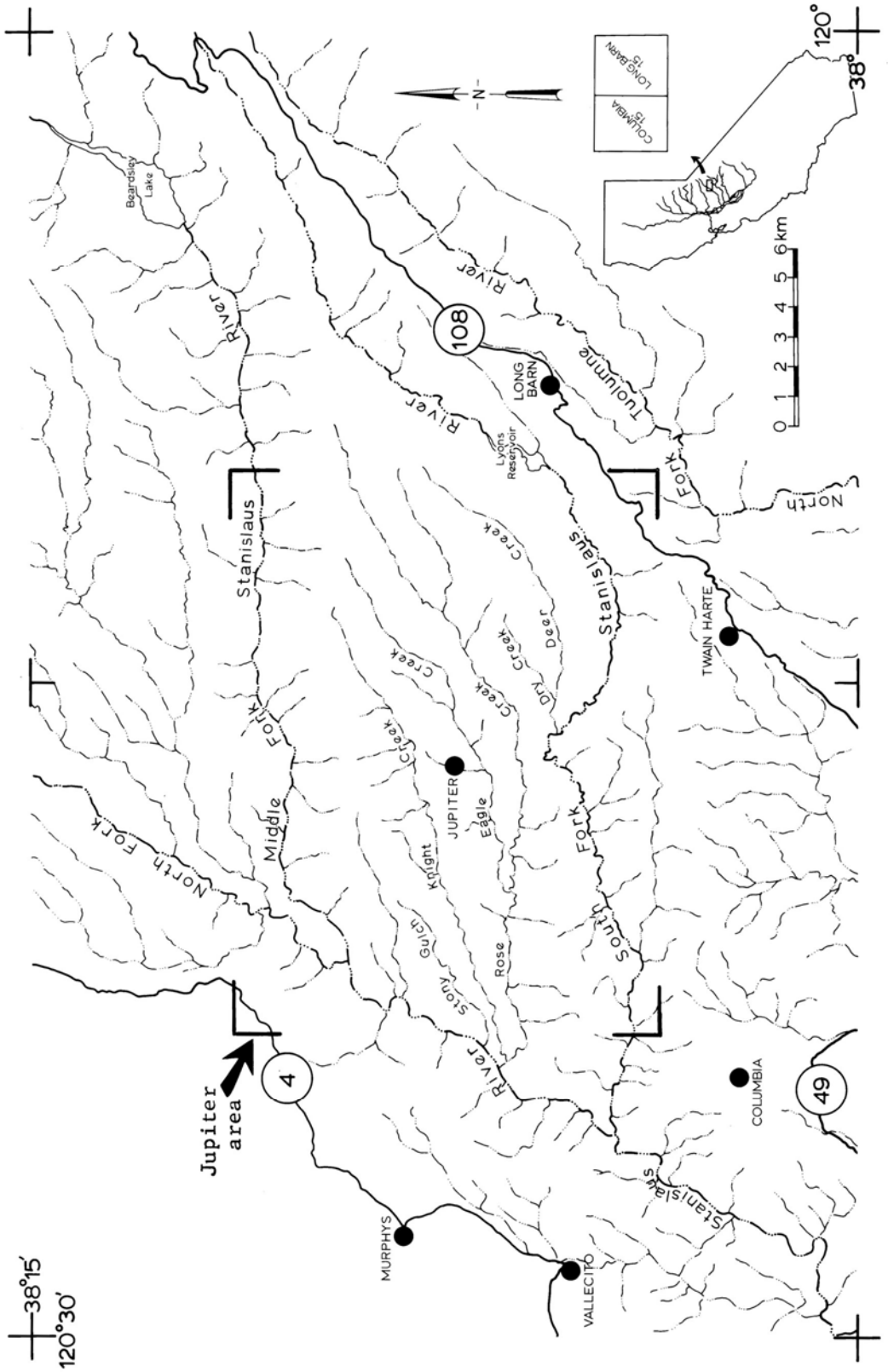

Figure 4 - Map of the Stanislaus river system in Tuolumne County, California. The Jupiter area is outlined. The river system describes a trellis pattern that is following young, brittle structural features trending NNE and ENE.

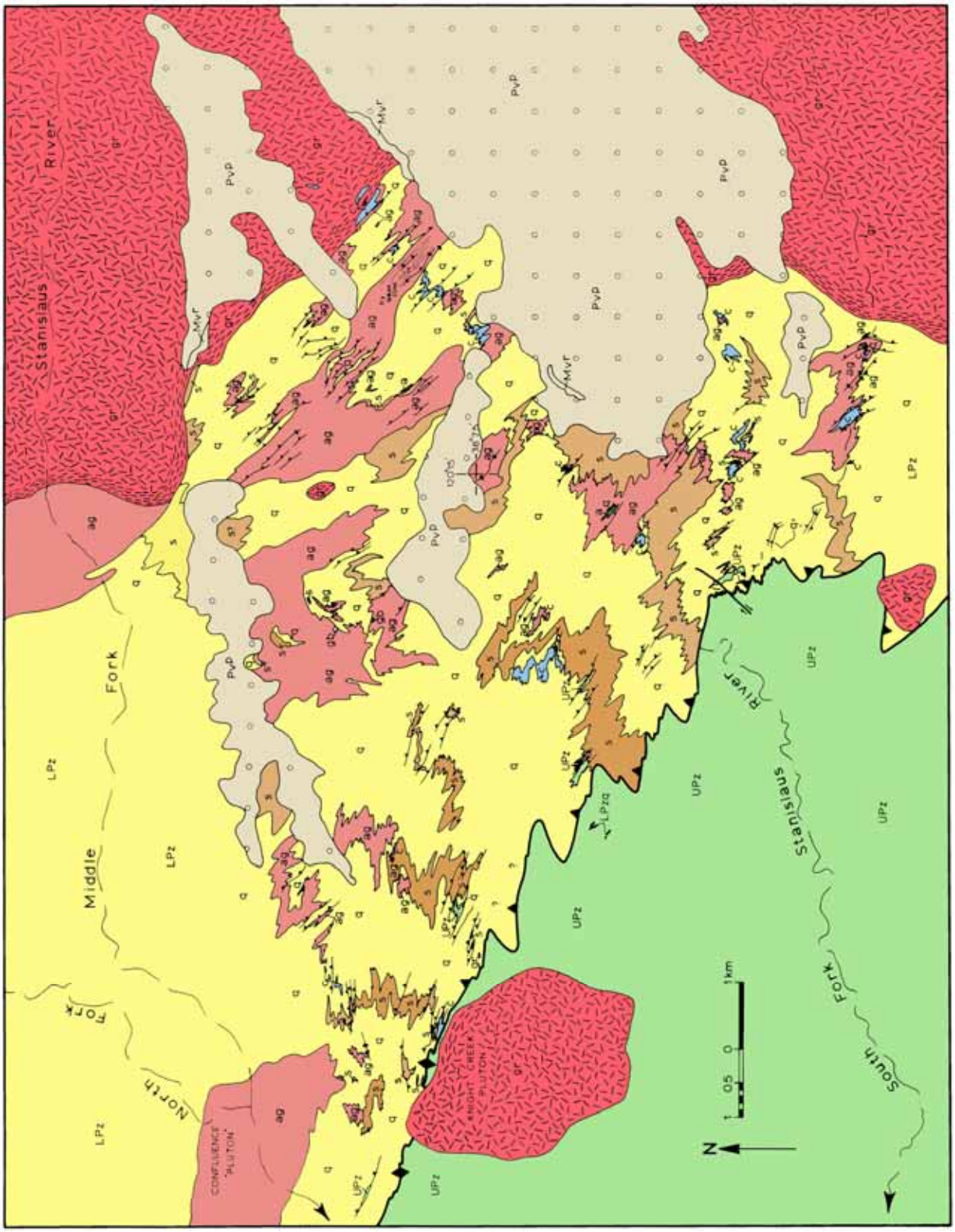

Figure 5 - Simplified bedrock geologic map of the Shoo Fly Complex of the Jupiter area encompassing parts of the Stanislaus, Columbia SE, Crandall Peak, and Twain Harte 7-1/2 minute quadrangles. Contacts are solid but actual contact control and explanation of symbols and lithologic units appear in the legend of Plate 1.

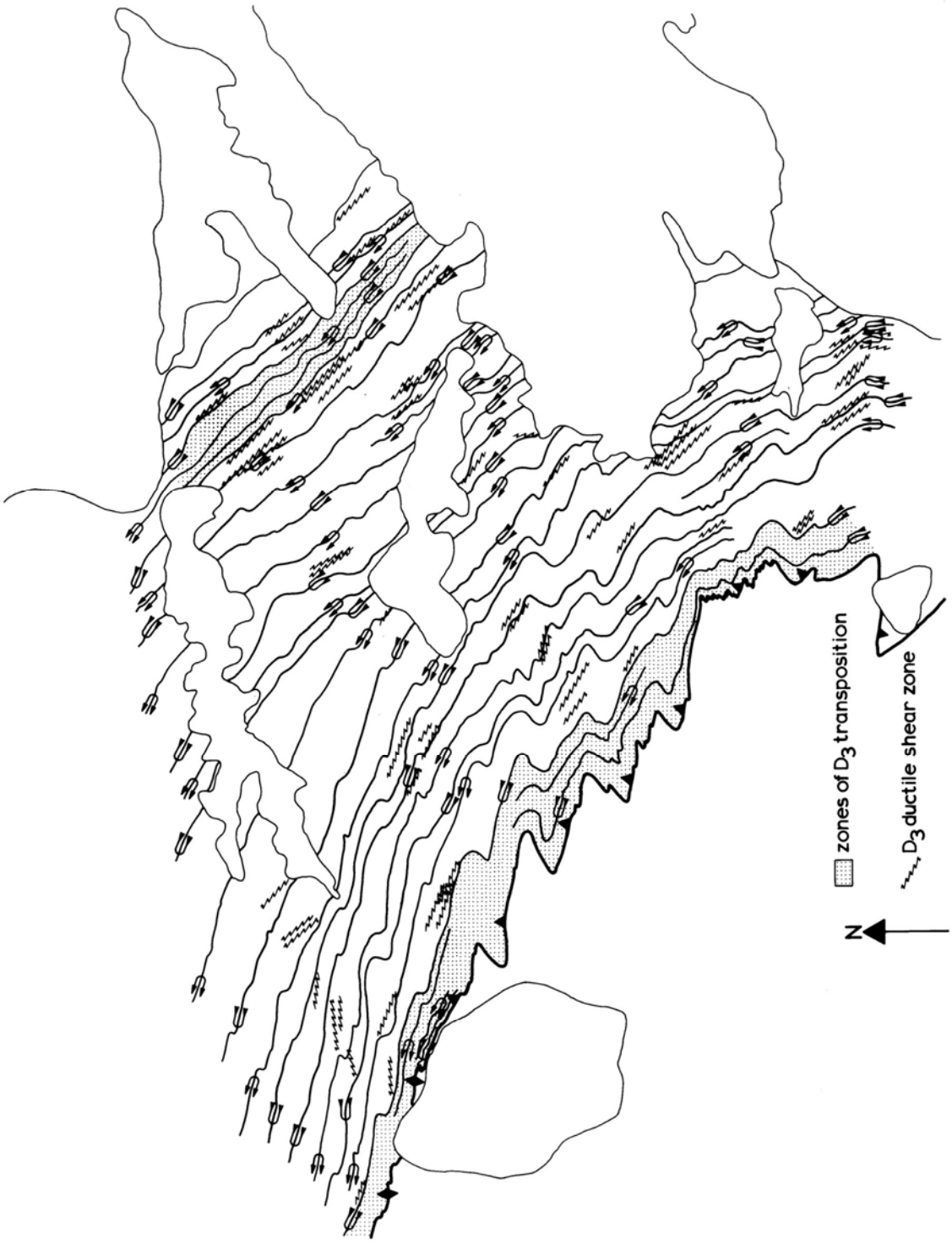

Figure 6 - S_3 axial surface trace map indicating zones of D_3 ductile transposition and mylonitization in the Shoo Fly Complex. The axial surface traces are schematic in that they are projected across stream channels and are not regionally continuous as indicated. This and figures 7 and 8 are intended for xerographic reproduction onto transparency in which form they may be used as overlays for figure 5 .

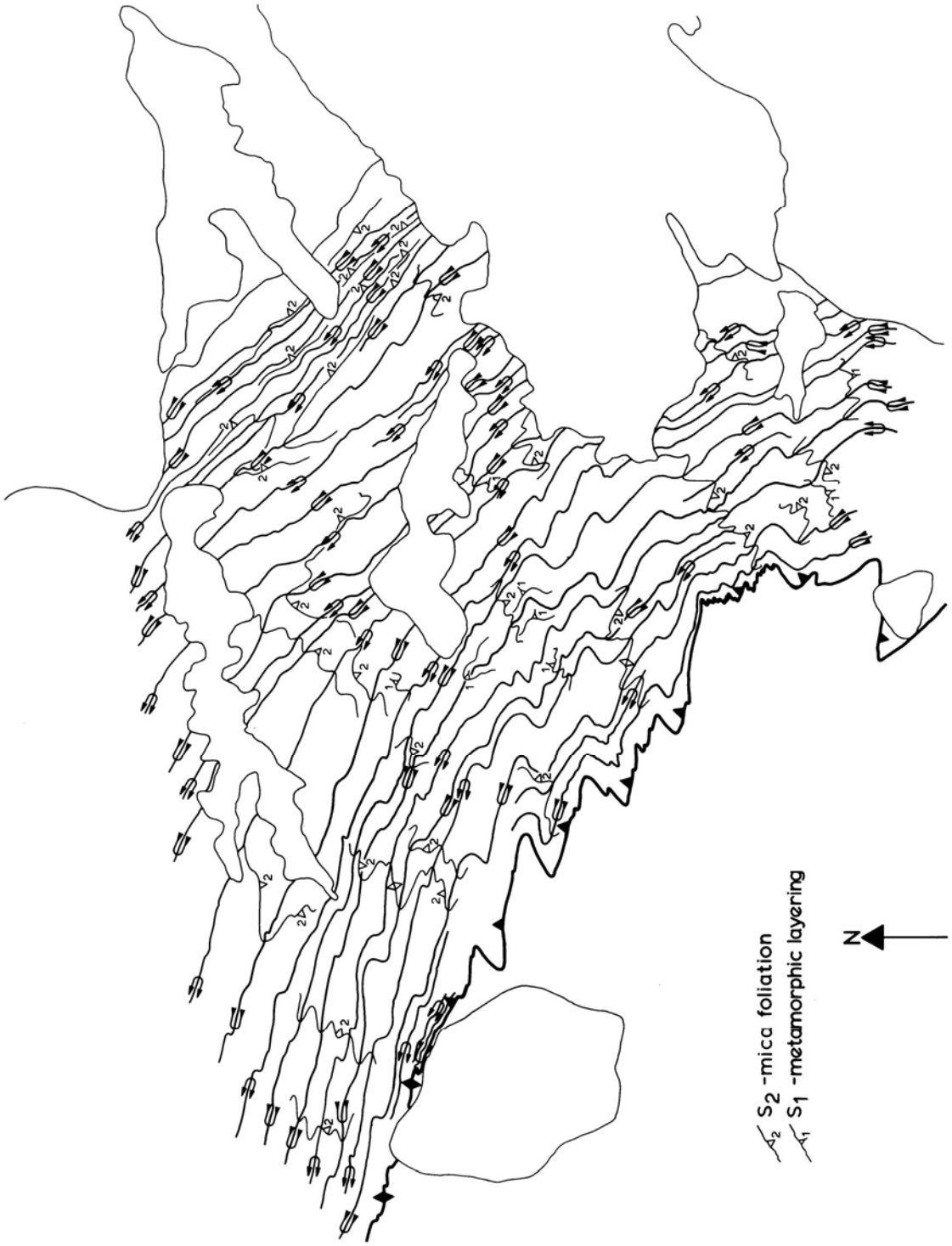

Figure 7 - S_3, S_2, and S_1 axial surface trace map to accompany geologic map.

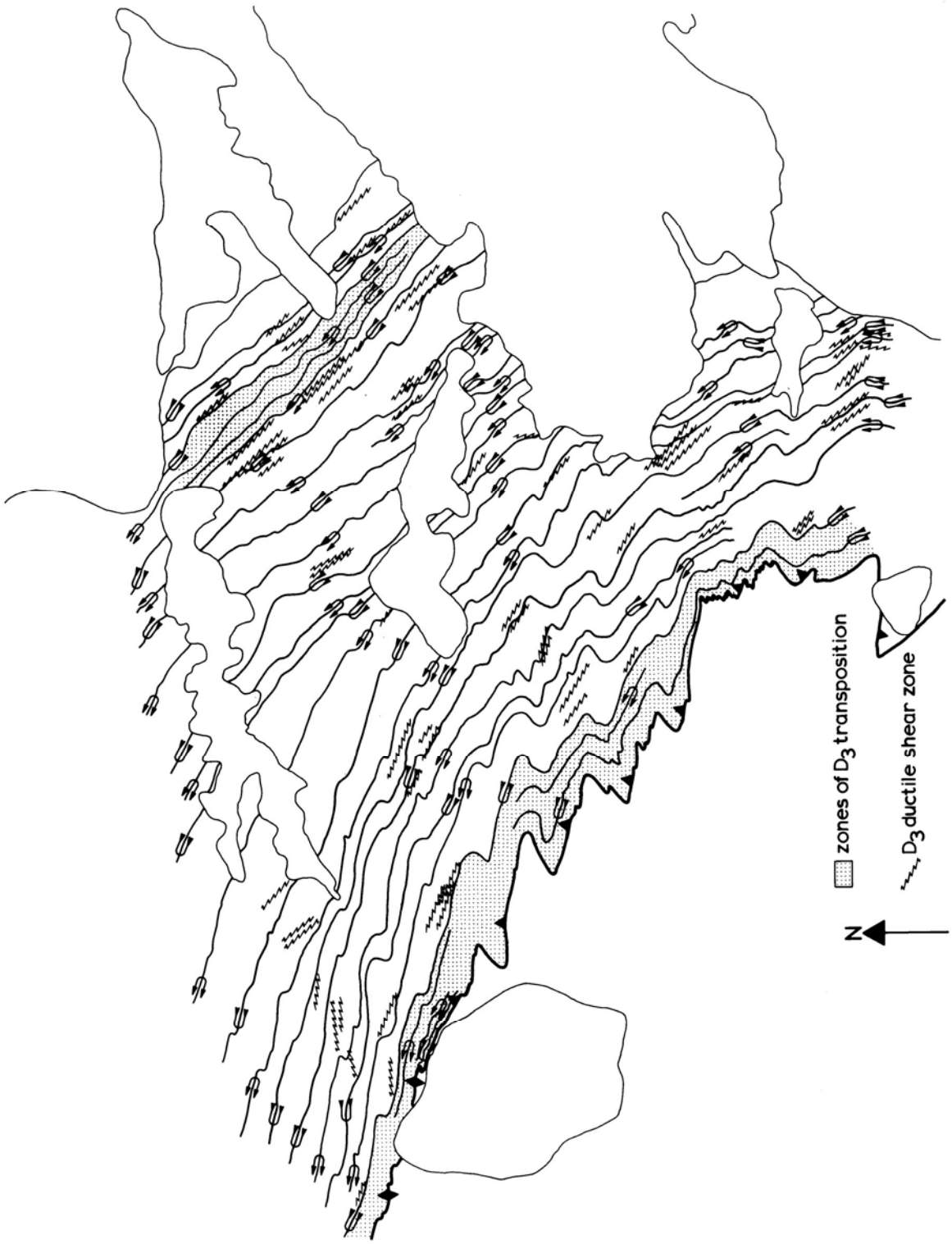

Figure 8 - S_3, S_4, and S_6 axial surface trace map to accompany geologic map.

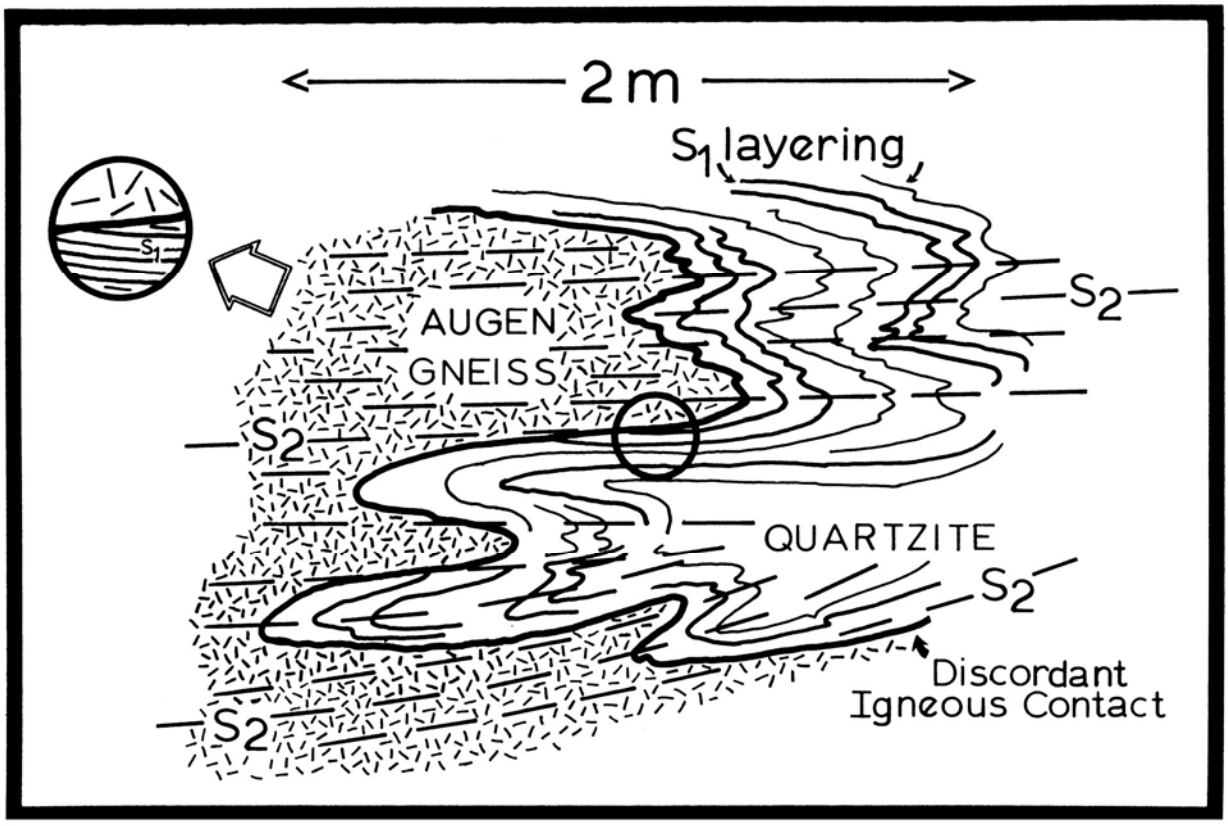

Figure 9 - A field drawing from Rose Creek showing the truncation of S_1 layering in quartzite by the discordant intrusive contact of the orthogneiss. During D_2, isoclinal F_2 folding of the contacts between the gneissic granitoid protoliths and their host rocks occurred. Syntectonic recrystallization produced a penetrative S_2 mica foliation in the gneissic granitoids and a mica foliation across S_1 in the Shoo Fly.

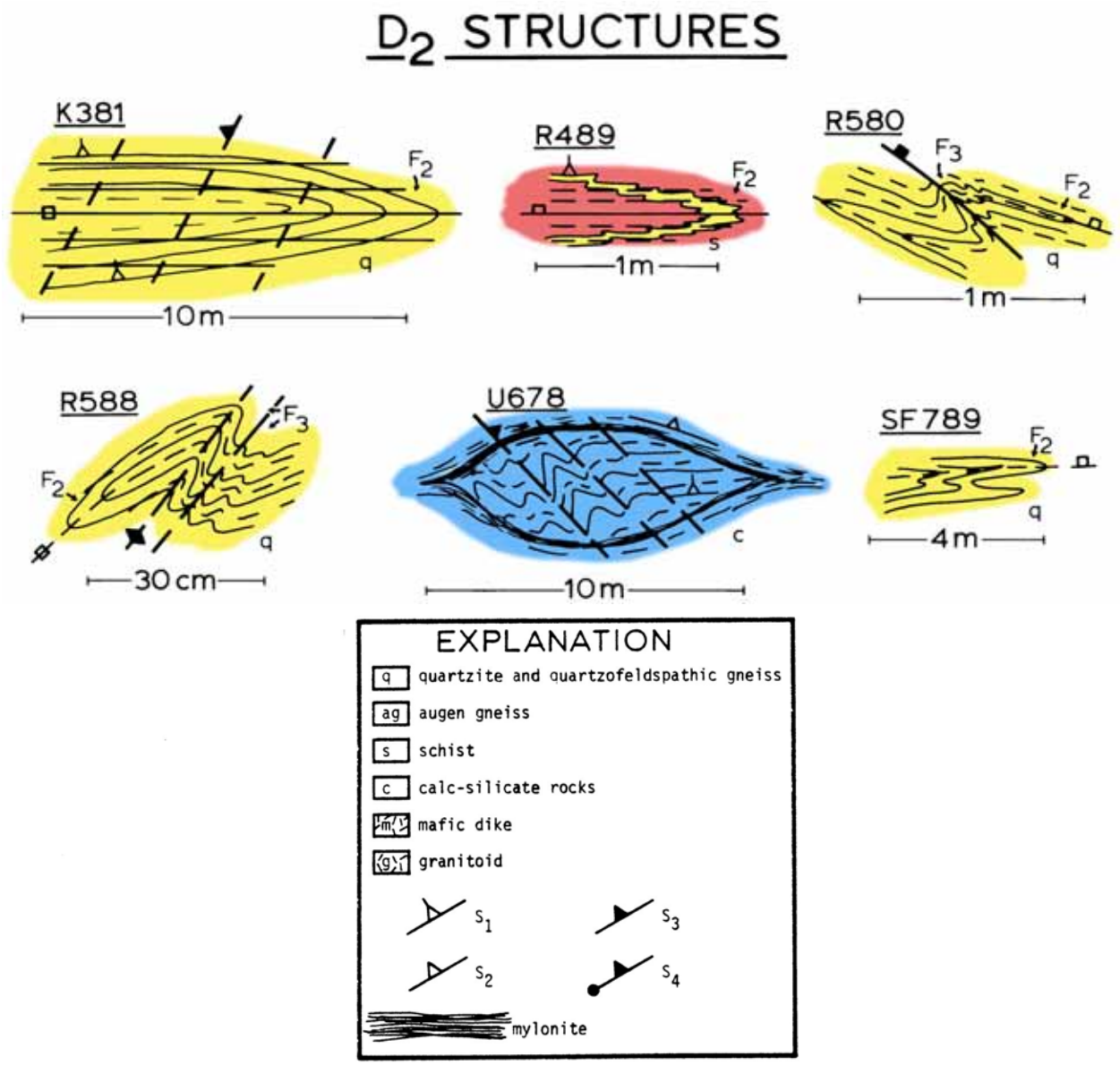

Figure 10 - Field drawings of D_2 structures in the Shoo Fly Complex of the southern Sierra Nevada Foothills, California. The field sketches illustrate the style of the F_2 isoclinal folds which deform and locally transpose the S_1 metamorphic layering of the Shoo Fly. The S_2 foliation is strongly penetrative and grades locally into mylonite. D_2 structures are locally overprinted by F_3 folds and related structures. In this and subsequent line drawings and photographs, structural symbols and lithologies are described in Plate 1 and Appendix 1. Solid axial surface traces indicate development of penetrative fabrics whereas dashed traces indicate weak or domainal fabrics. Thin continuous, closely-spaced lines indicate mylonitic shears. Field localities can be found in Plate 3.

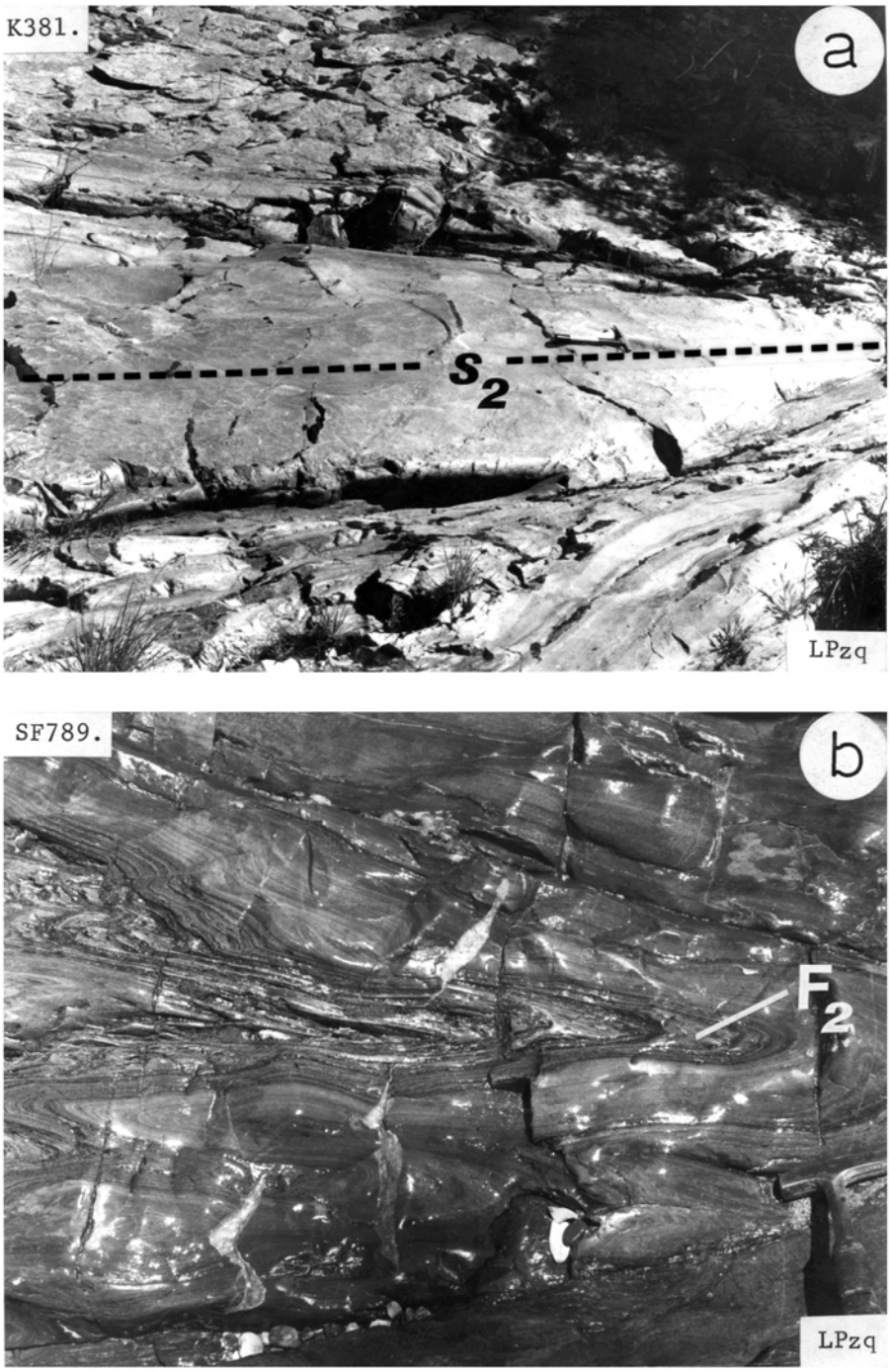

Figure 11 - Photographs of D_2 structures in the Shoo Fly Complex, Jupiter area, California. The photographs were chosen from regions that do not show strong refolding by D_3 although spaced mylonitic shears are (S_3) locally developed.

a. Loc. K381. F_2 isocline (10 m amplitude) folds interlayered black quartzite, schist, and gneiss possessing an S_1 foliation. An S_2+S_1 transposition foliation along the limbs is cut by a domainal S_3 biotite foliation. Hammer scale is 39 cm long.

b. Loc. SF789. F_2 isoclinal folds of laminated quartzite. Outside of the field of view an L_2 stretching lineation is parallel to the F_2 hingeline. Lamination in the quartzite is a highly penetrative S_1 mylonitic layering. Hammer scale at lower right.

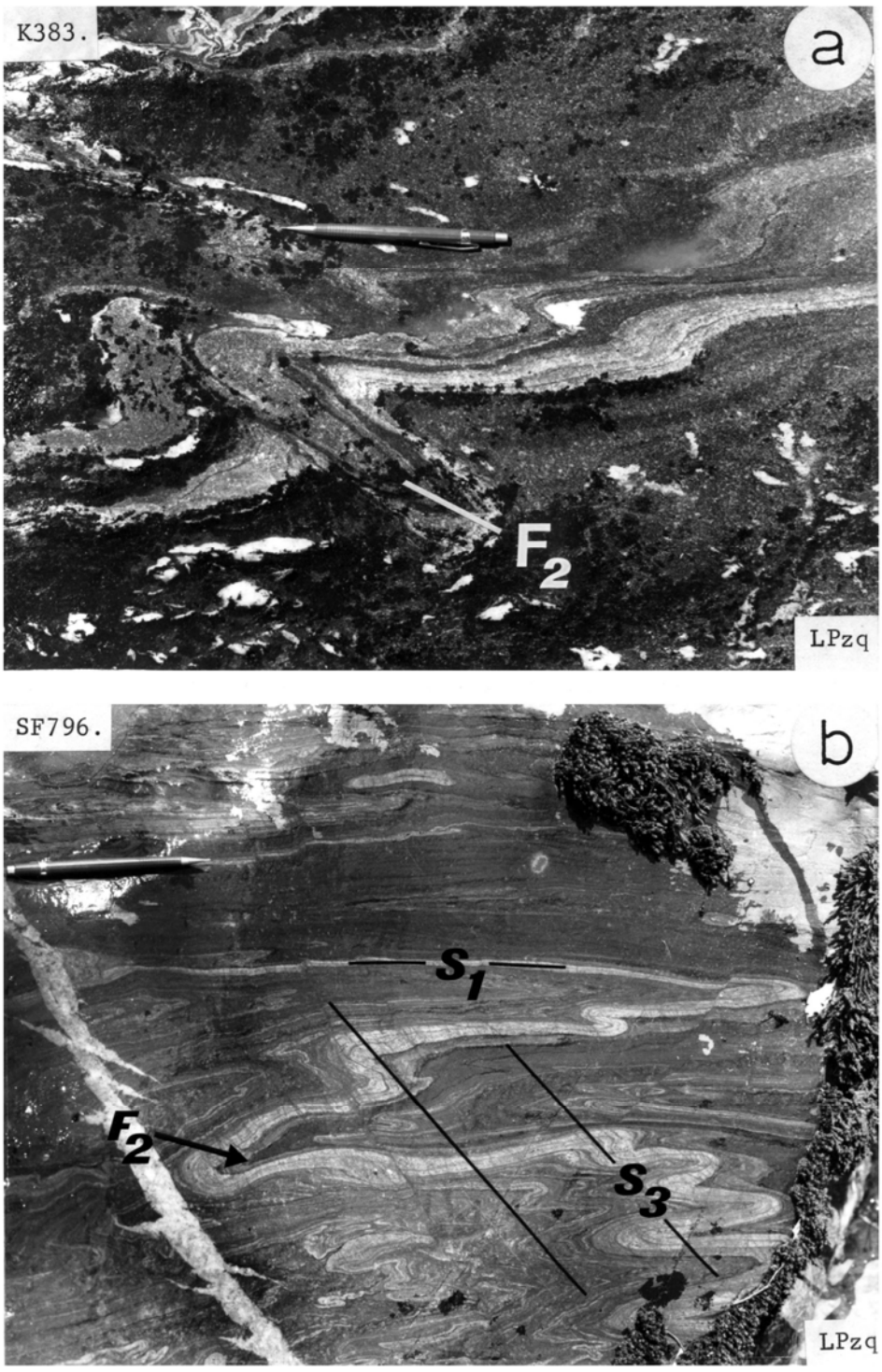

Figure 12 - Photographs of D_2 structures in the Shoo Fly Complex.
a. Loc. K383. F_2 isoclinal fold of S_1 layering in biotite quartzite is refolded by tight F_3 folds with some shearing along their axial surfaces. Pencil scale is 14.5 cm long.
b. Loc. SF796. F_2 isoclinal folds of laminated biotite quartzite deform a penetrative S_1 mylonitic foliation. Near the top of the photo, note the eye-fold possibly due to superposition of F_1 and F_2. Millimeter-scale spaced ductile shears can be traced into the axial surfaces of F_3 folds nearby. Pencil scale.

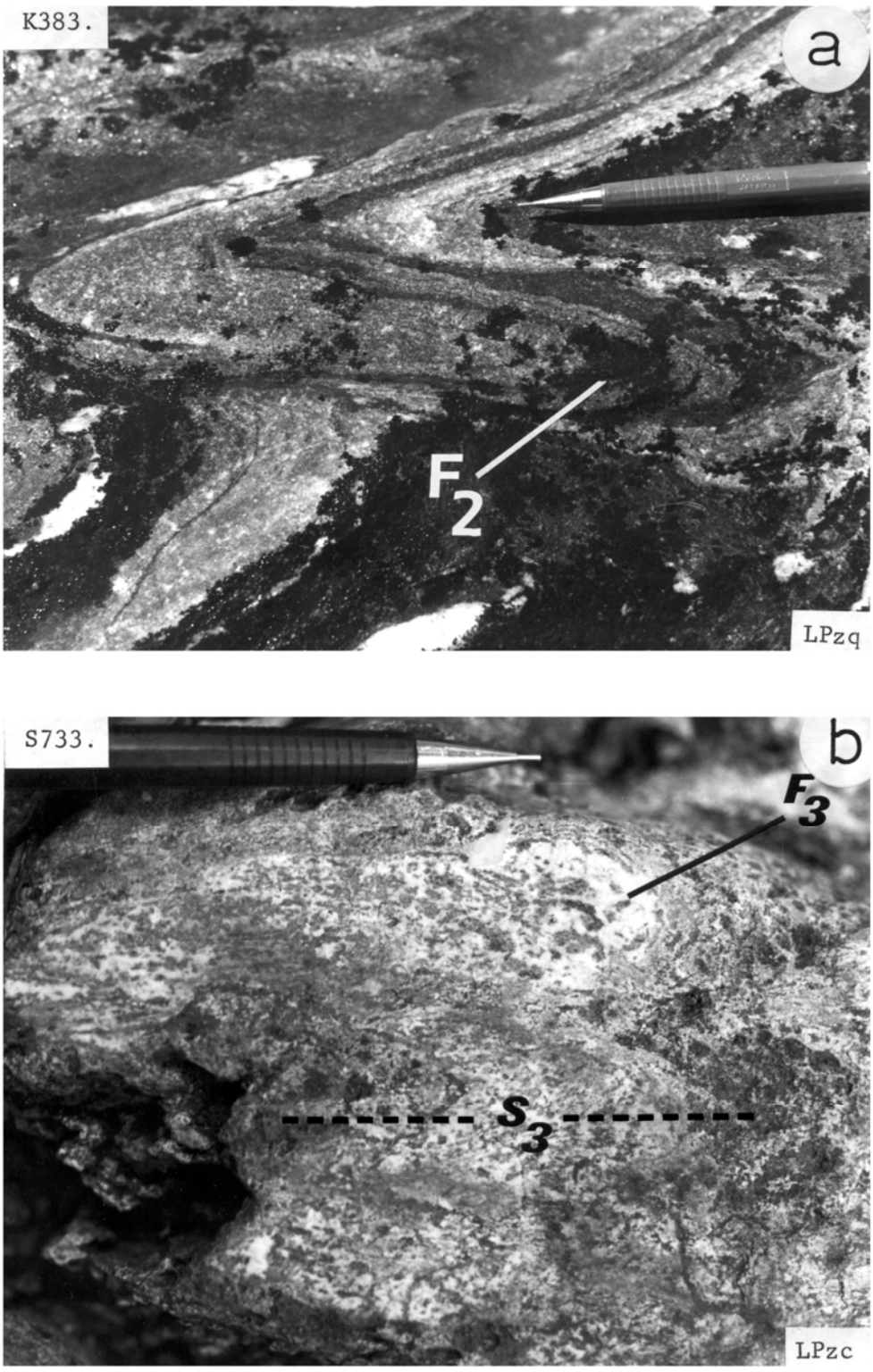

Figure 13 - Photographs of D_3 structures in the Shoo Fly Complex.
a. Loc. K383. Detail of F_3 fold which deforms the F_2 isocline of figure 12a. Pencil (scale) is parallel to S_3.
b. Loc. 5733. Isoclinal F_3 folds of diopside-tremolite calcsilicate rock deformed in the Calaveras-Shoo Fly thrust zone. On the fold limbs an L_3 stretching lineation is developed parallel to F_3 hingelines. Pencil scale.

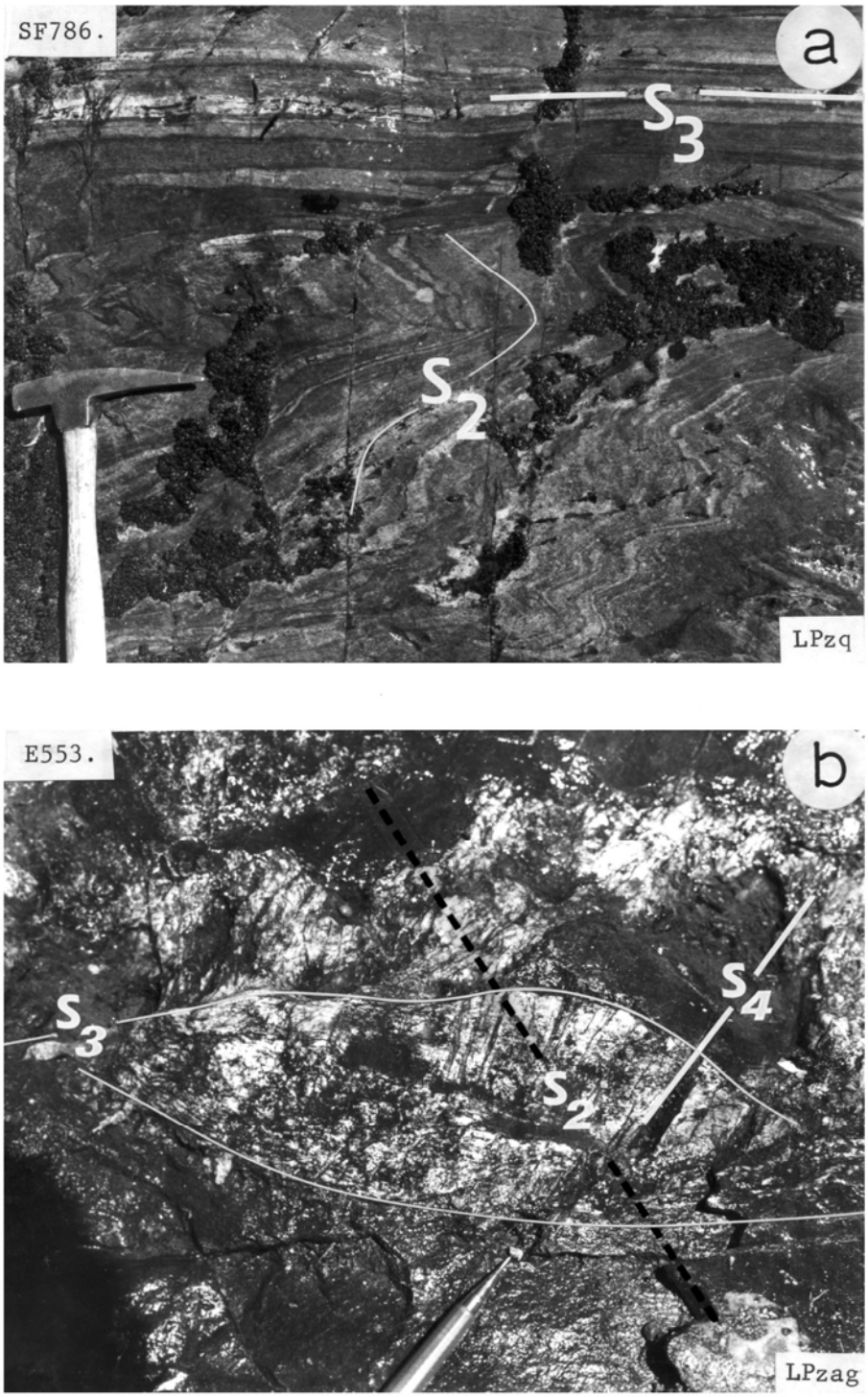

Figure 14 - Photographs of D_3 structures in the Shoo Fly Complex.
a. Loc. SF786. Long-limbed F_3 isoclinal folds in upper part of photo define a pronounced domain of D_3 ductile transposition in well-layered quartzite. The S_2 foliation is not obliterated, in the bottom two-thirds of the photo, but it is strongly folded by F_3. Hammer scale.
b. Loc. E553. Ellipsoidal mass of foliated augen gneiss. The sheared and tectonically eroded block of foliated gneiss is surrounded and cut by biotitic S_3 shears and occurs in a 14 cm wide D_3 shear zone (fig. 16) with local shears varying from 1 mm to 2 cm thick. The pencil (scale) is parallel to a spaced S_4 cleavage.

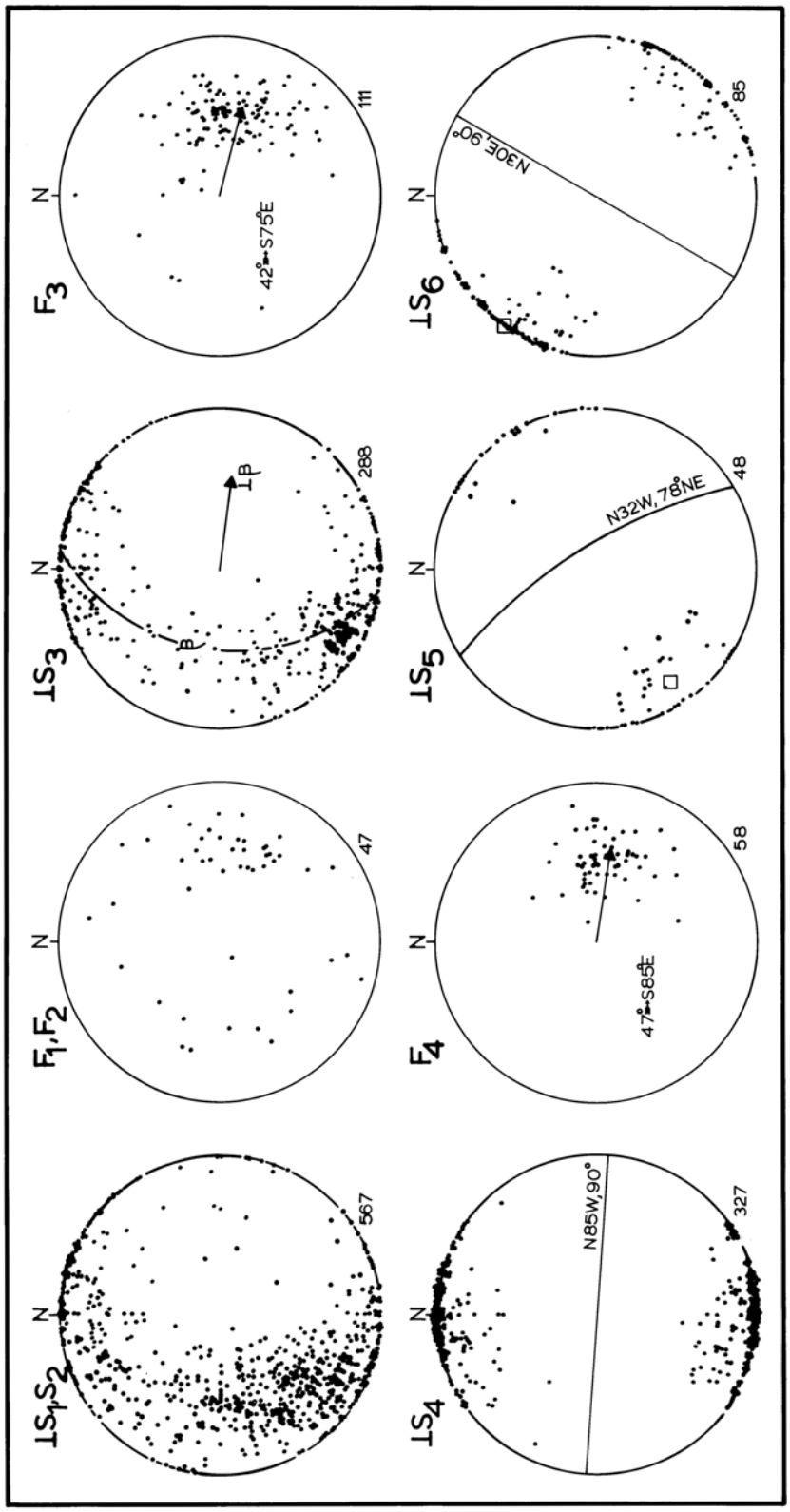

Figure 15 - Lower hemisphere equal-area stereograms showing poles (⊥) to foliations, and linear elements (fold hingelines and intersection lineations). The girdles are visual best-fits with their poles as open squares. The number of plotted points is indicated at the lower right of each stereogram.

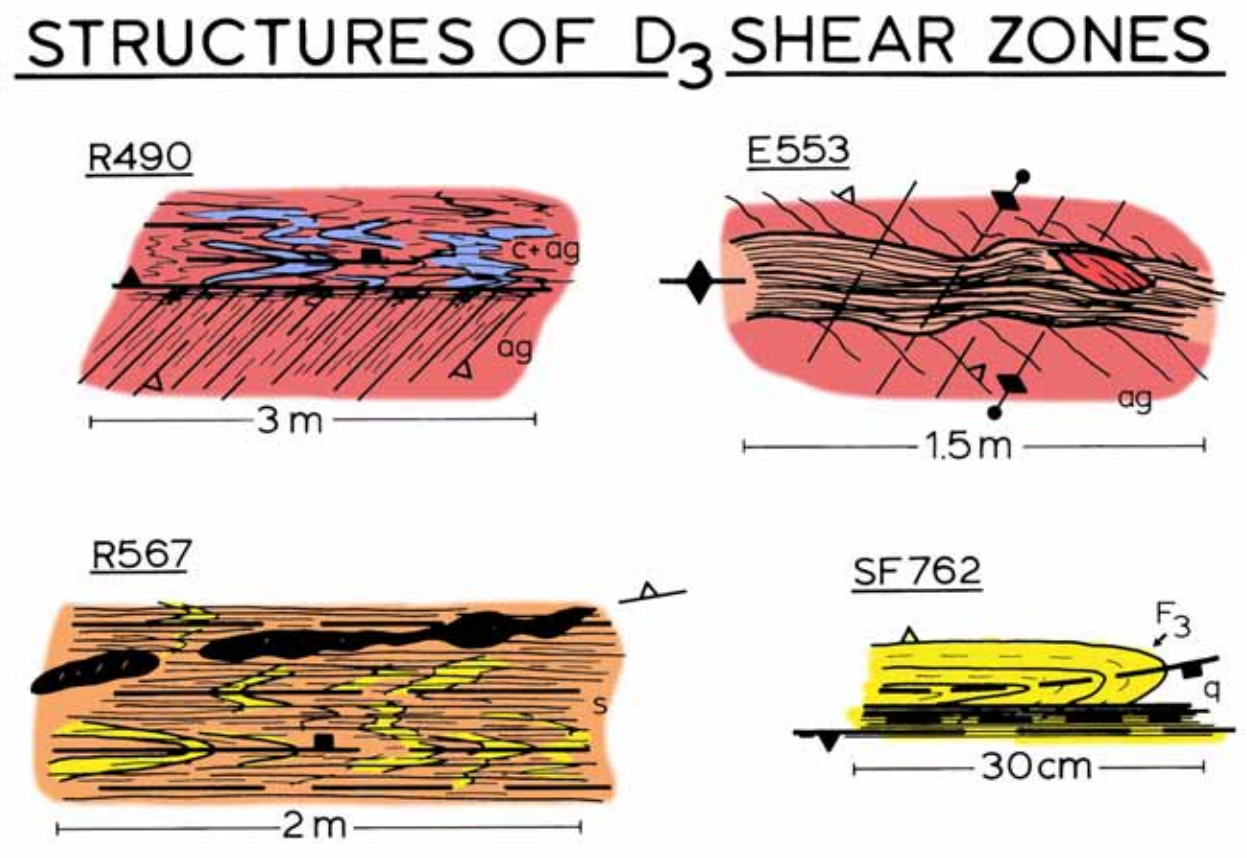

Figure 16 - Field drawings of D_3 structures in shear zones east of the Calaveras-Shoo Fly thrust. The field drawings illustrate the penetrative nature of S_3 with local transposition of S_2 (R490, 8567) and the development of mylonitic shears locally parallel to S_3 axial surfaces (E553, SF762).

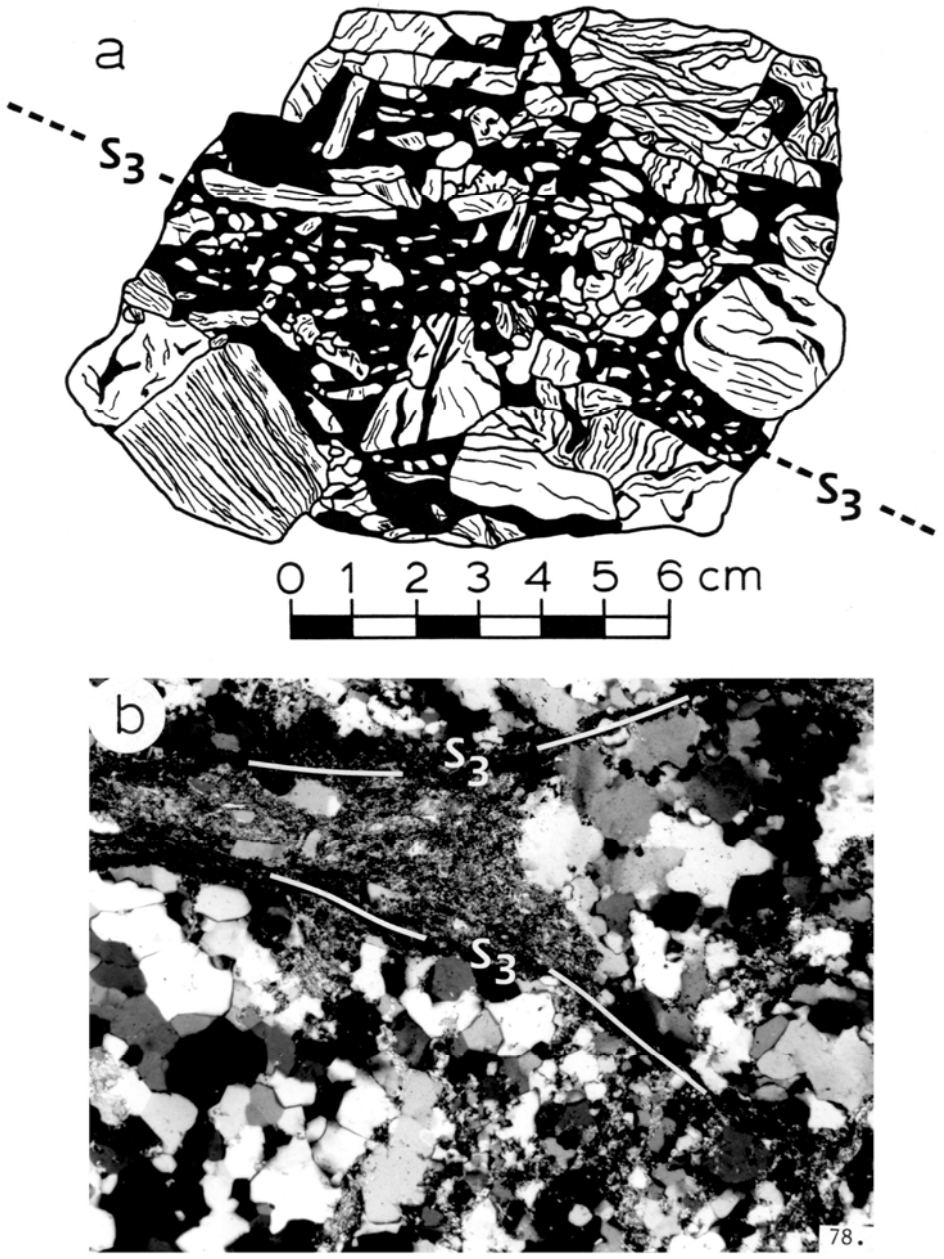

Figure 17 - Tracing from a sawn slab taken from a 2.5 m thick zone of random fabric protocataclasite **(a)**. Subangular Shoo Fly clasts, consisting of truncated foliated quartzite, schist, and phyllite, account for over 75% of the rock. They are surrounded by a finely comminuted matrix (black) of microcrystalline minerals. In the tracing, a 1 cm thick seam of matrix containing many prophyroclasts of strained quartz and feldspar separates areas of larger foliated clasts. The S_3 fabric here is defined by inosculating seams of matrix consisting of recrystallized quartz, mica, feldspar, and calcite. Matrix surrounds and locally injects across the margins of clasts.

The photomicrograph **(b)** shows parts of three strained quartzite clasts whose rounded margins are outlined by opaque minerals. The clasts show internal sutured grain boundaries, marginal granulation, local injection of matrix, and amalgamation. In the triangular area of matrix in the upper half of the photomicrograph, a few angular porphyroclasts of quartz and feldspar apparently escaped granulation in the pressure shadow between the larger clasts. The matrix probably represents a crush microbreccia or may, alternatively, be recrystallized pseudotachylyte. All photomicrographs taken with crossed nicols and frame width is 2.7 mm across unless otherwise noted.

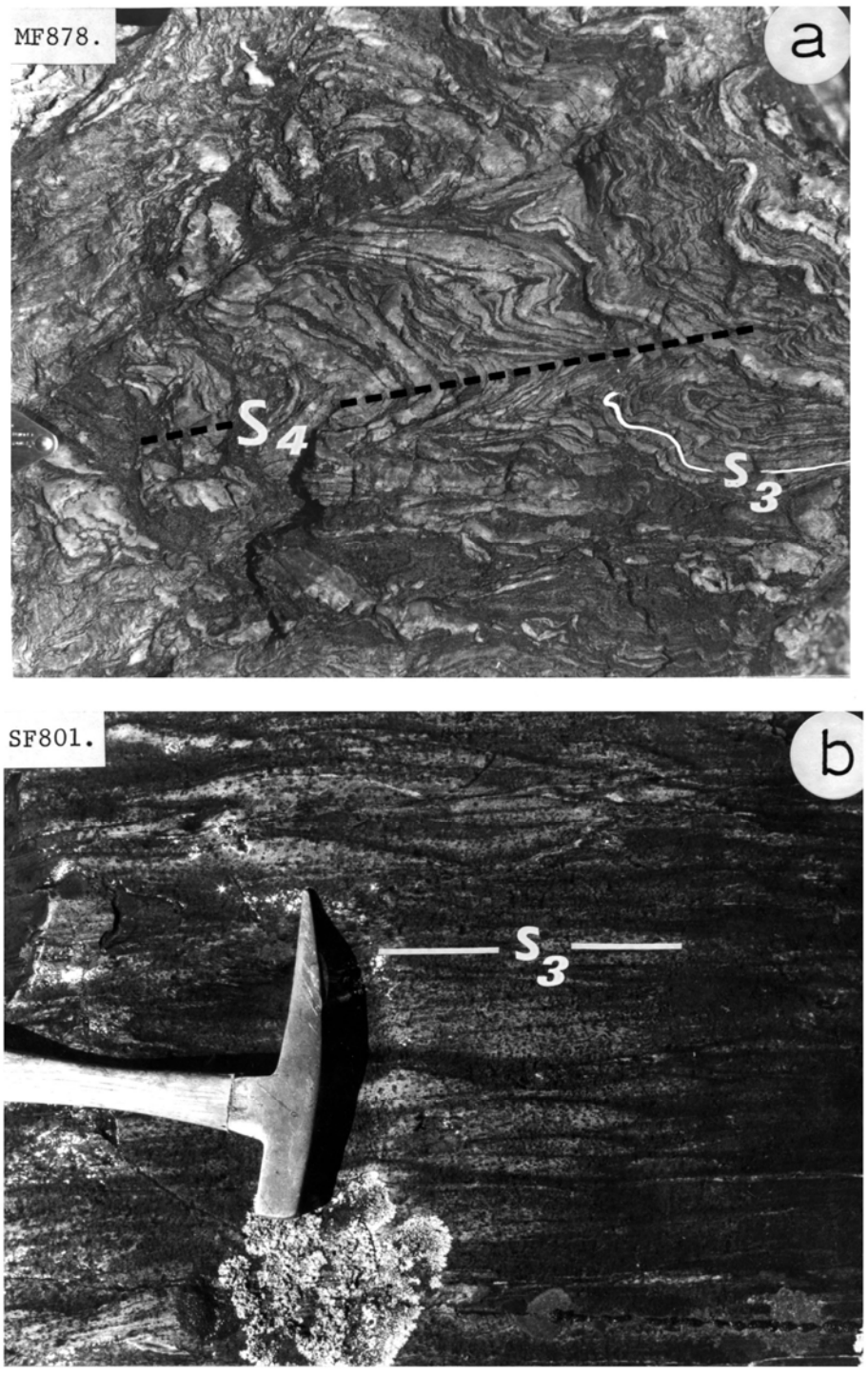

Figure 18 - Photographs of D_3 mylonites in the Calaveras-Shoo Fly thrust zone.
a. Loc. MF878. Intercalated black argillite (Calaveras) and laminated polydeformed quartzite and schist of the Shoo Fly define the S_3 mylonitic foliation. The heterogeneous S_3 fabric is crenulated by F_4 folds as indicated. Handlens scale.
b. Loc. SF801. Ghostlike S_2 in foliated quartzite is locally preserved among penetrative S_3 shears in a 4 m-wide zone of intense D_3 deformation. Inter sheaved foliated quartzite and black argillite are all recrystallized and flattened into parallelism with S_3. Hammer scale.

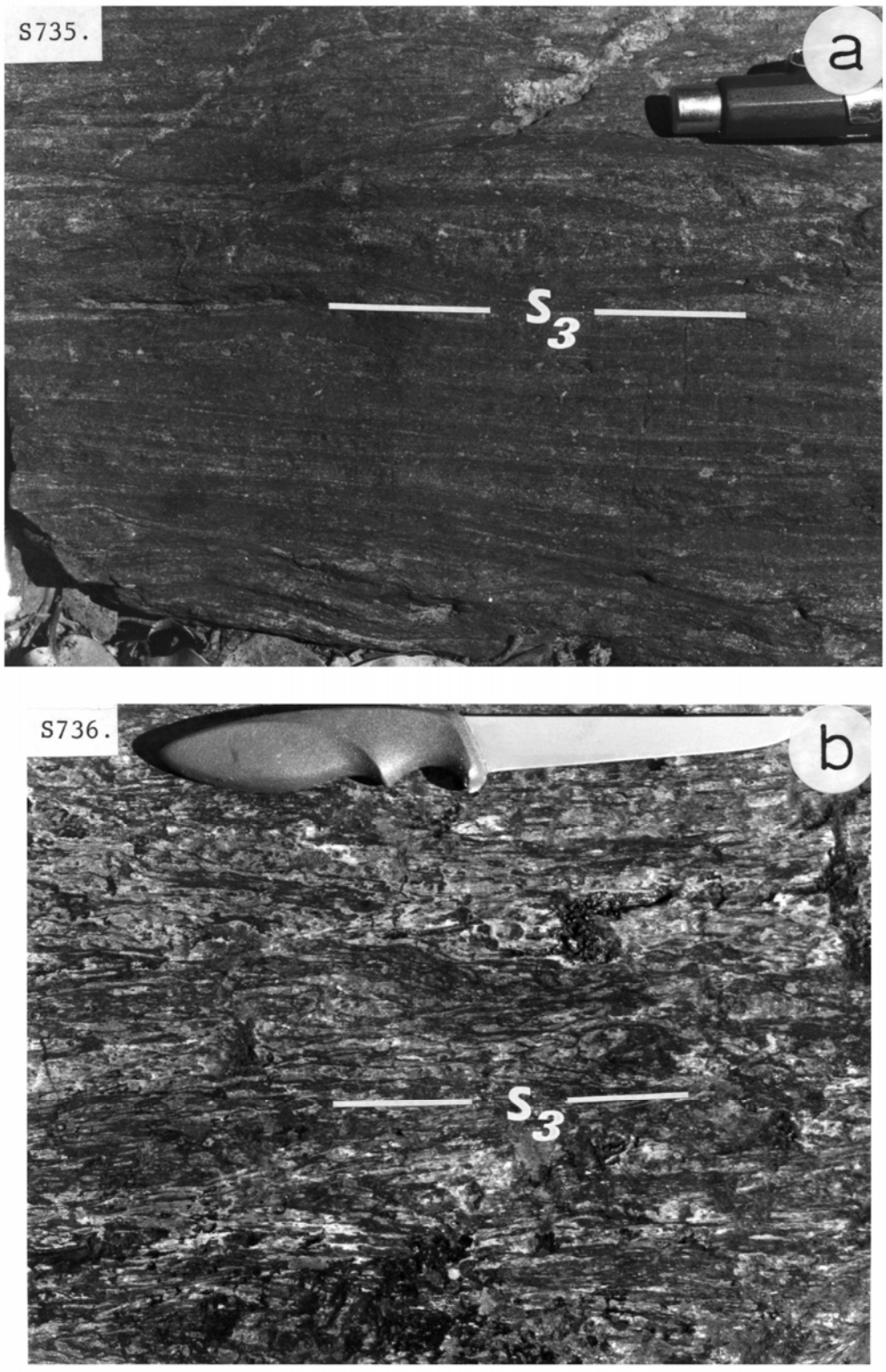

Figure 19 - Photographs of D_3 mylonites in the Calaveras-Shoo Fly thrust zone.
a. Loc. S735. Black to dark-gray laminated quartzite with 1 cm scale mylonitic layering. Total transposition into parallelism with S_3 produces a dense, penetrative flattening foliation. Pencil Scale.
b. Loc. S736. Tectonically shredded mica-quartzite with elongate flasers of recrystallized quartzite flattened into an S_3 blastomylonitic foliation. Knife (scale) is 21.5 cm long.

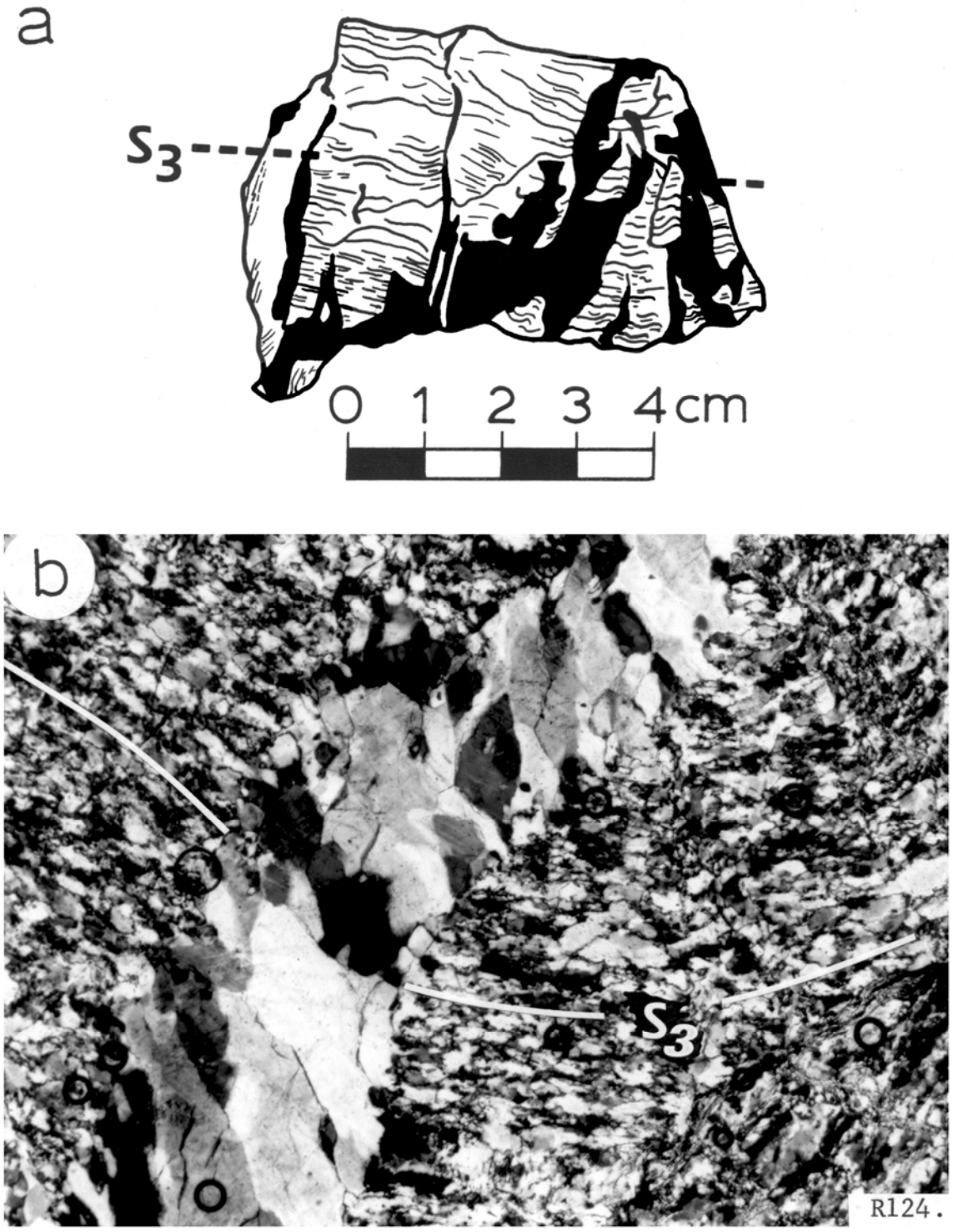

Figure 20 - Loc. 8124. Tracing of branching pseudotachylyte found near the Star Mine as float. In hand sample **(a)** the sinuous black veins permeate and clearly truncate the S_3 mylonitic foliation in tan colored vitreous quartzite. The photomicrograph **(b)** shows how a microvein, which is not composed of totally recrystallized strained quartz, truncates the S_3 mylonitic layering composed of flattened lenticles of highly-strained quartz. The veins may have originated as shear-heated glass during the late stages of D_3 thrusting along the Calaveras-Shoo Fly thrust zone.

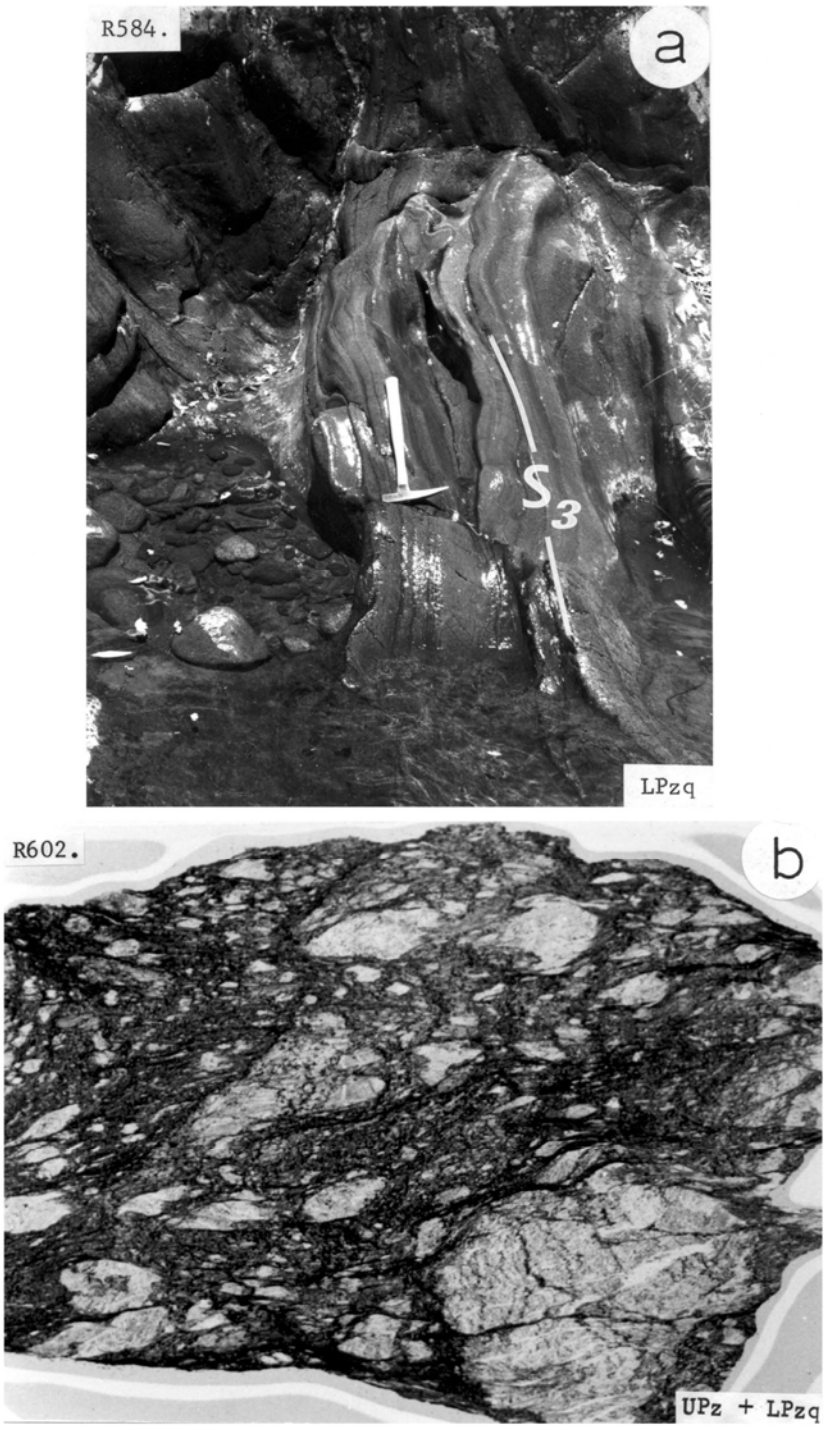

Figure 21 - Photographs of D_3 mylonitic rocks in the Calaveras-Shoo Fly thrust zone.
a. Loc. 8584. Highly flattened D_3 mylonite with abundant rootless isoclines (not visible) transposed into parallelism with S_3 in a laminated biotite quartzite. Note the low angle truncation of S_2 in thicker laminae. Hammer scale.
b. Loc. 8602. Internally folded ellipsoidal slivers of foliated Shoo Fly quartzite surrounded by finely recrystallized blastomylonite and intercalated black argillite of the Calaveras. This sample macroscopically illustrates the distinctive tectonic intermixing found to occur regionally between the Shoo Fly and Calaveras Complexes. Horizontal scale = 7 cm.

Figure 22 - Loc. SF809. Blastomylonitic layering produces a sugary textured, highly flattened and laminated quartzite with vestiges of older fabrics (S_1, S_2) at a small angle to S_3. The laminae vary from between 2 and 5 mm to 3 cm. Hammer scale.

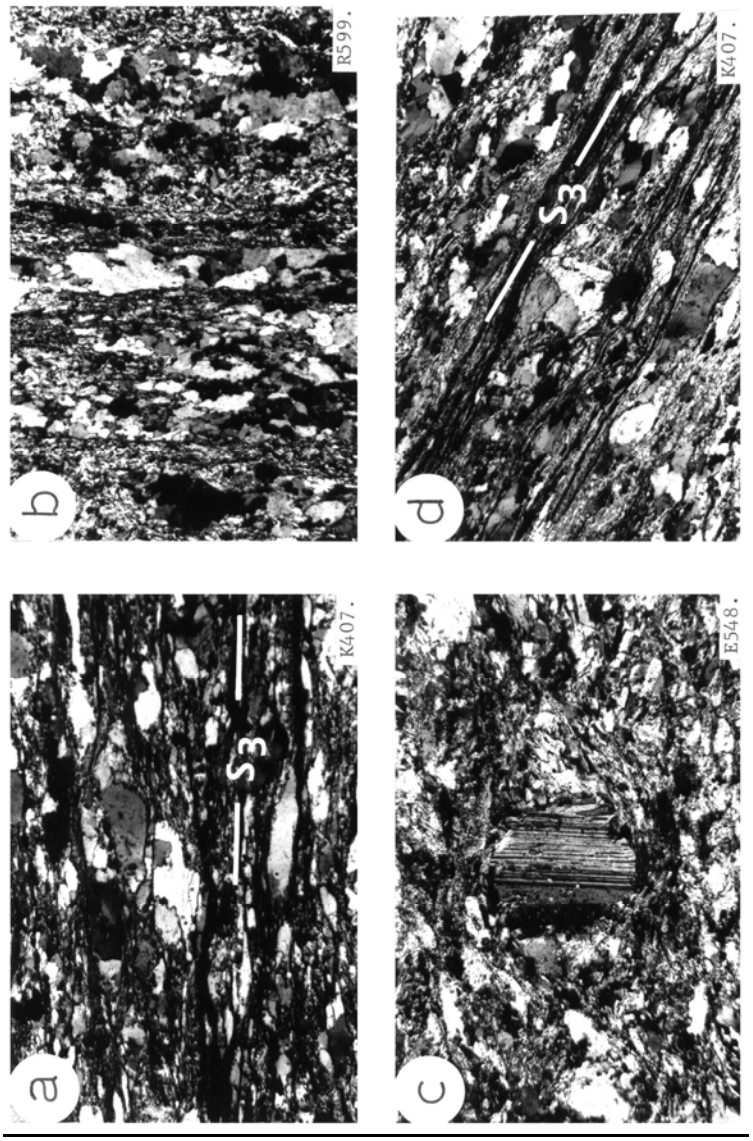

Figure 23 - Photomicrographs of mylonitic quartzite and quartzofeldspathic gneiss.
a. Loc. K407. Laminated mica quartzite with 0.5 mm strained quartz augen locally with internally sutured grain boundaries. The lenticular augen are separated and bounded by recrystallized mica, feldspar, and opaque minerals which together form a penetrative S_3 mylonitic layering. Some quartz augen have imbricated edges and others fine-grained tails containing recrystallized oriented muscovite which is continuous with the S_3 foliation. Rare feldspar augen are corroded and replaced by oriented (S_3) muscovite.
b. Loc. 8599. Quartzite mylonite defined by abrupt variations in the grain size of adjacent quartzose laminae. Here the S_3 foliation is vertical and is composed of the quartz-rich laminae with oriented mica and opaque minerals bounding them. Note the high degree of internal suturing of quartz grains composing the laminae.
c. Loc. E548. A rounded plagioclase porphyroclast in a quartzofeldspathic gneiss. Cracking and imbrication of the plagioclase and deformation of the polysynthetic twin lamellae occur at the margin of the porphyroclast which is surrounded by oriented mica crystals (S_3). The recrystallized feldspar+quartz tails contain oriented S_3 mica. Note scale here is 1.35 mm across.
d. Loc. K407. Lenticular quartz and feldspar augen with mica-rich tails flattened parallel to S_3. They are surrounded by opaque minerals and dark mineral films which may represent local injections of dark Calaveras argillite during formation of the Calaveras-Shoo Fly thrust. Note, in the central feldspar augen, the oriented opaque minerals which are truncated by S_3. They may be a vestige of S_2 or S_1 or, alternatively, may be S_3 rotated into this orthogonal position.

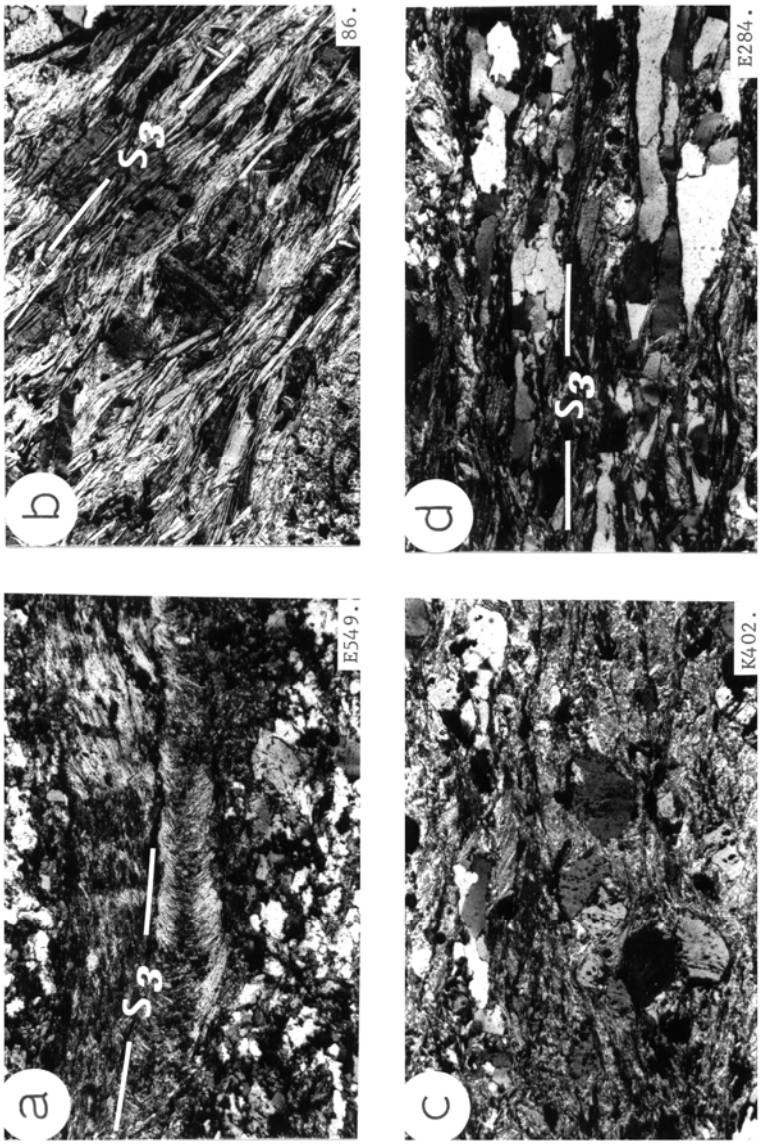

Figure 24 - Photomicrographs of mylonitic schist and phyllite.
a. Loc. E549. A localized 1 mm thick phyllonitic S_3 in quartzose schist is here composed of 0.01-0.05 mm microlites of finely intergrown muscovite, biotite, and graphite. The adjacent areas consist of recrystallized quartz, untwined plagioclase, muscovite, biotite, and chlorite with accessory garnet and tourmaline.
b. Loc. 86. Optically continuous augen of biotite is replaced and strongly overprinted by penetrative S_3 muscovite+biotite foliation. The augen possess frayed edges, dark internal deformation bands, and show evidence of intrafolial slip and concentration of opaque minerals. The remnant biotite predates S_3 and marks a regional metamorphic episode related to D_1 or D_2 deformation.
c. Loc. K402. Anastomosing S_3 foliation in porphyroclastic muscovite-quartz-plagioclase-biotite schist. The domains between the sinuous S_3 contain augen of quartz, feldspar, and mica. Note how the angular feldspar augen, which dominate the bottom two-thirds of the field of view, show a faint, truncated pre-S_3 fabric composed of oriented muscovite and opaque minerals. Quartz forms polygonized lenticles and ribbons and micas are largely recrystallized into a finely-intergrown phyllonitic matric between S_3 surfaces.
d. Loc. E284. Highly-laminated texture in mylonitic quartz-muscovite-chlorite-biotite schist is due to the S_3 mica foliation alternating with ribbons and augen of strained quartz. The 1 mm long quartz lenticles often occur with miniature lenticles adjacent to them. Phyllonitic muscovite+quartz+biotite intergrowths occur between the quartzose laminae.

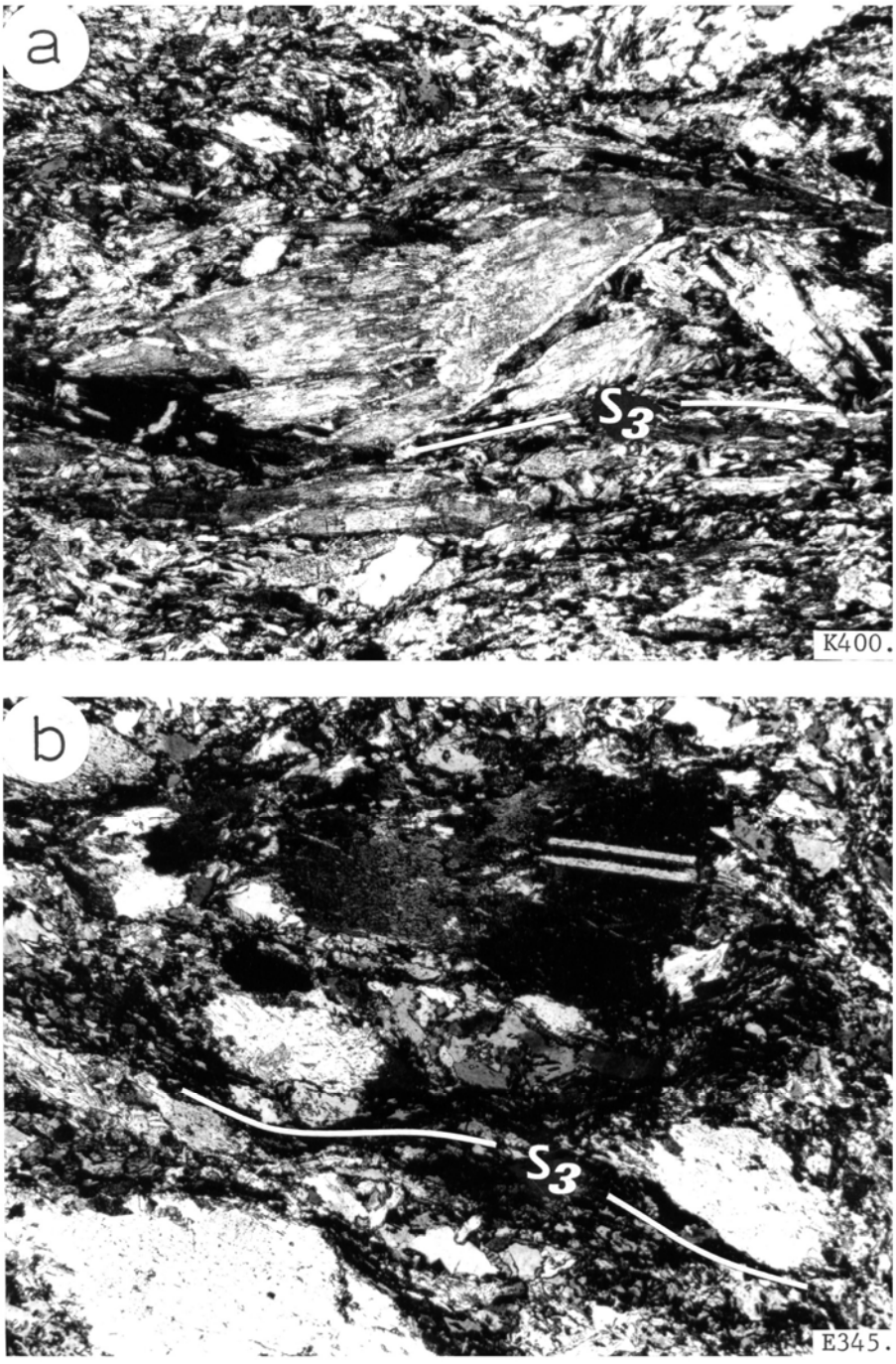

Figure 25 - Photomicrographs of mylonitic calc-silicate rocks.
a. Loc. K400. A colorless 2 mm strained augen of tremolite is bent with ragged edges and is cut by a penetrative S_3 foliation composed of recrystallized tremolite, quartz, calcite, plagioclase, and opaque minerals. At its margin, the tremolite is recrystallized to form a greenish amphibole and adjacent to the margin chlorite is concentrated. The large tremolite augen clearly predates S_3 and most likely formed during amphibolite-grade metamorphism during D_2 or D_1.
b. Loc. E345. Rounded, marginally recrystallized diopside augen flattened parallel to S_3 with recrystallized tails. The S_3 foliation is composed of recrystallized diopside, quartz, tremolite, biotite, plagioclase, and calcite which surrounds and locally crosscuts the augen. Note the deformation lamellae in the large diopside augen in the upper part of the view.

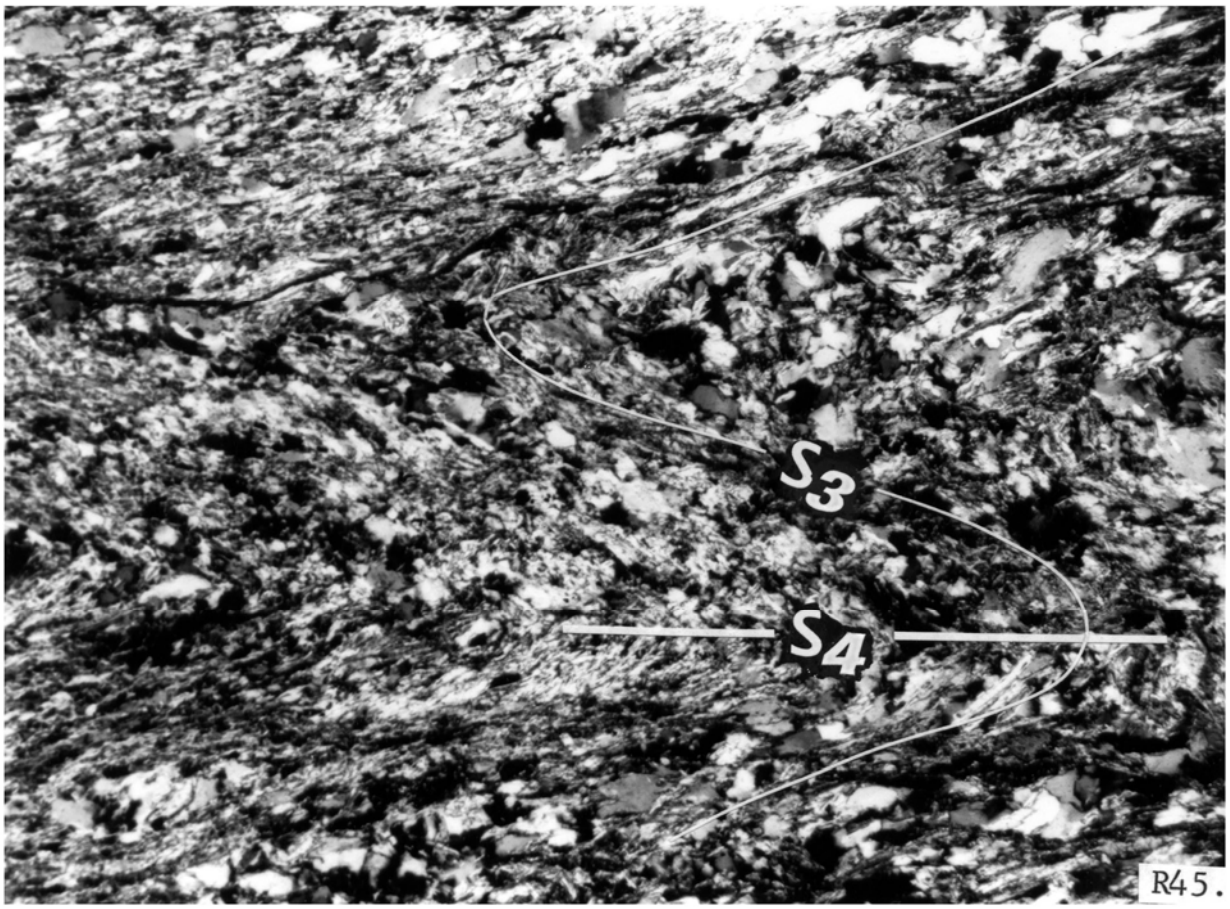

Figure 26 - Loc. R45. A tight F_4 fold of the S_3 mylonitic foliation in a quartz-biotite-muscovite phyllite. The S_4 foliation is composed of oriented biotite which formed parallel to the axial surface of F_4 folds. Older biotite within the highly flattened S_3 foliation is typically rimmed by retrograde chlorite. The chloritized S_3 biotite is deformed by F_4 and also cut by larger idioblastic S_4 biotite.

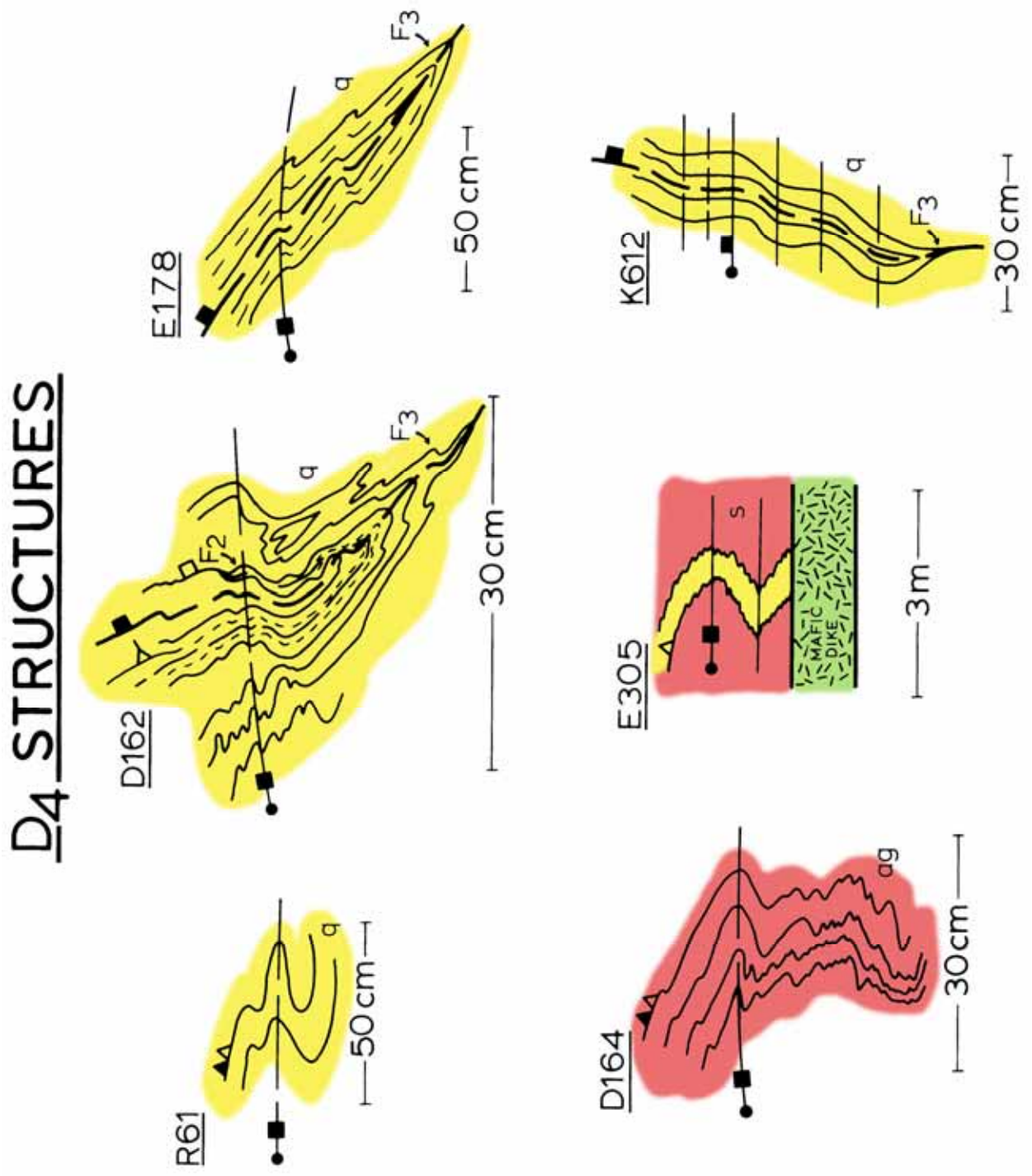

Figure 27 - Field drawings of D_4 structures in the Shoo Fly Complex of the Jupiter area. The D_4 structures, described in the text, consist of tight, asymmetric to isoclinal F_4 folds with a spaced S_4 axial surface mica foliation. F_4 and S_4 fold and cut older (F_3, F_2) fold hinges and related metamorphic fabrics and are themselves locally cut by dikes of the Sonora mafic dike swarm and F_5 and F_6 open folding episodes.

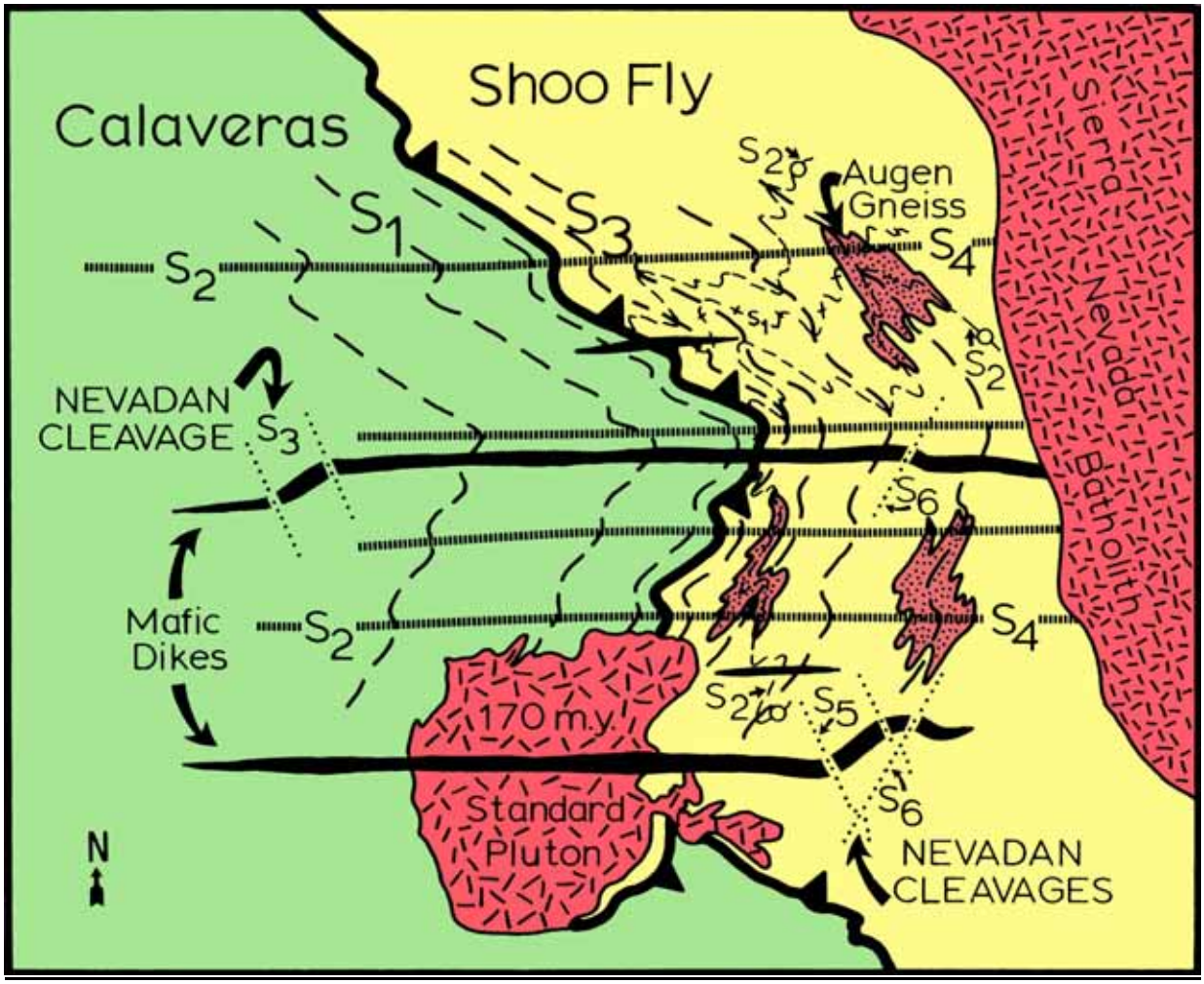

Figure 28 - Cartoon depicting the correlation and nomenclature of structural fabrics developed across the Calaveras-Shoo Fly thrust zone. Early folds and metamorphic fabrics in the Shoo Fly (S_1+S_2) are regionally truncated against the thrust and signify a tectonic history for the Shoo Fly that predates D_3 juxtaposition with the Calaveras. The regional parallelism of D_3 Shoo Fly (S_3) and Calaveras (S_1) foliations is due to the fact that D_3 thrusting marks the first in a series of tectonic events shared by both Paleozoic complexes. East-west folding of the thrust (dashed line = Shoo Fly (S_4) and Calaveras (S_2)), is followed by the middle Jurassic intrusion of the Standard pluton and by injection of mafic dikes (black). These igneous events are closely followed by folds and cleavage (dotted lines) developed during the Nevadan orogeny.

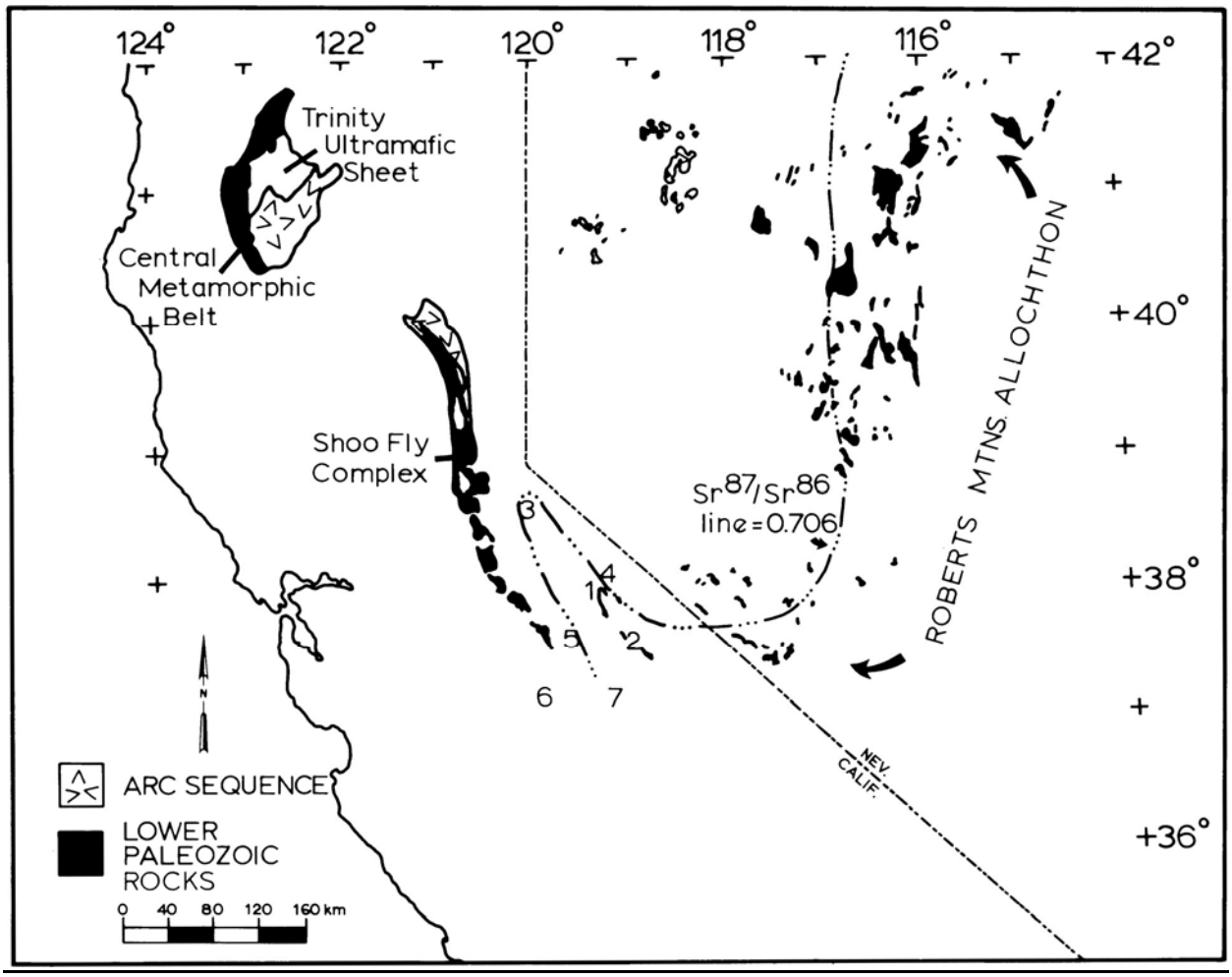

Figure 29 - Sketchmap of California and Nevada showing the distribution of the Shoo Fly Complex (black) and overlying upper Devonian arc volcanics. Lithologic correlatives of the Shoo Fly occur in the Roberts Mountains allochthon, in roof pendants of the Sierra Nevada batholith and in the central metamorphic belt of the Klamath Mountains. The 0.706 Sr^{87}/Sr^{86} isotopic line of Kistler and Peterman (1973, 1978), is inferred to mark the westward limit of buried Precambrian craton. Adapted from Schweickert, 1981.

LITHOLOGIC UNIT	DISTINGUISHING FEATURES	INTERPRETED PROTOLITH
Orthoquartzite	Massive with minor mica, pyrite, and dark quartz segregations; typically pure quartz; pebbly layers with quartz or bluish-quartz clasts.	Mature quartz sandstone with local chert lentils; local quartz- or chert-granule conglomerate.
Quartzofeldspathic Gneiss	Massive with schistose interlayers; plagioclase and/or orthoclase-rich; often micaceous; pebbly layers.	Subfeldspathic graywacke with pelitic intervals and local conglomerate.
Quartzite	White or dark-gray to black; massive to thinly-layered; very fine grained; no feldspar; minor mica; conchoidal fracture.	Chert and ribbon-chert.
Schist and Phyllite	Two-mica plagioclase schist and phyllite; pyritic and graphitic zones; dark quartz lentils, stringers, and layers; angular to to rounded pebbly layers.	Pelitic sediments with quartz sandstone and chert lenses and layers; periodic euxinic conditions; local breccia and conglomerate.
Calc-Silicate and Marble	Diopside-biotite-calc-silicate rock; locally graphitic calcite and dolomite marble, and siliceous marble. Only associated with quartzite.	Limestone, dolostone, and calcarenite.
Amphibolite	Elliptical areas 10-15 cm thick.	Mafic volcanic breccia.

Table 1 - Interpretive pre-metamorphic protoliths of the Shoo Fly Complex of Tuolumne and Mariposa Counties, California based upon distinguishing mineralogic and stratigraphic criterion. The gneissic granitoids are omitted since they are of plutonic parentage.

Table 2 - GEOLOGIC HISTORY OF THE JUPITER AREA TUOLUMNE COUNTY, CALIFORNIA

Holocene	Upland are affected by periglacial solifluxion.
Pleistocene	Accelerated uplift and development of trellised, deeply-incised, rejuventated stream system
Mio-Pliocene	I_8 Mudflow breccia ad volcanic flows of the Relief Peak Formation.
Oligo-Miocene	I_7 Rhyolitic ash flows of the Valley Spring Formation.
Eocene	Planation surface developed after post-Cretaceous uplift and erosion. Formation of consequent stream system.
Cretaceous	I_6 Intrusion of Sierra Nevada batholith and possibly other plutons.
Late Cretaceous (?)	D_7 N60°W to E-W, 90° fracture cleavage (S_7) parallel to axial surfaces of open F_7 folds.
Late Jurassic(?)	D_6 N30°E, 90° crenulation cleavage, black residue cleavage (S_6) parallel to axial surfaces of asymmetric open F_6 folds. Retrograde metamorphism.
NEVADAN OROGENY Late Jurassic	D_5 N32°W, 78°NE crenulation cleavage, black residue cleavage (S_5) parallel to axial surfaces of asymmetric open F_5 folds. Retrograde metamorphism.
Middle Jurassic(?)	I_5 Intrusion of the Knight Creek and possibly other plutons
Middle Jurassic	I_4 Intrusion of 159-157 m.y. Sonora dike swarm, sub-parallel to S_4.
Middle Jurassic	I_5 Intrusion of 170-164 m.y. Standard, Parrotts Ferry, and possibly other plutons.
Late Triassic(?)	D_4 N85°W, 90° spaced mica schistosity and crenulation cleavage (S_4) parallel to axial surfaces of isoclinal, tight, and crenulate F_4 folds plunging 47° into S85°E. Biotite-garnet grade metamorphism.
Permo-Triassic (?)	I_2 Intrusion of granitoid dikes and sills. Some foliated sills are late-syntectonic with respect to D_3

SONOMA OROGENY? Permp-Triassic (?)	D_3 Formation of the Calaveras- Shoo Fly thrust zone and intra-Shoo Fly ductile shear zones. Blastomylonitic foliation (S_3) parallel to the axial surfaces of isoclinal and rootless folds (F_3) plunging 42° into S75°E. There is significant tectonic imbrication within 2 km of the fault. The obliterative D_3 thrust fabric becomes a domainal blastomylonite and a mica foliation eastward from the thrust zone formed parallel to the axial surfaces of isoclinal to tight F_3 folds. Epidote-amphibolite grade metamorphism.
ANTLER OROGENY? Middle Paleozoic	D_2 Mica foliation and flattening foliation (+mylonite) (S_2) parallel to axial surfaces of isoclinal and rootless folds (F_2) with variable plunges. Folding and recrystallization of granitoid gneiss – Shoo Fly contacts. Amphibolite grade metamorphism.
Siluro-Ordovician to Permian (?)	I_1 Intrusion of protoliths of the gnessic granitoids as plutons into the Shoo Fly. Compositions range from mainly granite, granodiorite, and syenite to gabbro. Intrustive contacts are discordant, cutting the S_1 metamorphic layering.
ANTLER OROGENY? Pre-Silurian (?)	D_1 Metamorphic layering (S_1) in quartzite and quartz-mica-(feldspar)-gneiss parallel to axial surfaces of intrafolial and long-limbed isoclinal folds (F_1). Biotite grade metamorphism.
Late Precambrian (?) to Early Paleozoic	Deposition as a slope-rise sequence adjacent to the western edge of the North American miogeosyncline.

Table 2 - An interpretive geologic history of the Shoo Fly Complex of Tuolumne County, California. Numbered deformational (D_x) and igneous (I_x) events are listed in order of relative age based upon field relationships and geochronologic age data of Sharp and Saleeby (1979); Sharp (1980); Sharp and others (1982; in press), and Stern and others (1981). The absolute ages of the various D-events will be subject to change as more isotopic data becomes available.

DISTINCTIVE FEATURES OF D_3 DEFORMATION IN THE SHOO FLY COMPLEX

Rootless, isoclinal, to tight F_3 folding

Formation of ellipsoidal slivers of Shoo Fly rocks sheathed in mylonite and blastomylonite, flattened parallel to S_3 and elongated parallel to F_3 and L_3

Ductile transposition of $S_1 + S_2$ metamorphic layering and domainal recrystallization

Syn-metamorphic imbricaticn of Calaveras and Shoo Fly rocks

Formation of zones and seams of blastomylonite, mylonite, and ultramylonite, and injections of protocataclasite, and pseudotachylyte

Grain-size reduction, silicification, and general darkening of rock

Table 3 - Distinctive features of D_3 deformation in the Shoo Fly Complex.

	FEATHER AND YUBA RIVER AREA, D'Allura and others, 1977 (40° N - 39°15' N)	BOWMAN LAKE SEQUENCE, Girty and Schweickert, 1983c (39°30' N)	NORTH FORK AMERICAN RIVER, Harwood, 1980 (39° N)	NORTHWESTERN SIERRA NEVADA, Clark, 1976 (39°45' N - 38°30' N)	THIS REPORT (38°05' N - 37°30' N)
LITHOLOGY	Subfeldspathic lithic sandstone, quartz sandstone, shale with subordinate conglomerate, limestone, dolomite, chert, volcanics.	Subfeldspathic quartzose sandstone, quartz arenite, slate, chert-clast diamictite, bedded chert, calc-arenite.	Quartzose sandstone, quartz granule conglomerate, graywacke, slate, ribbon chert, lenses of limestone, dolostone.	Feldspathic quartz-rich sandstone, tuffaceous sandstone with graywacke texture, slate or very fine tuff with subordinate thin-bedded chert, mafic volcanic rocks, dolomite, limestone, conglomerate, breccia.	Quartzite, quartzofeldspathic gneiss, schist, phyllite with subordinate chert- and quartz-pebble conglomerate layers, calc-silicate rock, calcite and dolomite marble ± quartz, rare amphibolite.
RELATIVE ABUNDANCES OF MAJOR LITHOLOGIES	Graywacke> Quartz sandstone> Shale> Limestone and Dolomite.	Graywacke> Quartz arenite> Shale> Calc-arenite.	Quartzose sandstone> Slate> Graywacke> Chert> Limestone and Dolostone.	Graywacke> Quartz arenite> Slate> Calc-arenite.	Quartzite> Quartzofeldspathic Gneiss> Schist> Calc-silicate and Marble.
SMALL-SCALE STRATIGRAPHIC FEATURES	Conglomerate	Conglomerate	Quartz granule conglomerate	Conglomerate, pebbly mudstones, intraformational breccia	Chert and quartz pebble conglomerate, breccia
	Chert	Rhythmically-bedded radiolarian chert	Ribbon chert	Thin bedded chert	Massive to thinly-layered quartzite
			Dark slate with ribbon chert	Dark gray slate with chert	Dark quartz (meta-chert) lentils and layers in schist and quartzite (*)
	Graded beds, graywacke layering	Graded beds, flute casts, rip-up clasts, cross-lamination	Graywacke layering	Graywacke layering	Interlayed schist and and quartzofeldspathic gneiss
	Volcanic mudflow breccia	Mafic to intermediate volcanic rocks		Mafic volcanic rocks	Amphibolite
				Felsite dikes with quartz and feldspar phenocrysts	Felsic dikes with quartz phenocrysts

(*) - Also described by Diller (1908) at the type-locality.

Table 4 - Comparison of lithologic and small-scale stratigraphic features of the Shoo Fly Complex reported from the western Sierra Nevada metamorphic belt. The along-strike similitude of the Shoo Fly Complex is striking when compared to the interpretive pre-metamorphic lithologies of the study area (see Table 1). Terminology of the cited reports have been accurately recorded and have not been interpreted.

PLATES (As separate downloadable .pdf files)

Plate 1 - Bedrock geologic map of the Shoo Fly Complex in the Jupiter area, Tuolumne County, California. Map scale = 1:24,000.

Plate 2 - Contrasting style of D_3 folds and structures in the vicinity of the Calaveras-Shoo Fly thrust in the Jupiter area, California. F_3 folds were plotted as a function of relative distance from the thrust zone. Symbols are domainal when dashed. Square symbols indicate axial surfaces of folds. Horizontal scale indicated beneath drawings. Note how the F_3 folds become increasingly tighter with increased transposition and shearing of S_2 and S_1 upon approaching the thrust contact. Also note the local development of S_3 shear-bounded ellipsoidal slivers of foliated Shoo Fly lithologies, domainal seams of mylonite, and the presence of late-syntectonic granitoid injections.

Plate 3 - Locality index map (1:62,500 scale). Field localities are identified in the text and illustrations by stream, field station number, and lithology (i.e. - Loc. 8588 means field number 588 on Rose Creek). MF=Middle Fork Stanislaus River, U=unnamed creeks north of Stony Gulch, S=Stony Gulch, K=Knight Creek, E=Eagle Creek, DR=Dry Creek, D=Deer Creek, SF=South Fork Stanislaus River. Lithologies are q=quartzite and quartzofeldspathic gneiss, ag=gneissic granitoid, s=schist and phyllite, c=calc-silicate and marble, m=mafic dike, g=foliated granitoid sill.

Plate 4 - Detailed structural map of the Calaveras-Shoo Fly thrust zone illustrating the progressive transposition of S_2, S_1, and S_0 into parallelism with S_3 as well as the postions of fault-bounded slivers of Shoo Fly and Calaveras rocks and foliated, late-syntectonic granitoid sills.

APPENDIX 1

Descriptions of metamorphic rocks of the Shoo Fly Complex in the Jupiter area, Tuolumne County, California.

The Shoo Fly is subdivided not five major metasedimentary and metaigneous mappable units however the original stratigraphic relationships between the metasedimentary units is unknown due to extensive folding, shearing, and metamorphism.

The major units and their sub-units are listed below in order of decreasing map area. Minerals listed in order of decreasing relative abundance. Those minerals listed in parentheses are not found in all exposures.

Quartzite and quartzofeldspathic gneiss unit (LPzq) - a heterogeneous sequence of light- to dark-gray to brown- to maroon-weathering, generally gray-colored, massive to thickly-layered and slabby but locally highly laminated, fine- to coarse-grained quartzite, granoblastic quartz-mica and quartzofeldspathic gneiss, and black vitreous quartzite. The following four sub-units have been recognized:

1) light- to dark-gray, to white- to cream-colored, massive to well-layered biotite-muscovite-(chlorite)-(plagioclase)-(opaque) quartzite and vitreous biotite-opaque-(muscovite)-(chlorite)-(plagioclase)-(orthociase)(calcite) quartzite.

2) gray, well-layered quartz-plagioclase-biotite-muscovite-orthoclase)-(chlorite)-(garnet)-(tourmaline)-(zircon) gneiss. Locally the quartz grains have a bluish tint.

3) gray, well-layered to highly-foliated, quartz-muscovite-biotite(plagioclase)-(opaque)-(garnet)-(chlorite) gneiss and quartz-plagioclase-orthoclase-biotite-muscovite gneiss.

4) black to dark-gray, massive to thinly-layered to highly laminated, vitreous non-feldspathic opaque-(muscovite) quartzite with conchoidal fracture and radiating extinction (met a-chert?). Quartz typically comprises over 95% of the rock. Lentils and layers of this sub-unit occur within all metasedimentary units.

Gneissic granitoid metaplutonic unit (LPzag) - a compositionally variable assemblage of tan-, white-, and gray-weathering, white to dark gray, fine- to coarse-grained, massive hypidiomorphic-granular to highly foliated granitic, syenitic, and gabbroic orthogneiss typically with feldspar porphyroclasts set in a finer-grained recrystallized matrix. Felsic and alkalic rocks are most abundant although melanocratic internal zonations are common. The following three types have been recognized although transitional lithologies occur:

1) potash felspar-quartz-plagioclase-biotite-muscovite-(chlorite)(hastingsite)-(epidote)-(garnet)-opaque-(apatite)-(allanite)-(zircon) granite gneiss and quartz-plagioclase-muscovite-potash feldspar-(biotite)(chlorite)-(epidote)-(apatite)-(zircon) granodiorite and diorite gneiss. The potash feldspar commonly occurs as perthite and is locally myrmekitic.

2) perthite-hastingsite-plagioclase-biotite-(psilomelane)-(quartz)(epidote)-(opaque)-(allanite)-(sphene)-(zircon) syenite gneiss.

3) magnesian hornblende-epidote-plagioclase-biotite-(quartz)(chlorite)-(opaque)-(apatite) gabbro gneiss.

Schist unit (LPzs) - a heterogeneous sequence of brown- to gray weathering, tan to light-gray to dark-gray to black, well-foliated, medium- to coarse-grained schist, schistose gneiss, and phyllite. The following four sub-units have been recognized:

1) quartz-muscovite-biotite-plagioclase-(orthoclase)-(chlorite)(tremolite)-(calcite)-(garnet)-(graphite)-(tourmaline) schist and schistose gneiss.

2) quartz-plagioclase-muscovite-biotite-(chlorite)-(garnet) schistose gneiss.

3) biotite-muscovite-quartz-(plagioclase)-(orthoclase)-(garnet)-(chlorite)-(graphite)-(pyrite) schist and phyllite, and,

4) muscovite-biotite-quartz-(plagioclase)-biotite-(opaque) schist.

Calc-silicate and marble unit (LPzc) - a heterogeneous assemblage of calcareous rocks of diverse mineralogy and texture consisting of brown-, tan-, and green-weathering, light- to dark-green to gray-green to whitish well-layered, fine- to medium-grained calc-silicate rock, calcite and dolomite marble, and siliceous marble. The following four sub-units have been recognized:

1) dark-green to black-green, diopside-biotite-orthoclase-quartzplagioclase-(chlorite)-(muscovite)-(calcite)-(epidote)(apatite)-(sphene)-(zircon) calc-silicate rock.

2) light-green to dark-green, diopside-quartz-biotite-plagiociase(calcite)-(apatite)-(zircon) calc-silicate rock.

3) light-green, quartz-diopside-plagioclase-(tremolite)(vesuvianite)-(calcite)-(sphene) calc-silicate rock.

4) whitish to light-green, calcite-(dolomite)-quartz-muscovite(plagioclase)-biotite-graphite marble.

Amphibolite unit (LPza) - two exposures of green-weathering, green, crudely-foliated amphibolite were found in the study area. They are medium-grained hornblende-plagioclase-biotite-quartz-epidote-opaque amphibolite and amphibolitic gneiss.

CHAPTER 2

Paleozoic gneissic granitoids in the Shoo Fly Complex, central Sierra Nevada, California

ABSTRACT

Paleozoic gneissic granitoids are an important lithologic component of the Shoo Fly Complex of the central Sierra Nevada, California. Field relations, petrographic, and geochemical studies indicate that the gneisses were intruded as a series of plutons ranging from gabbro (oldest) to granite and granodiorite (median age) to syenite (youngest) with the granitoid types predominating. Compositionally they express a calcalkalic to alkalic rock suite. The plutons and related smaller injections truncate an early S_1 foliation in the Shoo Fly and were isoclinally folded and foliated under peak epidote-amphibolite grade conditions during regional D_2 and D_3 events.

During D_2 and D_3, the gneissic granitoids were penetratively deformed into augen gneiss, blastomylonite, and ultramylonite. The gneisses contain porphyroclasts of feldspar, quartz, mica, and amphibole, and granitic aggregates, surrounded by an anastomosing foliation of quartzose ribbons and recrystallized quartz, feldspar, amphibole, mica, and stilpnomelane. Later deformations (D_4-D_7) typically involved open folding with a spaced biotite schistosity (S_4) and non-penetrative cleavage (S_5, S_6, S_7) with recrystallization of older fabric elements.

Available geochronologic data (Sharp and others, 1982) suggests that the protoliths of the gneissic granitoids were intruded between middle Ordovician and late Devonian time, thus establishing a pre-late Devonian depositional age for the Shoo Fly Complex. D_1 and intrusion of the orthogneiss protoliths may have been precursors of the Late Devonian to Early Mississippian Antler orogeny or, alternatively, may have occurred significantly earlier than the Antler orogeny. Collectively, the gneisses may mark the remnants of a Paleozoic plutonic belt as their protoliths consisted of I-type, rather than S-type granitoids.

INTRODUCTION

The lower Paleozoic Shoo Fly Complex of the foothills metamorphic belt of the Sierra Nevada is intruded on the east by Mesozoic granitic rocks of the Sierra Nevada batholith and on the west is in thrust contact with upper Paleozoic-lower Mesozoic(?) chaotic rocks of the Calaveras Complex (Fig. 1) (Merguerian and Schweickert, 1980; Schweickert, 1977, 1981). Between lats. 37°45'N and 38°30'N, numerous bodies of gneissic granitoid are intimately associated with metasedimentary rocks of the Shoo Fly Complex (Fig. 2) (Schweickert and Merguerian, 1980; Merguerian, 1984). The orthogneisses consist predominantly of granite, granodiorite, and syenite with lesser amounts of gabbro.

This chapter reports on the geochemistry, petrography, and structural geology of the granitoid gneisses found in the Shoo Fly Complex of the Stanislaus River drainage in California. For this report, fieldwork was augmented by petrographic and XRF major-element geochemical studies of selected orthogneiss bodies. U-Pb and Rb-Sr ages and isotopic data of Sharp and others (1982, and in press) together with structural, petrographic, and geochemical data of this report, provide the first evidence for abundant Paleozoic plutonism in the Shoo Fly Complex. The tectonic significance of the deformed granitoid gneisses is evaluated on the basis of available evidence.

Previous Work. Gneissic granitic rocks were first noted in the North Forks of the Mokelumne and Tuolumne rivers by Turner (1894, 1896) during folio mapping of the Mother Lode gold belt. As a result of collaboration with C.R. Van Hise, who compared them with Archean rocks of the Lake Superior region, Turner (1896) and then Turner and Ransome (1898) suggested that the gneissic and schistose bands associated with quartzite in the Big Trees area (Shoo Fly Complex of this report) were Precambrian and were derived from igneous materials.

Although the gneisses were not mapped separately from undeformed granodiorites, Turner and Ransome (1898) distinguished two small masses of syenite on Rose Creek that we recognize as a part of the gneissic complex. The gneissic granitoids received no further study until Schweickert and others (1977) and Schweickert (1979) recognized them as being distinct from, and older than, undeformed Mesozoic granitic rocks in the Stanislaus River drainage.

Schweickert and Merguerian (1980), and Merguerian (1984) reported that the gneissic granitoids represent complexly deformed plutonic masses that were intruded into the Shoo Fly Complex early in its structural history but following an early dynamothermal episode. U-Pb and Rb-Sr ages ranging from about 275 to 450 m.y. reported by Sharp and others (1982; in press) from several samples of the gneissic granitoids indicated that they represent one or more episodes of Paleozoic plutonic activity, possibly ranging as far back as Middle Ordovician times.

Regional setting. Augen gneiss, intimately associated with the Shoo Fly Complex, occurs in the Mokelumne, Stanislaus, Clavey, and Tuolumne River drainage basins (Fig. 1). The augen gneiss appears to be most widely developed in the Stanislaus River drainage, and here we have mapped the gneisses in greatest detail (Fig. 2).

The Shoo Fly Complex, the host for the Paleozoic granitoids, is a metamorphosed sequence of quartzite, quartzofeldspathic gneiss, mica-garnet schist, calcite and dolomite marble, calc-silicate rocks, and rare amphibolite (Fig. 3). The Shoo Fly has endured a protracted deformational history, involving seven deformational events, each with distinctive structures and metamorphic fabrics (Table 1). The first four of these deformational events (D_1-D_4) involved ductile deformation and in many places were accompanied by the formation of zones and seams of mylonite. The last three events (D_5-D_7) were dominantly brittle in nature, were

non-penetrative and were accompanied by retrograde metamorphism and open folds of older fabric elements.

The gneissic granitoids were intruded as a series of plutons, stocks, sills and veins after the D_1 phase of Shoo Fly deformation and were subsequently involved in all later deformational events (see Chapter 1).

THE GNEISSIC GRANITOIDS

Form and evidence for intrusive origin

Granitoid gneisses compose roughly 40% of the Shoo Fly Complex and are found in contact with all lithologic units (Fig. 3). The foliated gneiss bodies of the Stanislaus River drainage range in size from 8-10 km-long masses that show complex internal zoning (Fig. 3) to meter-scale sills, stocks, and veins, and to centimeter-scale lit-par-lit injections. The larger bodies are commonly lenticular in shape and are composed of fine- to coarse-grained rocks that locally exhibit well preserved hypidiomorphic-granular and porphyritic textures. More typically, however, the gneisses are strongly deformed by numerous foliations, folds, and superposed cleavages.

A plutonic origin for the gneisses is indicated by the following features:

1) locally preserved discordant contacts,

2) discordant internal contacts and compositional zoning, and,

3) the presence of xenoliths and screens of wall rocks within the gneissic bodies.

Each of these will be discussed below.

At many field localities the gneissic granitoid contacts are irregular and truncate the S_1 layering in the Shoo Fly at a low angle although local high-angle relationships exist. Elsewhere, bosses and veins of gneiss cut the S_1 layering in quartzite, schist, and calcsilicate rock, F_1 folds in schist are crosscut by a 15 cm vein of gneiss, and long-limbed F_1 isoclines in both vitreous quartzite and mica schist are truncated. Many of the smaller bodies are sill-like masses up to 4 m wide that grade marginally into zones of lit-par-lit injection. Foliated xenoliths are commonly elongate parallel to S_1 and sill like lenses of gneiss up to 10 m wide permeate along the S_1 foliation. In the Shoo Fly wall rocks the S_1 fabric apparently had a strong controlling influence on the initial form of the intrusions generating sheet-like, rather than equidimensional bodies (Fig. 3).

On the North Fork Stanislaus River (Fig. 3) undeformed protoliths of the gneisses are locally well-exposed. Here, homogeneous biotite-hornblende granodiorite has a faint, northwest-trending igneous foliation (Fig. 4) defined by alignment of biotite flakes and hornblende prisms. This rock resembles Mesozoic granodiorite of the Sierra Nevada batholith. However, local mylonitic shears are widely spaced in the interior of the body, and as the southern margin is approached, the shears become more closely spaced. These shears eventually transpose the hornblende-biotite foliation into a west-northwest trending gneissic foliation. The southern part of the body is granodiorite gneiss, whose contact with Shoo Fly quartzite is transposed parallel to the gneissic fabric. However, at the northern contact of the granodiorite, dikes and intrusive sheets of granodiorite intrude a slightly older alaskite body. Just north of the alaskite, another narrow mass of granodiorite cut by sporadic mylonitic shears discordantly intrudes Shoo Fly quartzite. All of the prebatholithic rocks are cut by an Upper Jurassic mafic dike swarm (Fig. 4, Table 1).

In the larger internally zoned bodies, sharp contacts between chemically and petrographically distinct phases of gneiss are interpreted as a vestige of primary igneous zonation. In upper Rose Creek (Loc. 8240; Figs. 3, 5 - herein all numbered localities are field stop numbers found in Plate 3) xenoliths of granitic gneiss with blocky outlines and gradational margins are engulfed in syenite gneiss. Floating within the syenite gneiss are wisps and xenocrysts of granitic gneiss. Both gneisses are foliated and locally sheared.

The gneisses commonly enclose foliated subequant, angular to elongate (up to 2 m) xenoliths and screens of metasedimentary rocks of the Shoo Fly Complex. Smaller xenoliths (<0.5 m) are typically wispy with diffuse margins or highly injected with gneissic rock parallel to S_1. In addition, chilled marginal facies, permeated and discordant intrusive contact, veins, and scattered apophyses of gneiss crosscut the oldest metamorphic fabric (S_1) in the Shoo Fly (Fig. 6). The early S_1 foliation is locally preserved as oriented mica forming the axial surfaces of isoclinal F_1 folds. Structures related to the folds can not be traced into the gneissic granitoids, rather, the S_1 foliation is truncated along the contact of the gneiss. Mixed zones of augen gneiss and metamorphic country rock are common near the margins of the larger bodies but are not reproducible at the scale of Figure 3 or Plate 1.

These relations indicate that the gneisses represent discordant intrusions that locally involved injection of different batches of magma, and that they pried off fragments of foliated wall rocks. However, in many of the smaller, highly deformed bodies, evidence of this kind is no longer preserved.

The gneisses of the Stanislaus River drainage consist of three petrographically and geochemically distinct types, mafic gneiss, granitic to granodioritic gneiss, and syenitic gneiss. The granitic gneiss, the most common rock type, postdates the mafic gneisses and predates the

syenitic gneisses. For example, in upper Rose Creek (Loc. E216) 700 m downstream from the locality illustrated in Figure 5, granitic gneiss clearly crosscuts an older gabbroic gneiss body which, in turn, truncates S_1 in the Shoo Fly Complex. All of the gneisses share the same post-D_1, pre-D_2 structural relationship with the Shoo Fly.

The following sections describe the lithology, petrography, and geochemistry of the three types of gneiss, from oldest (gabbroic gneisses) to youngest (syenitic gneisses). We recognize that probable metasomatic exchange with the country rocks during polyphase deformation occurred and that "igneous" compositions reported in Table 2 may indeed reflect metamorphic and/or hybrid metamorphic-igneous compositions. Samples were carefully selected for analysis from xenolith deficient regions well-within the borders of orthogneisses. Detailed lithologic descriptions of the gneisses appear in Appendix 1 and modes calculated from stained slabs appear in Table 3.

Group 1 - Gabbroic gneiss

Lithology. This group is only locally represented with relatively few examples of undeformed protolith recognized in the study area. Group 1 gneisses are green in weathered and fresh color and vary from medium- to coarse-grained massive and dense hypidiomorphic to well-foliated rocks consisting of amphibole, plagioclase, epidote, and biotite with subordinate quartz, chlorite, and opaque minerals.

The gabbroic gneisses are typically well-foliated with amphibole augen separated and surrounded by a highly laminated foliation consisting or recrystallized amphibole, plagioclase, and epidote.

Petrography. The gabbroic gneiss is commonly mylonitic with porphyroclasts of magnesian hornblende up to 9 mm in length (Fig. 7a). The augen have cores of relict(?) igneous

brown amphibole that are cracked and highly-dusted with Fe and Ti oxides. The brown amphibole cores are optically continuous with, and mantled by, recrystallized clear to green magnesian hornblende of metamorphic origin (B-, 2V=70°). The composite amphiboles occur as porphyroclasts embedded in a foliated matric composed of untwined plagioclase, epidote, and magnesian hornblende with subordinate biotite, chlorite, quartz, apatite, and opaque minerals (Fig. 7b). This foliation cuts and locally recrystallizes that metamorphic green hornblende. Epidote always occurs in reaction relationship with plagioclase and its abundance (N30x) suggests albitization of originally calcic plagioclase during deformation of the Shoo Fly host rocks.

Geochemistry. Only one example of this lithology has been analyzed (#216 - solid triangle in Table 2 and Figs. 8, 9, 10). Compared to published analyses of Nockolds (1954), sample 216A resembles average alkali gabbro and gabbro except for its relative enrichment in Fe_2O_3 and Na_2O and relative depletion in MgO (Fig. 9, Table 4). As indicated in Fig. 10, sample 216A plots close to the gabbroic rocks of Table 4 on Na_2O-K_2O-CaO, normative Ab-Or-Q, and AFM diagrams.

Group 2 - Granitic to granodioritic gneiss

Lithology. The Group 2 gneisses are a texturally and compositionally variable assemblage of white- to gray- to tan-weathering, white to dark-gray, fine- to coarse-grained, massive hypidiomorphic and weakly foliated but typically strongly foliated and locally lineated granitoid rock. This group, which predominates over the Group 1 or 3 gneisses (Fig. 8), consists of rocks of granitic composition (locally melano- and leucocratic) but granodiorite and rare diorite occur. The rocks commonly contain augen of potash feldspar and to a lesser degree

plagioclase and granitoid rock, which are separated and surrounded by a foliation composed of recrystallized quartzose ribbons (± fine-grained plagioclase), biotite and muscovite (Table 3).

Petrography. The augen gneisses and less-deformed granitoids of Group 2 are composed of potash feldspar, oligoclase, quartz, biotite, and muscovite with accessory chlorite, epidote, hastingsite, calcite, zircon, apatite, allanite, magnetite, and pyrite.

Potash feldspars are often perthitic and sometimes twinned; local myrmekite occurs. Some perthites contain exsolution lamellae of polysynthetically twinned albite (Fig. 11a) or enclose equant polysynthetically twinned and inclusion-zoned plagioclase. The equant plagioclase and host perthite may mark original igneous equilibrium textures. The oligoclase is subhedral to anhedral is mostly untwined and highly recrystallized.

Biotite and muscovite occur as large subidioblastic flakes between recrystallized feldspar and quartz. The micas are partly to wholly recrystallized at their edges and replaced by fine-grained mica that forms, together with quartz and feldspar, a penetrative foliation. The biotite is commonly replaced by chlorite and rimmed by magnetite.

Geochemistry. The gneisses of Group 2 (solid circles in Table 2, Figs. 8, 9, 10) range from 70.47% to 73.73% silica and are similar in major element chemistry to average granite and granodiorite (Nockolds, 1954) and quartz monzonite of the Sierra Nevada batholith (Bateman and others, 1963) except for enrichment in Fe_2O_3 and depletion in CaO and alkalis (Fig. 9, Table 4). CIPW normative calculations (Table 2) indicate a peraluminous character with normative corundum (c) values of 0.53-2.25. In the Ab-Or-Q diagram (Fig. 10) the Group 2 gneisses cluster near the published analyses of Table 4 and within frequency distribution contours of over 570 granites reported by Tuttle and Bowen (1958). The Na20-K20-CaO and AFM diagrams illustrate depletion of CaO and alkalis in the Group 2 gneisses compared to published analyses.

The low alkalis and CaO content of the gneisses may be due in part to assimilation of non-calcic Shoo Fly rocks but has been strongly influenced by metamorphism to lower amphibolite grade (to be discussed below).

Group 3 - Syenitic gneiss

Lithology. The group consists of dark-gray to green-gray, medium to coarse-grained, massive hypidiomorphic, to fractured and veined, to highly foliated, syenite, hastingsite syenite, quartz syenite, and syenitic gneiss (Table 3). The syenite gneisses are dominantly coarse grained but in mylonite zones marked reduction in grain size to form finely-laminated textures occurs. The laminations are composed of segregated potash feldspar, amphibole, and minor amounts of biotite, and quartz.

Petrography. The syenitic gneisses are composed of potash feldspar with subordinate plagioclase, hastingsite, biotite, stilpnomelane, and accessory quartz, apatite, epidote, sphene, zircon, allanite, and opaque minerals. The potash feldspars are characteristically perthite and micro-perthite and occur as subhedral crystals to rounded porphyroclasts up to 6 mm in size (Fig. 12a). They are commonly mantled and separated by smaller, highly-recrystallized untwined potash feldspar. Twinned plagioclase also occurs but is markedly subordinate to perthite and mafic minerals comprise 13% or less of the mode (Table 3). The perthitic textures found in the Group 2 and 3 gneisses suggest original sub-solvus exsolution at $pH_2O \leq 5$ kbars. This might place the intrusion of these orthogneiss protoliths at crustal depths less than 15 km. Hastingsite is commonly xenoblastic and occurs between potash feldspars. At their margins the hastingsite is often recrystallized into acicular crystals that form a through-going foliation or anastomosing thin veins. Biotite and stilpnomelane always occur in domains rich in hastingsite.

Geochemistry. The Group 3 gneisses (solid squares in Table 2, Figs. 8, 9, 10 range from 60.29% to 67.04% silica. The gneisses, although sub-calcic, are similar to ferrohastingsite syenite (526) and aegerine syenite (240) and to average syenites reported by Nockolds (1954). The two analyses in Table 2 are from separate bodies (Fig. 8). They plot along with the published syenite compositions of Table 4 near the quartz-deficient edge of the Ab-Or-Q diagram (Fig. 10). The gneisses also plot close to published syenites on the Na_2O-K_2O-CaO and AFM diagrams except for their relative CaO depletion and alkali enrichment, respectively.

Major element and modal analyses (Tables 2, 3) as well as the AbOr-Q diagram indicate that the Group 3 syenites analyzed (samples 240 and 526) are quartz syenites. In addition, sample 240 has a chemistry that is shifted toward granitic compositions which is probably due to assimilation of Group 2 granitic gneiss (Fig. 5).

In summary, the gneissic granitoids of the Stanislaus River drainage were intruded as plutons, sills, and small injections into the Shoo Fly Complex. Petrographic studies and modal analyses show that they are mineralogically similar to granite, granodiorite, syenite and gabbro. Compared to published analyses of these igneous rocks, the gneisses are very similar in bulk chemistry except for relative depletion of CaO, Na20 and K20. The protoliths of the gneissic granitoids express a calcalkalic to alkalic chemistry and appear to represent I-type, rather than S-type granitoids. However, owing to field evidence of mixed zones and the pervasive recrystallization that the gneisses have experienced, it seems likely that assimilation and metasomatism have had an important effect of their bulk chemistry.

STRUCTURAL FABRICS IN THE GNEISSES

The geometric forms of gneissic granitoid bodies in the Stanislaus River drainage (Plate 1, Fig. 3) are due to their original post-S_1 sheet-like emplacement and the superposition of F_2, F_3, and to a lesser extent, F_4 folds (Table 1). Penetrative D_2 and D_3 deformation under amphibolite grade metamorphic conditions has resulted in the development of complex mylonitic textures in the gneisses at all scales of study. In general, the bodies have less deformed interiors and highly sheared marginal zones where seams of blastomylonite, mylonite, and ultramylonite separate less deformed regions of gneissic granitoid.

The gneisses commonly contain two penetrative foliations (S_2 and S_3) which are marked by recrystallized mica, quartz, feldspar, amphibole, and epidote. These foliations are cut by a younger S_4 spaced mica schistosity. The foliations can be separated in the field and in thin section sample by careful observation of crosscutting relations and by tracing foliations into the axial surfaces of folds in the bordering Shoo Fly Complex.

Because rocks of the various gneiss groups behaved differently during D_2 and D_3, their petrographic features are described separately below after a discussion of the field occurrence of the deformational features. Ductile fault rock terminology used in this report follows Sibson (1977) .

In the gneissic granitoids the S_2 foliation is characterized by oriented biotite, feldspar, and aggregates of quartz and feldspar, recrystallized parallel to the axial surfaces of F_2 folds. F_2 folds are rare in the interiors of the larger gneiss bodies but are common in thin-layered and lit-par-lit injection zones. Isoclinal to tight F_2 folds deform sills and lit-par-lit injections of orthogneiss, discordant igneous contacts, and xenoliths of quartzite and schist containing S_1 foliation near the borders of plutons (Fig. 13). Quartzite xenoliths are locally flattened into and

cut by S_2. The rarity of F_2 folds within the gneisses is probably due to the fact that no layered anisotropy a existed prior to the onset of D_2 deformation. As a result, in the more massive cores of larger bodies, recrystallization and flattening rather than folding occurred.

During the D_3 event broad zones of folding and shearing were developed in the gneissic granitoids. The gneisses were affected to varying degrees by D_3 deformation which is most intense in the Calaveras-Shoo Fly thrust zone and within many smaller ductile shear zones throughout the Shoo Fly Complex. In Rose Creek (Loc. 8572) a large-scale reclined F_3 fold deforms an original igneous contact between granitoid gneiss and interlayered quartz-mica schist and quartzite (Fig. 14). Here, a penetrative S_2 foliation in the gneiss and in the Shoo Fly, related to an F_2 isoclinal fold expressed in the quartzite, is cut by a domainal S_3 foliation. In Deer Creek (Loc. D842) centimeter-scale granitoid injections (Fig. 15a) were folded and foliated during F_2 isoclinal folding. Subsequent tight F_3 folds produced local axial-plane S_3 foliation. In the South Fork Stanislaus River (Loc. SF764) an S_3 mica foliation axial planar to F_3 isoclinal folds of a foliated quartzite can be traced directly into granitic augen gneiss where it forms S_3 mylonitic shears that truncate S_2.

Complete gradations of partial- to total-transposition of S_2 into parallelism with S_3 are common. Where transposition is prominent the augen texture is destroyed by pervasive grain-size reduction and recrystallization. Within domains of intense D_3 deformation shearing along the limbs and axial surfaces of F_3 folds ultimately creates ellipsoidal shear-bounded slivers of foliated (S_2) gneiss (compare Figs. 15a, b). Ellipsoidal slivers ranging from 20 cm to 2 m in length are flattened into S_3 and are strongly elongated parallel to F_3 hingelines. The tectonic slivers are sheathed in lineated mylonite and are internally folded by tight F_3 folds of the S_2 foliation (Fig. 16). An axial-planar S_3 biotitic foliation is related to the F_3 folds.

In an unnamed creek north of Stony Gulch (Loc. U705) near the trace of the D_3 Calaveras-Shoo Fly thrust, small (<1 m) sills of augen gneiss "floating" in schist are deformed into lineated (L_3) ellipsoidal slivers flattened into S_3. The schistose rocks have a shredded appearance in outcrop and show phyllonitic textures microscopically. The S_3 foliation, which anastomoses through and about the foliated (S_2) slivers, is locally folded by F_4 folds and cut by S_4 (Fig. 15b) and younger structures (S_5-S_7).

Near the Calaveras-Shoo Fly thrust and in D_3 shear zones the gneisses vary texturally from well-layered to finely-laminated rocks. They are cut internally by laterally extensive anastomosing S_3 shears which vary in thickness from 1 cm to 0.5 m (2-4 cm avg.). The shears are spaced throughout the study area with rapid decreases in spacing occurring at shear zones. The S_3 shears, which can be traced directly into the axial surfaces of F_3 folds, are characterized by recrystallization and grain-size reduction yielding mylonite and blastomylonite. Local flint-like 1-3 cm ultramylonite seams crosscut the S_2 foliation and related F_2 folds.

The deformational fabrics observed in the field are well-developed at the microscopic scale. In the granitic gneisses the feldspars reacted to strain by brittle failure and rotation with the development of segregated subhedral to anhedral 0.1 mm-1 cm porphyroclasts with bent perthite lamellae and twins, internal cracking, mineral replacement and recrystallization, and marginal granulation and/or recrystallization (Fig. llb). Finely recrystallized quartz and biotite±muscovite characteristically occur at feldspar edges. Plagioclase is commonly replaced by epidote and sericite and has biotite-rich margins. Quartz forms polycrystalline lenticles and ribbons (0.1-1 mm thick) that are locally undulose and that together with mica fill cracks in the feldspar augen. Biotite and muscovite augen formed during D_2 are sometimes undulose with frayed edges and adjacent neocrystallized oriented small micas. The micas, together with the

quartz and feldspar lenticles, ribbons, and porphyroclasts compose the S_3 mylonitic foliation which is superimposed on S_2. Severely sheared gneisses (example given below) have highly lineated textures composed of fine-grained minerals.

On Busse Road (Loc. BR221), gneiss within a 400 m wide D_3 shear zone 7 km east of the Calaveras Shoo Fly thrust (Figs. 3, 17a) shows extreme elongation (20:1) parallel to F_3 hingelines. Similarly lineated gneisses occur in drainages along strike to the southeast (Loc. R275). In thin sections cut parallel to L_3 (Fig. 17b), the lineation is composed of subangular porphyroclasts of orthoclase and plagioclase together with quartz lenticles and ribbons segregated between folia of biotite, muscovite and opaque minerals. In sections cut perpendicular to L_3 the feldspar augen are elliptical and flattened into S_3. Potash feldspar is typically untwined and shows edge granulation, internal cracks and internal recrystallization of quartz and white mica. Quartz subgrains occur at the boundaries of the quartz lenticles and ribbons and S_2 biotite flakes are bent, shredded and recrystallized into smaller crystals oriented parallel to the S_3 folia (Fig. 17c). Opaques are concentrated at the edges of the biotites. Along strike toward the south east the Busse Road granitoid gneiss becomes progressively more mylonitic with rotated and crushed potash feldspar with spalled, shattered rims set in an ultramylonitic matrix (Fig. 17d). Quartz flasers are surrounded by finely recrystallized S_3 muscovite and biotite.

In the syenite gneisses the lack of quartz and the feldspathic nature of the rocks generated a more brittle response to D_3 deformation. In regions of non-penetrative D_3 deformation the rocks are fractured and crudely foliated, cut by spaced 0.1 mm hastingsite±biotite±stilpnomelane folia (Fig. 12a). The hand sample takes on the appearance of a crushed mosaic due to the angular feldspar-rich domains separated by thin veins of amphibole±mica. Subidioblastic S_2

hastingsite occurs at the interstices of the cracked feldspars and are replaced by S_3 recrystallized hastingsite needles forming the veins.

In regions of high strain the potash feldspars are cracked and corroded with reaction rims and internal polycrystalline zones of feldspar±quartz±biotite. In more highly deformed rocks feldspars are rounded with abundant internal cracks, spalled-off and imbricated rims, deformed perthite exsolution lamellae, and granular, recrystallized edges. The porphyroclasts are surrounded by a blastomylonitic S_3 foliation composed of polycrystalline potash feldspar, quartz ribbons, hastingsite, and biotite±stilpnomelane (Fig. 12b).

Judging by the fold structures and coexisting minerals forming the S_2 and S_3 foliations, the gneissic granitoids were deformed under epidote-amphibolite facies metamorphic conditions as defined by Turner (1968). In addition, regardless of their bulk composition, the gneisses possess many of the macro- and microscopic features associated with deep-seated ductile shear zones. In zones of high shear strain the feldspars behaved in a brittle fashion, yet the quartz and mica responded by ductile deformational mechanisms. Such brittle-ductile behavior has been experimentally determined to occur at crustal depths of 10-15 km at temperatures of 350°-500°C (Tullis and Yund, 1977; Carter and others, 1981). Regional syntectonic metamorphism of the gneisses took place during D_2 and D_3 under epidote-amphibolite facies conditions which corroborates the P-T conditions suggested by the brittle-ductile mineral fabrics and the sub-solvus feldspar disequilibria textures discussed earlier. Together these P-T estimates suggest that plutonism of the gneissic granitoids and subsequent shearing took place at similar crustal depths.

RELATIONSHIP OF THE GNEISSES AND THEIR FABRICS TO STRUCTURAL EVENTS IN THE SHOO FLY

Protoliths of the gneissic granitoids and the Shoo Fly Complex have shared the effects of six deformational events in Phanerozoic time. The geologic relationships of the intrusion and subsequent deformation of the gneissic granitoids are now well-understood (Table 1). They truncate the S_1 foliation of the Shoo Fly Complex but are deformed along with their host rocks by D_2 and younger deformation.

D_1 - Pre-intrusive deformation. The first structural event to effect the Shoo Fly Complex involved the development of intrafolial and long-limbed isoclinal F_1 folds with an axial surface foliation (S_1). The S_1 layering is in part compositional but is also marked by recrystallized mica, quartz, and feldspar. The S_1 fabric, which is penetrative and locally mylonitic, is severely overprinted by D_2 and D_3 structures but is preserved around F_2 fold-hinges. F_1 fold-hinges are rare but do occur.

D_2 - Initial deformation of the granitoid rocks and second deformation of the Shoo Fly. Isoclinal folding and syn-tectonic recrystallization of S_1 and contacts between granitic rocks and their hosts during D_2 produced a micaceous foliation in the Shoo Fly Complex and a strong foliation in the gneisses. The S_2 foliation in both the Shoo Fly and gneisses is crosscut by a domainal S_3 foliation which is strongly mylonitic, particularly within 1-2 km of the Calaveras-Shoo Fly thrust (Fig. 13).

D_3 - Secondary deformation of the gneisses and development of the Calaveras-Shoo Fly thrust. Lithologic contacts and coplanar S_1 and S_2 of the Shoo Fly Complex are strongly deformed, recrystallized, and regionally truncated at the Calaveras-Shoo Fly thrust (Fig. 3). The

Shoo Fly experienced intense D_3 shearing and folding during development of the thrust and these structures can be traced into the gneissic granitoids.

During D_3, the S_2 foliation in the gneisses was isoclinally to tightly refolded by F_3 folds with local shearing along S_3 axial surfaces. Local seams of mylonite, blastomylonite, and ultramylonite are developed sub-parallel to S_3. F_3 folds of the S_2 gneissic layering are the most conspicuous folds in the gneiss. The relationship of the gneisses to the regionally developed structural episodes D_1, D_2, and D_3 in the Shoo Fly are illustrated in figure 18 from field drawings.

Post – D_3 deformational episodes

D_4 - Folding of the Calaveras-Shoo Fly thrust. F_4 folds with east-west-trending axial surfaces and east-plunging axes deformed S_3 and older fabrics in the Shoo Fly and the gneissic granitoids. Regionally, the Calaveras-Shoo Fly thrust was deformed into the digitated east plunging antiformal structure north of the Standard Pluton (Figs. 1, 3). A spaced biotite schistosity (S_4) crosscuts the S_3 mylonitic fabric in the Shoo Fly. Idiomorphic micas grown parallel to S_4 are, for the most part, smaller than those forming older fabrics (S_3, S_2, S_1)

In the gneisses penetrative S_2 and S_3 fabrics were deformed during D_4 with the development of a spaced biotite schistosity (S_4) parallel to the axial surfaces of F_4 folds. The F_4 folds are identical in style to those found throughout the Shoo Fly Complex varying from tight to asymmetric in profile (Fig. 19). Locally, inosculating black seams (S_4) composed of very fine-grained biotite±quartz±magnetite occur in the gneiss bodies. The seams post-date the S_3 mylonitic foliation and are cut by younger structures.

Prior to the onset of Nevadan deformation in Late Jurassic time the Shoo Fly and Calaveras Complexes were intruded by the Standard pluton, Sonora mafic dikes, and the Knight

Creek pluton (Fig. 3, Table 1). Based upon field superposition, brittle structures that overprint D_4 and older ductile fabrics as well as the Standard pluton, Sonora mafic dike swarm, and the Knight Creek pluton, are interpreted to have formed during the Nevadan orogeny (D_5, D_6) and a younger, possibly Cretaceous, event (D_7) (Table 1). Collectively, the F_5, F_6, and F_7 folds are asymmetric and open with a weak spaced cleavage formed parallel to their axial surfaces. The cleavage style varies from brittle quartz-filled to non-mineralized fractures to quartz+chlorite±muscovite lined crenulation cleavage which commonly retrogrades pre-existing ductile fabric elements.

Summary. Granitic, granodiorite, syenitic, and minor gabbroic protoliths of the gneissic granitoids were intruded into the Shoo Fly Complex after it experienced an early phase (D_1) of deformation. They were subsequently involved in two penetrative (D_2, D_3) and four relatively non-penetrative (D_4, D_5, D_6, D_7) regional deformations during Paleozoic and Mesozoic time. Although within regions of relatively nonpenetrative D_2 and D_3 deformation the gneisses contain relict igneous textures and marginal and internal intrusive contacts, typically the gneisses are strongly folded and recrystallized. They possess finely laminated mylonitic fabrics developed during superposed F_2 and F_3 isoclinal folding events resulting in a reduction in grain size and the development of augen (porphyroclasts of feldspars, amphibole, quartz, mica, and granitic aggregates).

The gneisses were further recrystallized during formation of the S_4 spaced mica schistosity and then by three discrete retrograde metamorphic episodes accompanying the development of S_5, S_6, and S_7 slip cleavage (Table 1; see Chapter 1). Clearly, the gneissic granitoids have experienced a complex post-intrusive history involving many episodes of folding and recystallization under varying metamorphic conditions.

DISCUSSION

The Shoo Fly Complex originated as a slope and rise sequence deposited adjacent to the Lower Paleozoic shelf edge of western North America but the Shoo Fly defies any simplistic genetic explanation due to its complex structure, pervasive syn-metamorphic shearing, lack of fossils, and paucity of geochronologic and isotopic data. The following is a discussion of the regional tectonic implications of the Shoo Fly orthogneisses.

Based on preliminary igneous ages of the Paleozoic orthogneisses and cross-cutting relations of other igneous rocks, the various D-events of the Shoo Fly Complex have been correlated with recognized tectonic events elsewhere in the Cordillera (Table 1). Most workers are in agreement that the first phase of compressive deformation to affect the lower Paleozoic Cordilleran margin was the Late Devonian-Early Mississippian Antler orogeny (Roberts and other, 1958).

U-Pb and Rb-Sr studies of the Group 2 granitic gneisses by Sharp and others (1982, in press) yield ages that cluster at 450 m.y.a. with one highly sheared locality (BR221) yielding a 275 m.y. age which may be spurious. A preliminary four-point Rb-Sr isochron by H.K. Brueckner (pers. comm. 1984) on the Group 3 syenites of upper Rose Creek (Loc. 8240) yields a 363 m.y. emplacement age. These data, although not conclusive, argue for Paleozoic and probably Ordovician or Devonian intrusive ages for the orthogneiss protoliths and therefore establish a prelate Devonian depositional age for the Shoo Fly Complex. The 363-450 m.y. range of igneous ages for the orthogneiss bodies suggest that D_1 in the Shoo Fly Complex may be of pre-middle Ordovician to Devonian age and places a Late Devonian maximum age on D_2.

If the 450 m.y. maximum age on the orthogneisses reported by Sharp and others (1982) is correct, then D_1 in the Shoo Fly and the intrusion of the orthogneiss protoliths would be older

than the Antler orogeny. This raises the intriguing possibility that the central Sierra Shoo Fly may record an orogenic pulse not identified elsewhere in the Cordillera. Alternatively, if the 363 m.y. age of Brueckner (pers. comm.) is correct, the D_1 event could be an expression of the Antler orogeny (Table 1).

The age and tectonic significance of the D_1 event in the Shoo Fly Complex is poorly understood. It marks an important initial episode of isoclinal folding and metamorphic recrystallization in the Shoo Fly but a discussion of the myriad of paleotectonic scenarios for D_1 is beyond the scope of this report. The D_2 event could be interpreted as a culmination of progressive D_1 Antler orogenesis which involved an early episode of F_1 folding and intrusion of the orthogneiss protoliths. However, if the 275 m.y. age on the Group 2 Busse Road gneiss (BR 119, 221) is correct, D_2 could be as young as Permian since the D_3 event is probably Permo-Triassic in age (Table 1). The 275 m.y. age is suspect, however, due to complicated isotopic systematics and intense deformation of the analyzed samples during D_2 and D_3. In the Shoo Fly Complex of the northern Sierra Nevada, a Late Devonian granitic batholith (Bowman Lake pluton of Hanson and others, 1983) may be correlative with the gneissic granitoids of this report, thus supporting the 363 m.y. age determination.

The lower Paleozoic intrusion of protoliths of the gneissic granitoids is an important mesozonal regional plutonic episode which occurred between the D_1 and D_2 events in the Shoo Fly (Table 1). Compositionally, the orthogneiss protoliths probably ranged from predominantly granite and granodiorite to syenite to gabbro, calc- alkalic to alkalic rocks typical of magmatic arcs. Crosscutting relations indicate that initially Group 1 gabbroic rocks then Group 2 granitic rocks and finally Group 3 syenitic rocks were emplaced along and locally across the early S_1 foliation in the Shoo Fly.

The protoliths of the gneisses may have been generated during an episode of continentward subduction but unlike typical ensialic marginal arcs the youngest magmas were syenitic. The crosscutting relations of the Group 1 , 2, and 3 gneisses might indicate a period of steep subduction which may have earlier created the S_1 foliation of the Shoo Fly. In this model, "roll-back" of the subducting oceanic lithosphere fostered a trenchward shift of the volcano-plutonic axis which may have resulted in a similar trenchward shift of the back-arc alkalic province (c.f. - Keith, 1978). In this way the Group 3 syenites would invade the earlier calc-alkaline plutons represented by the Group 1 and 2 gneisses during a protracted episode of subduction. Collectively, the gneisses may mark the remnants of a Paleozoic plutonic belt.

Another possible scenario for intrusion of the Group 2 gneiss protoliths would be that they represent in-situ partial melts. Sharp and others (in press) argue that the Sr^{87}/Sr^{86} ratio of 0.709±0.001 from the 450 m.y. Confluence and Rose Creek granite gneisses (Locs. SL-1, R1177) are characteristic of derivation from ancient crustal sources. More granodioritic gneisses (Locs. D163, K1176) have Sr^{87}/Sr^{86} ratios of 0.7067±0.0003 which suggests a different source than the 450 m.y.a. granitic gneisses but are still within the 0.706 isotopic line suggested by Kistler and Peterman (1973, 1978) to represent the westward limit of the Cordilleran craton (see Chapter 1, Fig. 29). A significant component of radiogenic lead from 1.9 b.y. zircon was detected in the Stanislaus River drainage orthogneisses analyzed by Sharp and others (in press) but it is unknown whether the zircon was assimilated during magmatic ascent through Precambrian crust or scavenged from rocks derived from such crust (i.e. - the Shoo Fly Complex). These isotopic studies suggest that the protoliths of the gneissic granitoids may have been derived from in-situ partial melting of western North American crust or from sediments eroded from it.

An anatectic origin for protoliths of the Group 2 gneisses is also suggested by their peraluminous chemistry. Peraluminous magmas generated near trenches have been documented from the Aleutian and Sumatran arcs (Hudson and others, 1977; Marshal and K arig, 1977). In these examples, high heat flow due to subduction of an active ridge segment led to melting within the accretionary prism with upward rise of peraluminous anatectic magmas. The syenites of Group 3 do not fit this model but it is possible that some of the granites of Group 2 originated in this way.

Syenites are commonly related to episodes of continental rifting with modern examples found near the East African rift system. The intrusion of the Group 3 syenites may have taken place during a post-D_1 rifting episode that post-dates intrusion of the Group 2 gneiss protoliths. This model would suggest a hiatus in igneous activity between the emplacement of Group 2 and Group 3 igneous rocks rather than them representing a consanguineous igneous suite as suggested above. Given the available data, it is not possible to distinguish between these two models and as a result the origin of the Group 3 syenites must remain enigmatic.

Thus, it is not possible at present to determine whether the gneissic granitoids of the Stanislaus River drainage originated as 1) subduction-related continental magmatism, as 2) in-situ partial melts from deep within a subduction complex, as 3) plutons related to rifting, or 4) as combinations of the above.

Metamorphic ages. Sharp and others (in press) report a 215±10 m.y. Late Triassic metamorphic event which affected the U-Pb systematics of the Indian Creek (IC686) and Confluence (SL-1) gneissic granitoids. Textural evidence discussed above indicates a complex post-intrusive polymetamorphic history for the gneissic granitoids that varied from epidote-amphibolite to chlorite grade between D_2 and D_7 (Table 1). Thus, interpretation of the

215±10 m.y. metamorphic ages indicated by lower intercepts of U-Pb concordia plots for localities SL-1 and IC686 and K-Ar analyses of amphibolites interlayered with gneiss at locality SL-1 is very complex. Field studies in the southern part of the Confluence body (Fig. 3) indicate the presence of strong, penetrative S_2 fabrics, locally isoclinally folded by F_3 and cut by S_3. S_3 is locally strong and subparallel to S_2. Both are cut by S_4 crenulations and spaced cleavages.

On Indian Creek (IC686) only a single, strong foliation (S_2) and lineation were noted. Conceivably, this could S_2xS_3, but there is no evidence for it. The following alternatives are possible: 1) the U-Pb lower intercept ages may represent a smeared out D_2/D_3 event, especially if the amphibolite has recrystallized parallel to S_2/S_3. This would fit IC686, which lacks obvious evidence of F_4. 2) Even though the penetrative fabrics in SL-1 are S_2/S_3, the D_4 event produced enough of a thermal pulse to reset K-Ar in amphibolite and somehow promoted lead loss in the zircons, so that both systems only closed after D_4 (F_4 folding of thrust, etc.). IC686 is relatively close to the axial surface of an F_4 synform, and thus may have felt the D_4 thermal disturbance, even though no obvious structures related to D_4 were observed.

The Busse Road granitic gneiss (Loc. BR221) is problematical. Although this sample plots on concordia and shows a lower intercept age of about 275 m.y., it shows evidence of intense lineation (Fig. 17) and open, crenulate F_3 folds of the S_2 foliation. It also contains an asymmetric kink band that could be an S_4 structure. Oddly enough, the isotopic systems in this sample do not appear to "see" the metamorphic events associated with F_2-F_4, even though the rock contains structures related to them. Based on these complications we consider a Late Triassic metamorphic event to represent an isotopically smeared-out minimum age for D_3 epidote-amphibolite grade regional metamorphism.

CONCLUSIONS

A significant lithology in the Shoo Fly Complex, Paleozoic gneissic granitoids represent former calc-alkalic to alkalic plutons, sills, and dikes intruded as a series ranging from gabbro (oldest) to granite and granodiorite (median age) to syenite (youngest) with the granitoid types predominating. They were subsequently folded and metamorphosed during regional deformational episodes but protoliths of the orthogneisses truncate F_1 folds and S_1 metamorphic layering in the Shoo Fly wall rocks. During regional D_2 and D_3 events the gneisses were penetratively deformed into augen gneiss and mylonitic gneiss. Later deformational events (D_4-D_7) involved open folding and weak metamorphic overprinting and are correlative with post-D_3 deformational events in the Shoo Fly wall rocks. Due to this structural correlation the gneisses represent an important structural marker for the region.

Available geochronologic data suggests that the gneissic granitoid protoliths were intruded between middle Ordovician and late Devonian time and establishes a pre-late Devonian age for deposition and subsequent D_1 deformation of the Shoo Fly. If the middle Ordovician age is reliable, D_1 in the Shoo Fly may have no counterpart elsewhere in the SW Cordillera. Collectively, the gneisses probably mark the remnants of a Paleozoic calc-alkaline plutonic belt as their protoliths consisted of I-type, rather than S-type granitoids.

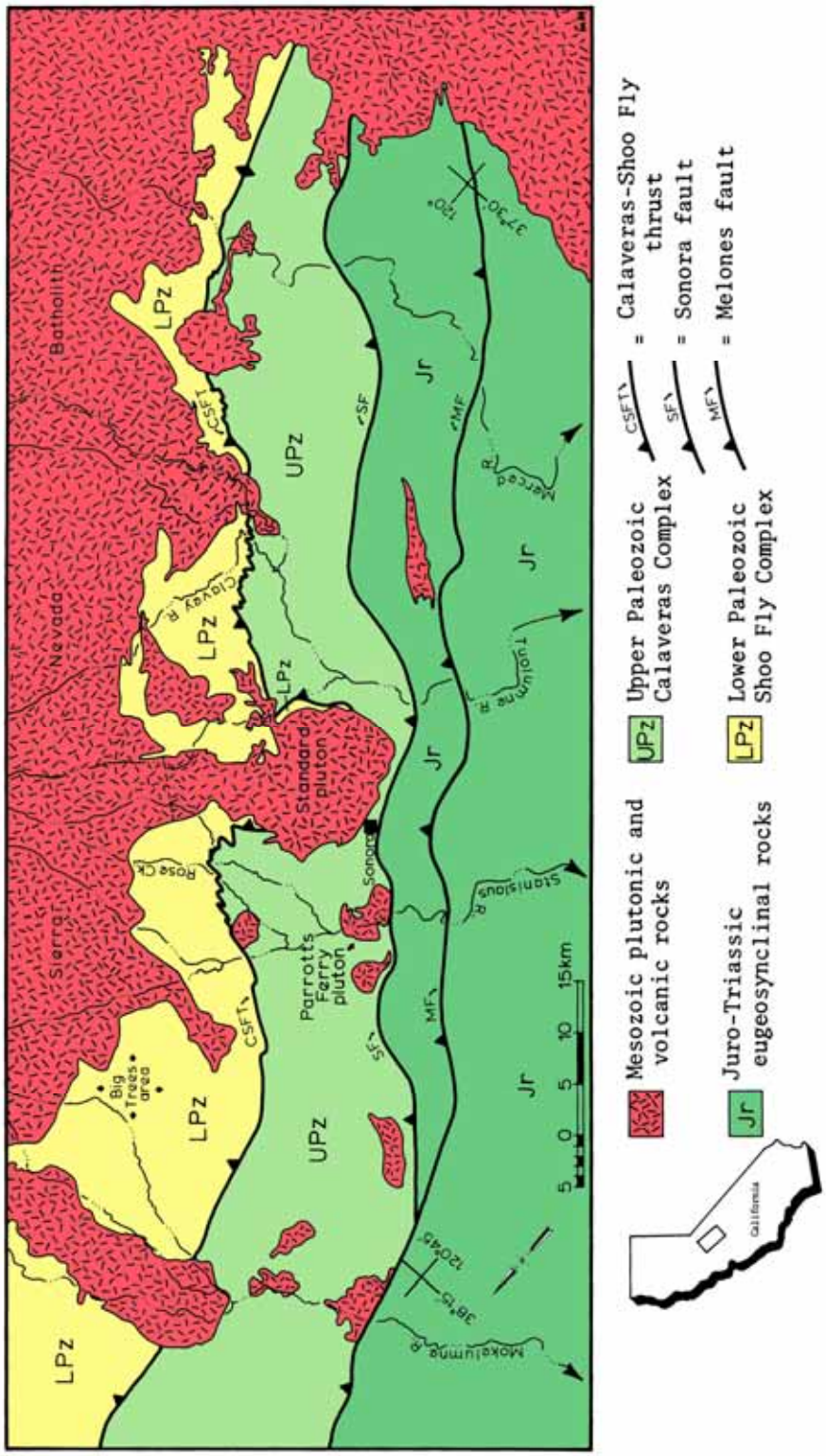

Figure 1 - Sketchmap of the Sierra Nevada Foothills metamorphic belt. The Shoo Fly Complex and other ductile-fault-bounded tectonostratigraphic units trend north-northwesterly and lie along the western edge of the Sierra Nevada batholith. Adapted from Bowen (1969), Merguerian (1981ms), Rogers (1966), Schweickert and Bogen (1983), Strand (1967), Tobisch (1960), and Wagner and others (1981).

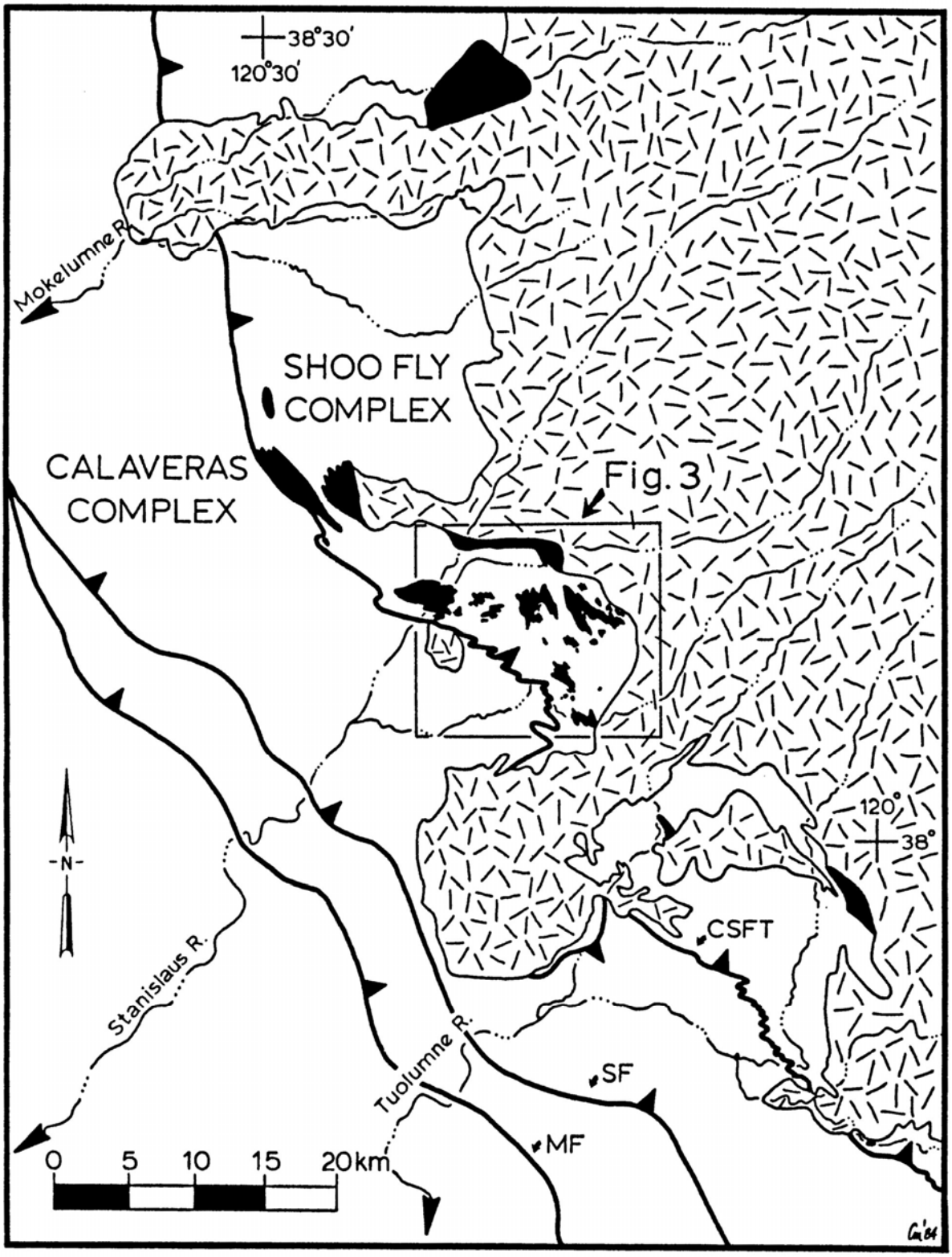

Figure 2 - Geologic sketch map showing all of the known occurrences of gneissic granitoids (black) between the Mokelumne and Tuolumne River drainages in the southern Sierra Nevada, California. The greatest concentration of gneiss occurs in the Stanislaus River drainage (inset). MF=Melones fault, SF=Sonora fault, CSFT=Calaveras-Shoo Fly thrust.

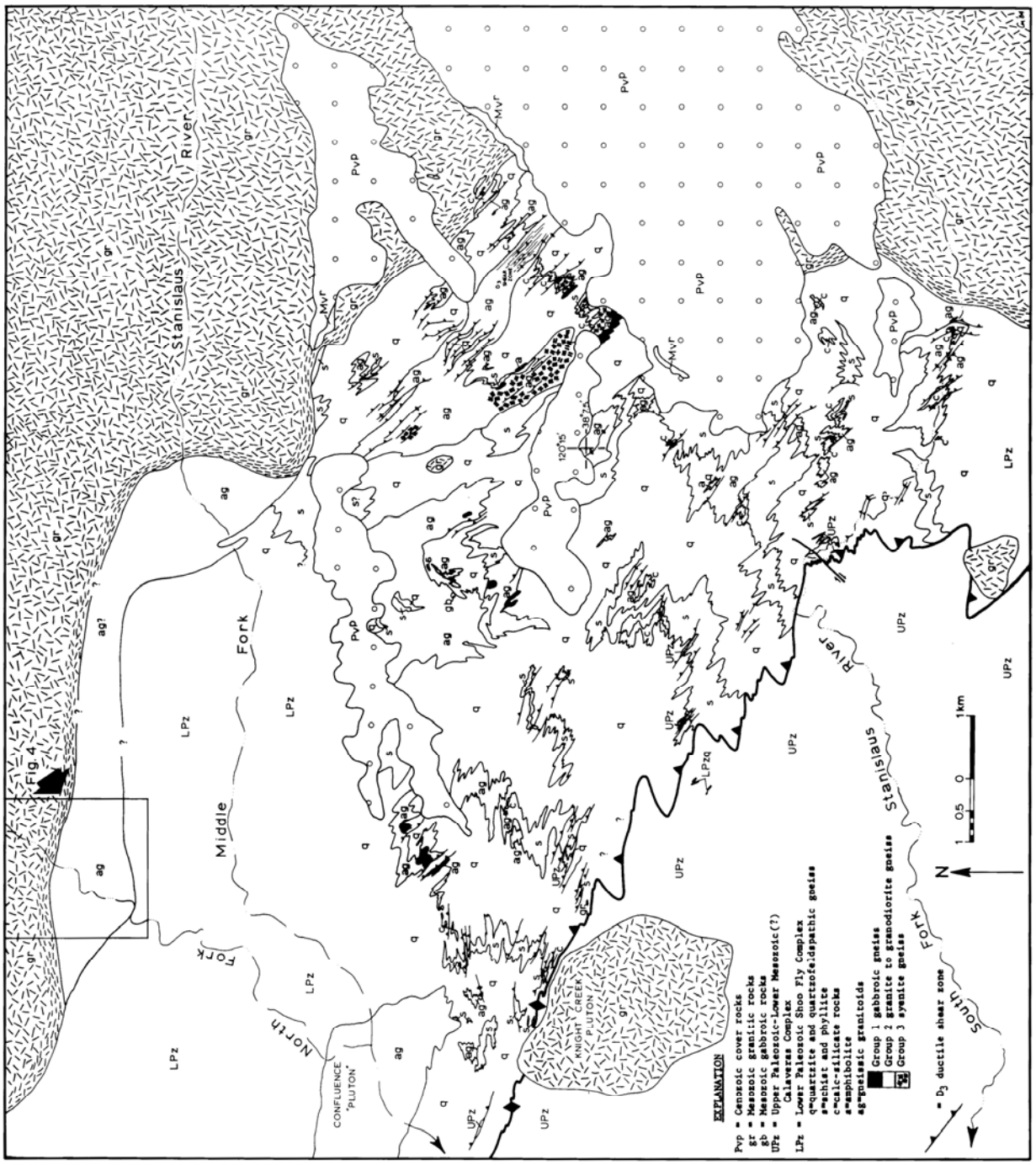

Figure 3 - Bedrock geologic map of the Shoo Fly Complex of Tuolumne County, California encompassing parts of the Stanislaus, Columbia SE, Crandall Peak, and Twain Harte 7-1/2 minute quadrangles. This map was compiled from 1:24,000 scale maps (Plate 1) and unpublished data from the North and Middle Forks of the Stanislaus River (Schweickert, unpub. data). Lithologies in the Shoo Fly Complex (LPz) are q=quartzite and quartzofeldspathic gneiss, s=schist and phyllite, c=calc-silicate and marble, and a=amphibolite. The gneissic granitoids (ag) are differentiated into Group 1 (gabbroic), Group 2 (granitic to granodioritic), and Group 3 (syenitic) gneiss.

Field localities mentioned in the text, figures, and tables of this report are shown in Plate 3. Streams and field station number are indicated (i.e. - 8237 means field number 237 in Rose Creek). MF=Middle Fork Stanislaus River, U=unnamed creeks to north of Stony Gulch, S=Stony Gulch, K=Knight Creek, E=Eagle Creek, DR=Dry Creek, D=Deer Creek, SF= South Fork Stanislaus River.

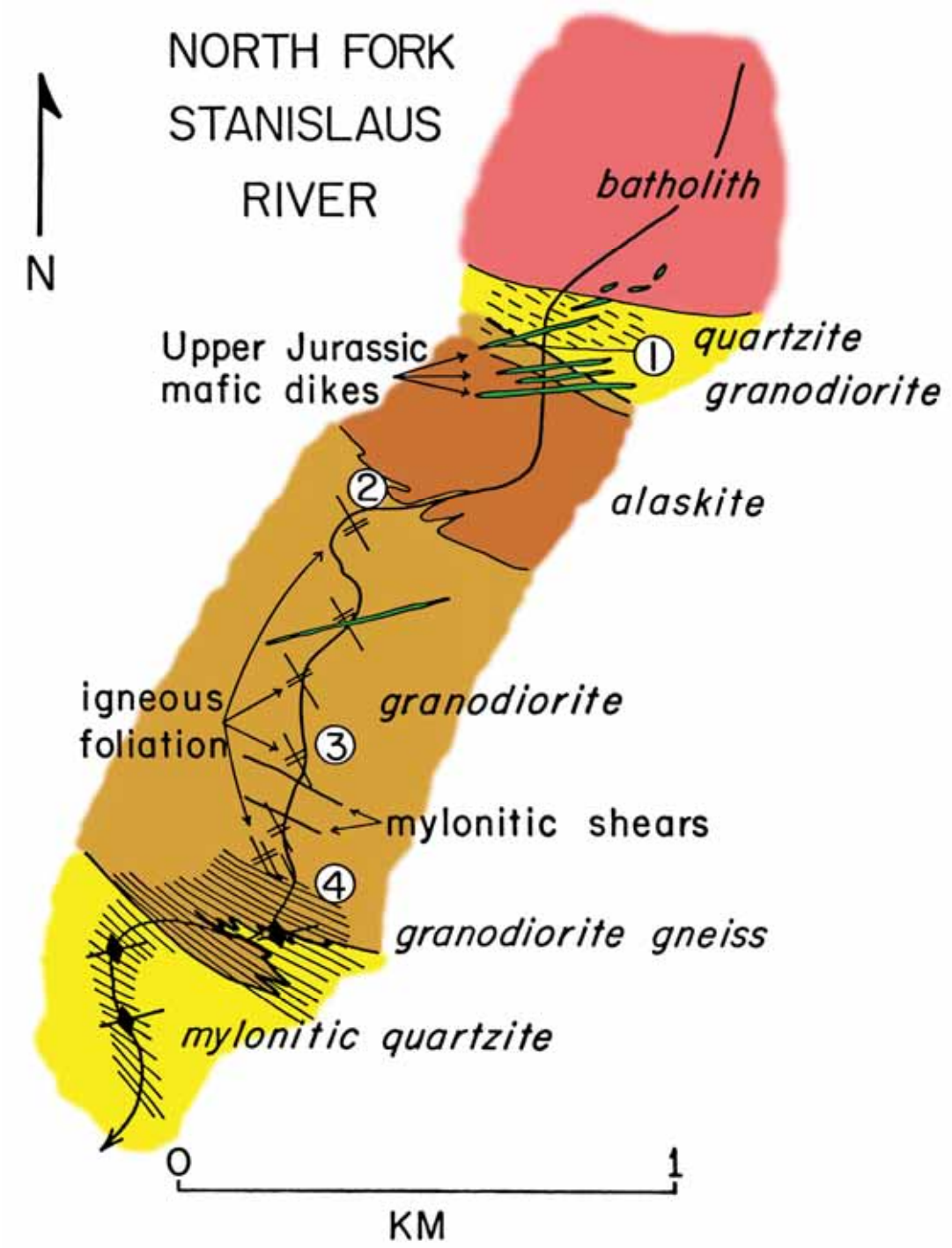

Figure 4 - Sketchmap of relations of deformed and undeformed granitoid rocks along North Fork Stanislaus River (see inset in Fig. 3). 1 -discordant contact between Shoo Fly quartzite with earlier foliation and granodiorite (protolith of augen gneiss). Both are cut by a 2 m mylonitic shear zone and in turn cut by Upper Jurassic mafic dikes that are disrupted by the Sierra Nevada batholith. 2 - granodiorite identical to 1 intrudes an alaskite body; granodiorite contains a northwest-trending igneous foliation of biotite and hornblende. 3 - igneous foliation in granodiorite locally cut by thin, mylonitic shears. 4 - mylonitic shears become more closely spaced and penetratively overprint the igneous foliation as a gneissic fabric. South of this point, rocks are granodioritic augen gneiss, whose contact with quartzite has been transposed into parallelism with the gneissic foliation of the augen gneiss. The quartzite is mylonitic.

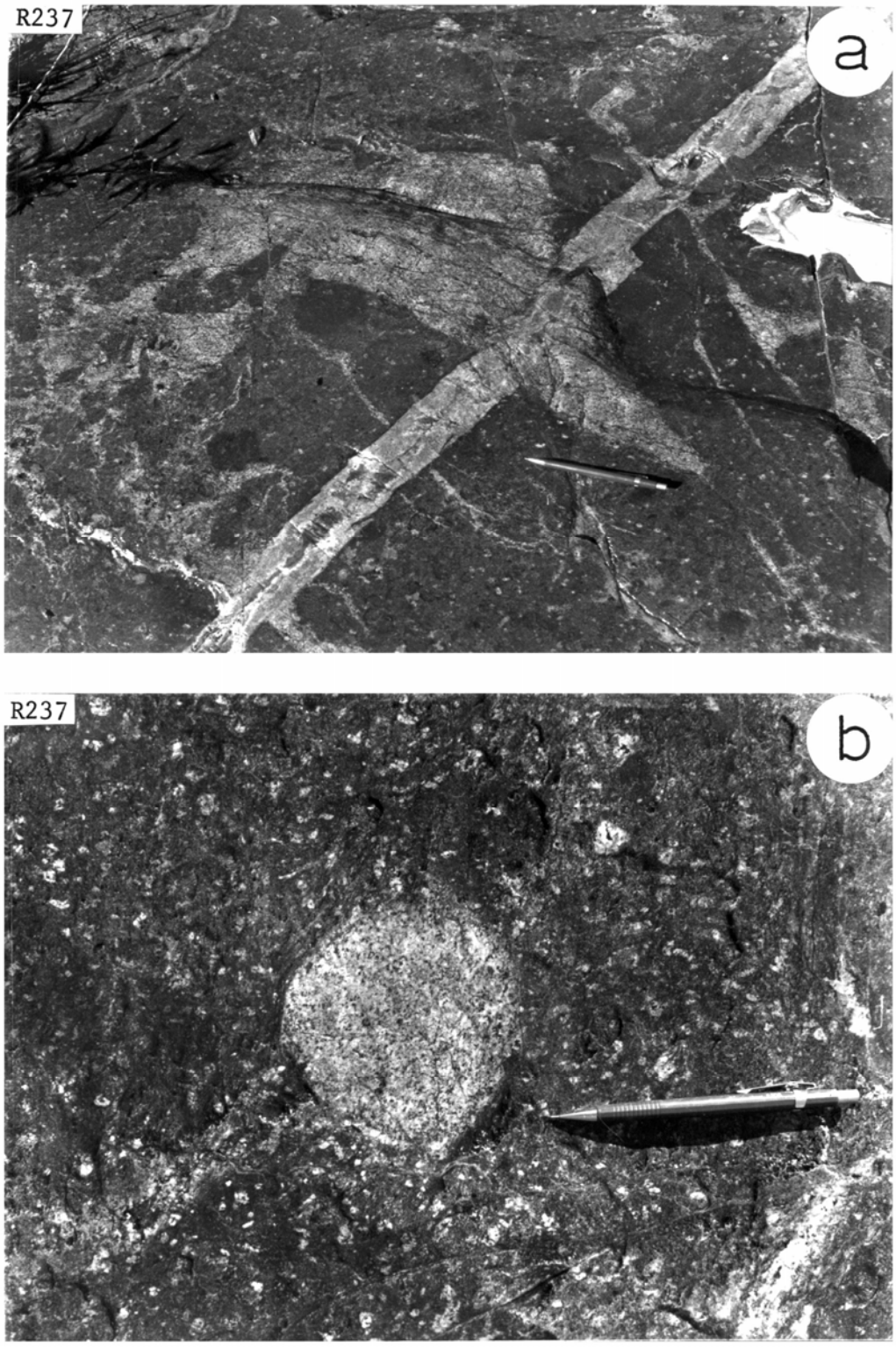

Figure 5 - Crosscutting intrusive relations exhibited in upper Rose Creek.
(a) Angular to rounded xenoliths of light-colored granitic gneiss (Group 2) enclosed in dark syenite gneiss (Group 3). Both the xenoliths and syenitic gneiss are cut by S2 and S3 shears and by granitic and mafic dikes.
(b) In detail, the Group 3 syenite contains many small xenoliths, xenocrysts, patches, and streaks of the Group 2 granitic gneiss. Pencil scale is 14.5 cm long.

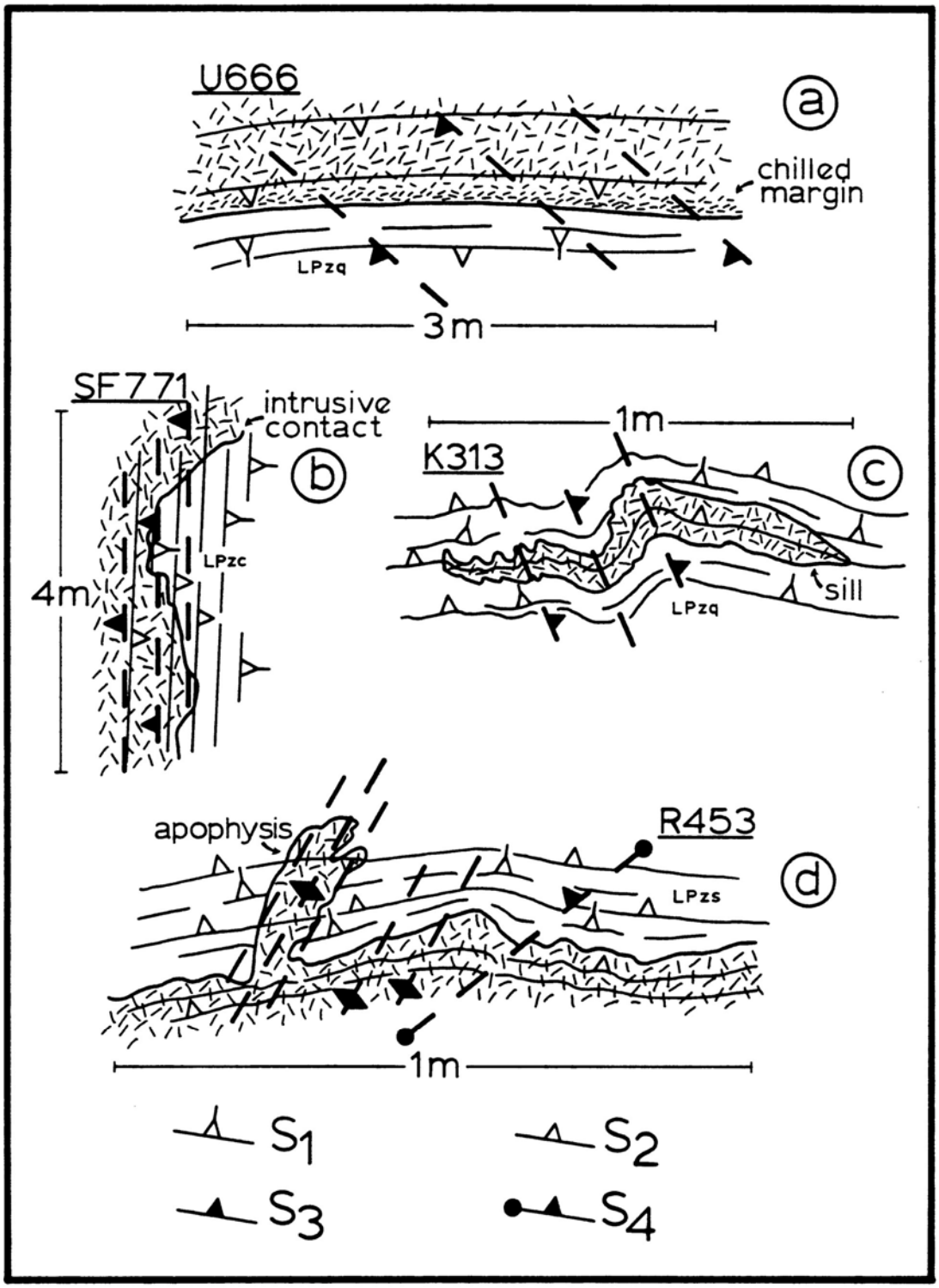

Figure 6 - Evidence for intrusive origin of the gneissic granitoid k bodies (stippled). The deformational fabrics are described in Table 1 and the text.
(a) A chilled margin at the contact of mylonitic quartzite.
(b) Discordant intrusive contact cutting S_1 in the Shoo Fly calcsilicate unit.
(c) Lensoidal form of gneissic granitoid suggesting control of sill emplacement by S_1 in quartzite.
(d) Apophyse of gneissic granitoid which cuts S_1 and contains S_2 and S_3 foliations.

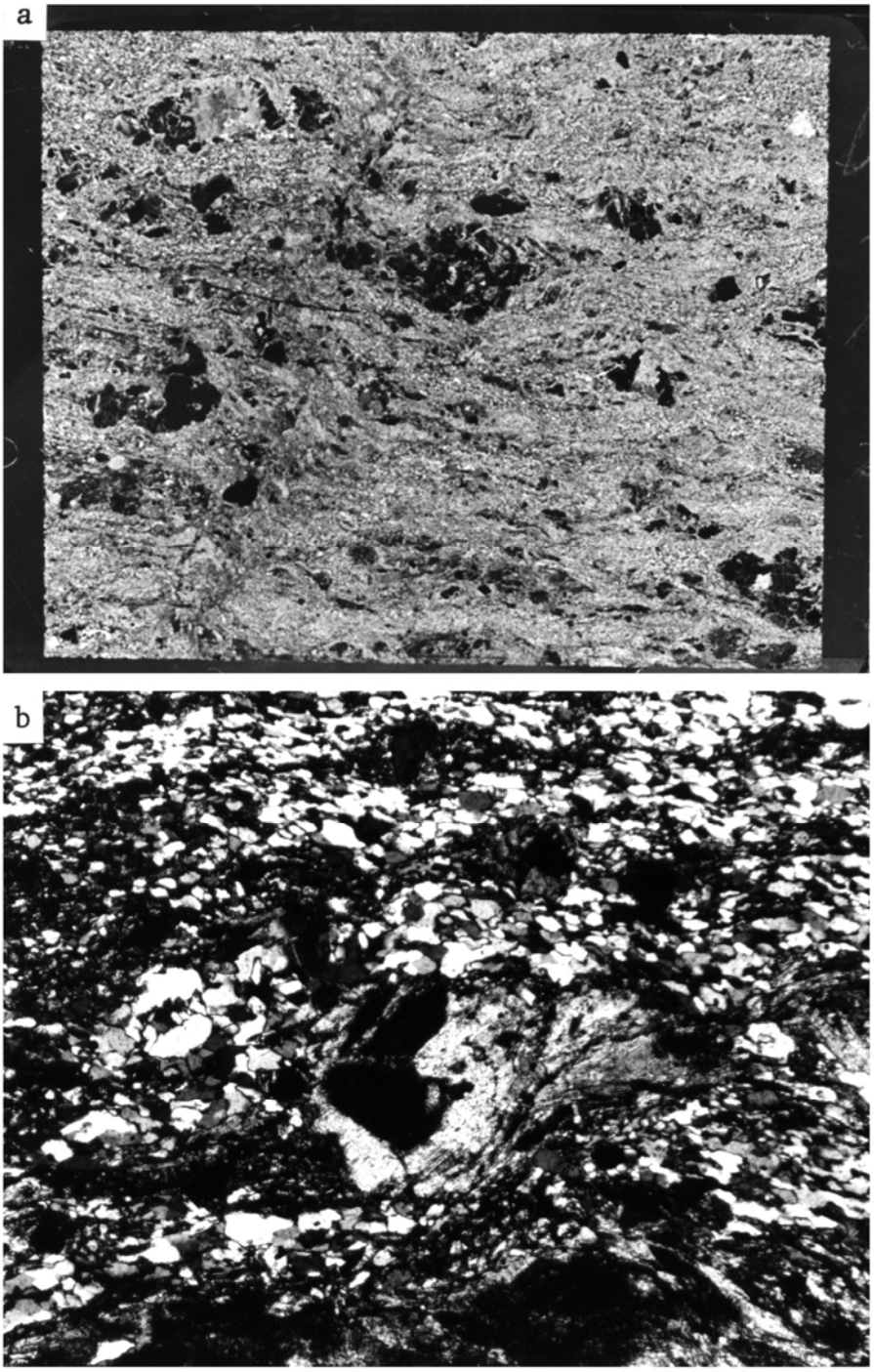

Figure 7 - **(a)** Macrophotograph of a mylonitic gabbro (R216A) showing highly recrystallized augen of green hornblende in various stages of deformation in a finely recrystallized S_3 foliation of untwined plagioclase and epidote in approximately equal proportions. Horizontal field of view is 40 mm; crossed polars.
(b) Photomicrograph of gabbroic gneiss showing composite amphibole porphyroclasts with fine-grained recrystallized tails. The opaque-rich core is composed of brown amphibole that is optically continuous with clear to green magnesian hornblende (B-, 2V = 70°). The S_3 foliation, which crosscuts and recrystallizes the green hornblende, is composed of untwined plagioclase (clear grains), epidote (gray, high relief grains), and prismatic green hornblende. All of the photomicrographs herein were taken with crossed polars with a horizontal frame width of 2.7 mm.

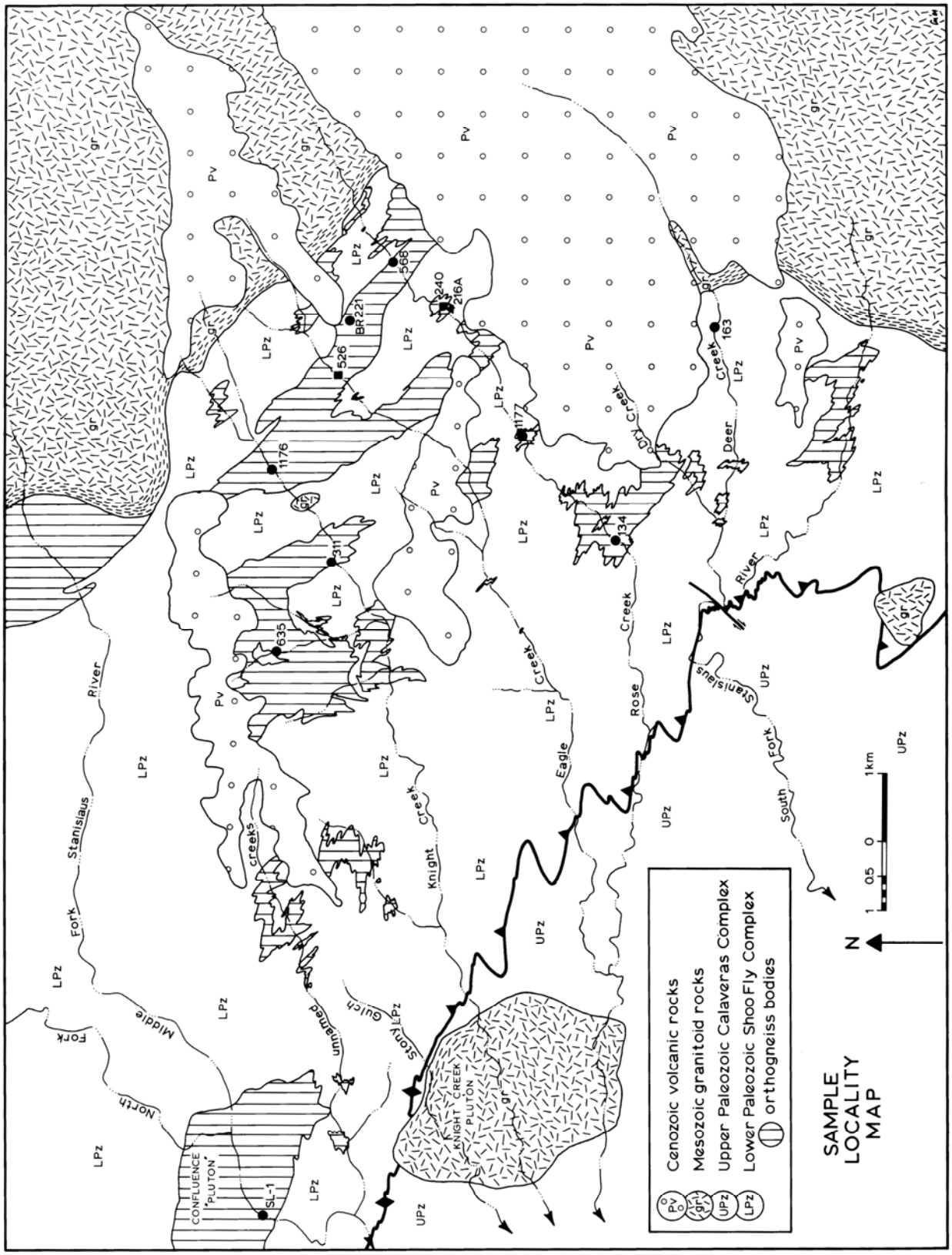

Figure 8 - Map showing the gneissic granitoids in the Stanislaus River drainage. Also shown are the localities of samples that have been analyzed for major element chemistry and geochronologic studies (see Table 2).

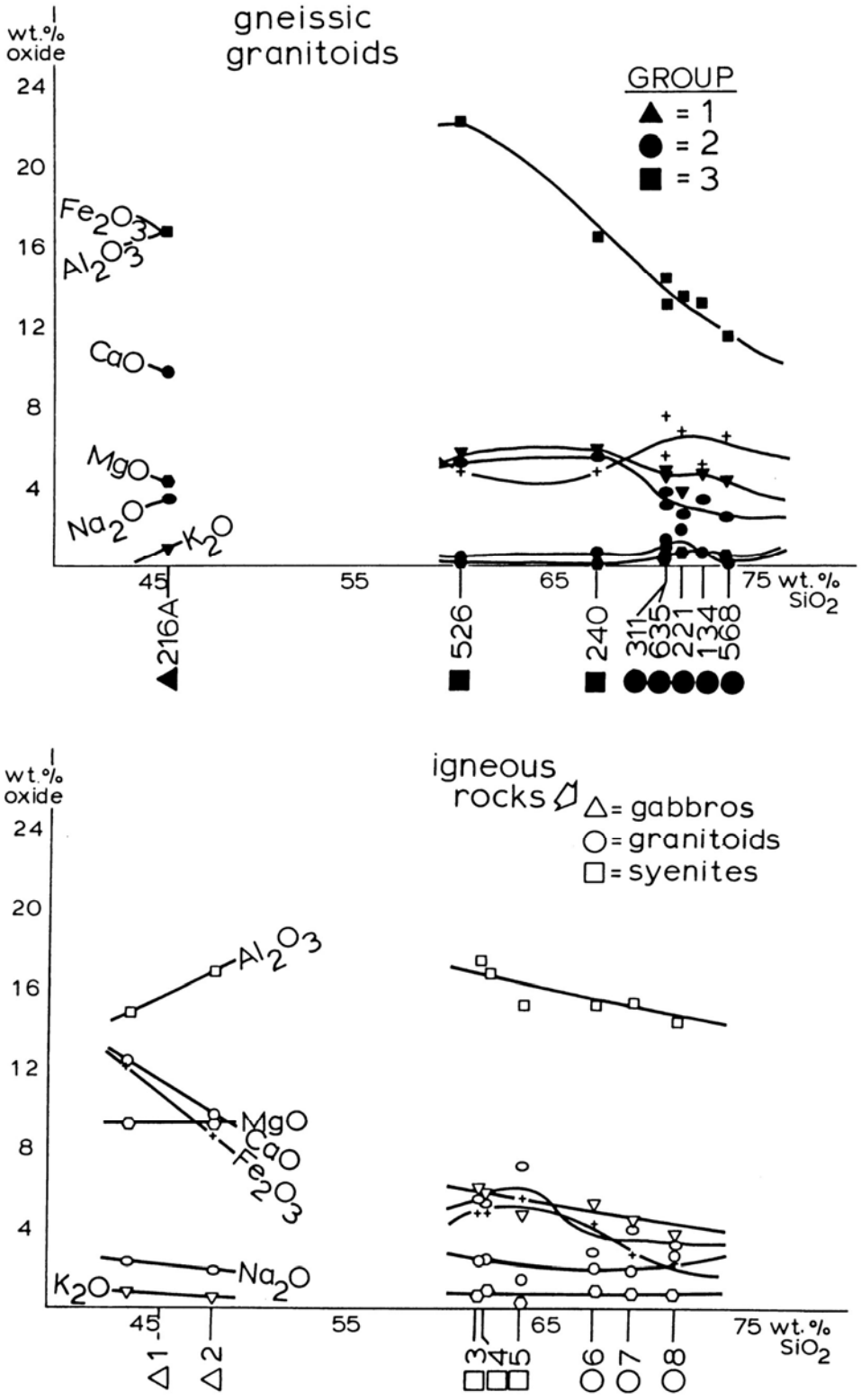

Figure 9 - Harker variation diagrams illustrating the major element trends of the Group 1, 2, and 3 gneisses in comparison to published igneous rock analyses of Table 4. Interpretation of this and the following diagram is problematical because of the likelihood that whole rock compositions of the gneisses reflect hybrid metamorphic-igneous origins.

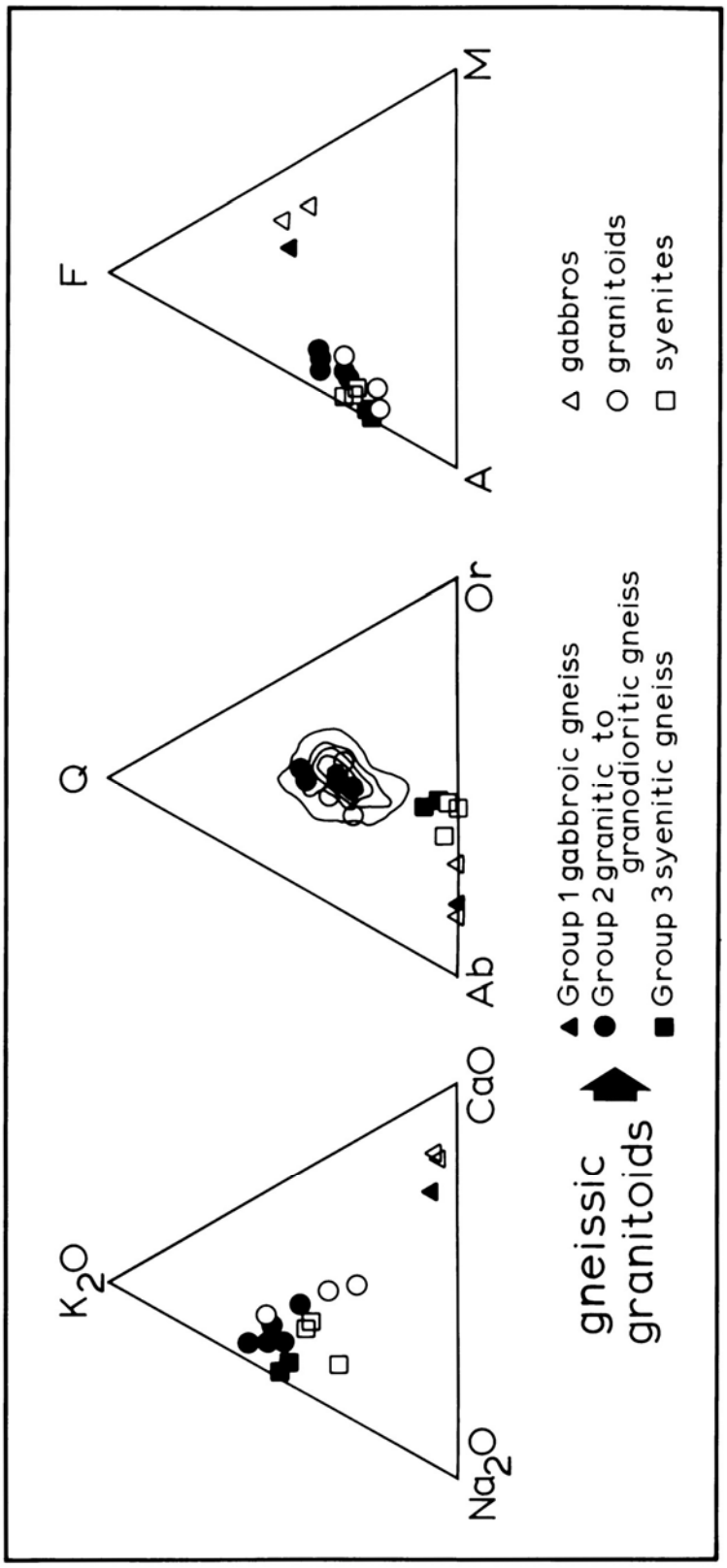

Figure 10 - Triangular variation diagrams indicating the relationship of alkalis (Na_20-K_20-CaO), normative Ab-Or-Q, and AFM.

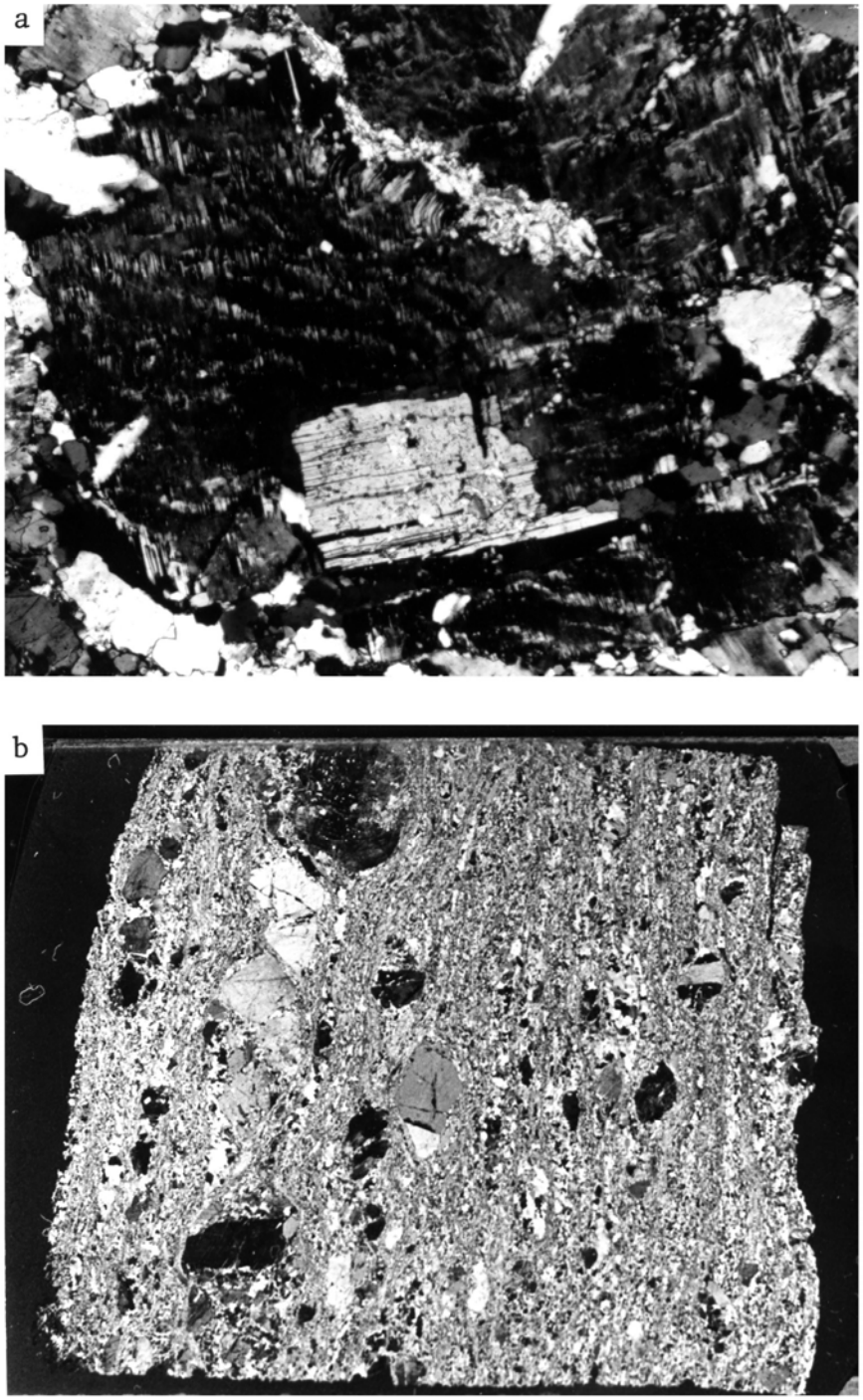

Figure 11 - **(a**) A relict perthite phenocryst in a granitic augen gneiss (R44) enclosing a twinned plagioclase crystal of probable comagmatic origin. Note that the perthite lamellae are internally deformed and locally folded along the borders of annealed fractures, and the incipient development of a recrystallized margin of feldspars, quartz, and mica.
(b) Macrophotograph of a potash feldspar granitic augen gneiss (K635) taken under crossed polars. The porphyroclasts (mostly perthite and microcline but some oligoclase and quartz) are rotated and cracked with local internal domains of recrystallized feldspar, quartz, and biotite. Fine-grained tails occur at the edges of the flattened augen. The vertical blastomylonitic S_3 foliation is composed of aggregates of finely recrystallized potash feldspar, quartz, plagioclase, biotite, and muscovite. Horizontal frame width is roughly 40 mm.

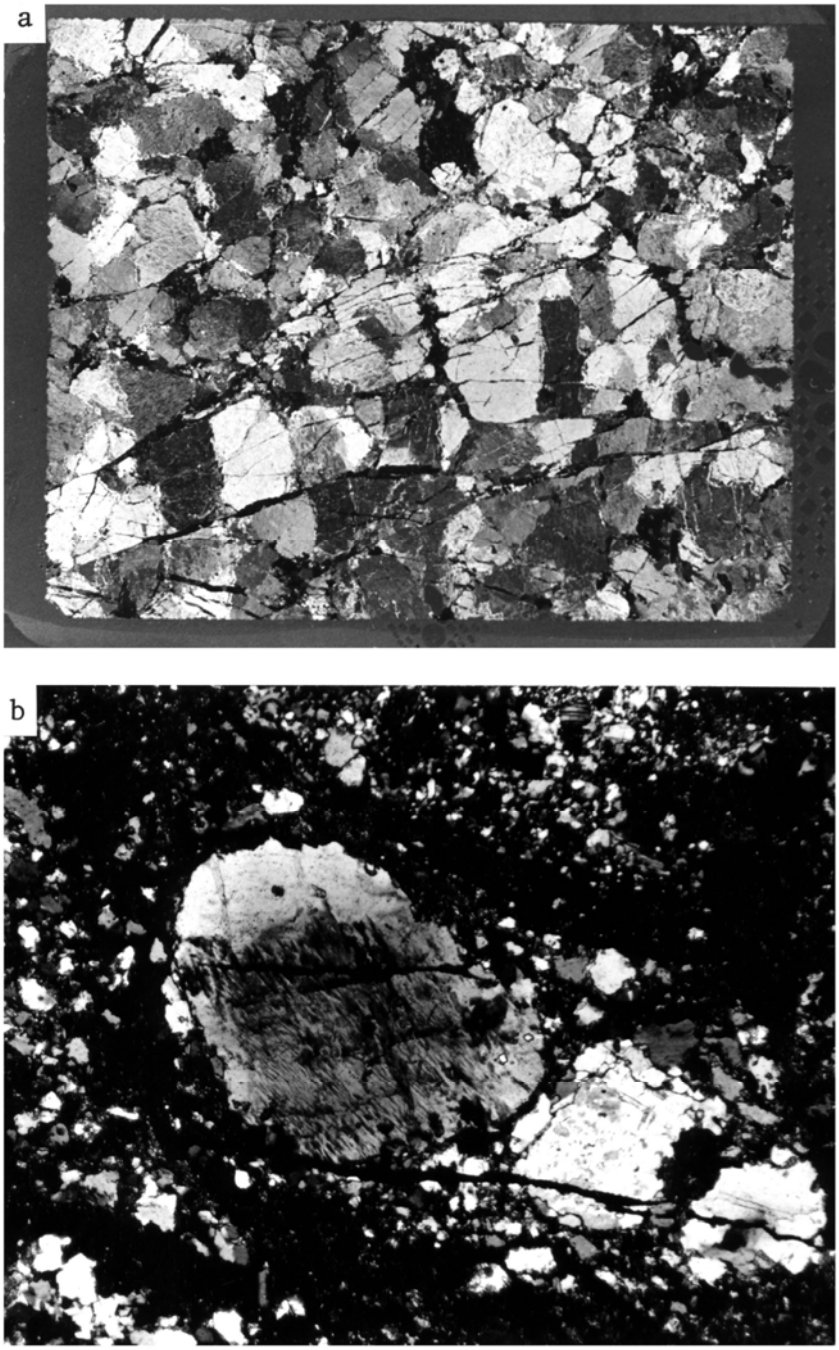

Figure 12 - **(a)** Deformed syenite (E212) with fractured angular perthite cut by microveins of recrystallized hastingsite, biotite, and locally, psilomelane. The hastingsite is optically distinct (B-, 2V = 0°-20°, birefringence = 0.019±0.003, x near a = yellow, y = b = medium khaki green, z near c = deep blue green, max. extinction = 19°t2°) and forms S_2 prismatic crystals in reaction with biotite in the interstices between feldspars. The hastingsite also forms subidioblastic S_3 acicular crystals within the veins and the S_3 veins locally cut the S_2 prismatic crystals. Macrophotograph taken with crossed polars; horizontal frame width is roughly 40 mm.
(b) Photomicrograph of two cracked and scaly-edged perthite porphyroclasts set in a fine-grained foliation composed of intergrown hastingsite, biotite, potash feldspar, and quartz (R255). Due to the fine grain size and strong absorption of both the hastingsite and biotite at extinction, the field of view is very dark. Note how shards of the feldspars, which may have once been continuous with the large augen, are spalled off their edges and incorporated into the S_3 foliation.

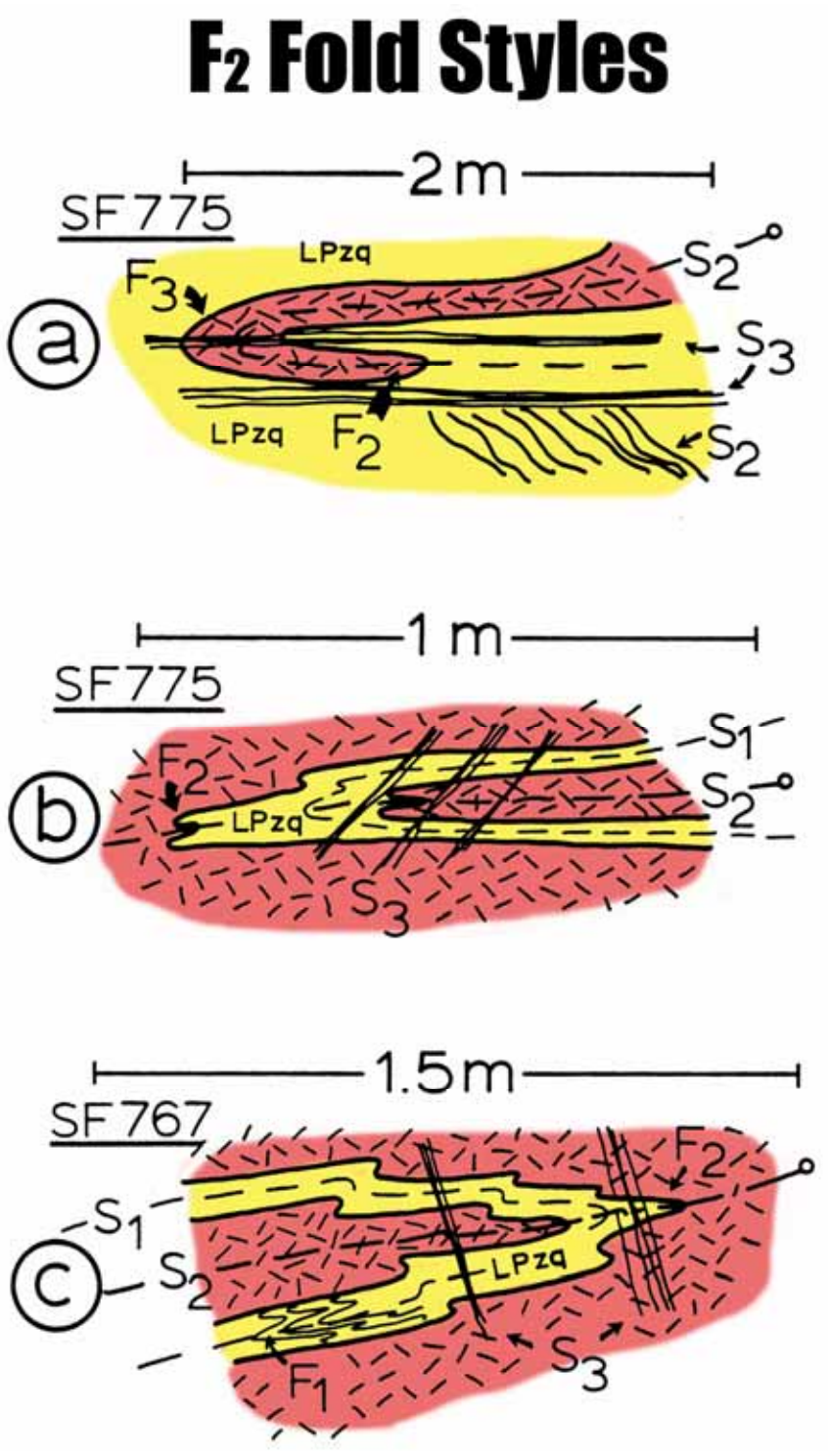

Figure 13 - Relationship of the gneissic granitoids (stippled) to F_2 and F_3 folds and related structures. Same symbols as Figure 6.
(a) An F_2 fold developed in granitic gneiss and Shoo Fly quartzite is redeformed by F_3 folds and S_3,mylonitic shears. Note the local high
(b) An F_2 isoclinal fold of a foliated (S_1) quartzite xenolith which is cut by domainal S_3 mylonitic shears.
(c) Local truncation of F_1 fold hinges in a deformed quartzite xenolith by granitoid gneiss. The quartzite and gneiss are folded by F_2 and cut by S_3 shears.

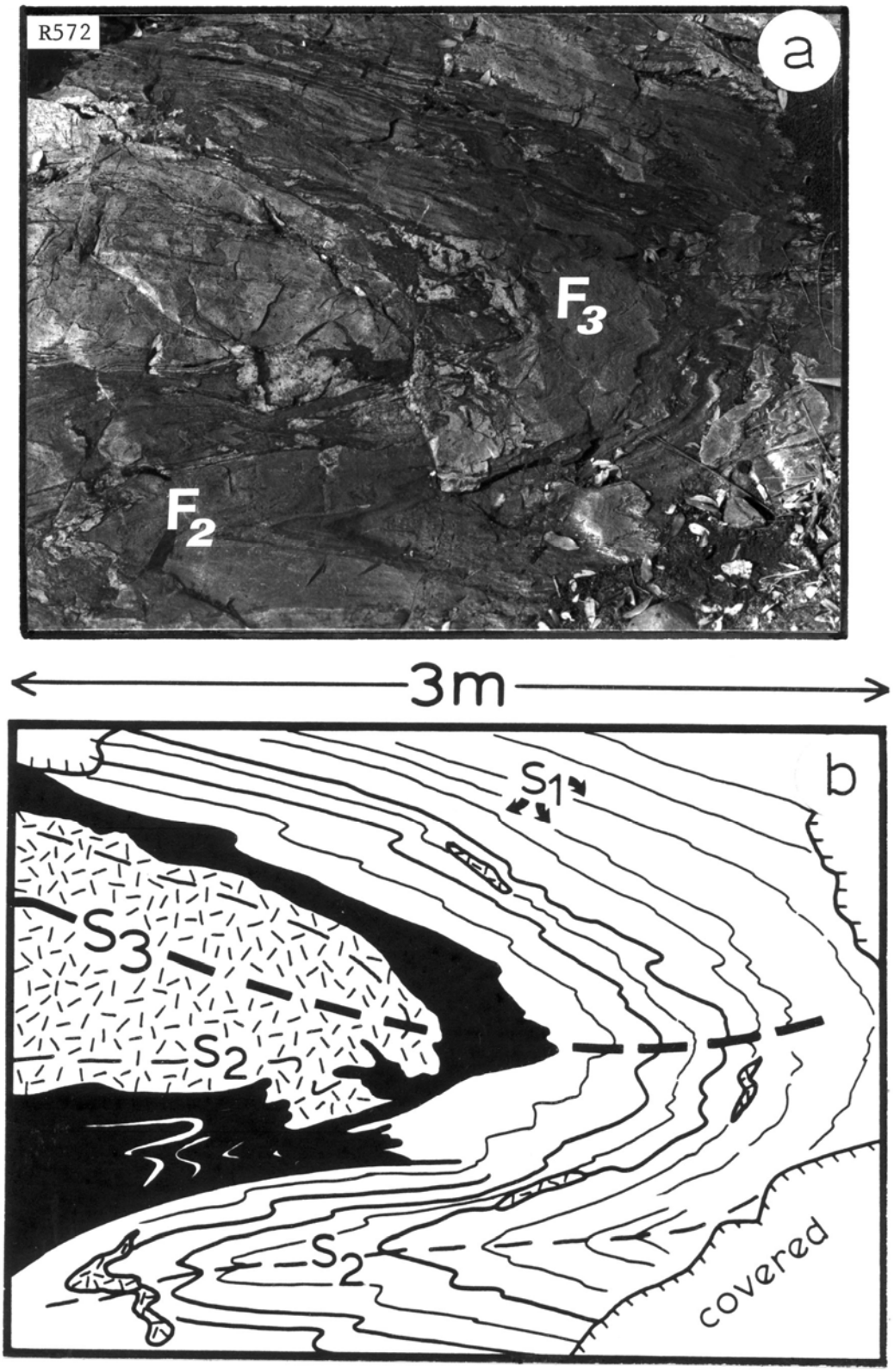

Figure 14 - Reclined F_3 fold of S_2 foliation in granitic gneiss (stippled). Note the irregular intrusive contact with laminated quartz-mica schist (black) and interlayered quartzite (uncolored). Smaller injections of gneissic granitoid occur in the quartzite. The warping of the S_3 axial surface is caused by F_4 folding.

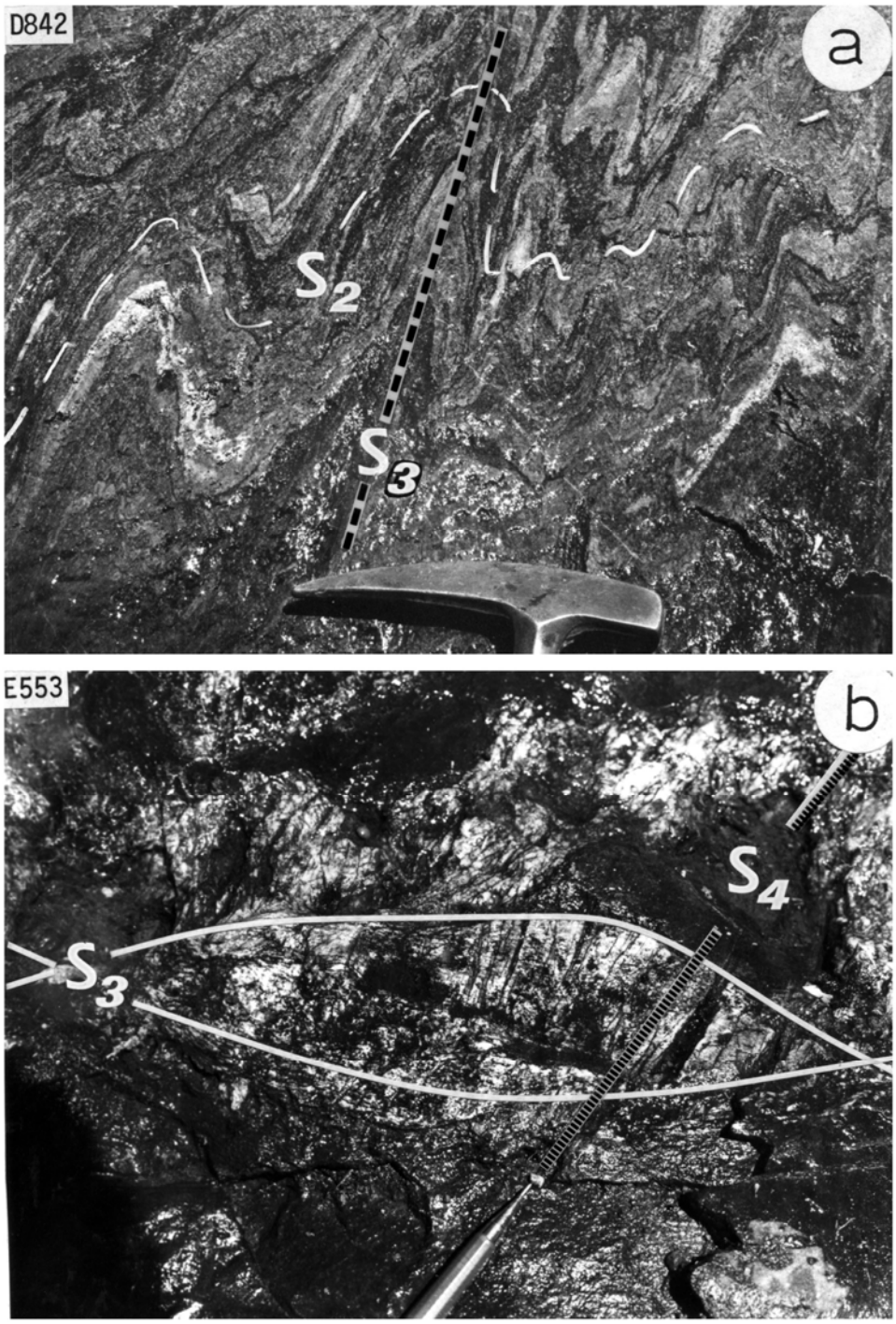

Figure 15 - Expression of D_3 deformation in gneiss varies from folding of S_2 foliation **(a)** to the creation of shear-bounded elipsoidal slivers **(b)**. In **(a)** cm-scale lit-par-lit injections of granitic gneiss in quartzite are isoclinally folded by F_2 folds and tightly refolded by F_3. The S_2 axial surface trends across the photo from upper right to center left where the F_2 hinge is located. Hammer head is 18 cm long.
(b) Mylonitic S_3 shears surround and crosscut a 24 cm long ellipsoidal sliver of foliated granitic gneiss. The sliver is flattened into parallelism with S_3 which can be traced into the axial surfaces of tight folds of S_2 foliation within the slivers of gneiss. The shears and sliver lie within a 14 cm thick ductile shear zone. The S_3 fabric and the sliver are cut by an anastomosing S_4 black residue cleavage composed of fine-grained biotite±quartz±magnetite. Pencil scale is 14.5 cm long.

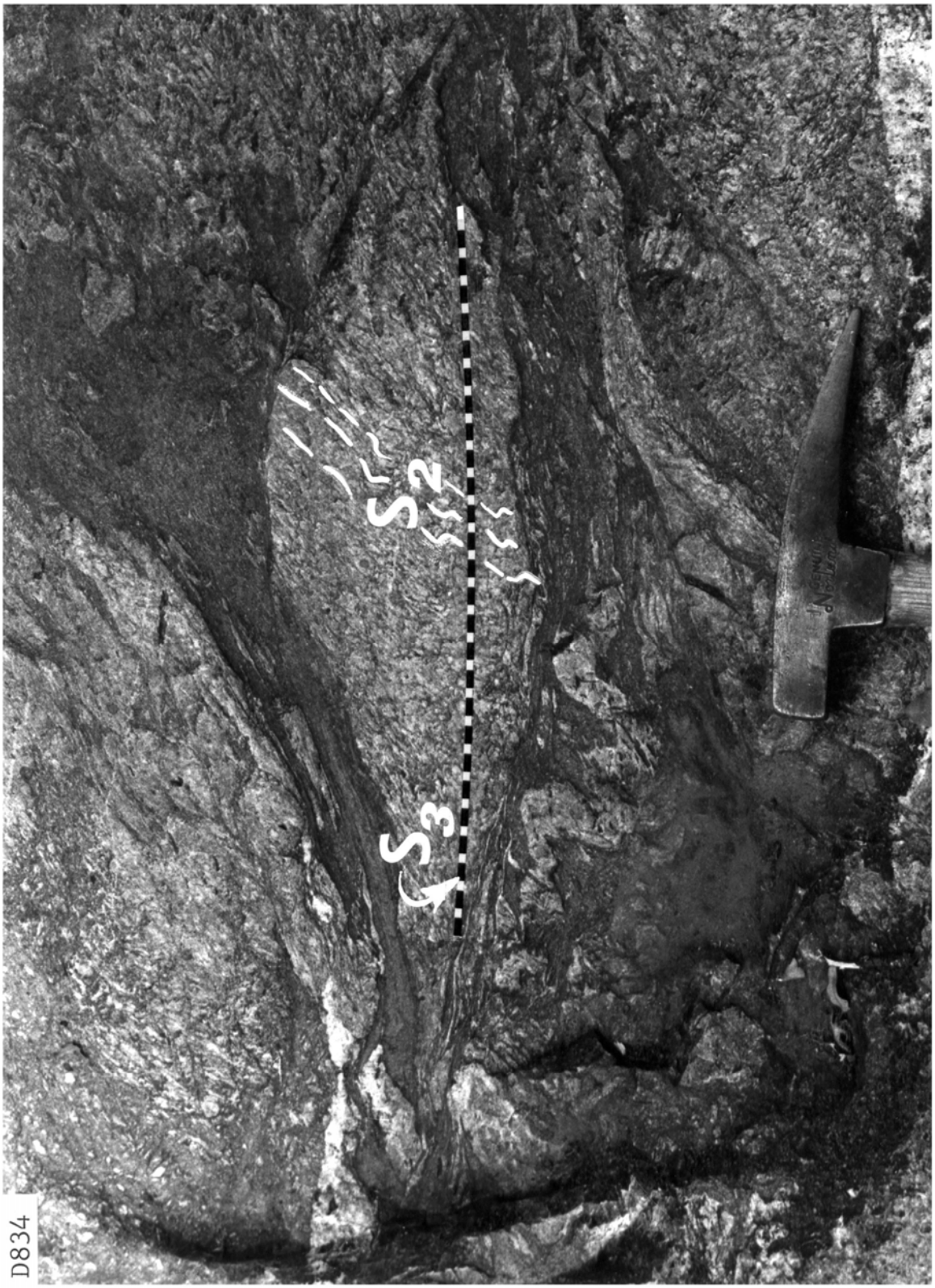

Figure 16 - A faint S_2 foliation is preserved in the interior of a 50 cm ellipsoidal sliver of augen gneiss (D834). The gneiss contains small isoclinal F_3 folds of S_2 foliation. The S_3 biotite-rich shears both cut across and form the boundaries of the sliver and can be traced throughout the outcrop.

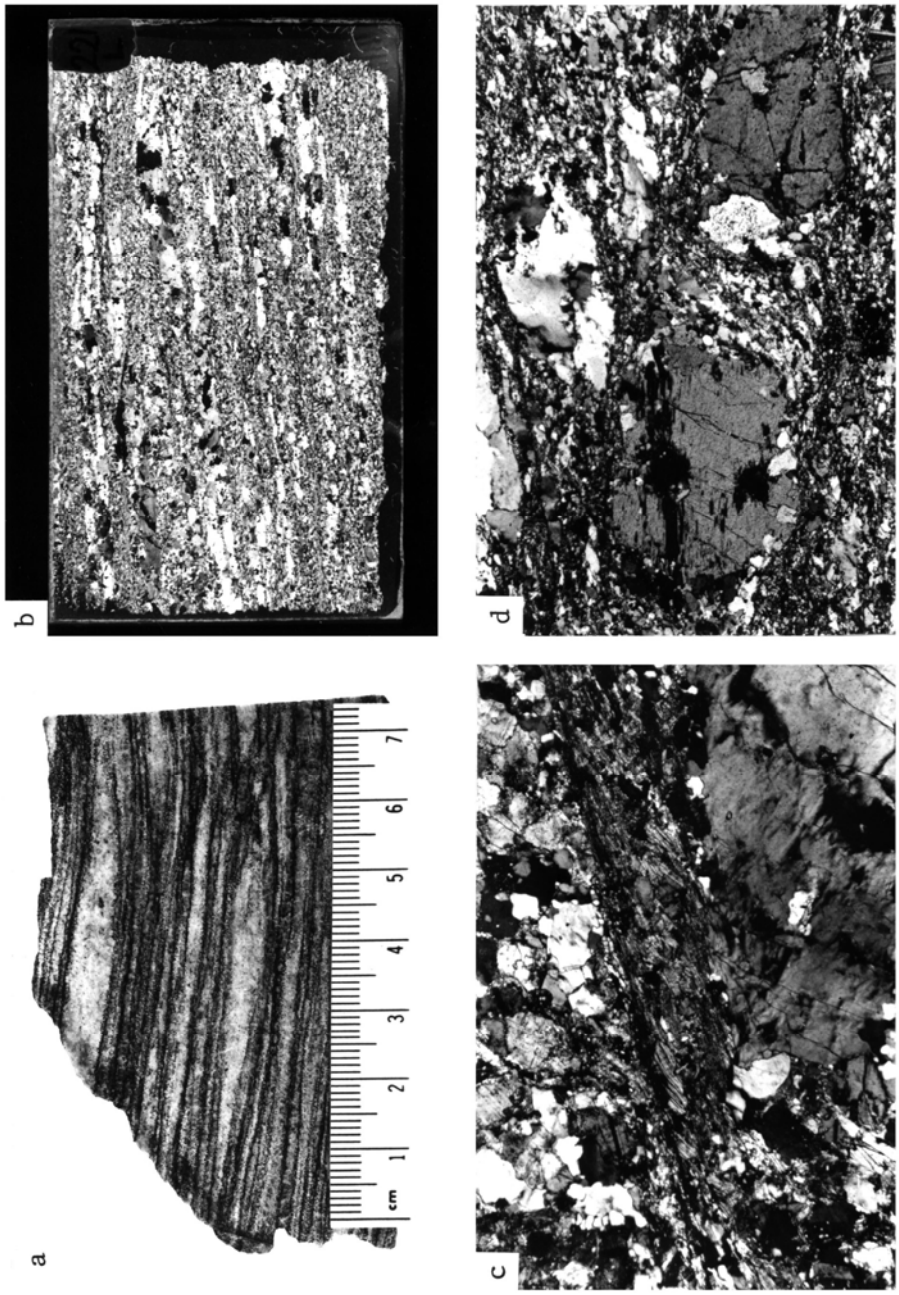

Figure 17 - **(a)** Macrophotograph of the Busse road granitic gneiss (BR221) cut parallel to the L_3 lineation showing the highly enlongate lenticular aggregates of quartz and feldspar bounded by micaceous layers. Rocks sectioned perpendicular to L_3 exhibit augen textures similar to that shown if Figure ll b.
(b) Macrophotograph of a thin section cut from the preceding slab (17a) taken with crossed polars. During D_3, stretching was accommodated by recrystallization of individual minerals and mineral aggregates producing the prominent banding shown here. Recrystallization during D_3 has obliterated the D_2 fabrics. The thin section is 46 mm long.
(c) Photomicrograph of a biotite-rich S_3 shear with finely recrystallized feldspar and quartz along its margin. A relict S_2 biotite porphyroblast of metamorphic parentage is deformed by internal slip and peripheral shredding, recrystallization, and grain-size reduction parallel to the S_3 shear.
(d) Photomicrograph of augen of potash feldspar and strained quartz from a highly sheared portion of the Busse road gneiss body. Rotation, internal cracks, edge corrosion, and marginal granulation with recrystallized rims occurred during D_3 deformation.

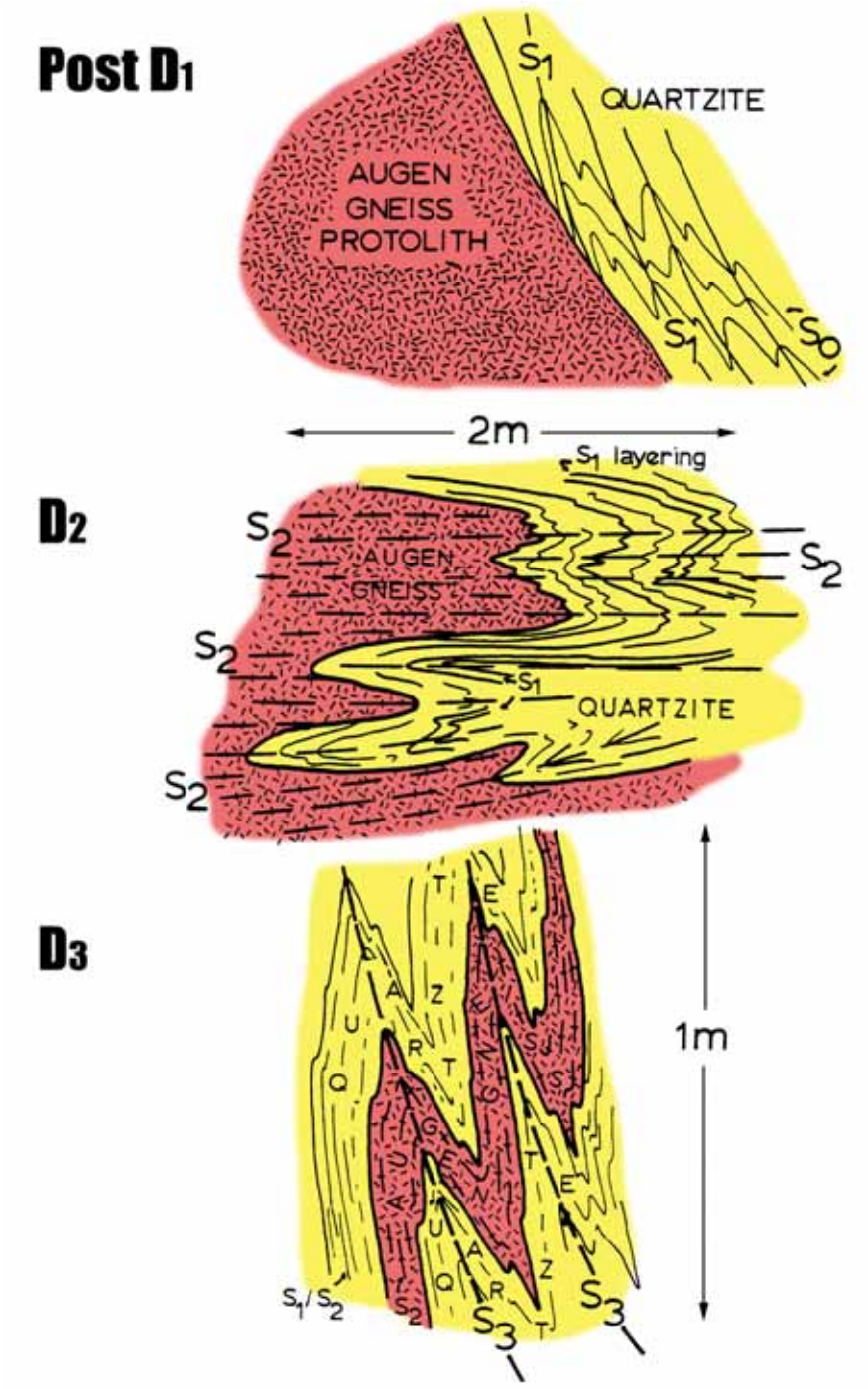

Figure 18 - Field drawings from various localities summarize the relationship of the augen gneisses (stippled) to structural elements formed during D_1, D_2, and D_3 in the Shoo Fly Complex.
(a) Contact relations of the augen gneiss protoliths indicate that they postdate an early (D_1) phase of folding and metamorphism in the Shoo Fly.
(b) The Shoo Fly and the augen gneiss protoliths are deformed by isoclinal F_2 folds and cut by a penetrative S_2 foliation.
(c) F_3 folding and shearing along S_3 axial surfaces redeforms the foliated gneiss and Shoo Fly host rocks in response to the D_3 regional deformation (formation of the Calaveras-Shoo Fly thrust). Curvature of the S_3 axial surfaces is due to F_4 and younger folding events (see Table 1).

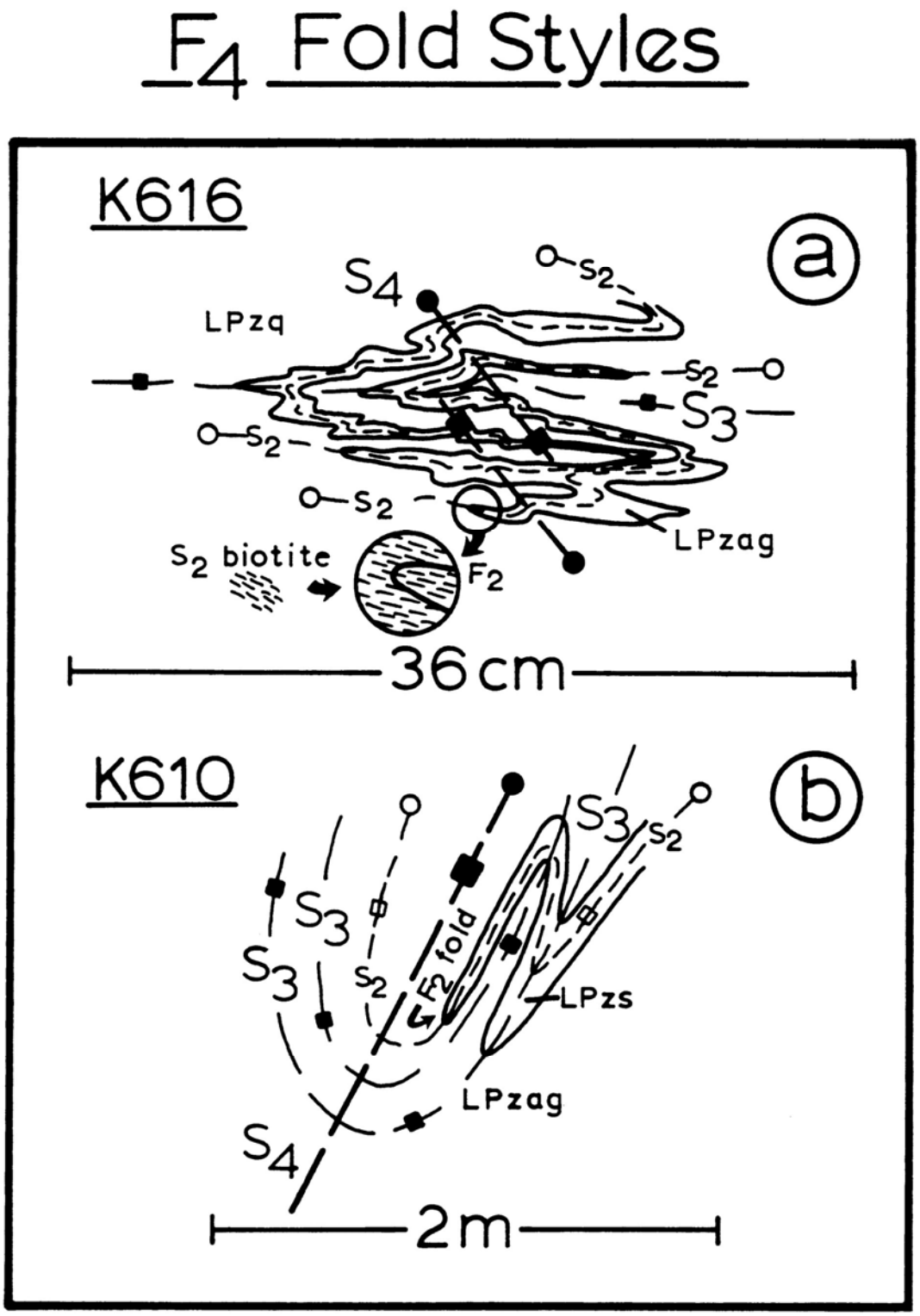

Figure 19 - Styles of F_4 folds and their relationship to older F_2 and F_3 folds and related structures. Same symbols as Figure 6. **(a)** Asymmetric F_4 folds superimposed on twice isoclinally folded (F_2 x F_3) "lit-parlit" in injections of gneissic granitoid. The circled area illustrates S_2 biotite flakes grown parallel to the axial surface of an F_2 isoclinal hinge.
(b) A tight F_4 fold deforms an already infolded (F_2 x F_3) contact between schist and granitic gneiss.

Table 1 - GEOLOGIC HISTORY OF THE JUPITER AREA TUOLUMNE COUNTY, CALIFORNIA

Holocene	Upland are affected by periglacial solifluxion.
Pleistocene	Accelerated uplift and development of trellised, deeply-incised, rejuventated stream system
Mio-Pliocene	I_8 Mudflow breccia ad volcanic flows of the Relief Peak Formation.
Oligo-Miocene	I_7 Rhyolitic ash flows of the Valley Spring Formation.
Eocene	Planation surface developed after post-Cretaceous uplift and erosion. Formation of consequent stream system.
Cretaceous	I_6 Intrusion of Sierra Nevada batholith and possibly other plutons.
Late Cretaceous (?)	D_7 N60°W to E-W, 90° fracture cleavage (S_7) parallel to axial surfaces of open F_7 folds.
Late Jurassic(?)	D_6 N30°E, 90° crenulation cleavage, black residue cleavage (S_6) parallel to axial surfaces of asymmetric open F_6 folds. Retrograde metamorphism.
NEVADAN OROGENY Late Jurassic	D_5 N32°W, 78°NE crenulation cleavage, black residue cleavage (S_5) parallel to axial surfaces of asymmetric open F_5 folds. Retrograde metamorphism.
Middle Jurassic(?)	I_5 Intrusion of the Knight Creek and possibly other plutons
Middle Jurassic	I_4 Intrusion of 159-157 m.y. Sonora dike swarm, sub-parallel to S_4.
Middle Jurassic	I_5 Intrusion of 170-164 m.y. Standard, Parrotts Ferry, and possibly other plutons.
Late Triassic(?)	D_4 N85°W, 90° spaced mica schistosity and crenulation cleavage (S_4) parallel to axial surfaces of isoclinal, tight, and crenulate F_4 folds plunging 47° into S85°E. Biotite-garnet grade metamorphism.
Permo-Triassic (?)	I_2 Intrusion of granitoid dikes and sills. Some foliated sills are late-syntectonic with respect to D_3

SONOMA OROGENY? Permp-Triassic (?)	D_3 Formation of the Calaveras- Shoo Fly thrust zone and intra-Shoo Fly ductile shear zones. Blastomylonitic foliation (S_3) parallel to the axial surfaces of isoclinal and rootless folds (F_3) plunging 42° into S75°E. There is significant tectonic imbrication within 2 km of the fault. The obliterative D_3 thrust fabric becomes a domainal blastomylonite and a mica foliation eastward from the thrust zone formed parallel to the axial surfaces of isoclinal to tight F_3 folds. Epidote-amphibolite grade metamorphism.
ANTLER OROGENY? Middle Paleozoic	D_2 Mica foliation and flattening foliation (+mylonite) (S_2) parallel to axial surfaces of isoclinal and rootless folds (F_2) with variable plunges. Folding and recrystallization of granitoid gneiss – Shoo Fly contacts. Amphibolite grade metamorphism.
Siluro-Ordovician to Permian (?)	I_1 Intrusion of protoliths of the gnessic granitoids as plutons into the Shoo Fly. Compositions range from mainly granite, granodiorite, and syenite to gabbro. Intrustive contacts are discordant, cutting the S_1 metamorphic layering.
ANTLER OROGENY? Pre-Silurian (?)	D_1 Metamorphic layering (S_1) in quartzite and quartz-mica-(feldspar)-gneiss parallel to axial surfaces of intrafolial and long-limbed isoclinal folds (F_1). Biotite grade metamorphism.
Late Precambrian (?) to Early Paleozoic	Deposition as a slope-rise sequence adjacent to the western edge of the North American miogeosyncline.

Table 1 - An interpretive geologic history of the Shoo Fly Complex of Tuolumne County, California. Numbered deformational (D_x) and igneous (I_x) events are listed in order of relative age based upon field relationships and geochronologic age data of Sharp and Saleeby (1979); Sharp (1980); Sharp and others (1982; in press), and Stern and others (1981). The absolute ages of the various D-events will be subject to change as more isotopic data becomes available.

WHOLE ROCK ANALYSES AND CIPW NORMS: ORTHOGNEISSES FROM THE SHOO FLY COMPLEX

	▲ 216A	■ 526	■ 240	● 311	● 635	● 221	● 134	● 568
SiO_2	45.77	60.29	67.04	70.47	70.54	71.24	72.57	73.73
Al_2O_3	16.77	22.04	16.34	12.99	14.27	13.39	13.11	11.41
Fe_2O_3*	16.75	4.78	4.68	7.48	5.46	6.78	5.12	6.41
MnO	0.26	0.10	0.09	0.07	0.05	0.08	0.06	0.06
MgO	4.24	0.22	0.09	0.41	0.58	0.69	0.57	0.56
CaO	9.66	0.26	0.74	0.86	1.13	1.81	0.68	0.37
Na_2O	3.39	5.19	5.53	3.66	3.09	2.64	3.35	2.47
K_2O	0.95	5.72	5.86	4.58	4.81	3.67	4.69	4.31
TiO_2	2.41	0.14	0.29	0.38	0.33	0.66	0.24	0.38
P_2O_5	0.67	0.04	0.03	0.04	0.14	0.18	0.10	0.11
TOTAL	101.01	98.78	100.69	100.94	100.40	101.14	100.49	99.81
Norms								
Q		4.65	8.43	25.15	28.24	33.86	30.21	38.01
C		6.93		0.53	2.23	2.17	1.50	2.25
Or	5.62	33.82	34.65	27.08	28.44	21.70	27.73	25.48
Ab	24.13	43.92	46.80	30.97	26.15	22.34	28.35	20.90
An	27.75	1.05	2.46	4.03	4.78	7.92	2.79	1.19
Wo	6.78		0.43					
En	8.16	0.55	0.23	1.02	1.44	1.72	1.42	1.39
Fs	14.87	6.06	5.69	9.08	6.53	7.73	6.28	7.69
Mt	3.64	1.04	1.01	1.62	1.19	1.48	1.12	1.39
Il	4.58	0.27	0.55	0.72	0.63	1.25	0.46	0.72
Ap	1.46	0.09	0.07	0.09	0.31	0.39	0.22	0.24
Ne	2.47							

*Total Fe as Fe_2O_3

■ GROUP 3 GNEISSES (Syenitic)

● GROUP 2 GNEISSES (Granite to Granodiorite)

▲ GROUP 1 GNEISSES (Gabbroic)

Table 2 - Whole-rock X-ray fluorescence major element analyses and CIP W norms using the fused-disc method of Harvey and others (1973). Samples were crushed then powdered on a rotary disc pulverizer which introduced up to 2.2 wt. % Fe according to Johnson and Maxwell (1981). The analytical error was confirmed by utilizing hand-crushed control specimens. No correction for iron was made on Table 2 and as a result the other elements are proportionately underreported.

GNEISSIC GRANITOIDS – MODAL ANALYSES

	216A	526	240	311	635	221	134	568
Potash Feldspar	--	51+	80*	36+	48	25	35	31
Quartz	tr	10	5	29	23	28	20	30
Plagioclase	30	19	3	19	20	24	26	19
Biotite	tr	3	2	8	4	15	6	12
Muscovite	--	7	--	5	2	4	10	4
Amphibole	35	10	8	--	--	--	--	--
Epidote	30	--	--	--	tr	tr	tr	--
Chlorite	tr	--	--	3	2	4	1	--
Opaques	5	tr	2	tr	1	tr	2	4

+ = mostly perthite tr = trace * = some perthite

Based on 500 counts per stained slab.

Table 3 - Modal analyses of the gneissic granitoids of Table 2 based upon 500 counts per stained thin section chip.

	1	2	3	4	5	6	7	8
SiO_2	43.94	48.36	61.54	61.86	63.75	66.88	71.42	72.08
Al_2O_3	14.87	16.84	17.45	16.91	15.32	15.66	14.47	13.86
Fe_2O_3*	12.15	8.76	4.92	4.95	5.64	3.92	2.41	2.55
MnO	0.16	0.14	0.09	0.11	0.17	0.07	0.08	0.06
MgO	9.31	9.27	0.74	0.96	0.36	1.57	0.78	0.52
CaO	12.37	9.72	2.39	2.54	1.52	3.56	2.86	1.33
Na_2O	2.32	1.96	5.59	5.46	7.28	3.84	3.44	3.08
K_2O	0.92	0.63	5.97	5.91	4.62	3.07	3.69	5.46
TiO_2	2.86	1.32	0.59	0.58	0.66	0.57	0.25	0.37
P_2O_5	0.44	0.21	0.19	0.19	0.15	0.21	0.10	0.18
TOTAL	99.34	97.21	99.47	99.47	99.47	99.35	99.50	99.49
Rock Type	Average Alkali Gabbro	Average Gabbro	Ferro-hastingsite Syenite	Average Alkali Syenite	Aegerine Syenite	Average Granodiorite	Quartz Monzonite	Average Granite

* Total Fe as Fe_2O_3

References: Bateman and others (1963) = 7
Nockolds (1954) = 1-6, 8

Table 4 - Major element analyses of representative igneous rocks similar in composition to the gneissic granitoids. Data from Bateman and others (1963) and Nockolds (1954)

CHAPTER 3

Geology and geochemistry of the Sonora dike swarm;

central Sierra Nevada foothills belt, California

ABSTRACT

The Sonora dike swarm, an areally extensive (>1500 km^2) consanquineous suite of dikes of amphibole-, plagioclase-, and augite-phyric andesite, lamprophyre, and basalt intrudes the foothills metamorphic belt of the central Sierra Nevada near lat. 38°N in California. The swarm is subvertical and trends east-west across two polyphase deformed Paleozoic-Mesozoic(?) tectonostratigraphic units. These units, the Shoo Fly and Calaveras Complexes, also form the basement to a middle Jurassic calc-alkaline arc (Jawbone granitoid sequence of Stern and others, 1981) that is partly obscured on the east by granitoids of the Sierra Nevada batholith.

Geochronologic data of Sharp (1980) indicates that the dikes are also middle Jurassic (157-159 m.y.), which suggests that they are petrogenetically related to the Jawbone granitoid sequence. Crosscutting igneous relations and similarities in modal mineralogy between the Sonora dikes and the Jawbone plutons helps substantiate their association. Field, petrographic, and geochemical studies indicate that the Sonora dikes are derived from calc-alkaline magmas that probably formed during subduction of oceanic crust beneath a continental arc.

The dikes have provided an important structural marker in the Shoo Fly and Calaveras Complexes. Since the dikes truncate and intrude along an east-west-trending regional foliation in the metamorphic belt that formed parallel to the axial surfaces of folds of the Calaveras-Shoo Fly thrust, clearly the juxtaposition of the Shoo Fly and Calaveras Complexes and the east-west folds are pre-middle Jurassic events. In addition, the dikes are deformed by two superimposed phases of Nevadan (late Jurassic) folds and related cleavage development.

Dilation of the east-west-trending metamorphic fabric in the marginal arc basement preceded and probably was coeval with intrusion of the dike swarm. Such north-south extension was most likely the result of crustal compression due to subduction which was transmitted into

the overriding plate. The north-south extension was probably enhanced by the nearly orthogonal relationship between the trend of the arc (NNW-SSE) and the east-west-trending spaced achistosity of the Shoo Fly and Calaveras.

INTRODUCTION

An extensive swarm of andesite, lamprophyre, and basalt dikes (called the Sonora dike swarm in this paper) intrudes deformed and metamorphosed rocks of Paleozoic and Mesozoic(?) age in the central part of the Sierra Nevada foothills, California. The dikes occur in the lower Paleozoic Shoo Fly Complex and the upper Paleozoic to lower Mesozoic(?) Calaveras Complex and cut across the Calaveras-Shoo Fly thrust, a ductile shear zone which separates the two metamorphic units (Fig. 1).

The dike swarm also cuts across several Jurassic granitic plutons and predates some younger granitoid plutons. A 157-159 m.y. K-Ar hornblende age on some mafic dikes near Sonora by Sharp (1980) indicates that the dikes were intruded in middle Jurassic time.

The Sonora dike swarm is similar in age to sheeted dikes of the Smartville ophiolite and other mafic rocks found in the western belt (Unit 3 in Fig. 1) of the Sierra Nevada and to rocks in the Coast Range ophiolite (Saleeby, 1982, 1983). However, as shown in this paper, the Sonora dikes are similar in lithology and chemistry to calc-alkaline rocks of the 148 m.y. Independence dike swarm in eastern California (Moore and Hopson, 1961; Chen and Moore, 1979). In view of the tectonic setting of the dike swarm near a Jurassic convergent margin, detailed field, petrographic, and geochemical studies of the swarm were conducted to establish possible clues as to its petrogenesis, its position as a structural marker in the Shoo Fly Complex, and the significance of the swarm as a paleostress indicator.

Regional Setting

Highly deformed and metamorphosed Paleozoic and Mesozoic rocks occur in the western foothills of the central Sierra Nevada. Intruded on the east by the Sierra Nevada batholith and overlain unconformably to the west by post-Jurassic rocks of the Great Valley, the metamorphic rocks have been subdivided into three east-dipping ductile-fault-bounded tectonostratigraphic units (Fig. 1). The units are the upper Precambrian(?)-lower Paleozoic (LPz) Shoo Fly Complex (Unit 1), the upper Paleozoic-lower Mesozoic(?) (UPz) Calaveras Complex (Unit 2), and a western belt (Unit 3) composed of Jurassic and Triassic volcanic and volcaniclastic rocks (Jrp) (Schweickert and others, 1984).

The Shoo Fly Complex (Unit 1) consists of a polyphase deformed, epidote-amphibolite grade assemblage of quartzite, quartzofeldspathic gneiss, granitoid orthogneiss, schist, and phyllite with subordinate marble and calc-silicate rocks (Merguerian and Schweickert, 1980, Merguerian, 1981, 1982, 1983). The Calaveras Complex (Unit 2) is a deformed oceanic assemblage of chaotic argillite, chert-argillite, massive and rhythmically-bedded chert, and marble (Schweickert and others, 1977). The western belt (Unit 3) consists of folded slate, graywacke, phyllite, and augitic greenstone and pyroclastic rocks (Clark, 1964, 1970; Schweickert and Bogen, 1983). Thus, from east to west across the foothills metamorphic belt the rocks become progressively younger and exhibit progressively less deformation and metamorphism (Merguerian and others, 1983).

Regionally important tectonic boundaries occur between the tectono-stratigraphic units (Figs. 1, 2). Both the Calaveras-Shoo Fly thrust and the Sonora fault are east-dipping syn-metamorphic ductile shear zones that truncate and transpose structural and metamorphic fabrics in older units to the east. The Calaveras-Shoo Fly thrust truncates lithologic units of the

Shoo Fly (Fig. 3). The thrust is marked by a 1-2 km wide zone of syn-metamorphic ductile deformation characterized by intense localized isoclinal and rootless folds, sheared and imbricated rock units, and blastomylonite and other ductile fault rocks. Detailed maps and structural, stratigraphic, and petrographic descriptions of the Shoo Fly Complex and the Calaveras-Shoo Fly thrust appear in Chapter 1.

The Sonora fault (Fig. 1) is a ductile shear zone that separates actinolite-stilpnomelane bearing phyllite and green schist (Jrp) from the Calaveras Complex (Schweickert and Bogen, 1983). Locally, dikes of the Sonora swarm are deformed and truncated by the Sonora fault. The Jurassic oceanic rocks of the western belt (Unit 3) are internally imbricated along the Melones fault zone which occurs west of the Sonora fault (Figs. 1, 2).

Dikes of the Sonora swarm occur to the east of the Sonora fault in both the Shoo Fly and Calaveras Complexes. They occupy a 1550 km^2 area over 55 km long and 25 km wide centered near lat. 38°N and long. 120°15'W (Fig. 4). Over 1000 dikes have been mapped in the Shoo Fly and Calaveras Complexes by Merguerian and Schweickert (unpub. data), respectively.

THE SONORA DIRE SWARM

Form and occurrence

The Sonora dike swarm is most prominently developed between the North Fork Stanislaus and Tuolumne rivers (Fig. 1). South of the Tuolumne and north of the Stanislaus Rivers only sporadic dikes occur. The study area of this report (Fig. 3) includes one of the denser parts of the swarm in parts of the Stanislaus, Crandall Peak, Columbia SE and Twain Harte 7-1/2-minute quadrangles. The area lies north of Twain Harte and east of Columbia, California (Plate 1).

Over 270 solitary dikes and zones of multiple dikes were examined in the Shoo Fly Complex (Figs. 3, 4). Solitary dikes vary from 3 cm to 15 m thick, averaging 1 m, and zones of profuse injections range up to 25 m thick. Due to the lack of continuous exposure the regional density of dikes is probably greater than indicated in figure 4. Individual dikes exposed along creek beds can commonly be traced for over 100 m with little variation in thickness (Fig. 5). Individual dikes have offshoots and chilled margins. Locally, the dikes contain elliptical xenoliths of foliated orthogneiss and quartzite (Fig. 6), typical Shoo Fly lithologies. The dikes clearly crosscut all subunits of the Shoo Fly Complex (Figs. 3, 4), and ductile fabrics in the Calaveras-Shoo Fly thrust zone and related structures in the Calaveras (discussed later) (Schweickert, 1981).

The dikes are divided into three distinct groups based upon lithology, petrography, and geochemistry:

A - dark gray, mottled, fine- to coarse-grained, plagioclase-phyric, pyroxene-free basalt and amphibole-phyric, labradorite andesite. The phenocrysts are euhedral and subhedral and are up to 4 mm in length. These dikes average 3 m in thickness.

B - gray-green to gray-black, dense, dominantly aphyric basalt and andesite which possess minor amounts of augite phenocrysts and brown amphibole microphenocrysts. These dikes have microgabbro and microdiorite cores when thicknesses exceed 2 m but their average thickness is 1.1 m.

C - light-gray to dark-gray lamprophyres (spessartite and vogesite) with non-oriented euhedral to subhedral pargastitic amphibole, light-green to colorless amphibole, augite, and plagioclase phenocrysts up to 4 mm long. Their average thickness is 0.4 m.

Numerous examples of cross-cutting relations, truncated flow layering, chilled margins, and cognate xenoliths indicate that the Group B dikes, which comprise roughly 30% of the dike swarm, are of median relative age. They always crosscut dikes of Group A, both Groups A and B are cut by dikes of Group C (Fig. 7). Observations throughout the swarm suggest that Groups A and B occur in subequal numbers and are slightly less common than Group C (A N B < C). The three groups of dikes appear to be randomly distributed throughout the study area and are not clustered into zones. Older dikes are thicker, on average, than younger dikes, suggesting either that the rate of intrusion decreased with time or that extension waned with time.

All three types of dikes strike roughly east-west with vertical dips (Fig. 9). They fill tension gashes and zig-zag fractures in the wall rocks and are statistically parallel to a pre-existing east-west trending spaced schistosity in the Calaveras and Shoo Fly Complexes which formed during a regionally important folding episode.

Petrography

The microscope shows that the Sonora dikes are holocrystalline andesite, basalt, and lamprophyre ranging in texture from porphyritic to aphanitic. Local hiatal seriate textures occur. In the interiors of thicker dikes with microgabbro and microdiorite cores, granophyric textures occur. The Group A and C dikes contain non-aligned, twinned and zoned phenocrysts of plagioclase, pargasite, light-green to colorless amphibole and augite. The Group B dikes are generally aphyric with the exception of rare augite (Table 1). Phenocrysts in all dikes are commonly highly altered and replaced or rimmed by amphibole, biotite, chlorite, and epidote minerals presumably due to Nevadan (Late Jurassic) lower green schist metamorphism of the Shoo Fly Complex (see Chapter 1, Table 2).

The groundmass of the dikes has a diabasic texture which consists of moderately altered intergrown crystals and microlites of plagioclase, brown and light-green to colorless amphibole, biotite, with some quartz and alkali feldspar (Table 1). Finely recrystallized fibrous amphibole, biotite, chlorite, calcite, and epidote minerals replace the groundmass minerals. Petrographically, the Group A and B dikes span the broad lithologic range of calc-alkaline andesite and basalt. The three dike groups are described in more detail below.

Group A - Plagioclase-phyric dikes. The oldest dikes of the Sonora swarm range from pyroxene-free porphyritic basalt to amphibole-bearing labradorite andesite (Table 1). They contain abundant, highly clouded, euhedral to subhedral plagioclase phenocrysts ranging from 0.5-4 mm in length set in a diabasic groundmass. The plagioclase exhibits oscillatory zoning and polysynthetic twinning (Fig. l0a) and shows little range in composition, varying from An_{56-62} (labradorite) as measured on a homogeneous crystal (sample #244) by the combined Albite-Carlsbad method of Tobi and Kroll (1975). The abundance of oscillatory zoned and twinned plagioclase and amphibole both as phenocrysts and as groundmass phases characterizes the Group A dikes.

Unlike the example shown in figure 10a, the plagioclase phenocrysts of Group A are commonly altered and turbid and are replaced by finely intergrown epidote, calcite, colloform and crystalline chlorite, quartz, sericite, pyrite, and opaque mineral dusts. In some extreme cases, the plagioclase phenocrysts are rounded, resorbed ghosts with preferentially darkened cores. The high degree of alteration of plagioclase phenocrysts and the local abundance of calcite and epidote in the groundmass suggests that they may have been more calcic than An_{62} originally. Plagioclase is locally glomerocrystic.

Some plagioclase-phyric dikes contain microphenocrysts (0 .1-0.2 mm) of oscillatory-zoned plagioclase and phenocrysts of partly resorbed light-green to colorless amphibole (Table 1). In one sample of basalt (238B), abundant, highly-twinned augite phenocrysts showing exsolution lamellae occur with minor plagioclase (Fig. l0b).

The groundmass in Group A dikes displays diabasic, granular, and locally pilotaxitic textures with omnipresent zoned and twinned plagioclase, twinned olive to yellow amphibole laths, biotite, light-green to colorless amphibole microlites, accessory acicular apatite, and opaque minerals. The groundmass plagioclases have labradorite cores (An_{60}) and rims as sodic as oligoclase (An_{l8}), but groundmass plagioclase is irregularly twinned and zoned, making accurate measurement of An content very difficult. Post-magmatic green schist metamorphic recrystallization strongly affected the groundmass textures. Locally, oval regions (former vesicles?) are filled with calcite and quartz±pyrite.\

Group B - Aphanitic dikes. Aphanitic dikes range from augitebearing basalt to basaltic andesite to andesite. Included in this group are altered dikes whose phenocrysts have been completely resorbed and replaced by fibrous amphibole, chlorite, biotite, calcite, and opaque mineral dusts. With the exception of augite, which is sometimes rimmed with green amphibole, large phenocrysts (>1 mm) do not occur in dikes of Group B (Table 1). The Group B aphanitic dikes exhibit diabasic, inter granular, and local hiatal-seriate textures. They are principally composed of abundant intergrown twinned plagioclase laths, prismatic yellow-brown and green amphibole, sparse biotite, and opaque minerals (Table 1). In comparison to the other dike groups the Group B dikes contain little calcite.

Microphenocrysts (0 .1-1 mm) of oscillatory zoned and twinned plagioclase and twinned brown and green composite amphiboles occur in many specimens (Fig. 1la). The composite

amphibole microphenocrysts are euhedral, highly twinned and although generally replaced, show green rims and brown cores containing local patches of clear amphibole. The brown amphibole is typically not associated with the augite phenocrysts but instead is restricted to the groundmass.

Post-magmatic metamorphic alteration produced fibrous amphibole and plagioclase coronas around primary amphiboles (Fig. llb), which were replaced by biotite, chlorite, epidote, actinolite, and hematite. Metamorphic recrystallization of the groundmass yielded amphibole-biotitechlorite-quartz assemblages.

Group C - Lamprophyre dikes. The youngest dikes of the Sonora swarm are markedly porphyritic amphibole and clinopyroxene-bearing lamprophyres with several generations of mafic phenocrysts set in a groundmass showing diabasic to granophyric texture. Ferromagnesian constituents, occurring both in the groundmass and as phenocrysts, account for up to 40% of the rock (Table 1). Locally glomeroporphyritic, the dominantly euhedral mafic phenocrysts consist of 0.5-4 mm prismatic pargasitic amphibole, light-green amphibole, augite, and rare biotite (Figs. 12a, b). Together, the amphiboles account for 70%-100% of the mafic phenocrysts in the Group C dikes. Augite can occur alone or comprises up to 30% of the phenocrysts when coexisting with amphibole (Table 1).

The pargasitic amphibole forms composite crystals with common, simple, and lamellar twinning, and compositional zoning (Fig. 12c). These crystals are moderately pleochroic with brown- to olive cores, pale olive- to pale yellow mantles, and light-green rims of hornblende. Optically, the pargasitic amphibole is biaxial (-) to (+) with 2V=90°, β=1 .67, Y=b, Z/\ c=18°, and varies in maximum birefringence from second order blue to second-order green (0.020-0.025). Generally, 2V is close to 90° but appears as low as 70°±5° in biaxial negative crystals. These optical properties indicate that this distinctive brown amphibole lies in the

pargasitic amphibole field but is not an end member. Both the brown and green amphiboles form single crystals and occur in the groundmass of the Group C dikes (Table 1).

Augite forms large subequant to equant phenocrysts that are preferentially altered, having globular outlines. The augite is biaxial + with 2V=45° and may therefore be diopsidic. Composite phenocrysts with augite cores and pargasitic rims are locally abundant (Fig. 12d) and may represent primary disequilibrium textures or be due to subsolidus reactions. It seems likely that the clinopyroxene-amphibole reaction textures are of magmatic origin because pargasitic amphibole is an important mineral phase in both the phenocrysts and groundmass of the dike group (Table 1).

The mafic phenocrysts, often remarkably fresh and crisp, are sometimes embayed, pseudomorphed, or rimmed by light-green to colorless amphibole or chlorite and replaced, commonly along cleavage traces, by biotite, chlorite, calcite, epidote minerals, talc, and hematite.

Plagioclase phenocrysts are rare and are commonly replaced by calcite, chlorite, sericite, zeolites, and opaque minerals and dusts. In some cases the cores of plagioclase crystals are clouded. Curiously, despite the survival of the mafic phenocrysts even in moderately altered dikes, plagioclase phenocrysts and groundmass laths are commonly completely resorbed and replaced.

The diabasic to granophyric groundmass of the Group C dikes consists of intergrown prismatic brown pargasitic amphibole, green amphibole, plagioclase, potash feldspar, and quartz with accessory biotite, apatite, and epidote and opaque minerals. Plagioclase microlites locally flow around pargasitic amphibole phenocrysts creating trachytic textures. The groundmass is

commonly clouded due to metamorphic growth of colorless, fibrous amphibole, biotite, epidote mineral aggregates, and veinlets of calcitetchlorite.

Calcite is widespread in the groundmass and in phenocrysts, and locally comprises up to 15% of the volume of the dikes. The calcite often occurs in oval areas (vesicles?) up to 1.5 mm in size. Other mineral phases in the vesicles include epidote, chlorite, green amphibole, chalcedonic and euhedral quartz, pyrite, and opaque minerals. The oval areas are commonly zoned, with calcite cores mantled by quartz and both rimmed by intergrown epidotefplagioclase.

In summary, Group C dikes are strongly porphyritic and exhibit several generations of euhedral mafic minerals including augite. These facts, together with the overall abundance of calcite and the selective resorption of feldspar are definitive characteristics of calc-alkaline lamprophyres as described by Williams and others (1982, p. 228-229). According to Streckeisen (1979) such amphibole- and clinopyroxene-phyric lamprophyres range from spessartite to vogesite depending upon whether plagioclase or potash feldspar, respectively, predominate the felsic phase.

Geochemistry

Fourteen dikes were analyzed for major elements with a Model 303 Perkin-Elmer atomic-absorption spectrophotometer (Tables 2, 3, 4). After removal of weathered rinds, the amount of rock crushed was 150-250 gm. Sample preparation and methodology is modified, after Johnson and Maxwell (1981) utilizing both natural and synthetic standards. Unfortunately, pulverization introduced from 3%-7% iron-contamination in the samples. The iron-contamination was analytically re-determined from the remaining samples and subtracted from the total and the remaining elements were increased according to their relative

concentrations. Due to the degree of alteration of the dikes, more sophisticated chemical analyses of the samples were deemed unwarranted.

These difficulties aside, questions concerning the degree of contamination of the original magmas and the effects of metamorphism must be evaluated. The presence of elliptical xenoliths of Shoo Fly rocks in a few dikes (Fig. 6) argues for some contamination, but xenoliths are exceedingly rare. Typically the dikes have sharp, chilled contacts with host rocks and are homogeneous in thicknesses less than 2 m.

The dikes were weakly recrystallized under lower green schist grade metamorphic conditions. Some are highly altered, but the survival of fresh, euhedral plagioclase, amphibole, and augite phenocrysts and groundmass minerals in many dikes suggests that metamorphic overprinting was domainal in nature (Table 1). In addition, some dikes of the swarm are strongly modified by deuteric mineralization. Considered together, the dikes show moderate effects of chemical alteration and as a result the interpretation of their analyses is somewhat tentative. Modifications of the original alkali content of the dikes has occurred and diagrams utilizing Na_20 and K_20 should not be interpreted rigorously. In addition, due to the overall abundance of calcite in many dikes, the normative calculations are best considered semi-quantitative. Despite these disclaimers, the geochemistry of the dike swarm is consistent with their calc-alkaline petrographic characteristics.

Major element analyses. Silica content of the dikes varies from 49.5% to 60.5% and most of them are quartz normative (Tables 2, 3, 4). A Harker variation diagram (Fig. 13) shows that Group A, B, and C dikes have similar major element patterns. In general, MgO, total Fe, and Ca0 decrease and $A1_20_3$, Na_20, and K_20 increase with increasing silica content. The major element trends define smooth curves suggesting that they form a consanguineous rock suite.

With few exceptions the major elements of the Group A and B dikes are similar to published analyses of andesite and basalt (Tables 5, 6). With $Na_20+K_20=CaO$ at $Si0_2=60\%$, the dikes form a calc-alkaline suite. As indicated in figure 14 the Group A and B dikes plot dominantly in the calc-alkaline field (CA) of the AFM diagram as defined by Irvine and Baragar (1971). The dikes are scattered but define a calc-alkaline trend as indicated by the solid line. The Group C dikes show a markedly different trend (solid line) reflecting their more variable chemistry.

On a potash-silica plot, most of the dikes comprising Groups A and B are medium-K orogenic andesites as defined by Gill (1981 , p. 6) (Fig.15). One of the samples (#216B) plots as a medium: basic andesite based on its low silica content. Sample #206 was not plotted due to its anomalously high K_20. The andesites are all quartz and hypersthene normative (Tables 2, 3) and typically contain modal amphibole and/or labradorite phenocrysts and groundmass phases (Table 1). As indicated by comparing Tables 2, 3, and 5, andesites of Groups A and B are strongly similar to Gill's (1981) average of 2500 orogenic andesites and to the average of 24 hornblende andesites reported by Daly (1933) and are similar to Recent feldsparphyric basaltic andesite erupted from the Solomon arc (Stanton and Bell, 1969). These analyses are also plotted on figure 15.

The Group A and B basalts range from 49.5% to 51.7% in silica content. They are petrographically curious in that they contain no phenocrystic olivine or orthopyroxene (Table 1). They do contain phenocrysts of augite (#167, 238B) and sometimes amphibole and/or plagioclase (552A), traits similar to the andesites of Group A. No pyroxene exists in the groundmass but, rather, green and brown amphibole occurs (Table 1). As a result the two samples of Group A with silica content less than 53% are termed "basalts" due to their

nontypical petrography. They both contain normative olivine together with nepheline (#238B) or hypersthene 0552A) but neither are quartz-normative (Table 2). These "basalts" plot in the alkali basalt field of Kuno (1966) (Fig. 16) and are similar in chemistry and normative mineralogy to alkalic and high alumina basalts from the Japanese and Korean arcs (Fig. 16; compare Tables 2 and 6).

The unique augite-bearing basalt of Group B (#167-Tables 1, 3) contains clinopyroxene phenocrysts but does not contain groundmass pyroxenes thus disqualifying it as a tholeiite sensu stricto, despite the fact that the sample shows normative quartz and hypersthene. Nevertheless, the sample plots in the arc tholeiite field of Kuno (1966) (Fig. 16). The remaining basalts and andesites of Groups A and B plot in the alkali and high-alumina basalt fields.

As indicated in comparing Tables 3 and 6, sample #167 is very similar in major element chemistry and normative mineralogy to low-$Ti0_2$ quartz-normative diabase dikes of eastern North America (Weigand and Ragland, 1970, p. 200) and is less similar to the average of 137 tholeiitic basalts and diabases reported by Nockolds (1954). The augite basalt (167) does not constitute a significant geochemical or petrographic type and its classification as a tholeiite is not characteristic of the dike swarm.

The Group C lamprophyres vary in silica content from 50.3% to 57.3%, never reaching the high silica content of the andesites (compare Tables 2, 3, 4). They are chemically variable but broadly similar to the Group A and B dikes in chemistry and mineralogy (Fig. 13; Table 1). The Group C dikes show enrichment in alkalis at low silica ratios. They are mildly enriched in Fe_20_3 compared to the Group B dikes (Tables 2, 4).

Chemically they are strongly similar to spessartite lamprophyres from the Independence dike swarm in eastern California (Chen and Moore, 1979), and to the average of 14 spessartites

and 15 vogesites reported by Johannsen ((1937, v.III), p. 39, 192). In comparing Tables 4 and 7, compositionally the Group C lamprophyres show a similar range in $Si0_2$, $A1_20_3$, and $Ti0_2$, they are somewhat enriched in total Fe, CaO, and MgO, and are somewhat low in alkalis. These chemical comparisons are in accord with their petrographic classification as calc-alkaline spessartite and vogesite as discussed earlier.

Minor- and trace-element analyses. Eleven of the dikes were analyzed for minor- and trace-elements by semi-quantitative emission spectrographic methods (Table 8). The standard deviation of this method is plus 50% and minus 33%. The use of immobile trace-element discrimination diagrams to help classify the tectonic setting of mafic volcanic rocks has grown in the last decade (cf- Pearce and Cann, 1973; Pearce, 1975; Floyd and Winchester, 1975; Smith and Smith, 1976). Such plots are strictly applicable to fresh, aphyric basaltic volcanic rocks. Although the Sonora dikes commonly show petrographic evidence for moderate alteration, the major element analyses and Harker diagram suggest that significant redistribution of major elements has not occurred in most analyzed samples. Another problem, however, is that the dikes are porphyritic basalt and andesite. Together with the uncertainties introduced by the analytical error of the semi-quantitative analyses, this means that discrimination diagrams cannot be interpreted rigorously.

Three diagrams of Pearce and Cann (1973) are shown in Fig. 17. A plot of Y/Nb (Fig. 17a) differentiates between tholeiitic and alkalic basalts. The three analyzed basalts of the Sonora dike swarm (Y /N b=1.6-2.1) plot in the transition between the alkalic oceanic island and tholeiitic provinces. Andesites and lamprophyres of the dike swarm have similar Y/Nb values.

A triangular plot of Zr vs. Ti/100 vs. Y x3 (Fig. 17b) shows that the analyzed basaltic dikes, as well as related andesites and lamprophyres, fall within field D which includes oceanic

island or within plate continental basalts (Pearce and Cann, 1973). A Ti vs. Zr plot (Fig. 17c), although not strictly applicable to within-plate basalts according to Pearce and Cann (1973), shows that basalts of the Sonora swarm plot mostly in the A and C fields which suggests affinities both with island arc low -K tholeiites and calc-alkaline basalts. Addition of the andesites and lamprophyres produces a spread of points between the A, B and C fields in support of this conclusion. No single discrimination diagram is conclusive but together they suggest that the basalts and presumably related rocks of the Sonora dike swarm have within-plate tholeiitic to calc-alkaline affinities and are unlike typical ocean floor basalts. This conclusion, although very tentative, is consistent with the petrographic character of the dike swarm.

Petrologic interpretation

Petrographic and geochemical studies indicate that the Sonora mafic dike swarm is composed dominantly of calc-alkalic andesite and subordinate basalt and slightly younger calc-alkalic lamprophyres. The dikes are mineralogically interesting in that they are strongly enriched in primary amphibole and plagioclase phenocrysts and groundmass phases. According to Jakes and White (1972) hornblende andesites are found in both island arc and marginal arc settings. Typically, the marginal arc rocks contain abundant hornblende, less than 25% clinopyroxene (typically calcic), some biotite, and rare hypersthene phenocrysts. These traits are shared by the Sonora dikes (Table 1).

The abundance of hydrous primary igneous phases as phenocrysts and in the groundmass of the dikes is probably due to the original high water content of the magma. Such hydrous magmas are commonly generated at active magmatic arcs where significant water can be introduced during dehydration of wet sediments off-scraped from subducted lithosphere.

Oscillatory zoning in plagioclase, compositional zoning and multiple twinning in amphibole, exsolution in clinopyroxene, embayed and rimmed phenocrysts, and marked porphyritic textures suggest a two-stage cooling history for the parent magma. Glomeroporphyritic textures suggest that early-formed crystals clumped together either within the magma chamber or during upward rise of the partly-crystallized magma. Sequential intrusion of the dikes of Groups A, B, and C could- mark periodic rise of phenocryst-enriched magmas tapped from such a chamber or chambers. Mineralogic and chemical similarities between the Group A, B, and C dikes suggest they had a similar ancestry.

Despite the fact that mafic dike swarms in continental regions are commonly interpreted to represent injection of new ocean-floor basalt during regional extension, the calc-alkaline dikes of the Sonora swarm were probably related to subduction and marked a stage in the development of a marginal arc. Significantly, the dikes are temporally and spatially associated with a belt of middle-Jurassic calc-alkaline plutons intruded across the Paleozoic and Mesozoic basement rocks of the foothills metamorphic belt (Figs. 1, 2). The dikes provide an important structural marker in the Shoo Fly and Calaveras Complexes and, as discussed below, provide important constraints on the style and geometry of post-middle Jurassic tectonism in the foothills metamorphic belt.

REGIONAL STRUCTURAL RELATIONS

The Sonora dike swarm was intruded during the Middle Jurassic into a complexly deformed and metamorphosed Paleozoic basement complex (Units 1, 2 in Figs. 1, 2, 4). North of the Tuolumne river, between lats. 38°15'N and 37°45'N, the dikes are closely associated with a suite of calc-alkaline plutons (i.e. - San Andreas, Vallecitos, Parrotts Ferry, Knight Creek, Standard, Basin Creek, and Hazel Green plutons) that together form a northwest-striking

intrusive sequence in the central Sierra Nevada. The plutons are phaneritic and similar in mineralogy and probably represent a comagmatic intrusive suite.

The limited geochronologic data available (Table 9) indicates that some of the plutons were intruded during middle Jurassic time about 164170 m.y. ago. These dated plutons, such as the Parrotts Ferry, Standard, and parts of the Sierra Nevada batholith northeast of the Jawbone Flats and Hazel Green plutons in Fig. 1, comprise the Jawbone granitoid sequence of Stern and others (1981) . The full extent of this middle Jurassic intrusive suite is unknown at present.

Dikes of the Sonora swarm crosscut the Vallecitos, Parrotts Ferry, and Standard plutons (Table 9), but occur as xenoliths along the west edge of the Knight Creek pluton (Schweickert, unpub. data). Both the plutons and the Sonora dikes locally contain a cleavage related to folds produced during the Late Jurassic Nevadan orogeny (Table 9). These observations plus the available geochronologic data indicate that the intrusion of calc-alkaline mafic dikes of the Sonora swarm and the calcalkaline plutons are related pre-Nevadan igneous episodes that affected the pre-batholithic wall rocks of the Sierra Nevada range.

Structural framework of the Paleozoic basement rocks

Prior to intrusion of the Sonora dike swarm the Shoo Fly and Calaveras Complexes experienced protracted but dissimilar deformational histories. The discussion to follow (use Table 10) briefly outlines similarities in the structural evolution of the three foothills tectonostratigraphic units; detailed descriptions appear elsewhere (Schweickert, 1981; Schweickert and others, 1984; Schweickert and Bogen, 1983).

Several regional deformational events have affected more than one foothills unit at various times throughout the development of the metamorphic belt. In this report these events (D_l, D_2, D_3, etc) are numbered from oldest (D_1) consecutively to youngest (D_{l+n}) within each

tectonostratigraphic unit. Regional foliations (S_1, S_2, S_3, etc) and related folds (F_1, F_2, F_3, etc.) were formed during deformational events D_1, D_2, D_3, etc. The following nomenclature is used to denote synchronous events between various foothills units:

D_1/D_3 or D_2/D_4 - episodes affecting the Calaveras Complex (UPz)
/Shoo Fly Complex (LP z)

$D_1/D_3/D_5$ or $D_2/D_4/D_6$ - episodes affecting the western belt (Jrp)/Calaveras Complex/Shoo Fly Complex

In this system the units (Jrp/UPz/LPz or UPz/LP z) are listed in their geographical west to east positions; the slash (/) marks either the Sonora fault (SF) or the Calaveras-Shoo Fly thrust (CSFT) of Figs. 1, 2.

D_1/D_3 - Development of the Calaveras-Shoo Fly thrust. The Shoo Fly and Calaveras Complexes are in contact along a 1-2 km wide zone of synmetamorphic ductile deformation (see Chapter 1). The Shoo Fly contains two coplanar metamorphic fabrics that, together with lithologic units, are regionally truncated along the thrust zone (Fig. 3). The D_3 event in the Shoo Fly is coeval with initial isoclinal folding and flattening in the Calaveras (D_1) and formation of the Calaveras-Shoo Fly thrust (Merguerian, 1981) . The absolute age of the D_1/D_3 event is unknown but it is bracketed between late Paleozoic and pre-middle Jurassic time and probably is an expression of the Permo-Triassic Sonoma orogeny (see Chapter 1, Table 2).

D_2/D_4 - East-west folding of the thrust. The Calaveras and Shoo Fly Complexes were folded during the D_2/D_4 event into map scale tight to crenulate folds (Figs. 1 , 3). The F_2/F_4 folds, which deform the Calaveras-Shoo Fly thrust, have steep to vertical east-west-trending axial surfaces and hingelines that plunge moderately toward the east. Regionally, the S_2/S_4 surfaces range from slip cleavage to a spaced mica schistosity. This event must be pre-middle

Jurassic in age because the 164-170 m.y. Standard pluton cuts across and deflects the S_2/S_4 axial surface traces, and the dikes intrude along S_2/S_4.

Dike intrusion as an indicator of regional stress

The dikes were intruded parallel to the east-west-trending spaced schistosity of the Paleozoic basement complexes, indicating that the S_2/S_4 regional schistosity exerted a strong influence on the orientation of the dikes (compare Fig. 9 with Chapter 1, Fig. 15). However, in the vicinity of the D_1/D_3 Calaveras-Shoo Fly thrust, the dikes locally intrude parallel to and bifurcate across thrust-related folds and Mylonitic fabrics in the Shoo Fly. The strong layered anistropy of the thrust zone locally produced atypical dike orientations, but these instances are rare.

The overall geometry of the dike swarm (Figs. 4, 9) suggests that a period of north-south regional extension leading to dilation of the S_2/ S_4 regional schistosity may have preceded or accompanied intrusion of the dikes. Such extension may have been related to east-west compression of the basement complexes or related to uplift or rifting. These possibilities are explored more fully in the last section of this report.

Structures related to the Nevadan orogeny

The Late Jurassic Nevadan orogeny deformed the pre-batholithic wall rocks of the Sierra Nevada range in California (Knopf, 1929; Taliaferro, 1942; Clark, 1964; Bateman and Clark, 1974). The Nevadan orogeny produced two deformational episodes in the Paleozoic basement rocks that also affected the Sonora dike swarm. The first of these ($D_1/D_3/D_5$) involved folding about northwest-trending axial surfaces and the second ($D_2/D_4/D_6$) produced folds with northeast-trending axial surfaces (Table 10). The variable regional style and correlation of

Nevadan structures along the length of the Sierra Nevada metamorphic belt is described by Schweickert and others (1984).

In the study area, the axial surfaces of Nevadan and late-Nevadan folds statistically trend N32°W, 78°NE and N30°E, 90°, respectively (see Chapter 1, Table 2, Fig. 15). The steeply-plunging folds and related cleavages that deform the Sonora dikes are oriented N15°W-N30°W (Nevadan) and N20°E-N40°E (late-Nevadan). The stereonet showing poles to 264 dikes (Fig. 9) shows a marked scatter in the NW and SW quadrants due to the effects of the Nevadan folds on originally east-west-trending dikes.

The northwest- and northeast-trending folds have similar structural styles and will be discussed together below. Nowhere were the northwest- and northeast-trending folds observed to be superimposed on one another, but northwest-trending folds are commonly crosscut by northeast-trending slip cleavage and spaced fractures. Collectively, the Nevadan folds can best be described as 2-8 m wavelength asymmetric to open folds and kinks with an associated spaced axial-surface slip cleavage or spaced fracture cleavage that can be traced from the wall rocks through the dikes (Fig. 18). The dike margins are commonly offset along the cleavage.

Typically, the dikes lack a pervasive cleavage and are neither boudinaged, strongly sheared, nor foliated. Instead, the northwest- to northeast-trending open to asymmetric fold geometries suggest modest east-west shortening during the Nevadan orogeny. Lower green schist grade metamorphic recrystallization occurred in the western belt (Clark, 1964), the Calaveras Complex (Schweickert, unpub. data), and the Shoo Fly Complex during the Nevadan orogeny (see Chapter 1). As described earlier the Sonora swarm shows moderate effects of metamorphic recrystallization and deformation.

TECTONIC INTERPRETATIONS

A model has recently been proposed to explain the tectonic setting of the Sonora dike swarm. Based on lithologic and geochronologic comparisons, Sharp (1980) and Saleeby (1982, 1983) have correlated the Sonora dike swarm with mafic dikes related to the Smartville ophiolite sequence near lat. 39°N. In their view, the dike swarms are the products of incipient ophiolite generation during middle Jurassic intra arc continental rifting of a marginal arc terrane.

There are dramatic differences, however, between the dikes of the Sonora and Smartville swarms. In comparison to the east-west, vertical trend of the Sonora swarm, the Folsom dike swarm of the Smartville ophiolite (Xenophontos and Bond, 1978) is oriented N40°W to N15°W with dips averaging 60°NE. Their orientation is broadly parallel to the trend of the Nevadan cleavage in the northern Sierra (Schweickert and others, 1984).

Compared to the andesites, basalts, and lamprophyres of the Sonora dike swarm, the Folsom dikes show a great range in lithology from basalt, andesite, olivine clinopyroxenite, and gabbro to quartz-diorite, trondjemite, soda rhyolite, and quartz-feldspar porphyry (Xenophontos and Bond, 1978). The Smartville dikes are predominantly nonporphyritic to clinopyroxene- and plagioclase-bearing diabases however the Sonora dikes are strongly enriched in amphibole and plagioclase phenocrysts and contain little clinopyroxene. There is therefore little reason to correlate the Sonora and Folsom dike swarms.

In the western belt, west of the Sonora fault (Unit 3 in Figs. 1 , 2), middle Jurassic mafic rocks form significant lithologic components of the accreted Nevadan arc terrane. Mafic rocks of the western belt are strongly dissimilar to the Sonora dike swarm in occurrence, petrography, and geochemistry. The western belt contains thick regionally conformable sequences of massive augite-porphyry basalt, plagioclasephyric basaltic pillow lavas, nonporphyritic volcanic breccia,

and associated volcaniclastic rocks (Clark, 1964, 1970; Duffield and Sharp, 1975). These rocks, which rarely occur as dikes, are interlayered with oceanic sediments.

The range of lithologies documented for the Sonora dike swarm does not occur in the western belt and the augite-bearing basalts of the western belt are geochemically distinct in that they show higher $Ti0_2$ and MgO and lower total Fe and K_20 in comparison to augite-bearing basalts of the Sonora dike swarm (compare samples 167, 238B in Tables 2, 3, with analyses # 1, 2, 6, 7, 8 in Table 1 of Duffield and Sharp (1975)). The western belt is composed of island arc rocks that may have formed at some distance from the Cordilleran margin.

In eastern California, the Independence dike swarm forms a regionally extensive, northwest-trending, steeply-dipping array of dikes that intrude across the Sierran crest, the Inyo range, and the Argus range (Moore, 1954ms; Moore and Hopson, 1961; Chen and Moore, 1979). The Independence dikes average 1 m in thickness (compare Fig. 8) and form a series from lamprophyre (spessartite) through diorite and quartz diorite porphyry to granodiorite porphyry (Moore and Hopson, 1961). Petrographically, the lamprophyres are strongly similar in texture and modal mineralogy to those in the Sonora swarm (compare Fig. 12 a-d, Table 1 to Moore and Hopson (1961) Fig. 7, Tables 1, 2) and, as discussed earlier, are geochemically comparable to the Group C lamprophyres of the Sonora swarm (compare Tables 4, 7).

Aside from these similarities they share an equivalent geologic setting in that both swarms are intruded into calc-alkaline plutons of a marginal arc terrane. Silicic dikes of the Independence swarm yield concordant U Pb ages of 148 m.y.a. (Chen and Moore, 1979) which suggests that the post-Nevadan plutonic axis of the Sierra Nevada occurred east of the middle Jurassic Jawbone granitoid sequence. The northwest-trend of the Independence dike swarm may

reflect the fact that it was intruded after the 153-158 m.y.a. Nevadan orogeny affected the pre-batholithic wall rocks of the eastern Sierra (Schweickert and others, 1983).

Despite the difference in their ages, the Sonora dike swarm appears to have a tectonic setting most similar to that of the Independence dike swarm. The Sonora dikes, however, are markedly different in occurrence, orientation, petrography, and lithology than both the dike swarm of the Smartville ophiolite and the Jurassic volcanic rocks of the western belt. The geology of the Sonora dike swarm suggests that it was closely related to the development of a marginal magmatic arc in mid-Jurassic time and that it formed an important structural marker in the later Mesozoic tectonic development of the Sierra Nevada.

The Sonora dike swarm occurs within the region of closest spacing of the Jawbone granitoid plutons (Figs. 1, 3, 4; Table 9) and intrusion of the Sonora dikes and the marginal arc plutons probably were related igneous events. Together they mark the locus of a middle Jurassic plutonic belt developed within a polyphase deformed Paleozoic basement complex.

The Vallecitos, Parrotts Ferry, Sonora, Basin Creek, Jawbone Flats, and Hazel Green plutons (Fig. 1, Table 9) contain mafic-ultramafic zones as well as amphibole- and pyroxene-rich granitoid phases. The presence of amphibole- and clinopyroxene phenocrysts in the Sonora dikes suggest that they might be petrologically related to the Jawbone suite. Calcalkaline lamprophyres, such as the Group C dikes, are commonly associated with intrusive complexes and are interpreted to represent residual magmas related to subduction (Carmichael and others, 1974, p. 510). Magmas that formed the dikes may have ascended through a thermally weakened crust of deformed Paleozoic basement rocks and middle Jurassic calc-alkaline plutons in a convergent plate setting where their orientation (Figs. 4, 9) may have been governed by the regional tectonic stress regime.

Nakamura and others (1977) found that in the Aleutian and Alaskan arcs, a swarm of coeval dikes and extension fractures formed in the magmatic arc perpendicular to the trend of the trench axis. Their study suggested that compressive stress related to subduction can be directly transmitted into the overriding plate with maximum compression oriented parallel to the net slip vector of the down going slab.

The Alaskan-Aleutian arc may thus provide a modern analog of the Sonora dike swarm and the middle Jurassic Jawbone arc system in the Sierra foothills. Dilation of the east-west-trending S_2/S_4 metamorphic surfaces possibly resulted from the transmission of subduction stress into competent, polyphase deformed rocks of the Shoo Fly and Calaveras Complexes forming the upper-plate arc basement (Figs. 1, 2, 19). In addition, regional extension in the north-south direction may have been enhanced by the "perpendicular to arc" paleogeometry of the S_2/S_4 schistosity of the Paleozoic terranes.

Alternatively, or perhaps in concert, the extension that accompanied and/or preceded intrusion of the dike swarm could be accommodated by post-D_2/D_4 regional uplift and relaxation of the S_2/S_4 metamorphic fabrics or be controlled by deviatoric stress related to thermally induced crustal arching during middle Jurassic marginal arc plutonism. The Sonora dikes may represent deep-seated residual magmas of the middle Jurassic Jawbone arc complex that were released upward during the north south regional extension in the overriding plate which accompanied subduction (Fig. 19).

Because the Jawbone granitoid sequence and the Sonora dike swarm lie landward of and are cut by the late Jurassic Nevadan suture, the Sonora fault (Schweickert and Bogen, 1983), they are evidently the products of near-trench marginal arc activity possibly related to a period of steep subduction in the middle Jurassic (Fig. 19). The orientation of the dike swarm suggests

that mid-Jurassic convergence was nearly perpendicular to the trend of the marginal magmatic arc. The dikes also record minor east-west shortening in the Calaveras and Shoo Fly Complexes during the late Jurassic Nevadan orogeny.

CONCLUSIONS

The Sonora dike swarm is an areally extensive consanguineous calcalkaline suite of amphibole-, plagioclase-, and augite-phyric andesite, lamprophyre, and basalt. The subvertical, east-west-trending dike swarm intrudes both the Shoo Fly and Calaveras Complexes of the Sierra Nevada foothills metamorphic belt. The dikes are temporally and spatially associated with a series of middle Jurassic calc-alkaline plutons known as the Jawbone granitoid sequence. Field, petrographic, and geochemical studies presented here indicate that the Sonora dikes are derived from calc-alkaline magmas that probably formed during subduction of oceanic lithosphere beneath a marginal continental arc.

The dikes are an important structural marker in the Shoo Fly and Calaveras basement complexes. They are intruded parallel to a steep, east-west-trending spaced regional schistosity that formed in both basement complexes after the development of the Calaveras-Shoo Fly thrust. While these relationships set a minimum middle Jurassic age on development of the thrust, the dikes are also deformed by northwest- and northeast-trending folds and cleavage related to the Late Jurassic Nevadan orogeny.

Calc-alkaline plutonism and coeval intrusion of the Sonora dike swarm are evidently the products of middle Jurassic subduction of oceanic lithosphere beneath a marginal (Jawbone) arc whose basement consisted of polyphase deformed metasedimentary and metaigneous rocks of the Calaveras and Shoo Fly Complexes. Dilation of the east-west trending metamorphic fabrics in the Jawbone arc basement, which preceded and was probably contemporaneous with intrusion

of the dike swarm, was most likely the result of east-west-directed compression transmitted into the overriding plate during subduction.

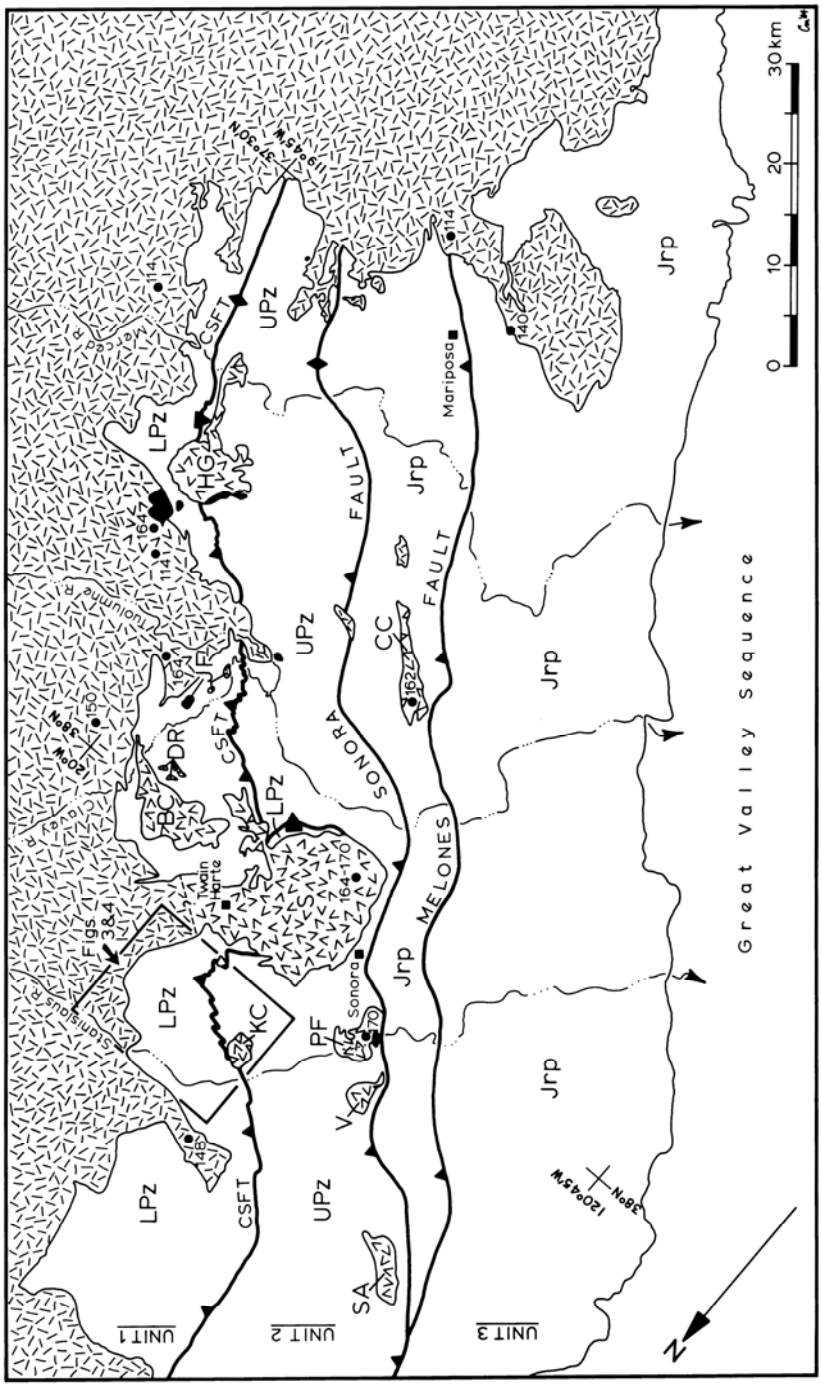

Figure 1 - Geologic map of the southern end of the foothills metamorphic belt in Calaveras, Tuolumne, and Mariposa Counties, California. Unit 1 = Shoo Fly Complex (LPz), Unit 2 = Calaveras Complex (UPz), Unit 3 = western belt (Jrp). Contacts of the Shoo Fly Complex and the geometry of the Calaveras-Shoo Fly thrust (CSFT) are from bedrock mapping as 1:24,000 scale (1978-1981). Some map contacts from: Bowen (1969); Merguerian (1981 ms, 1984); Morgan (1977); Rogers (1966); Schweickert and Bogen (1983); Schweickert (unpub. data); Strand (1967); Strand and Koenig (1965); Tobisch (1960); Turner and Ransome (1897, 1898); and Wagner and others (1981). Middle Jurassic plutons indicated by V pattern are the San Andreas (SA), Vallecitos (V), Parrotts Ferry (P F), Knight Creek (KC), Standard (S), Basin Creek (BC), Duckwall Ridge (DR), Jawbone Flats (J F), Cobb Creek (CC), and Hazel Green (HG). Mafic-ultramafic plutons and phases are solid black. Granitoids of the Sierra Nevada batholith are stippled. Geochronologic dates are indicated by a filled circle. Sources of data listed in Table 9.

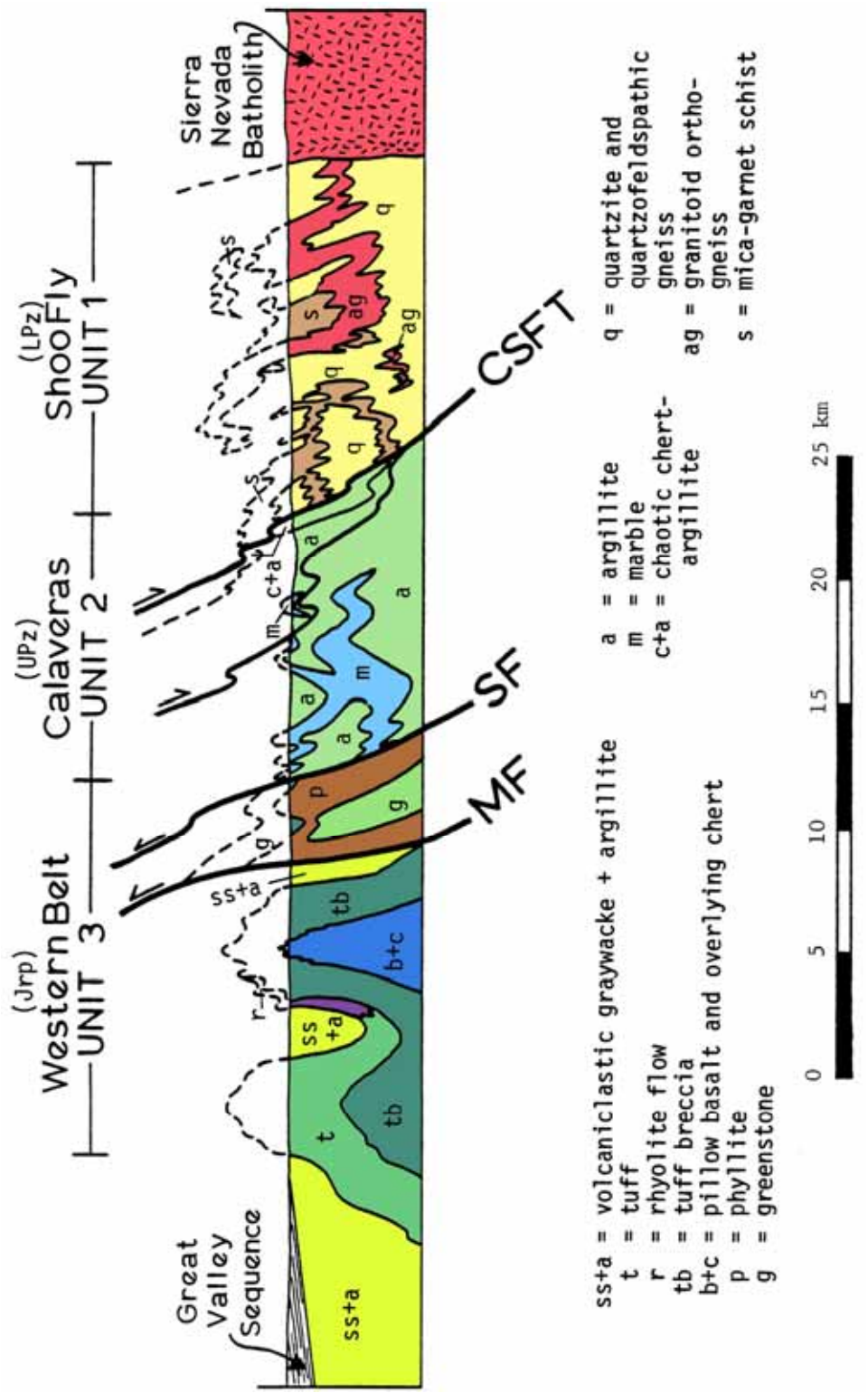

Figure 2 - Structure section across the foothills metamorphic belt illustrating the westward decrease in age, structural complexity, metamorphism, and eugeosynclinal character of the tectonostratigraphic units. The section is composite; data for Units 1 and 2 come from the Stanislaus River but data for Unit 3 is from the Merced River. MF= Melones fault, SF=Sonora fault, CSFT= Calaveras-Shoo Fly thrust. Data for Unit 2 from Schweickert (unpub. data), Unit 3 from Bogen (1983 ms). No vertical exaggeration.

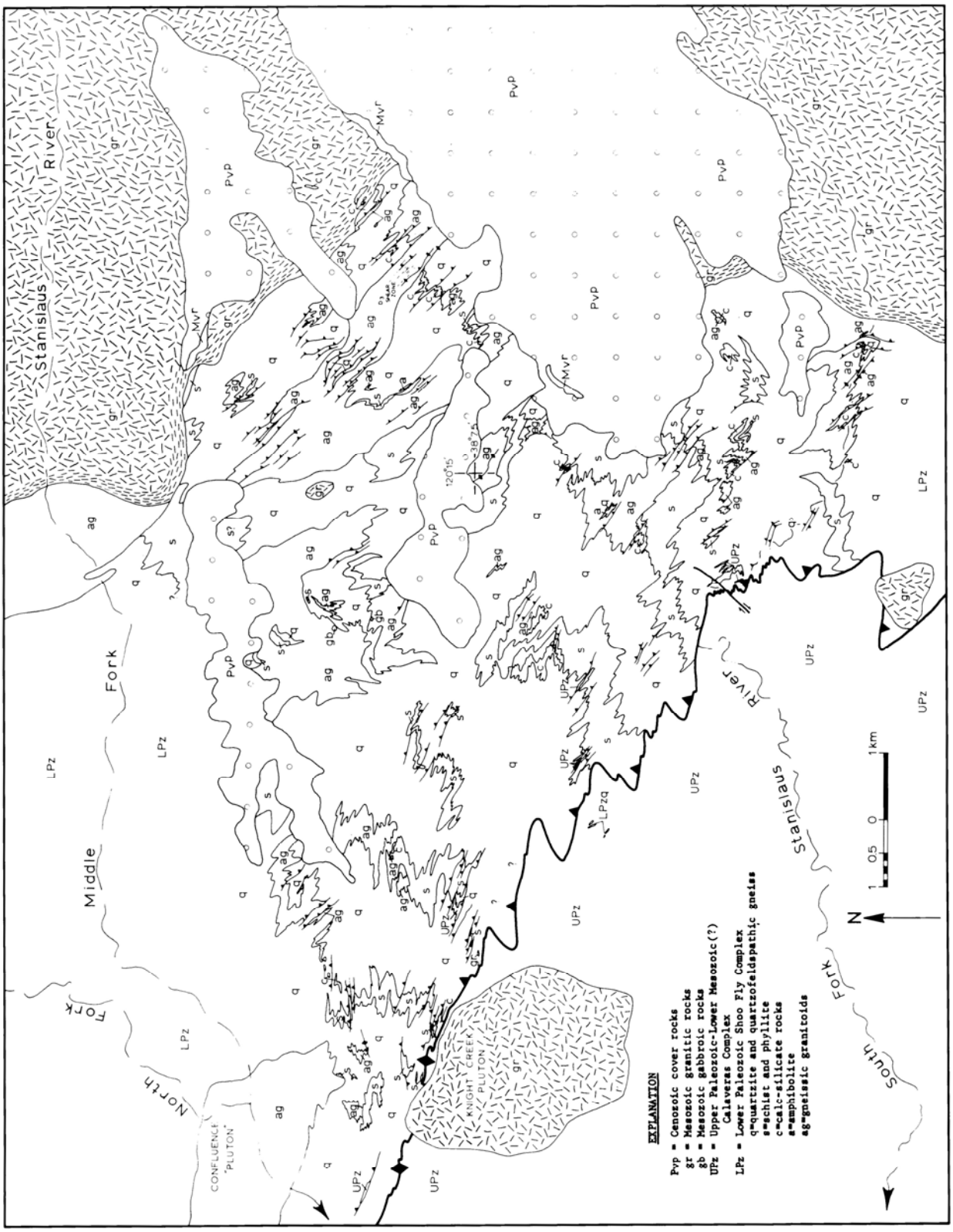

Figure 3 - Bedrock geologic map of the Shoo Fly Complex of Tuolumne County, California encompassing parts of the Stanislaus, Columbia SE, Crandall Peak, and Twain Harte 7-1/2 minute quadrangles. Detailed maps appear elsewhere (Merguerian, 1984).

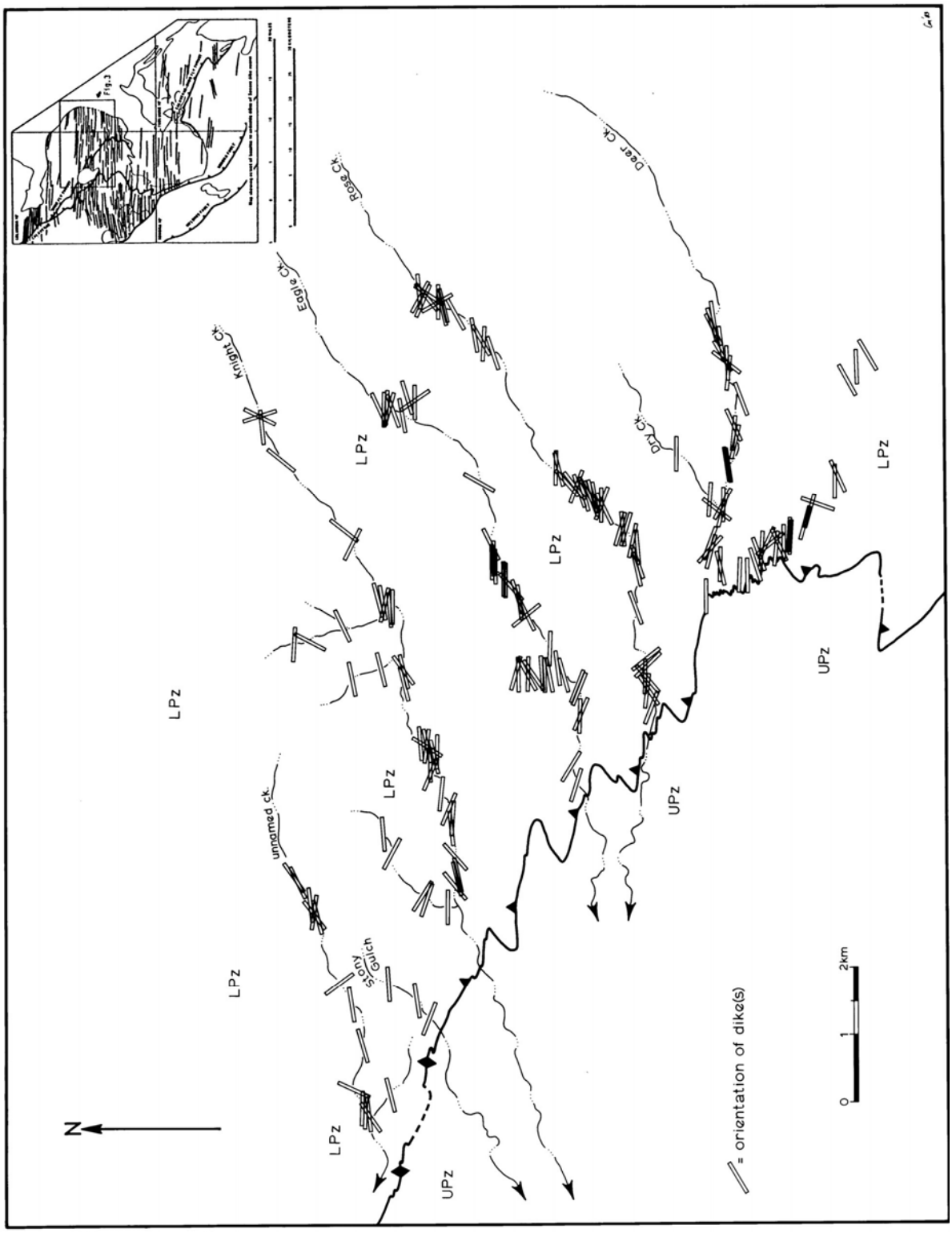

Figure 4 - Map showing the location of mafic dikes exposed in deeply incised tributaries of the Middle and South Forks of the Stanislaus River. This figure can be xerographically reproduced onto acetate and employed as an overlay for Figure 3 (same scale). Azimuthal trends of dikes are plotted. Open symbol can indicate a single observation or the average orientation of a zone of multiple dikes. Regionally they trend east-west (see Figure 9). Inset (from Schweickert and Bogen (1983)) shows the regional distribution of the Sonora mafic dike swarm.

Figure 5 - Aphanitic dike (Group B = N85°W, 86°NE) exposed along Knight Creek. The dike is more resistant than the schistose rocks it intrudes.

Figure 6 - Part of a massive, composite dike swarm (25 m wide) showing internal chilled margins and crosscutting relations. Rounded xenoliths (up to 10 cm long) of foliated quartzite and orthogneiss are typical lithologies of the Shoo Fly Complex.

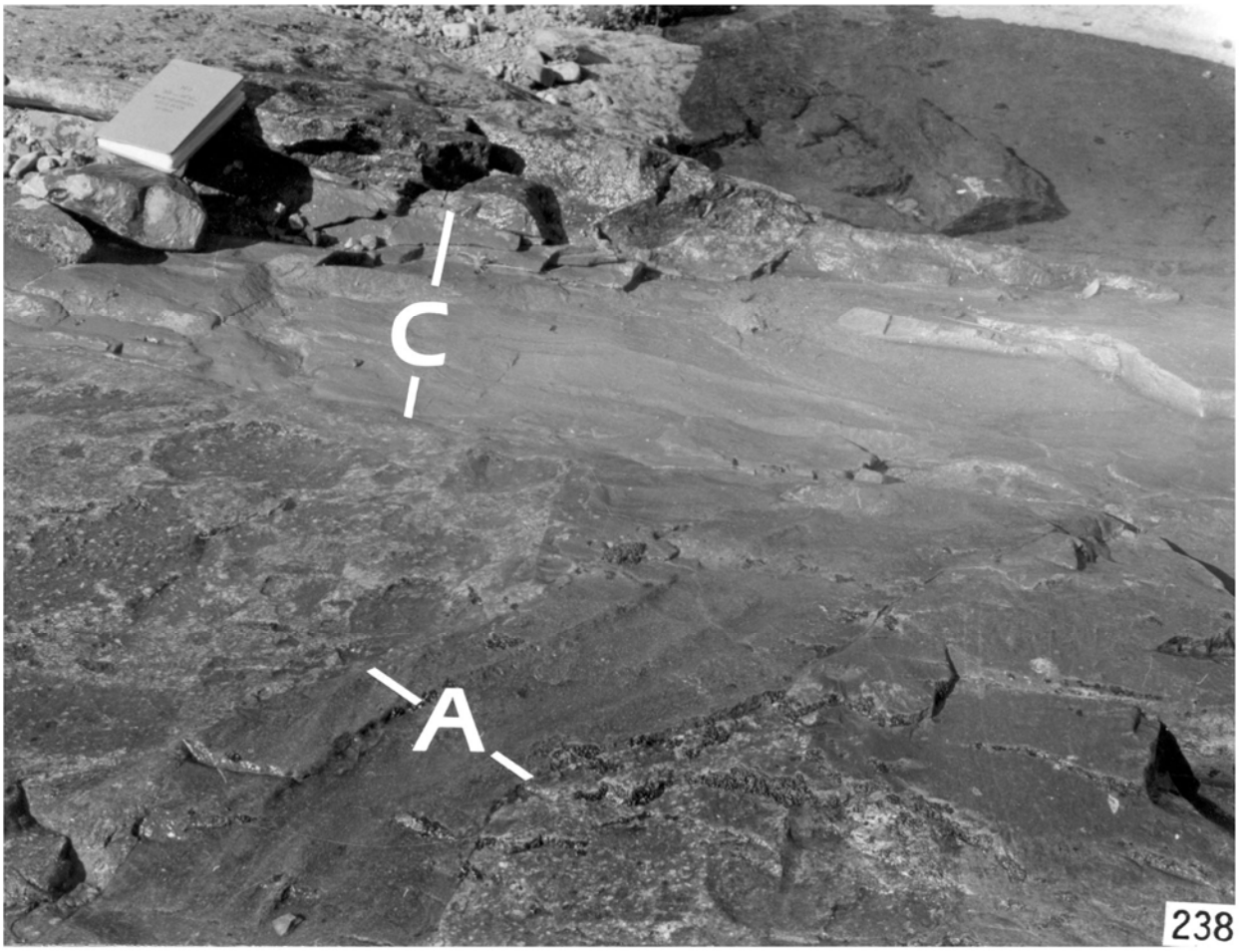

Figure 7 - Two crosscutting mafic dikes that intrude foliated syenitic orthogneiss in upper Rose Creek. The plagioclase-phyric dike in the foreground (Group A) has opened a pre-existing zig-zag fracture in the gneiss. It is cut at a high angle by a 30 cm thick lamprophyre dike (Group C). Field book is 18.5 cm long.

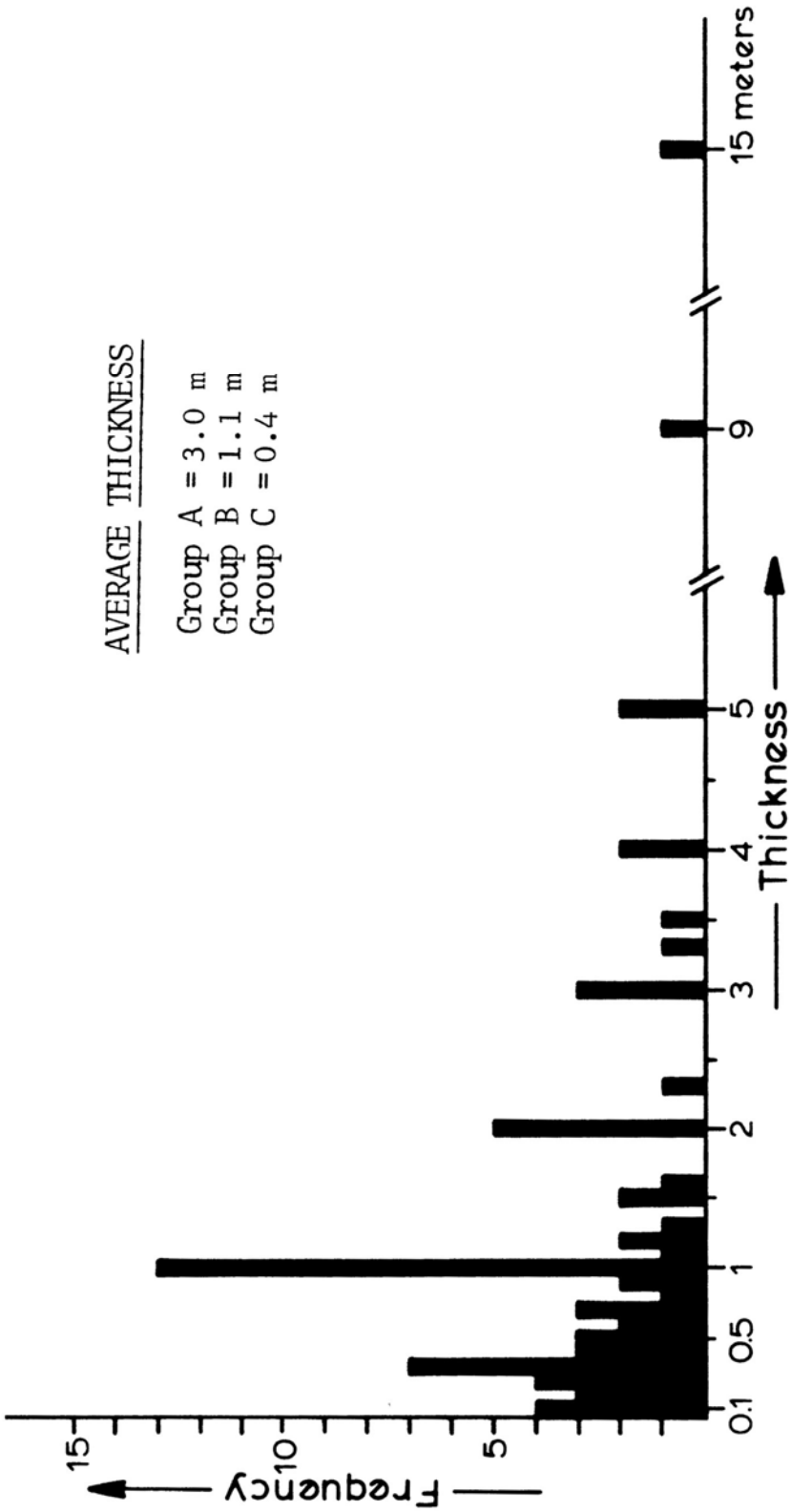

Figure 8 - Frequency distribution plot of thicknesses of 70 mafic dikes measured in the field. Average thicknesses shown for the Group A, B, and C dikes are based on a sampling of 278 measurements.

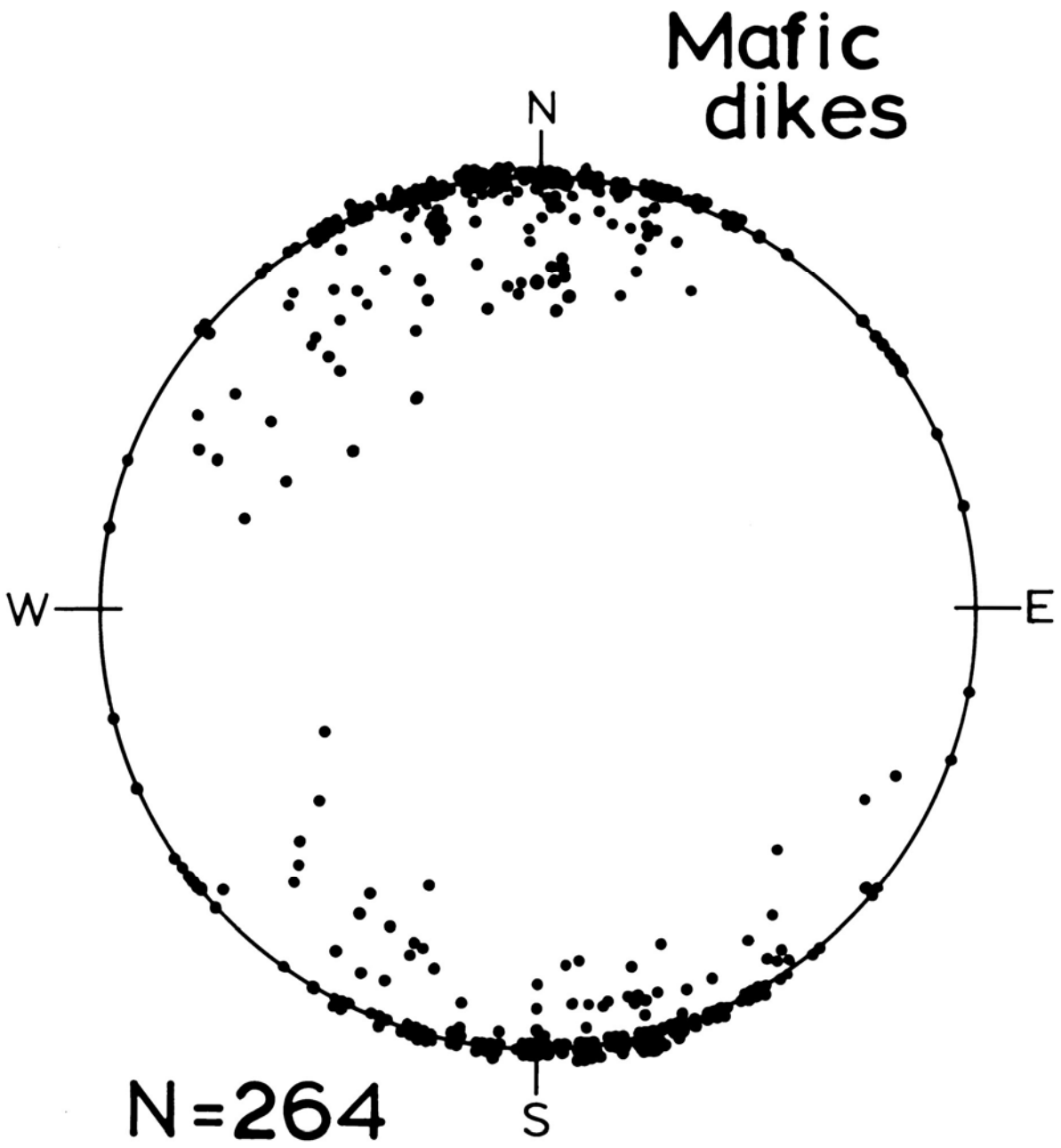

Figure 9 - Equal-area plot of poles to 264 dikes with zones of multiple dikes plotted as a single point. Note the dominant east-west, vertical trend of the dike swarm and the scatter in the NW and SW quadrants. The scattering is mostly due to post-intrusive Nevadan and younger folding.

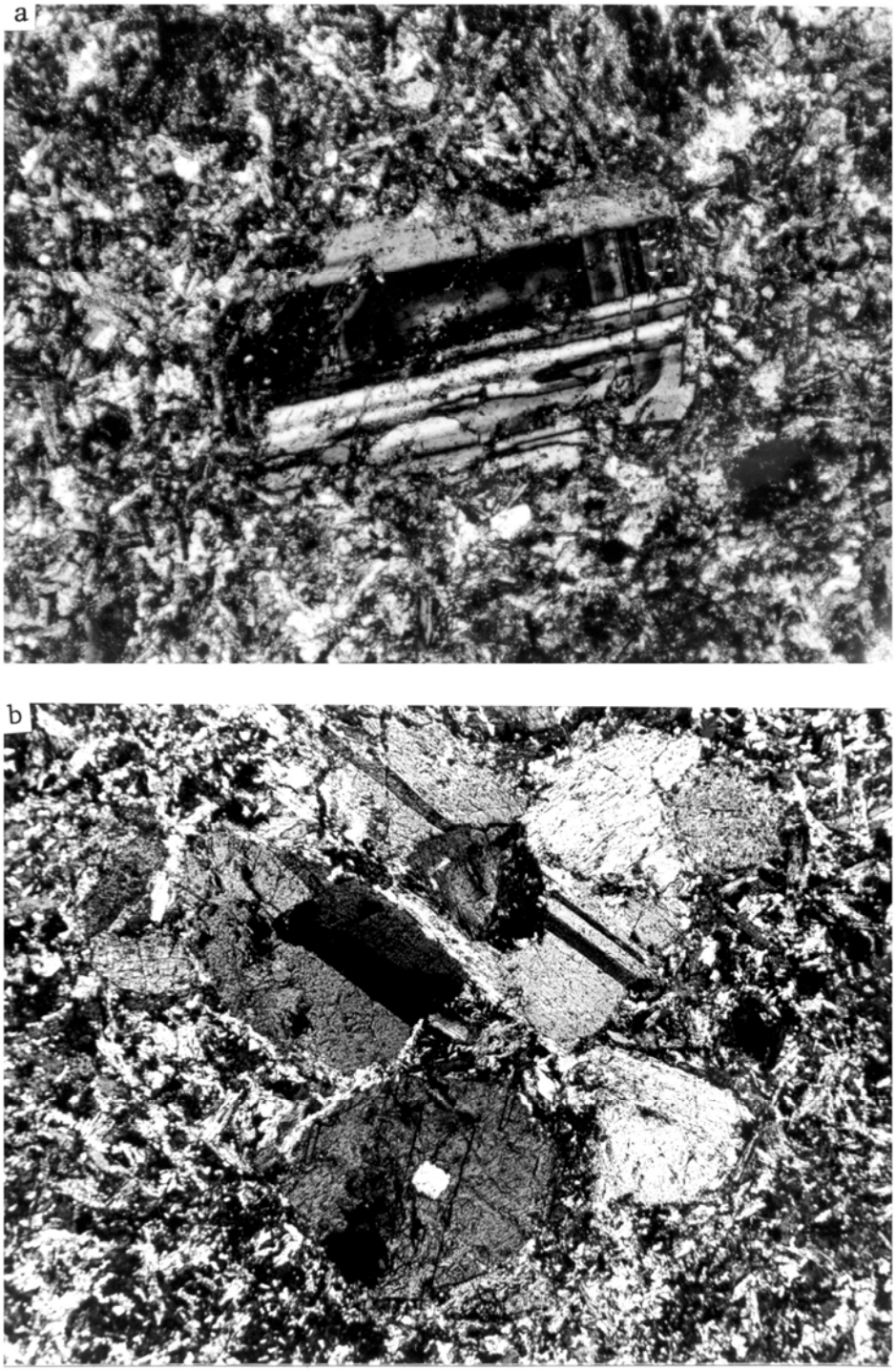

Figure 10 (a) - Subhedral plagioclase tectoblast from a labradorite andesite dike (244) of Group A showing oscillatory zoning and polysynthetic twins sets in an aphanitic groundmass consisting of plagioclase, biotite, calcite, epidote, chlorite, and opaque minerals. Reaction with the matrix, internal cracks and marginal alteration of the phenocrysts are evident. Two conjugate strain-slip cleavages intersect above and crosscut the plagioclase crystal (Nevadan structures D_5, D_6). All photomicrographs taken with crossed nicols and horizontal frame width = 2.7 mm unless otherwise indicated.
(b) - Subhedral to anhedral augite glomerocryst from an augiteplagioclase basalt dike (238B) of Group A pictured in Figure 7 showing a reaction rim composed of plagioclase, quartz, and epidote. Horizontal frame width = 1.35 mm.

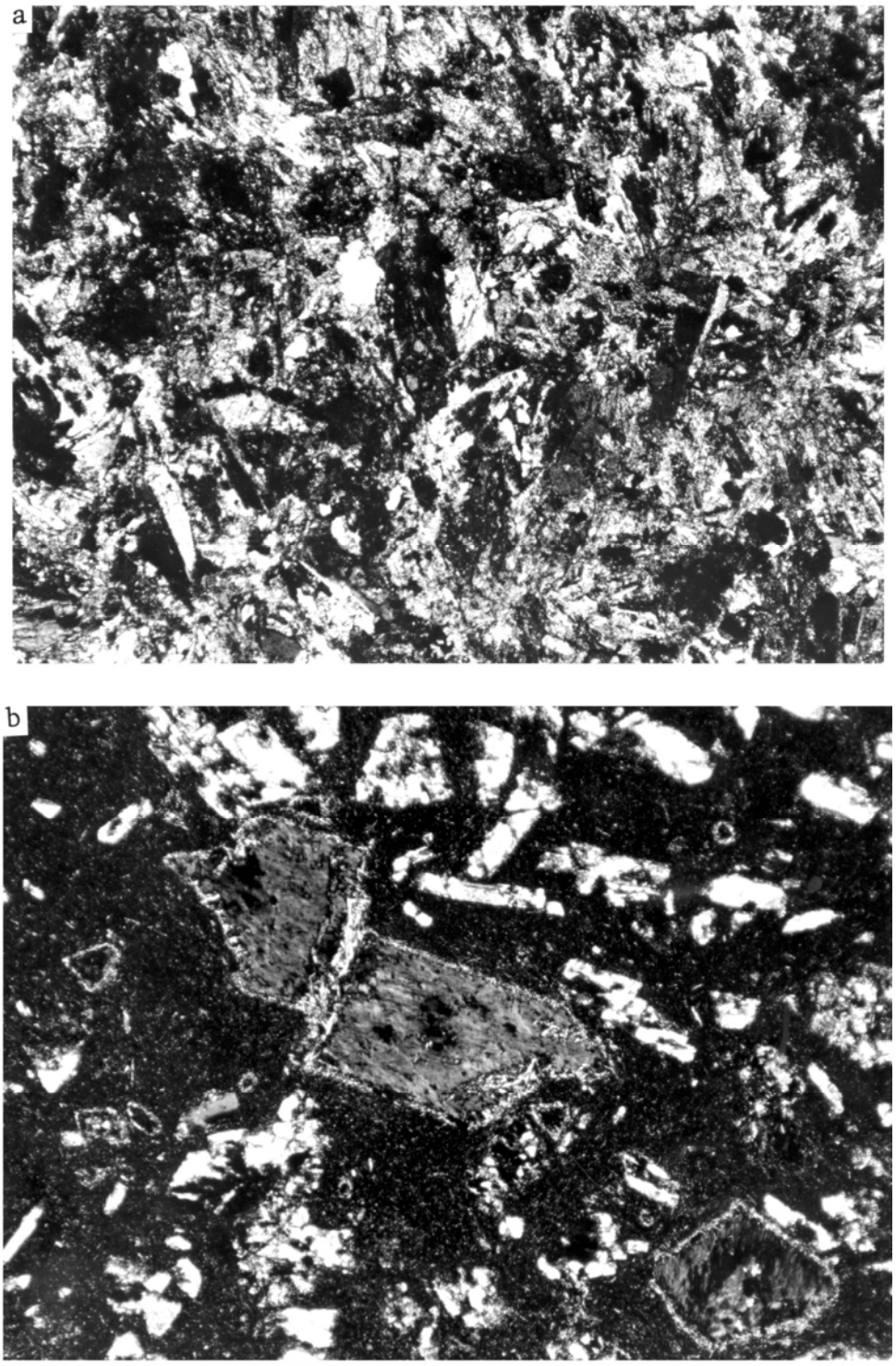

Figure 11 (a) - Ophimottled Group B basic andesite dike (216B) with twinned brown amphibole and plagioclase microphenocrysts set in a groundmass of clouded sericitized plagioclase, green and brown amphibole, biotite, epidote, quartz, and opaque minerals.
(b) - Chloritized subhedral amphibole tectoblast from a Group B dike (321A) showing cracking and a reaction corona of fibrous amphibole and plagioclase. Light-colored subhedral crystals are epidote and zoisite replacements of plagioclase, and to a lesser extent, mafic minerals. The dike is part of a zone of multiple dikes that are locally phenocrystic as pictured here.

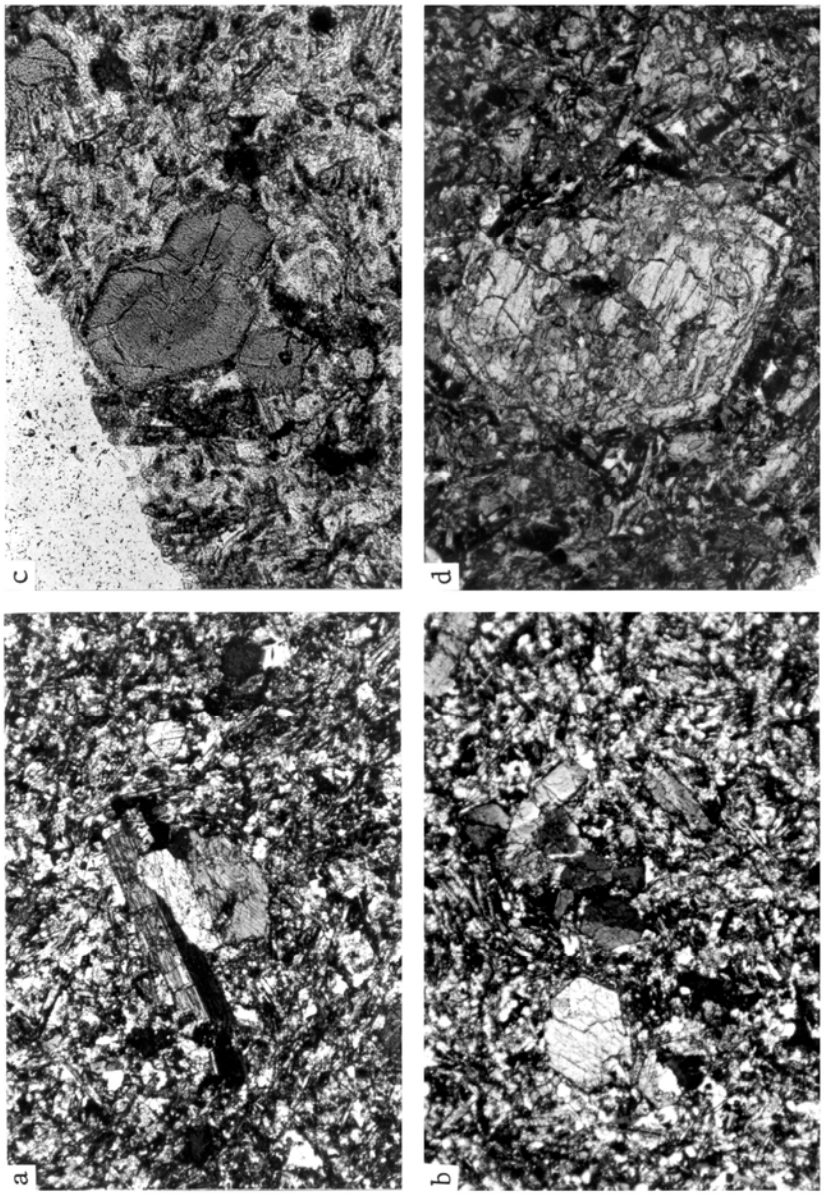

Figure 12 (a) - Prismatic and equant pargasitic amphibole crystals in a Group C dike (143) amalgamated to form a glomerocryst. Both crystals exhibit simple twinning. Note how microlites of plagioclase and pargasitic amphibole flow around the composite grain. Smaller pargasitic microphenocrysts are scattered throughout the altered groundmass.
(b) - Twinned pargasite phenocrysts and glomerocrysts (143) set in a diabasic groundmass of plagioclase and pargasite. Note the 56° amphibole cleavage in the twinned crystal (end-section) to the left of center.
(c) - A pleochroic parallel-twin clinoamphibole showing core and doublemanting zoning. The dark core is composed of dark brown to olive pargasitic amphibole (2V = 90°, B+ and B-) and the thick mantle is pale olive to pale yellow pargasitic amphibole (2V = 70°, B-). The zoned crystal is rimmed by a light green hornblende of possible magmatic or metamorphic origin. Taken with plane polarized light; horizontal frame width is 1.35 mm. (Field #238A - pargasite-plagioclase lamprophyre).
(d) - Subequant zoned augite phenocryst from a Group C pargasite-augite lamprophyre dike (323) partly replaced (upper half of crystal) and rimmed by pale yellow pargasitic amphibole. The dark crystals in contact with the rim are resorbed, highly-clouded plagioclase laths. Prismatic plagioclase, light green to colorless amphibole, and pargasitic amphibole occurs in the groundmass together with epidote, chlorite, alkali feldspar, quartz, opaque minerals, and abundant calcite.

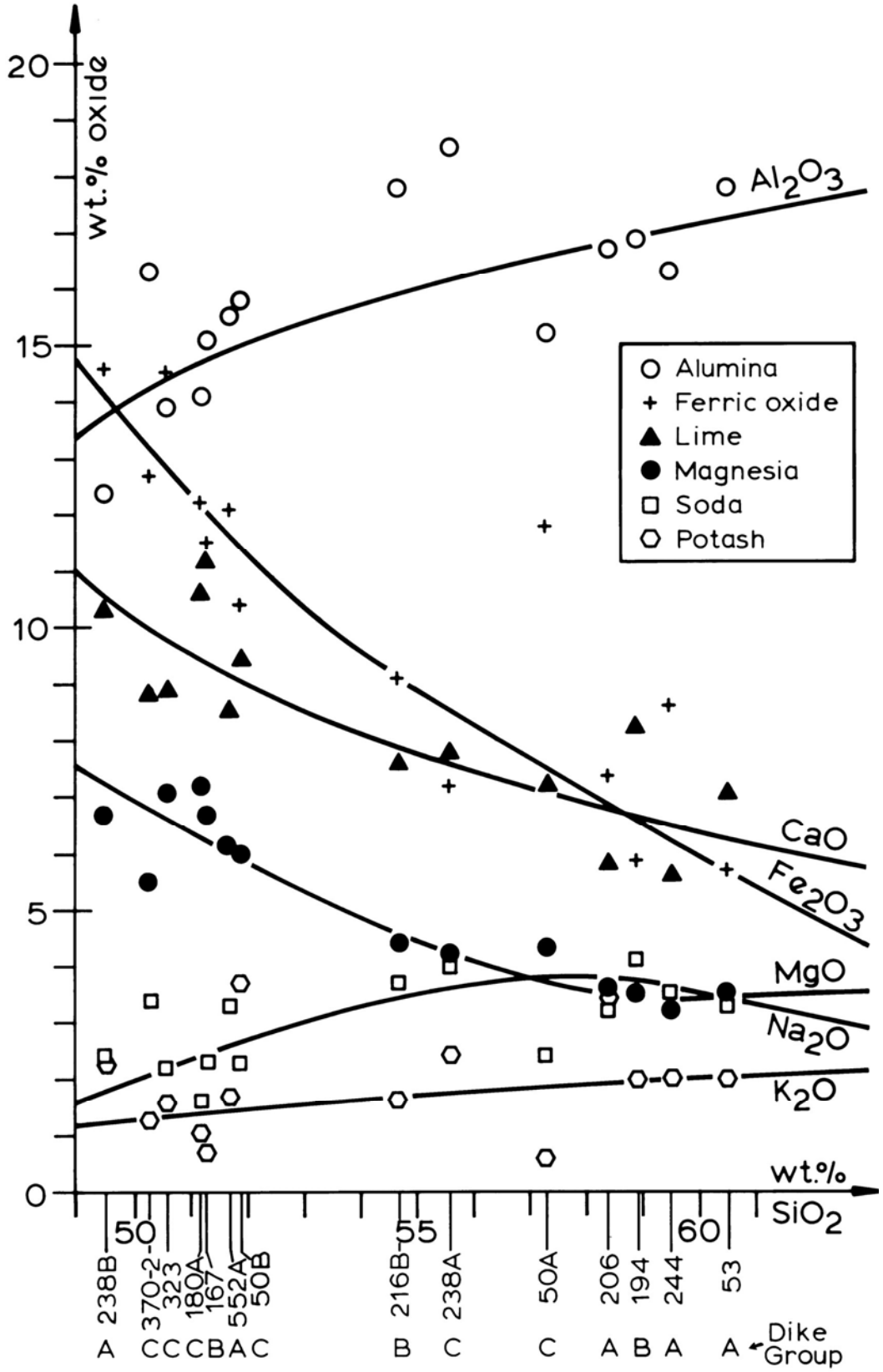

Figure 13 - Harker variation diagram for the Sonora dike swarm.

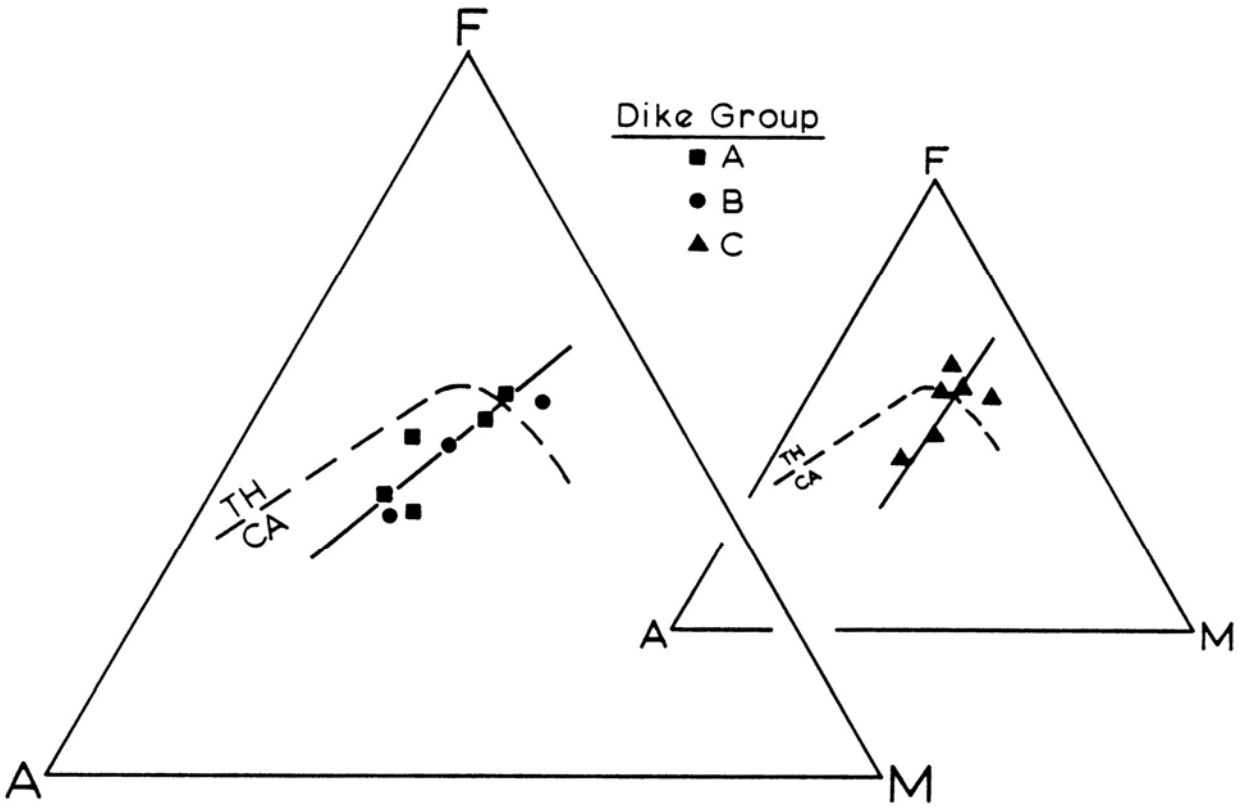

Figure 14 - AFM diagram after Irvine and Baragar (1971) of the Group A and B dikes showing a trend toward the alkali corner, typical of calcalkaline magmas. Inset shows atypical trend of chemically variable lamprophyres of Group C.

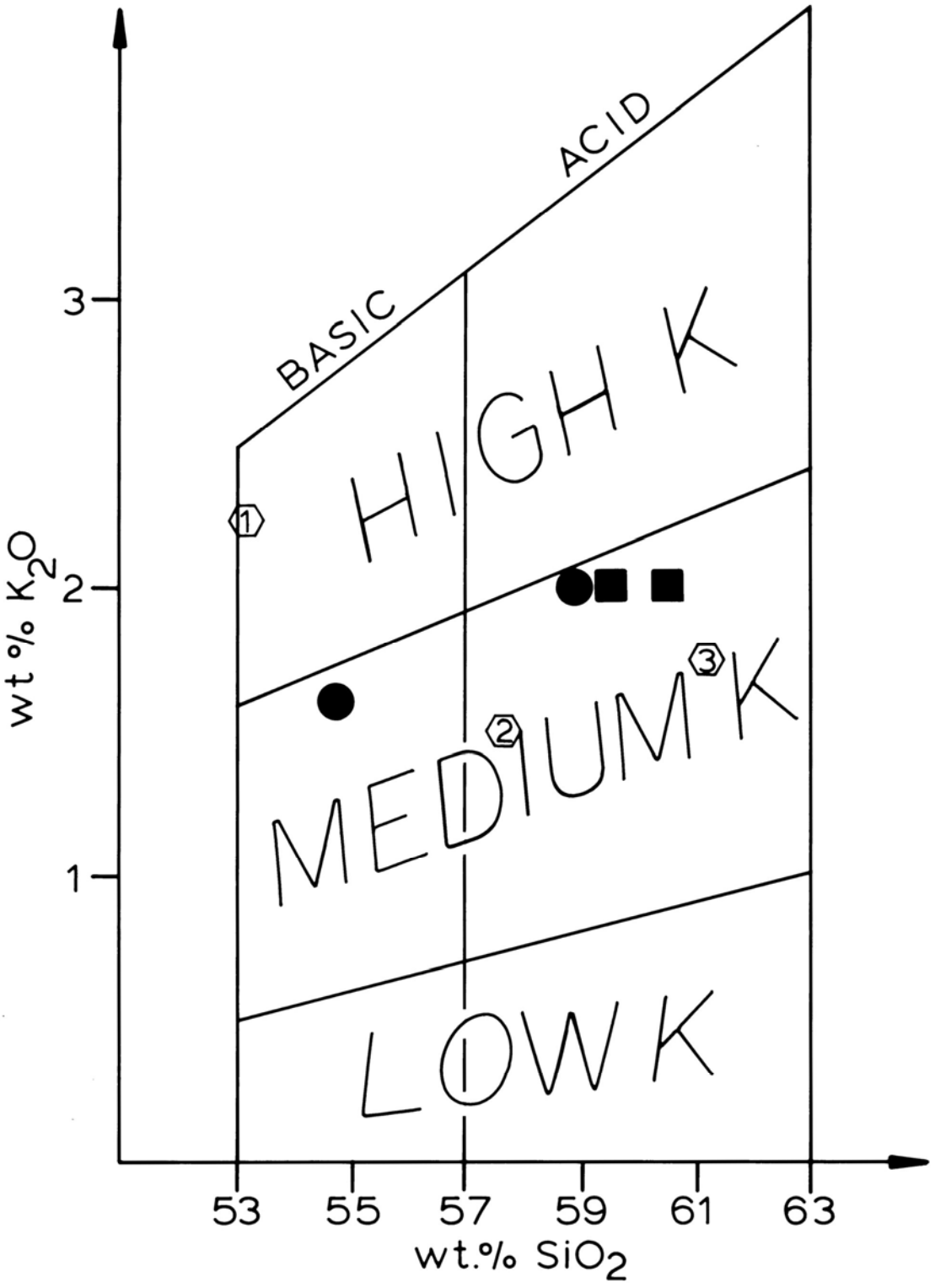

Figure 15 - Orogenic andesite diagram from Gill (1981, p. 6) showing nomenclature for andesites of the Group A and B dikes (solid squares and circles). Sample 1206 was not plotted due to its high K_20 reported in Table 3. Numbered hexagons refer to 1) Recent feldsparphyric basaltic andesite from the Solomon arc (Stanton and Bell, 1969), 2) the average of 2500 orogenic andesites (Gill, 1981, p. 3), and 3) the average of 24 hornblende andesites (Daly, 1933).

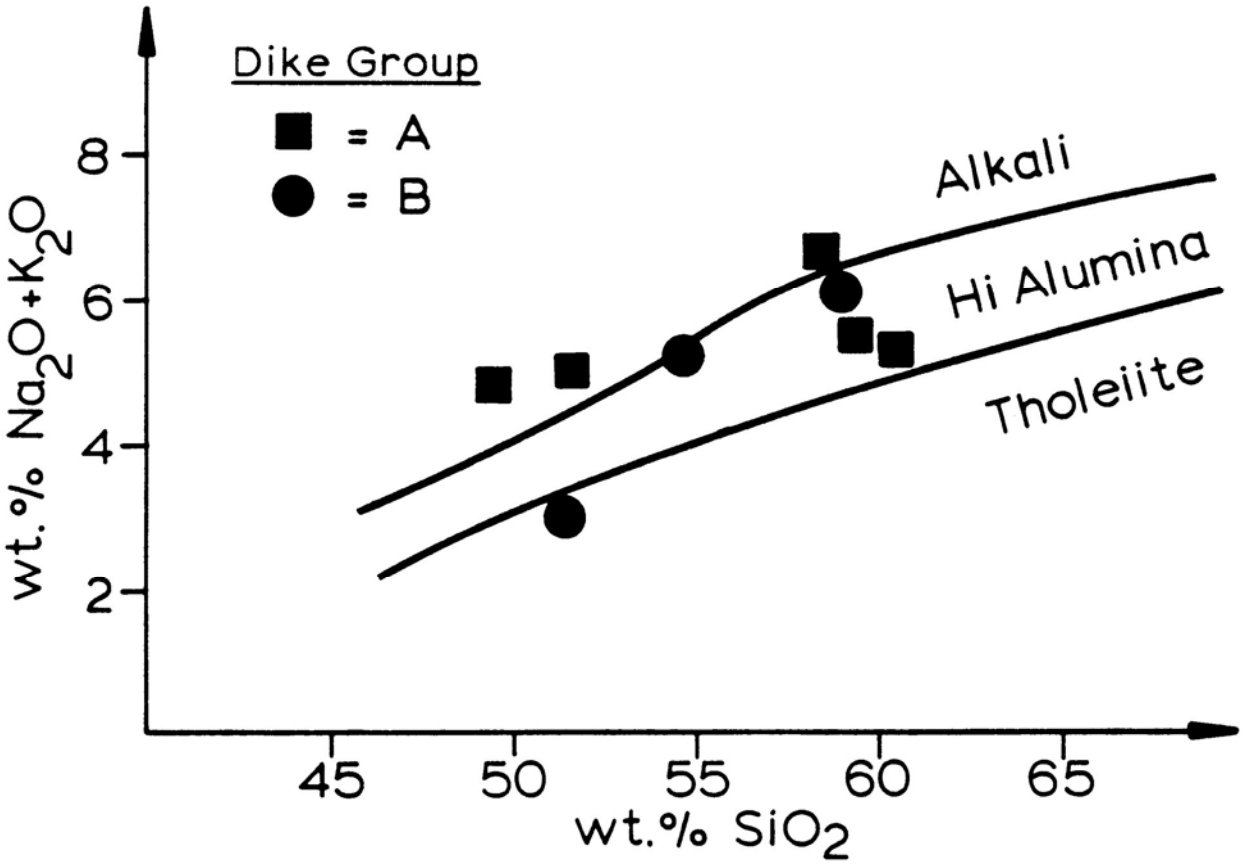

Figure 16 - Total alkali vs. $Si0_2$ diagram discriminating between the tholeiitic, high-alumina, and alkali-olivine basalt series of the Japanese arc (after Kuno, 1966). Most basalts and all andesites of the Sonora swarm plot in the high-alumina and alkali basalt fields.

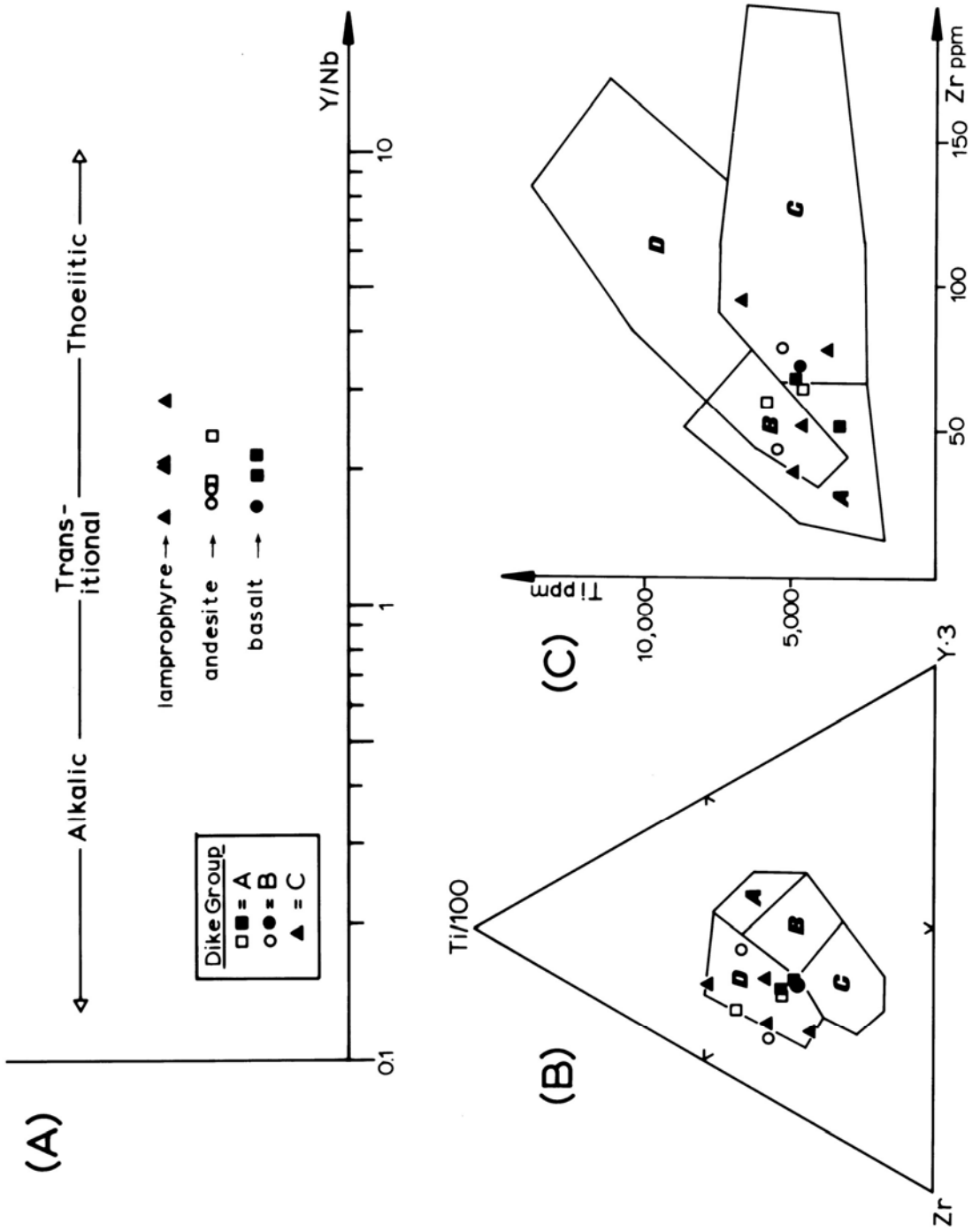

Figure 17 **(a)** - Y/Nb diagram to illustrate the petrologic character of the Sonora dike swarm after Pearce and Cann (1973). The basaltic dikes (solid circle and squares) are transitional between alkalic and tholeiitic basalts although discrimination between within-plate basalts or ocean floor basalts is not possible in this diagram.
(b) - Zr-Ti-Y discrimination diagram after Pearce and Cann (1973). Low potassium tholeiites occur in fields A and B, calc-alkaline basalts in fields B and C, ocean-floor basalts in field B, and oceanic island or continental "within-plate" basalts in field D. The Sonora dikes are concentrated in field D.
(c) - Ti-Zr discrimination diagram after Pearce and Cann (1973). Low potassium tholeiites plot in fields A and B, ocean-floor basalts plot in fields B and D, and calc-alkaline basalts plot in fields B and C. Basalts of the Sonora Swarm occupy the A and C fields which suggests affinities with island arc low-K tholeiites and calc-alkaline basalts.

Figure 18 - A 20 cm thick, flow-layered basaltic dike trending N80°W in Eagle Creek deformed by late Nevadan (N35°E, 80°SE) folding. The hammer handle is parallel to the late-Nevadan cleavage which crenulates and disrupts the flow-layering of the dike and forms a strain-slip cleavage in the Shoo Fly quartzite surrounding it.

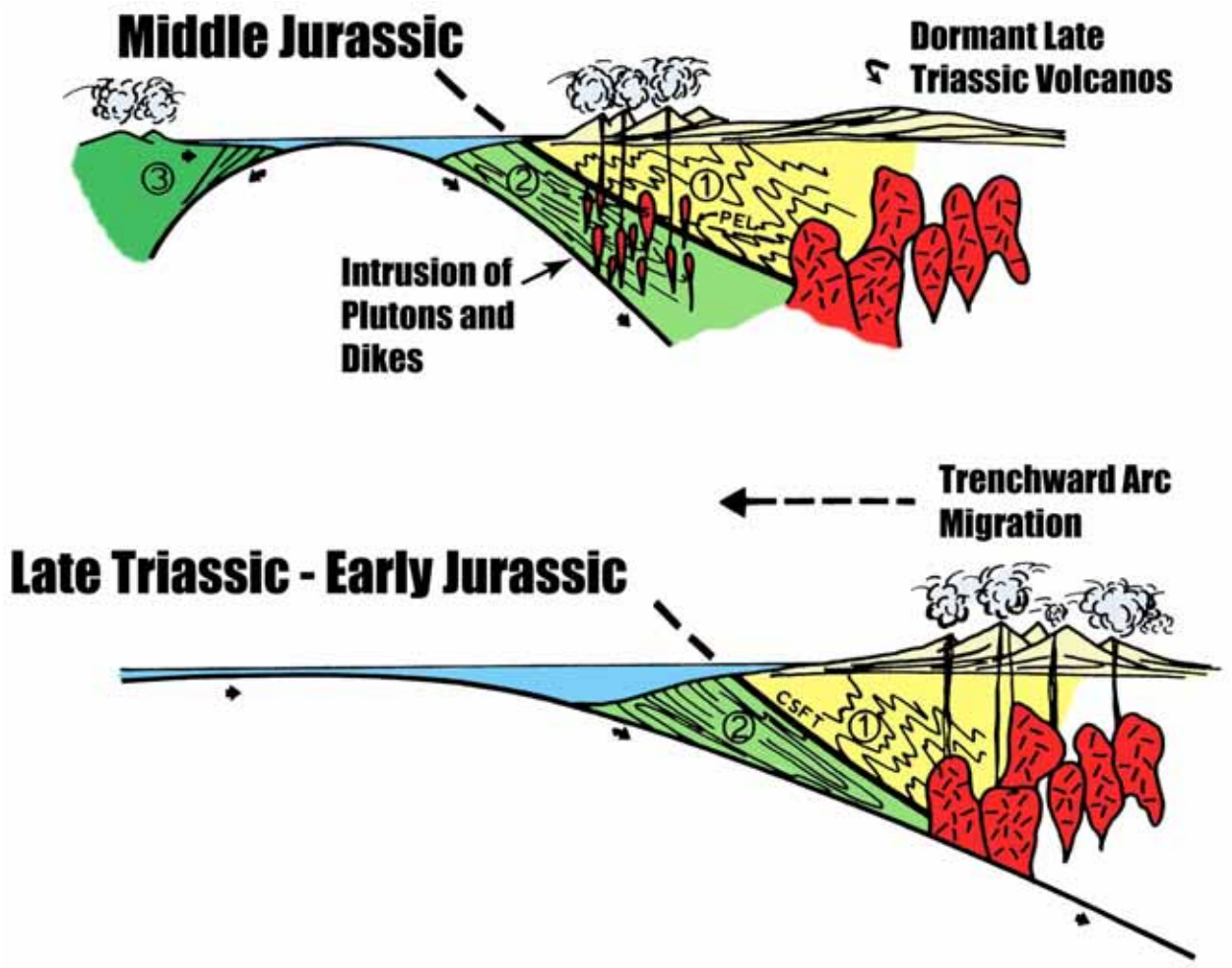

Figure 19 - Cartoon showing the pre-Nevadan development of the Cordilleran margin between late Triassic and middle Jurassic time. The Sonora dike swarm probably formed in a near-trench subductive regime with opening of east-west S_2/S_4 metamorphic surfaces (maximum extension perpendicular to page) due to subduction stress transmitted into the overriding plate. PEL=present erosion level, S=Standard pluton, CSFT= Calaveras-Shoo Fly thrust, SF=Sonora fault. The cross-section is at 38°N lat. Units 1, 2, and 3 are circled.

MODAL MINERALOGY OF THE DIKE SWARM

	A ■ BASALT & ANDESITE						B ● APHANITES			C ▲ LAMPROPHYRES				
PHENOCRYSTS	2388	552A	206	244	53		167	216B	194		370-2	323	180A	50B	238A	50A
Plagioclase	✓	A	A	A	A						✓				✓	
Pargasitic Amphibole											A	A		A	A	
Light Green to Colorless Amphibole		✓		✓	✓											A
Augite	A						A					✓	A			
GROUNDMASS																
Plagioclase	✓	✓	A	✓	✓		A	✓	✓		✓	✓	✓	✓	✓	✓
Pargasitic Amphibole												✓		✓	✓	
Brown Amphibole							✓+	✓+	✓+				✓			
Light Green to Colorless Amphibole	✓	A	✓		✓		✓	✓			✓	✓	✓	✓	✓	A
Biotite	✓		✓	✓	✓			✓	✓					✓		✓
Calcite	✓	A*	✓	✓	✓						A	A	A	A	✓	A
Epidote	✓	✓		✓	✓			✓			✓	✓	✓	✓	✓	✓
Chlorite		✓		✓	✓		✓				✓	✓	✓	✓		✓
Alkali Feldspar											✓	✓				
Quartz			✓		✓			✓			✓	✓		✓	✓	A
Opaques	✓	✓	✓	✓	✓		✓	✓	✓		✓	✓	✓	✓	✓	✓
Degree of Alteration	L	H	M	M	H		M	M	M		M	L	L	M	L	H
LITHOLOGY	Augite-Plagioclase Basalt	Pyroxene-Free Plagioclase Basalt	Plagioclase Andesite	Amphibole-bearing Labradorite Andesite	Amphibole-bearing Labradorite Andesite		Augite Basalt	Basic Andesite	Andesite		Pargasite-Plagioclase Lamprophyre	Pargasite-Augite Lamprophyre	Augite Lamprophyre	Pargasite Lamprophyre	Pargasite-Plagioclase Lamprophyre	Amphibole Lamprophyre

KEY

✓ = present
A = abundant
L = low
M = moderate
H = high

* = abundance of carbonate due to high degree of alteration

\+ = also occurs as microphenocrysts

Table 1 - Petrographic modal mineralogy of phenocrysts and groundmass of the Group A, B, and C dikes of the Sonora dike swarm.

■ GROUP A – PLAGIOCLASE-PHYRIC ANDESITE & BASALT

	238B	552A	206	244	53
SiO_2	49.5	51.7	58.4	59.5	60.5
TiO_2	0.8	0.6	0.7	0.8	1.0
Al_2O_3	12.4	15.5	16.7	16.3	17.8
Fe_2O_3*	14.6	12.1	7.4	8.6	5.7
MnO	0.2	0.2	0.2	0.1	0.1
MgO	6.7	6.1	3.6	3.2	3.5
CaO	10.3	8.5	5.8	5.6	7.0
Na_2O	2.4	3.3	3.2	3.5	3.3
K_2O	2.4	1.7	3.5	2.0	2.0
TOTAL	99.3	99.7	99.5	99.6	100.9
Q			7.35	12.08	13.55
or	14.18	10.05	20.68	11.82	11.82
ab	17.98	27.92	27.08	29.62	27.92
an	15.97	22.46	20.87	22.86	27.85
ne	1.26				
di	29.15	16.28	6.47	4.08	5.51
hy		7.87	12.28	14.07	9.07
ol	15.07	10.07			
mt	2.90	2.90	2.90	2.90	2.90
il	1.52	1.14	1.33	1.52	1.90
TOTAL	98.04	98.69	98.96	98.94	100.53
	Augite-Plagioclase Basalt	Pyroxene-Free Plagioclase Basalt	Plagioclase Andesite	Amphibole-bearing Labradorite Andesite	Amphibole-bearing Labradorite Andesite

* TOTAL IRON AS Fe_2O_3

Table 2 - Chemical composition (major element, wt. %) and CIPW norms of the Group A plagioclase- and augite-phyric andesites and "basalts" of the Sonora dike swarm. In Tables 2, 3, and 4, CIPW norms were calculated assuming 2% Fe203 and remaining iron = FeO.

● GROUP B - APHANITES

	167	216B	194
SiO_2	51.3	54.7	58.9
TiO_2	0.8	0.9	0.9
Al_2O_3	15.1	17.8	16.9
Fe_2O_3*	11.5	9.1	5.9
MnO	0.2	0.2	0.2
MgO	6.7	4.4	3.5
CaO	11.2	7.6	8.2
Na_2O	2.3	3.7	4.1
K_2O	0.7	1.6	2.0
TOTAL	99.8	100.0	100.6
Q	1.07	2.39	7.01
or	4.14	9.46	11.82
ab	19.46	13.31	34.69
an	28.81	27.24	21.80
ne			
di	21.96	8.60	15.21
hy	19.00	15.69	5.06
ol			
mt	2.90	2.90	2.90
il	1.52	1.71	1.71
TOTAL	98.85	99.29	100.21
	Augite Basalt	Basic Andesite	Andesite

* TOTAL IRON AS Fe_2O_3

Table 3 - Chemical composition (major element, wt. %) and CIPW norms of the Group B dominantly aphanitic andesites and basalt of the Sonora dike swarm.

▲ GROUP C – LAMPROPHYRES

	370-2	323	180A	50B	238A	50A
SiO_2	50.3	50.6	51.2	51.9	55.6	57.3
TiO_2	1.1	0.8	0.8	0.6	1.2	0.9
Al_2O_3	16.3	13.9	14.1	15.8	18.5	15.2
Fe_2O_3*	12.7	14.5	12.2	10.4	7.2	11.8
MnO	0.2	0.2	0.2	0.2	0.1	0.2
MgO	5.5	7.1	7.2	6.0	4.2	4.3
CaO	8.8	8.9	10.6	9.4	7.8	7.2
Na_2O	3.4	2.2	1.6	2.3	4.0	2.4
K_2O	1.3	1.6	1.0	3.7	2.4	0.6
TOTAL	99.6	99.8	98.9	100.3	101.0	99.9
Q			3.36		0.69	14.55
or	7.68	9.46	5.91	21.87	14.18	3.55
ab	28.77	18.62	13.54	18.97	33.85	20.31
an	25.38	23.33	28.34	21.86	25.44	28.93
ne				0.27		
di	15.16	17.24	19.91	20.33	10.73	5.66
hy	4.73	20.72	22.40		10.41	21.31
ol	11.82	4.77		12.13		
mt	2.90	2.90	2.90	2.90	2.90	2.90
il	2.09	1.52	1.52	1.14	2.28	1.71
TOTAL	98.53	98.55	97.88	99.46	100.48	98.92
	Pargasite-Plagioclase Lamprophyre	Pargasite-Augite Lamprophyre	Augite Lamprophyre	Pargasite Lamprophyre	Pargasite-Plagioclase Lamprophyre	Amphibole Lamprophyre

* TOTAL IRON AS Fe_2O_3

Table 4 - Chemical composition (major element, wt. %) and CIPW norms of the Group C pargasitic amphibole-, plagioclase-, and augite-bearing lamprophyres of the Sonora dike swarm.

	Feldsparphyric Basaltic Andesite 1	Average of 2500 Orogenic Andesites 2	Average of 24 Hornblende Andesites 3
SiO_2	53.07	57.6	61.12
TiO_2	0.70	0.77	0.42
Al_2O_3	18.21	17.3	17.65
Fe_2O_3	2.98	3.1	2.89
FeO	4.76	4.3	2.40
MnO	0.22	0.15	----
MgO	4.28	3.6	2.44
CaO	8.93	7.2	5.80
Na_2O	3.10	3.2	3.83
K_2O	2.21	1.5	1.72
H_2O	1.09	1.0	1.43
P_2O_5	0.34	0.21	----
TOTAL	100.05	99.93	100.0
Q	2.49		15.41
or	13.06		10.16
ab	26.23		32.41
an	29.25		25.89
di	9.58		2.34
hy	11.52		8.04
ol	----		----
mt	4.32		2.90
il	1.33		0.80
ap	0.80		----
TOTAL	98.58		97.94

1 = Stanton and Bell (1969)
2 = Gill (1981, p. 3)
3 = Daly (1933)

Table 5 - Chemical composition (major element, wt. %) and where reported CIPW norms of orogenic andesites.

	Average of 7 Alkali Basalts 1	Average of 11 High-Alumina Basalts 2	Average of 137 Tholeiitic Basalts and Diabases 3	Low TiO_2 Q-norm type Diabase 4
SiO_2	48.11	50.19	50.83	51.66
TiO_2	1.72	0.75	2.03	0.76
Al_2O_3	15.55	17.58	14.07	14.95
Fe_2O_3	2.99	2.84	2.88	11.77*
FeO	7.19	7.19	9.00	----
MnO	0.16	0.25	0.18	0.20
MgO	9.31	7.39	6.34	7.44
CaO	10.43	10.50	10.42	10.80
Na_2O	2.85	2.75	2.23	2.23
K_2O	1.13	0.40	0.82	0.48
H_2O	----	----	0.91	----
P_2O_5	0.56	0.14	0.23	----
TOTAL	100.00	99.98	99.94	100.29
Q	----	----	3.5	3.38
or	6.67	2.22	5.0	2.84
ab	24.10	23.58	18.9	18.87
an	26.41	34.47	25.9	29.37
di	9.16	7.08	10.3	19.67
hy	8.22	22.62	27.0	18.81
ol	16.73	4.29	----	----
mt	4.41	4.18	4.2	5.12
il	3.19	1.52	3.8	1.44
ap	1.34	0.34	0.5	----
TOTAL	100.23	100.30	99.1	99.47

1, 2 = Kuno (1960)
3 = Nockolds (1954)
4 = Weigand and Ragland (1970, p. 200)

*** Total Fe as Fe_2O_3**

Table 6 - Chemical composition (major element, wt. %) and CIPW norms of alkali, high-alumina, and tholeiitic basalts.

	Average of 16 Vogesites	Spessartite	Average of 14 Spessartites	Spessartite
	1	2	3	4
SiO_2	50.32	52.71	52.85	56.32
TiO_2	1.47	1.48	1.03	0.68
Al_2O_3	15.38	16.01	15.74	18.40
Fe_2O_3	3.71	5.17	3.04	3.36
FeO	5.29	4.58	4.81	4.23
MnO	0.11	0.21	0.06	0.15
MgO	6.33	4.25	6.24	3.46
CaO	7.58	8.14	7.58	7.01
Na_2O	3.03	3.49	3.58	3.60
K_2O	2.74	1.46	2.39	1.54
H_2O	2.87	1.32	2.05	1.17
P_2O_5	0.40	0.78	0.07	0.18
CO_2	0.78	0.01	0.12	0.02
TOTAL	100.01	99.61	99.56	100.12

1 = Johannsen (1937, v. III, p. 39)
2 = Chen and Moore (1979)
3 = Johannsen (1937, v. III, p. 192)
4 = Chen and Moore (1979)

Table 7 - Chemical composition (major element, wt. %) of vogesite and spessartite lamprophyres.

EMISSION SPECTROGRAPHIC ANALYSIS

PROGRAM NO. 1284202
PLATE NO. CE-1938

MAFIC DIKES
Tuolumne Co., California

J. HARRIS/C. SKEEN (ANALYST)
W. B. CRANDELL (PLATE RECORDER)
D. M. GOLIGHTLY (PROJECT LEADER)

FIELD #	147	180A	194	206	216B	230A	230B	244	323	376-2	552A
SAMPLE	U-217365	U-217366	U-217367	U-217368	U-217369	U-217370	U-217371	U-217372	U-217373	U-217374	U-217375
SI %	18	17	21	19	15	18	16	21	17	18	17
AL %	7.2	5.5	8.2	8.5	7.7	8.7	5.9	7.8	6.1	4.8	7.2
FE %	14	13	9.0	11	14	17	15	11	10	8.9	15
MG %	3.7	5.1	2.5	2.1	2.4	2.5	4.6	1.9	3.9	2.3	3.6
CA %	5.7	5.1	5.5	5.2	4.9	4.7	5.4	4.0	5.5	3.7	5.3
NA %	1.8	1.7	4.7	3.9	2.6	2.3	1.9	2.6	2.6	3.9	2.6
K %	0.45	0.75	0.56	3.7	1.4	2.1	1.4	1.8	1.9	1.1	1.5
TI %	0.23	0.12	0.24	0.15	0.19	0.25	0.18	0.19	0.17	0.16	0.25
P %	< 0.068	< 0.068	0.21	< 0.068	< 0.068	< 0.068	< 0.068	< 0.068	< 0.068	0.13	< 0.068
MN %	0.28	0.19	0.19	0.18	0.26	0.25	0.24	0.16	0.24	0.20	0.27
AG PPM	0.22	0.81	< 0.10	0.36	< 0.10	< 0.10	1.7	< 0.10	0.29	< 0.10	0.21
AS PPM	< 150	< 150	< 150	< 150	< 150	< 150	< 150	< 150	< 150	< 150	< 150
AU PPM	< 10	< 10	< 10	< 10	< 10	< 10	< 10	< 10	< 10	< 10	< 10
B PPM	< 6.8	< 6.8	< 6.8	< 6.8	< 4.6	< 6.8	< 6.8	< 6.8	< 6.8	< 6.8	< 6.8
BA PPM	280	120	310	530	410	520	490	510	340	370	160
BE PPM	< 1.0	< 1.0	< 1.0	< 1.0	< 1.0	< 1.0	1.5	1.3	< 1.0	< 1.0	< 1.0
BI PPM	< 10	< 10	< 10	< 10	< 10	< 10	< 10	< 10	< 10	< 10	< 10
CD PPM	< 32	< 32	< 32	< 32	< 32	< 32	< 32	< 32	< 32	< 32	< 32
CE PPM	< 63	< 63	< 63	< 63	< 63	< 63	< 63	< 63	< 63	< 63	< 63
CO PPM	39	45	25	21	39	33	44	20	37	29	41
CR PPM	310	710	150	130	220	310	670	140	340	180	310
CU PPM	220	88	160	90	260	440	300	260	380	240	160
DY PPM	< 22	< 22	< 22	< 22	< 22	< 22	< 22	< 22	< 22	< 22	< 22
ER PPM	< 10	< 10	< 10	< 10	< 10	< 10	< 10	< 10	< 10	< 10	< 10
EU PPM	< 2.2	< 2.2	< 2.2	< 2.2	< 2.2	< 2.2	< 2.2	< 2.2	< 2.2	< 2.2	< 2.2
GA PPM	14	14	26	22	20	21	14	17	17	18	16
GD PPM	18	< 15	< 15	< 15	< 15	< 15	< 15	< 15	< 15	< 15	< 15
GE PPM	< 1.5	< 1.5	< 1.5	< 1.5	< 1.5	< 1.5	< 1.5	< 1.5	< 1.5	< 1.5	< 1.5
HF PPM	< 15	< 15	< 15	< 15	< 15	< 15	< 15	< 15	< 15	< 15	< 15
HG PPM	< 6.8	< 6.8	< 6.8	< 6.8	< 6.8	< 6.8	< 6.8	< 6.8	< 6.8	< 6.8	< 6.8
IN PPM	< 6.8	< 6.8	< 6.8	< 6.8	< 6.8	< 6.8	< 6.8	< 6.8	< 6.8	< 6.8	< 6.8
IR PPM	< 15	< 15	< 15	< 15	< 15	< 15	< 15	< 15	< 15	< 15	< 15
LA PPM	< 10	< 10	11	< 10	< 10	17	25	< 10	< 10	11	< 10
LI PPM	< 68	< 68	< 68	< 68	< 68	< 68	N	< 68	< 68	< 68	N
LU PPM	< 15	< 15	< 15	< 15	< 15	< 15	< 15	< 15	< 15	< 15	< 15
MN PPM	2800	1900	1900	1800	2600	2500	2400	1600	2400	2000	2700
MO PPM	10	3.0	12	10	25	25	14	5.3	7.0	4.9	14
NB PPM	8.0	< 3.2	< 3.2	< 3.2	6.1	3.8	5.2	4.2	< 3.2	4.2	5.0
ND PPM	< 32	< 32	< 32	< 32	< 32	< 32	< 32	< 32	< 32	< 32	< 32
NI PPM	85	220	61	42	70	110	120	44	76	51	89
OS PPM	< 22	< 22	< 22	< 22	< 22	< 22	< 22	< 22	< 22	< 22	< 22
PB PPM	16	8.4	14	17	15	49	33	14	8.7	15	15
PD PPM	< 1.0	< 1.0	< 1.0	< 1.0	< 1.0	< 1.0	< 1.0	< 1.0	< 1.0	< 1.0	< 1.0
PR PPM	< 68	< 68	75	< 68	< 68	< 68	< 68	< 68	< 68	< 68	< 68
PT PPM	< 4.6	< 4.6	< 4.6	< 4.6	< 4.6	< 4.6	< 4.6	< 4.6	< 4.6	< 4.6	< 4.6
RE PPM	< 10	< 10	< 10	< 10	< 10	< 10	< 10	< 10	< 10	< 10	< 10
RH PPM	< 2.2	< 2.2	< 2.2	< 2.2	< 2.2	< 2.2	< 2.2	< 2.2	< 2.2	< 2.2	< 2.2
RU PPM	< 2.2	< 2.2	< 2.2	< 2.2	< 2.2	< 2.2	< 2.2	< 2.2	< 2.2	< 2.2	< 2.2
SB PPM	< 32	< 32	< 32	< 32	< 32	< 32	< 32	< 32	< 32	< 32	< 32
SC PPM	39	17	10	9.9	20	17	31	15	34	19	32
SN PPM	< 10	< 10	< 10	< 10	< 10	< 10	< 10	< 10	< 10	< 10	< 10
SN PPM	< 1.5	< 1.5	4.9	< 1.5	2.4	5.9	< 1.5	< 1.5	1.5	< 1.5	< 1.5
SR PPM	610	260	1400	560	690	920	970	660	470	680	490
TA PPM	< 460	< 460	< 460	< 460	< 460	< 460	< 460	< 460	< 460	< 460	< 460
TB PPM	< 32	< 32	< 32	< 32	< 32	< 32	< 32	< 32	< 32	< 32	< 32
TH PPM	< 22	< 22	< 22	< 22	< 22	< 22	< 22	< 22	< 22	< 22	< 22
TL PPM	< 4.6	< 4.6	< 4.6	< 4.6	< 4.6	< 4.6	< 4.6	< 4.6	< 4.6	< 4.6	< 4.6
TM PPM	< 4.6	< 4.6	< 4.6	< 4.6	< 4.6	< 4.6	< 4.6	< 4.6	< 4.6	< 4.6	< 4.6
U PPM	< 320	< 320	< 320	< 320	< 320	< 320	< 320	< 320	< 320	< 320	< 320
V PPM	190	210	100	110	170	120	140	110	180	200	170
W PPM	< 10	< 10	< 10	< 10	< 10	< 10	< 10	< 10	< 10	< 10	< 10
Y PPM	13	5.1	5.4	6.6	11	7.8	11	10	9.2	8.7	9.7
YB PPM	0.67	0.29	0.63	0.70	0.74	2.6	3.3	1.8	0.61	1.2	0.43
ZN PPM	140	95	100	93	120	120	150	120	110	95	170
ZR PPM	73	36	79	60	44	78	68	65	92	95	52
dike group →	B	C	B	A	B	C	A	A	C	C	A

Table 8 - Chemical composition (minor and trace elements, ppm) of the Sonora dike swarm. Utilizing semi-quantitative emission spectrographic analysis, accuracy is limited to +50% and -33%.

Pluton name	Symbol	Intrusive into Unit #	(m.y.) Age	cut by Sonora dike swarm?	NW or NE cut by Nevadan cleavage?	References
San Andreas	SA	2		?	NW + NE	Clark (1970); Merguerian (unpub. data) = (A)
Vallecitos	V	2		YES	NW	Baird (1962); Schweickert and Merguerian (unpub. data) = (B)
Parrotts Ferry	PF	2	170[a]	YES	NW + NE	Baird (1962); Sharp and Saleeby (1979); (B)
Knight Creek	KC	1+2		NO dikes=xenoliths	NE	Merguerian (1984); (B)
Standard	S	1+2	170[a] 153-164[a] 147-166[b]	YES	NW + NE	Sharp and Saleeby (1979); Stern and others (1981); Sharp (unpub. data); (B)
Basin Creek	BC	1		?	NW	Merguerian, 1981 ms = (C)
Duckwall Ridge	DR	1		?	?	(C)
Jawbone Flats	JF	1		?	?	Turner and Ransome (1897); (C)
Cobb Creek	CC	3	162[a]	NO	?	Morgan (1977)
Hazel Green	HG	1+2		NO	NO	Tobisch (1960, unpub. data); Bowen (1969); (C)

Table 9 - Field relationships of middle Jurassic plutons of the Sierra Nevada foothills compared to the Sonora dike swarm and Nevadan structures. Geochronologic data is indicated where possible (see Fig. 1). The plutons are tabulated (top to bottom) from northwest to southeast. Blank spaces indicate a lack of data.

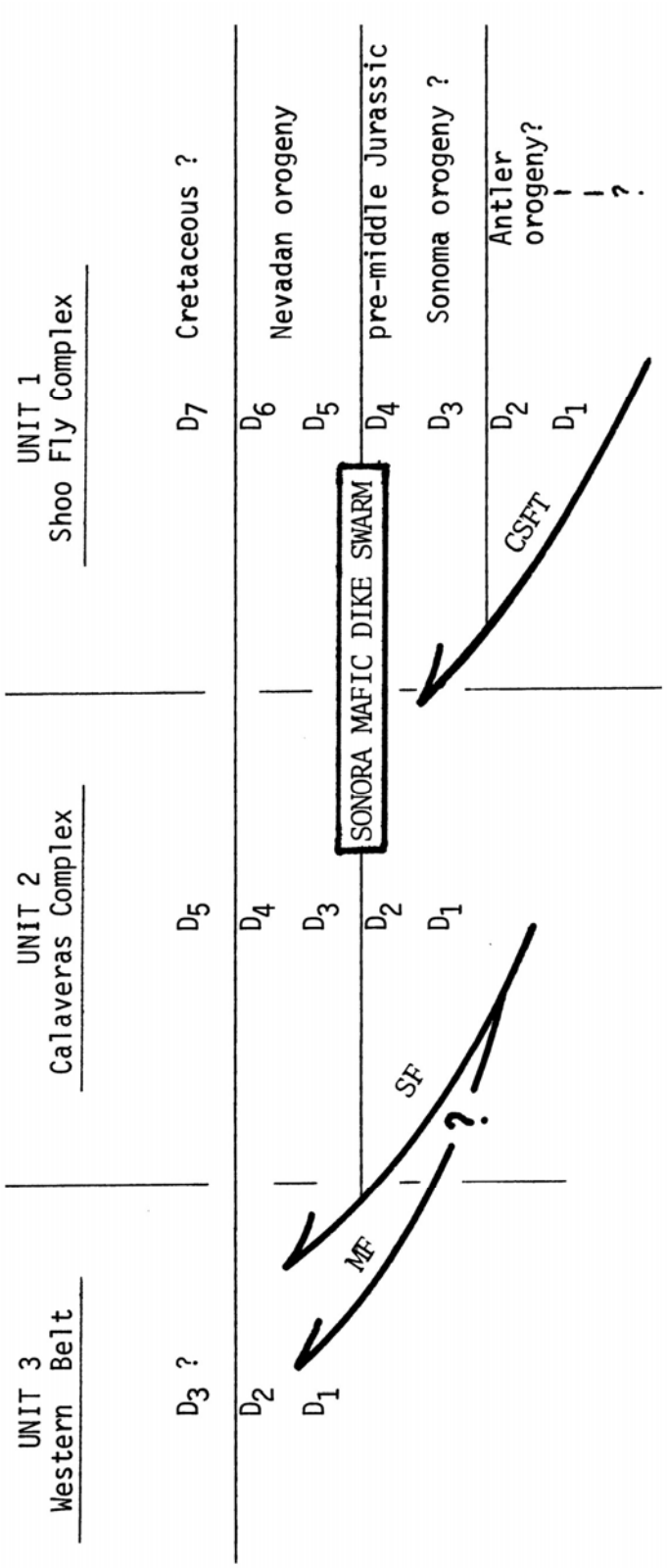

Table 10 - Structural correlation chart illustrating the regionally developed deformational episodes recognized in Units 1, 2, and 3 of the foothills metamorphic belt. See Figs. 1, 2; Schweickert and others (1984).

REFERENCES CITED

Baird, A.K., 1962, Superposed deformation in the central Sierra Nevada foothills east of the Mother Lode: University of California Publications in Geological Sciences, v. 42, p. 1-70.

Bateman, P.C., Clark, C.D., Huber, N.K., Moore, J.G., and Rinehart, C.D., 1963, The Sierra Nevada batholith - a synthesis of recent work across the central part: U.S. Geological Survey Professional Paper 414D, p. D1-D46.

_____, and Clark, L.D., 1974, Stratigraphic and structural setting of the Sierra Nevada batholith, California: Pacific Geology, v. 8, p. 79-89.

Busacca, A. J., Marchand, D.E., and Sawka, W.N., 1982, Geologic map of the Raymond quadrangle, Madera and Mariposa Counties, California: U.S. Geological. Survey Map GO-1555, 1:62,500 scale.

Bell, T.H., and Etheridge, M.A., 1976, The deformation and recrystallization of quartz in a mylonite zone, central Australia: Tectonophysics, v. 32, p. 235-267.

Bond, G.C., and DeVay, J.C., 1980, Pre-Upper Devonian quartzose sandstones in the Shoo Fly Formation northern California - petrology, provenance and implications for regional tectonics: Journal of Geology, v. 88, p. 285-308.

_____, and Schweickert, R.A., 1981, Significance of pre-Devonian melange in the Shoo Fly Complex, northern Sierra Nevada, California (abs.): Geological Society of America Abstracts with Programs, v. 13, p. 46.

Bowen, O.E., 1969, Geology of the E1 Portal - Coulterville area: California Divison of Mines and Geology Open-File Report, Kinsley, Feliciana Mtn., E1 Portal, and Buckingham Mtn. quadrangles, 1:24,000 scale.

Brook, C.A., 1977, Stratigraphy and structure of the Saddlebag Lake roof pendant, Sierra Nevada, California: Geological Society of America Bulletin, v. 88, p. 321-334.

Carmichael, I.S.E., Turner, F.J., and Verhoogen, J., 1974, Igneous petrology: McGraw Hill, New York, 739p.

Carreras, J., Julivert, M., and Santanach, P., 1980, Hercynian mylonite belts in the eastern Pyrenees: an example of shear zones associated with late folding: Journal of Structural Geology, v. 2, no. 1/2, p. 5-9 .

Carter, N.L., Anderson, D.A., Hansen, F.D., and Kranz, R.L., 1981, Creep and creep rupture of granitic rocks: *in* Mechanical behavior of crustal rocks, N.L. Carter, M. Friedman, J.M. Logan, and D.W. Stearns *(editors)*, American Geophysical Union Monograph 24, p. 61-82.

Cashman, S.M., 1980, Devonian metamorphic event in the northeastern Klamath Mountains, California: Geological Society of America Bulletin, Part 1, v. 91, p. 453-459.

Chen, J.H. and Moore, J. G., 1979, Late Jurassic Independence dike swarm in eastern California: Geology, v. 7, p. 129-133.

Christie, J.M., 1960, Mylonitic rocks of the Moine thrust zone in the Assynt region, northwest Scotland: Transactions Geological Society of Edinburgh, v. 18, p. 79-93.

Churkin, M., and Langenheim, R.L., 1960, Silurian strata of the Klamath Mountains, California, *in* Geological Survey research 1965: U.S. Geological Survey Professional Paper 525-C, p. C72-C73.

_____, and Eberlein, G.D., 1977, Ancient borderland terranes of the North American Cordillera: correlations and microplate tectonics: Geological Society of America Bulletin, v. 78, p. 651-668.

Clark, L.D., 1964, Stratigraphy and structure of part of the western Sierra Nevada metamorphic belt, California: U.S. Geological Survey Professional Paper 410, p. 69.

_____, 1970, Geology of the San Andreas 15 - minute quadrangle: California Division of Mines and Geology Bulletin 195, 23p.

_____, 1976, Stratigraphy of the north half of the western Sierra Nevada metamorphic belt, California: U.S. Geological Survey Professional Paper 923, 26p.

_____, Imlay, R.W., McMath, V.E., and Silberling, N.J., 1962, Angular unconformity between Mesozoic and Paleozoic rocks in the northern Sierra Nevada, California: U.S. Geological Survey Professional Paper 450B, B15-B19.

D'Allura, J.A., Moores, E.M., and Robinson, L., 1977, Paleozoic rocks of the northern Sierra Nevada: their structural and stratigraphic relations: *in* Stewart, J.H., Stevens, C.H., and Fritsche, A.E. *(editors)*, Paleozoic paleography of the western United States: Society of Economic Paleontologists and Mineralogists, Pacific Section, Pacific Coast Paleogeography Symposium I, p. 395-408.

Daly, R.A., 1933, Igneous rocks and the depths of the Earth: McGraw Hill, New York, 598p.

Diller, J. S., 1892, Geology of the Taylorsville region, California: Geological Society of America Bulletin, v. 3, p. 370-394.

_____, 1908, Geology of the Taylorsville region, California: U.S. Geological Survey Bulletin 352, 128p.

Dixon, H.R., 1968, Bedrock geology of the Plainfield-Danielson area, Connecticut: U.S. Geological Survey Open-file report.

Dodge, F.C.W., 1982, Geologic map of the Dinkey Lakes Roadless Area, Fresno County, California: U.S. Geological Survey Miscellaneous Field. Investigation Map MF-1389-A, scale 1:62,500.

duBray, E.A., 1981, Generalized bedrock geologic map of the John Muir Wilderness, Fresno, Inyo, and Mono Counties, California: U.S. Geological Survey Miscellaneous Field. Investigation Map MF-1185-A, 1:125,000 scale.

Duffield, W.A., and Sharp, R.V., 1975, Geology of the Sierra Foothills melange and adjacent areas, Amador County, California: U.S. Geological Survey Professional Paper 827, 30p.

Evernden, J.F. and Kistler, R.W., 1970, Chronology of emplacement of Mesozoic batholithic complexes in California and western Nevada: U.S. Geological Survey Professional Paper 623, 42p.

Floyd, P. A., and Winchester, J.A., 1975, Magma type and tectonic setting discrimination using immobile elements: Earth and Planetary Science Letters, v. 27, p. 211-218.

Gill, J., 1981, Orogenic andesites and plate tectonics: Springer-Verlag New York, 390p.

Girty, G.H., and Schweickert, R.A., 1979, Preliminary results of a detailed study of the "lower" Shoo Fly, Bowman Lake, northern Sierra Nevada, California (abs.): Geological Society of America Abstracts with Programs, v. 11, no. 3, p. 79.

_____, and Schweickert, R.A., 1985a, The Culbertson Lake Allochthon, a newly identified structural unit within the Shoo Fly Complex, California: evidence for four phases of deformation and extension of the Antler Orogeny to the northern Sierra Nevada: Geological Society of America Bulletin, in press.

_____, and Schweickert, R.A., 1985b, The Bullpen Lake sequence, geochemical evidence for an intraplate setting: Geological Society of America Bulletin, in press.

_____, and Schweickert, R.A., 1985c, Lower Paleozoic sandstones in part of the Shoo Fly Complex, northern Sierra Nevada, California: the case for an early Paleozoic collisional complex: Geological Society of America Bulletin, in press.

Hanson, R.E., Schweickert, R.A., and Brueckner, H.B., 1983, The Bowman Lake Batholith: a probable Upper Devonian composite pluton in the northern Sierra Nevada, CA (abs.): Geological Society of America Abstracts with Programs, v. 15, no. 5, p. 323.

Harvey, P.K., Taylor, D.M., Hendrey, R.D., and Bancroft, F., 1973, An accurate fusion method for the analysis of rocks and chemically related materials by x-ray fluorescence spectrometry: X-ray Spectrometry, v. 2, p. 33-44.

Harwood, D.S., 1980, Geologic map of the North Fork of the American River Wilderness Study Area and adjacent parts of the Sierra Nevada, California: U.S. Geological Survey Map MF-1177-A, scale 1:62,500.

Huber, N.K., 1981, Amount and timing of Late Cenozoic uplift and tilt of the central Sierra Nevada, California - Evidence from the upper San Joaquin River Basin: U.S. Geological Survey Professional Paper 1197, 28p.

_____,1982, Geologic map of the Mount Raymond roadless area, central Sierra Nevada, California: U.S. Geological. Survey Miscellaneous Field. Investigation Map MF-1417-A, scale 1:62,500.

Hudson, T., Plafker, G., and Lanphere, M.A., 1977, Intrusive rocks of the Yakutat-St. Elias area, south-central Alaska: U.S. Geological Survey Journal of Research, v. 5, no. 2, p. 155-172.

Irvine, T.N., and Baragar, W.R.B., 1971, A guide to the chemical classification of the common igneous rocks: Canadian Journal of Earth Sciences, v. 8, p. 523-548.

Irwin, W.P., 1966, Geology of the Klamath Mountains province, *in* Bailey, E.H. *(editor)*, Geology of Northern California: California Divison of Mines and Geology Bulletin 190, p. 19-37.

1981, Tectonic accretion of the Klamath Mountains: in Ernst, W.G., ed., The geotectonic development of California, Rubey vol. 1, Prentice-Hall, NJ, p. 29-49.

Jakes, P., and White, A.J.R., 1972, Hornblendes from calc-alkaline volcanic rocks of island arcs and continental margins: American Mineralogist, v. 57, p. 887-902.

Johannsen, A., 1937, A descriptive petrography of the igneous rocks, volume 3: University of Chicago Press, Chicago, Illinois, 360p.

Johnson, W.M., and Maxwell, J.A., 1981, Rock and mineral analysis: John Wiley and Sons, New York, 489p.

Keith, S.B., 1978, Paleosubduction geometries inferred from Cretaceous and Tertiary magmatic patterns in southwestern North America: Geology, v. 6, p. 516-521.

Keith, W.J., and Seitz, J.F., 1981, Geologic map of the Hoover Wilderness and adjacent study area, Mono and Tuolumne Counties, California: U.S. Geological Survey Map MF-1101-A, 1:62,500 scale.

Kerrick, D.M., 1970, Contact metamorphism in some areas of the Sierra Nevada, California: Geological Society of America Bulletin, v. 81, p. 2913-2938.

Kistler, R.W. and Peterman, Z.E., 1973, Variations in Sr, Rb, K, Na, and initial Sr^{87}/Sr^{86} in Mesozoic granitic rocks and intruded wall rocks in central California: Geological Society of America Bulletin, v. 84, p. 3489-3512.

Kistler, R.W. and Peterman, Z.E., 1978, Reconstruction of crustal blocks of California on the basis of initial Strontium isotopic compositions of Mesozoic granitic rocks: U.S. Geological Survey Professional Paper 1071, 17p.

Knopf, A., 1929, The Mother Lode System of California: U.S. Geological Survey Professional Paper 157, 88p.

Kuno, H., 1966, Lateral variation of basalt magma type across continental margins and island arcs: Bulletin of Volcanology, v. 29, p. 195-222.

Lanphere, M.A., and Irwin, W.P., 1965, Carboniferous isotopic ages of metamorphism of the Salmon Hornblende Schist and Abrams Mica Schist, southern Klamath Mountains, California: U.S. Geological Survey Professional Paper 525-D, p. D27-D33.

Marshak, R.S., and Karig, D.E., 1977, Triple junctions as a cause for anomalously near-trench igneous activity between the trench and the volcanic arc: Geology, v. 5, p. 233-236.

McKee, E.H. and Howe, R.A., 1981, Geologic map of the Mokelumne Wilderness and contiguous Rare II further planning areas, central Sierra Nevada, California: U.S. Geological. Survey Miscellaneous Field. Investigation Map MF-1201-A, 1:62,500 scale.

McMath, V.E., 1966, Geology of the Taylorsville area, northern Sierra Nevada, California: California Division of Mines and Geology Bulletin 190, p. 173183.

Merguerian, C., 1981, Tectonic significance of the Calaveras - Shoo Fly Thrust (CSFT), Tuolumne County, California (abs.): Geological Society of America Abstracts with Programs, v. 13, no. 2, p. 96.

_____,1981ms, The extension of the Calaveras - Shoo Fly Thrust to the southern end of the Sierra Nevada metamorphic belt, California: Preliminary geologic maps of the Tuolumne, Duckwall Mountain, Groveland, Jawbone Ridge, Lake Eleanor NW, SW, and NE 1/4s, Buckhorn Peak, Kinsley, E1 Portal, and Buckingham Mountain 7-1/2' quadrangles. Accompanied by lop. report plus 5 figs., 1 table; California Division of Mines and Geology, Ferry Bldg., San Francisco.

_____, 1982, The extension of the Calaveras - Shoo Fly Thrust (CSFT) to the southern end of the Sierra Nevada Metamorphic Belt (SNMB), California (abs.): Geological Society of America Abstracts with Programs, v. 14, no. 4, p. 215.

_____, 1983, Structural geology of the Calaveras - Shoo Fly Thrust (CSFT), Tuolumne and Mariposa Counties, California (abs.): Geological Society of America Abstracts with Programs , v. 15, no. 6, p. 643.

_____, 1984, Bedrock geologic map of the Shoo Fly Complex, Stanislaus River drainage, Tuolumne County, California: California Division of Mines and Geology, open-file map, scale 1:24,000.

_____, and Schweickert, R.A., 1980, Superposed mylonitic deformation of the Shoo Fly Complex in Tuolumne County, California (abs.): Geological Society of America Abstracts with Programs, v. 12, no. 3, p. 120.

_____, Bogen, N.L., and Schweickert, R.A., 1983, Tectonostratigraphic units in a transect across the central Sierra Nevada, California (abs.): Geological Society of America Abstracts with Programs, v. 15, no. 5, p. 272.

Mitra, G., 1978, Ductile deformation zones and mylonites: The mechanical processes involved in the deformation of crystalline basement rocks: American Journal of Science, v. 278, p. 1057-1084.

Moore, J. G., 1954ms, Geology of the Sierra Nevada front, near Mount Baxter, California: Ph.D. thesis, John Hopkins University, 105p.

_____, and Hopson, C.A., 1961, The Independence dike swarm in eastern California: American Journal of Science, v. 259, p. 241-259.

Morgan, B.A., 1977, Geologic map of the Chinese Camp and moccasin quadrangles, Tuolumne County, California: U.S. Geological Survey Miscellaneous Investigations Map MF-840, scale 1:24,000.

_____, and Rankin, D.W., 1972, Major structural break between Paleozoic and Mesozoic rocks in the Eastern Sierra Nevada, California: Geological Society of America Bulletin, v. 83, p. 3739-3744.

Nakamura, K., Jacob, K.H., and Davies, J.N., 1977, Volcanoes as possible indicators of tectonic stress orientation - Aleutians and Alaska: Pageoph, v. 115, p. 87-112.

Nockolds, S.R., 1954, Average chemical compositions of some igneous rocks: Geological Society of America Bulletin, v. 65, p. 1007-1032.

Nokleberg, W.J., and Kistler, R.J., 1980, Paleozoic and Mesozoic deformation in the central Sierra Nevada, California: U.S. Geological Survey Professional Paper 1145, 24p.

Pearce, J.A., 1975, Basalt geochemistry used to investigate past tectonic environments on Cyprus: Tectonophysics, v. 25, p. 41-67.

_____, and Cann, J. R., 1973, Tectonic setting of basic volcanic rocks determined using trace element analyses: Earth and Planetary Science Letters, v. 19, p. 290-300.

Pique, A., Jeannette, D., and Michard, A., 1980, The Western Mesata shear zone, a major and permanent feature of the Hercynian belt in Morocco: Journal of Structural Geology, v. 2, no. 1/2, p. 55-61.

Reed, J.J., 1964, Mylonites, cataclasites, and associated rocks along the Alpine Fault, South Island, New Zealand: New Zealand Journal of Geology and Geophysics, v. 7, p. 645-684.

Reesor, J.E., and Moore, J.M., Jr., 1971, Petrology and structure of the Thor-Odin Gneiss dome, Shuswap Metamorphic Complex, British Columbia: Geological Survey Canada Bulletin, 195, 149p.

Rinehart, C.F., and Ross, D.C., 1964, Geology and mineral deposits of the Mount Morrison quadrangle, Sierra Nevada, California: U.S. Geological Survey Professional Paper 385, 106p.

Roberts, R.J., Hotz, P.E., Gilluly, J., and Ferguson, H.G., 1958, Paleozoic rocks of north-central Nevada: Bulletin of the American Association of Petroleum Geologists, v. 42, p. 2813-2857.

Rogers, T.H., 1966, San Jose sheet, Geologic Map of California: California Division of Mines and Geology, scale 1:250,000.

Rowell, A.J., Rees, M.N., and Suczek, C.A., 1979, Margin of the North American continent in Nevada during Late Cambrian time: American Journal of Science, v. 279, p. 1-18.

Russell, S., and Nokleberg, W., 1977, Superimposition and timing of deformations in the Mount Morrison roof pendant and in the central Sierra Nevada, California: Geological Society of America Bulletin, v. 88, p. 335-345.

Saleeby, J., 1981, Ocean floor accretion and volcano plutonic arc evolution of the Mesozoic Sierra Nevada: *in* Ernst, W.G., *(editor)*, The geotectonic development of California: Rubey volume I: Prentice Hall, Englewood Cliffs, NJ, p. 132-181.

_____,1982, Polygenetic ophiolite belt of the California Sierra Nevada: geochronological and tectonostratigraphic development: Journal of Geophysical Research., v. 87, no. B3, p. 1803-1824.

_____, 1983, Accretionary tectonics of the North American Cordillera: Annual Reviews of Earth and Planetary Science (1983), v. 15, p. 45-73.

Schweickert, R.A., 1974, Probable late Paleozoic thrust fault near Sierra City, California (abs.): Geological Society of America Abstracts with Programs, v. 6, p. 251.

_____, 1977, Major pre-Jurassic thrust fault between the Calaveras and Shoo Fly Complexes, Sierra Nevada, California (abs.): Geological Society of America Abstracts with Programs, v. 9, p. 497.

_____, 1979, Structural sequence of the Calaveras Complex between the Stanislaus and Tuolumne Rivers (abs.): Geological Society of America Abstracts with Programs, v. 11, p. 127.

_____, 1981, Tectonic evolution of the Sierra Nevada Range: *in* Ernst, W.G., *(editor)*, The geotectonic evolution of California, a symposium in honor of W.W. Rubey, Prentice-Hall, Englewood Cliffs, NJ, p. 87-131.

_____, and Cowan, D.S., 1975, Early Mesozoic tectonic evolution of the western Sierra Nevada, California: Geological Society of America Bulletin, v. 86, p. 1329-1336.

_____, and Wright, W.H., III, 1975, Structural studies of the CalaverasFormation along the Stanislaus River and their tectonic implications, *in* Hulbe, W.H., ed. Stanislaus River Guide - Camp Nine to Melones, Annual Field Trip of the Geological Society of Sacramento, 1975, p. 30-47.

_____, Saleeby, J.B., Tobisch, O.T., and Wright, W.H., III, 1977, Paleotectonic and paleogeographic significance of the Calaveras Complex, western Sierra Nevada in Stewart, J.H., Stevens, C.H., and Fritsche, A.E., *(editors)*, Paleozoic paleogeography of the western United States: Society of Economic Paleontologists and Mineralogists, Pacific Section, Pacific Coast Paleogeography Symposium I, p. 381-394.

_____, and Merguerian, C., 1980, Augen gneiss in the Shoo Fly Complex, Tuolumne County, California - a pre Middle Jurassic plutonic episode (abs.) : Geological Society of America Abstracts with Programs, v. 12, no. 3, p. 152.

_____, and Snyder, W.S., 1981, Paleozoic plate tectonics of the Sierra Nevada and adjacent regions: *in* Ernst, W.G., *(editor)*, The geotectonic development of California, a symposium in honor of W.W. Rubey, Pr entice-Hall, Englewood Cliffs, NJ, p. 182-202.

_____, and Bogen, N.L., 1983, Tectonic transect of Sierran Paleozoic through Jurassic accreted belts: Pacific Section, Society of Economic Paleontologists and Mineralogists, Ann. Mtg., Sacramento, Calif., 22p.

_____, Bogen, N.L., Girty, G.H., Hanson, R.E., and Merguerian, C., 1983 Timing and structural expression of the Nevadan orogeny, Sierra Nevada, California (abs.): Geological Society of America Abstracts with Programs, v. 15, no. 5, p. 293.

_____, Girty, G.H., and Merguerian, C., 1983, The Shoo Fly Complex - a profile of early Paleozoic sedimentation, plutonism, and deformation in the Sierra Nevada of California (abs.): Society of Economic Paleontologists and Mineralogists Abstracts, Pacific Sect., p. 132.

_____, Bogen, N.L., Girty, G.H., Hanson, R.E., and Merguerian, C., 1984, Timing and structural expression of the Nevadan orogeny, Sierra Nevada, California: Geological Society of America Bulletin, v. 95, p. 967-979.

_____, and Merguerian, C., in press, The Calaveras - Shoo Fly thrust, a major pre-Nevadan ductile shear zone in the Sierra Nevada, California: Geology, v. , p.

Seitz, J.F., 1983, Geologic map of the Tioga Lake, Hall Natural Area, Log Cabin, Saddlebag and Horse Meadows Roadless Areas, Mono County, California: U.S. Geological Survey Miscelaneous Field Investigations, Map MF-1453-A, scale 1:62,500.

Sharp, W.D., 1980, Ophiolite accretion in the northern Sierra (abs.): Transactions American Geophysical Union, Eos, v. 61, no. 46, p. 1122.

_____, 1984ms, Structure, petrology, and geochronology of a part of the central Sierra Nevada Foothills Metamorphic Belt, California: Ph.D. thesis, Berkeley, 183p.

_____, W.D., and Saleeby, J. B., 1979, The Calaveras Formation and syntectonic mid-Jurassic plutons between the Stanislaus and Tuolumne Rivers, California (abs.): Geological Society of America Abstracts with Programs, v. 11, p. 127.

_____, Saleeby, J.B., Schweickert, R.A., Merguerian, C., Kistler, R., Tobisch, 0., and Wright,W.H., 1982, Age and tectonic significance of Paleozoic orthogneisses of the Sierra Nevada Foothills Metamorphic Belt, California (abs.): Geological Society of America Abstracts with Programs, v. 14, no. 4, p. 233.

_____, Saleeby, J., Schweickert, R.A., Merguerian, C., Kistler, R., Tobisch, 0., and Wright, W.H., III, in press, Age and tectonic significance of Paleozoic orthogneisses of the Sierra Nevada Foothills Metamorphic Belt, California: American Journal of Science.

Sibson, R.H., 1977, Fault rocks and fault mechanisms: Journal Geological Society of London, v. 133, p. 191-213.

_____, 1980, Transient discontinuities in ductile shear zones: Journal of Structural Geology, v. 2, no. 1/2, p. 165-171.

Slemmons, D.B., 1966, Cenozoic volcanism of the central Sierra Nevada, California: *in* Bailey, E.H., *(editor)*, Geology of northern California, California Divison of Mines and Geology Bulletin 190, p. 199-208.

Smith, R.E., and Smith, S.E., 1976, Comments on the use of Ti, Zr, Y, Sr, K, P, and Nb in classification of basaltic magmas: Earth and Planetary Science Letters, v. 32, p. 114-120.

Stanton, R.L., and Bell, J.D., 1969, Volcanic and associated rocks of the New Georgia Group, British Islands Protectorate: Overseas Geology and Mineral Resources (G.B.), v. 10, p. 113-145.

Stern, T.W., Bateman, P.C., Morgan, B.A., Newell, M.F., and Peck, D.L., 1981, Isotopic U-Pb ages of zircon from the granitoids of the central Sierra Nevada, California: U.S. Geological Survey Professional Paper 1185, 17p.

Strand, R.G., 1967, Mariposa sheet, Geologic Map of California: California Division of Mines and Geology, scale 1:250,000.

_____, and Koenig, J.B., 1965, Sacramento Sheet, Geologic map of California: California Division of Mines and Geology, scale 1:250,000.

Streckeisen, A., 1979, Classification and nomenclature of volcanic rocks, lamprophyres, carbonatites, and melilitic rocks: recommendations and suggestions of the IUGS Subcommission on the systematics of igneous rocks: Geology, v. 7, p. 331-335.

Taliaferro, N.L., 1933, Bedrock complex of the Sierra Nevada, west of the southern end of the Mother Lode (abs.): Geological Society of America Bulletin, v. 44, no. 1, p. 149-150.

_____, 1942, Geologic history and correlation of the Jurassic of southwestern Oregon and California: Geological Society of America Bulletin, v. 53, p. 71-112.

_____, 1943, Manganese deposits of the Sierra Nevada, their genesis and metamorphism: California Divison of Mines and Geology Bulletin 125, p. 277332.

Tobisch, O.T., 1960ms, Geology of the Crane Flat - Pilot Peak area, Yosemite District, California: University of California Berkeley, M.A. Thesis,p. plus 1:24,000 scale map.

_____, and Fiske, R.S., 1976, Significance of conjugate folds and crenulations in the central Sierra Nevada, California: Geological Society of America Bulletin, v. 87, p. 1411-1420.

_____, and Fiske, R. S., 1982, Repeated parallel deformation in part of the eastern Sierra Nevada, California and its implications in the dating of structural events: Journal of Structural Geology, v. 4, no. 2, pp. 177-195.

Tullis, J., and Yund, Y.A., 1977, Experimental deformation of the Westerly granite: Journal of Geophysical Research, v. 82, p. 5705-5718.

Turner, F.J., 1968, Metamorphic Petrology: McGraw Hill, New York, p.

Turner, H.W., 1893, Some recent contributions to the geology of California: American Geology,v. 11, p. 307-324.

_____, 1894, Geological notes on the Sierra Nevada: American Geology, v. 13, p. 228-249.

_____, 1896, Further contributions to the geology of the Sierra Nevada: Seventeenth annual report of the U.S. Geological Survey to the Secretary of the Interior, 1895-96, Part I, p. 529-770.

_____, and Ransome, F.L., 1897, Sonora, California: U.S. Geological Survey Folio 41, 7p., 4 maps.

_____, and Ransome, F.L., 1898, Big Trees, California: U.S. Geological Survey Folio 51, 8p., 3 maps.

Wagner, D.L., Jennings, C.W., Bedrossian, T.L., and Bortugno, E.J., 1981, Geologic map of the Sacramento Quadrangle: California Division of Mines and Geology, Regional Geologic Map Series Map No. lA, Scale 1:250,000.

Weathers, M.S., Bird, J.M., Cooper, R.F., and Kohlstedt, D.L., 1979, Differential stress determined from deformation-induced microstructures of the Moine Thrust Zone: Journal of Geophysical Research, v. 84, no. B13, p. 7495-7509.

Weigand, P.W., and Ragland, P.C., 1970, Geochemistry of Mesozoic dolerite.dikes from eastern North America: Contributions to Minerology and Petrology., v. 29, p. 195-214.

White, S.H., Burrows, S.E., Carreras, J., Shaw, N.D., and Humphreys, F.J., 1980, On mylonites in ductile shear zones: Journal of Structural Geology, v. 2, no. 1/2, p. 175-187.

Williams, H., Turner, F.J., and Gilbert, C.M., 1982, Petrography - an introduction to the study of rocks in thin sections: W.H. Freeman, San Francisco, 626p.

Wright, W.H., and Schweickert, R.A., 1977, Tectonics and stratigraphy of the Calaveras Complex - Central Sierra Nevada Foothills: Guidebook for 73rd Ann. Mtg. Geological Society of America, Sacramento, California, 17p.

Xenophontos, C., and Bond, G.C., 1978, Petrology, sedimentation and paleogeography of the Smartville terrane (Jurassic) - bearing on the genesis of the Smartville ophiolite: *in* Howell, D.G., and McDougall, K.A., *(editors)*, Mesozoic Paleogeography of the Western United States: Pacific Section, Soc. Econ. Paleontologists and Mineralogists, Pacific Coast Paleogeography Symposium 2, p. 291-302.

To Cite This Thesis:

Merguerian, Charles, 1985, Stratigraphy, structural geology, and tectonic implications of the Shoo Fly Complex and the Calaveras-Shoo Fly thrust, Central Sierra Nevada, California: Ph.D. dissertation, Columbia University, New York, 255 p.

[**Note:** *The electronic version you are reading contains only 207 p. because margins and spacing of figures were slightly adjusted to save pages. No changes in wording or content were made from the original document which is on-file at the Geology Library of Columbia University (available through Interlibrary Loan) or for free download at* ***www.dukelabs.com****.*

Filename: CM1985ms.doc